

**Developing a novel methodology to investigate the
biomechanics and wear in natural patello-femoral joints**

Divya Baji (MEng, Hons)

Submitted in accordance with the requirements for the degree of
Doctor of Philosophy.

The University of Leeds

School of Mechanical Engineering

Institute of Medical and Biological Engineering (iMBE)

September 2016

The candidate confirms that the work submitted is her own and that appropriate credit has been given where reference has been made to the work of others.

All the work in this thesis was performed by Divya Baji.

This copy has been supplied on the understanding that it is copyright material and that no quotation from the thesis may be published without proper acknowledgement.

© 2016 The University of Leeds and Divya Baji

The right of Divya Baji to be identified as author of this work has been asserted by her in accordance with the Copyright, Designs and Patents Act 1988

Acknowledgements

“Surround Yourself With Positive People”

A PhD might be an individual project but it is a huge mission that requires the right guidance, help and support from many outstanding individuals without which it could be a mission impossible. So it is time to express my gratitude towards the individuals who have helped me through this journey. It is an acknowledgement to these individuals for the help and advice they have contributed to accomplish this multi-disciplinary project, as well as a tribute to some extraordinary people without whom I could not have come this far.

I would like to thank my primary supervisor Dr Louise Jennings and my co-supervisors Prof Eileen Ingham and Prof John Fisher. Thank you for all your help and patience throughout the years. It has been an incredible journey and your support is very much appreciated.

Thanks to Phil Wood, Irvin Homan and Lee Wetherill for all the technical support, Dr Hazel Fermor for your help with human dissection, Dr Abdul Abdellatif for your help with the indentation testing and Dr Raelene Cowie for the last minute Talysurf study. Thanks to Philippa, Rachel and Mahsa for being a great lab team; we worked together to save a lot of porcine legs!

I would like to thank Raman who has been a great friend and mentor. It has been great working with you and I have learnt a great deal from you. Also I would like to offer my sincere gratitude to Diana Higgins, my Disability Strategy Tutor, who has supported me in innumerable ways in the writing of this thesis. A big hug to my star team Ayesha, Emily and Nivi who have listened to my PhD stories and kept me sane! Special thanks to Ayesha for being a great house mate and all the moral support you have provided. You are one of the most honest and reliable people I know.

I sincerely thank my family without whom I would not be here today. Their support and encouragement has lifted my spirits on many occasions. Words cannot express the gratitude I have for my parents. Their belief in me has kept me going even at difficult times. Thanks to my beautiful sister, for her constant nagging and entertainment. Thank you for putting up with my constant ramblings and my not so often Eureka moment stories. And last but not least, my absolutely lovely husband. I thank them all from the bottom of my heart.

Dedicated

To the Lotus Feet of my Lord

Abstract

Patello-femoral problems affect nearly a quarter of the population and remain a common cause of knee replacement revision surgery. Minimally invasive treatments such as osteochondral substitutions are early interventions that can be used to prevent or delay the need for these replacements. Lack of pre-clinical testing is a major challenge in getting these promising treatments to clinical trials. The purpose of this research was to develop a platform that can get these products one step closer to clinical trials and hence getting them out in the market as a viable product for treating osteochondral lesions.

The aim of this project was to develop and validate a design specification for the pre-clinical testing of natural patello-femoral joint (PFJ). A characterization study was carried out to investigate the suitable animal model required to simulate a human joint that requires osteochondral substitutions. The size of the porcine PFJ was closer to the human PFJ and the material properties of its cartilage were also similar to the human cartilage. Therefore, the porcine PFJ was chosen as the animal model to develop the methodologies for this project.

A methodology was developed to investigate wear of the natural porcine PFJ by adapting a single station knee simulator to apply the porcine PFJ gait cycle to the joints. The position of the patella with respect to the femur determined through a contact point study was used to set up the samples in the simulator. A positive (cobalt chrome on natural cartilage) and negative (cartilage on cartilage) control was used to investigate the wear. This study showed the potential of using an Alicona Infinite focus G5 optical profiler to assess the change in cartilage topography in natural joints. The contact area and pressure in the PFJ was measured using Tekscan pressure sensors. This study showed the change in contact mechanics across a gait cycle and the effect of sample geometry on the contact mechanics of a joint.

In-vitro simulation can reduce the need for animal testing and progress the preclinical trials for new tissue substitutions. Developing the methodology in a human knee is not practical. However, by establishing an animal model can bring this a step closer. The methods developed in this thesis can contribute towards creating a pre-clinical testing system that can be used to assess early interventions to the PFJ.

Nomenclature

A/A	Adduction/ Abduction
AF	Axial Force
ANOVA	One-way analysis of variance
A/P	Anterior/Posterior
CL	Confidence Limit
ECM	Extra cellular matrix
F/E	Flexion/ Extension
GAG	Glycosaminoglycan
ISO	International Organization for Standardization
LVDT	Linear Variable Differential Transformer
Micro-CT	Micro Computed Tomography
M/L	Medial/ Lateral
MRI	Magnetic resonance imaging
MSD	Minimum significant difference
OA	Osteoarthritis
PBS	Phosphate Buffered Saline
PFJ	Patello-femoral joint
S/I	Superior/Inferior
SD	Standard deviation
SSKS	Single station knee simulator
TFJ	Tibio-femoral joint

Table of Contents

Acknowledgement	i
Abstract	iii
Nomenclature	iv
Table of Contents	v
List of Figures	x
List of Tables	xvi
Chapter 1. Literature Review	1
1.1 Patello-femoral joint	1
1.1.1 Biomechanics	2
1.1.2 Contact mechanics	5
1.2 Articular cartilage	9
1.2.1 Structure.....	10
1.2.2 Composition	13
1.2.3 Biphasic theory.....	14
1.2.4 Mechanical properties	15
1.3 Pathology and treatments.....	23
1.3.1 Patello-femoral disorders	23
1.3.2 Treatment options	28
1.4 Biotribology	35
1.4.1 Lubrication	35
1.4.2 Friction and wear	39
1.4.3 Tribology models for assessment of cartilage wear and friction	44
1.5 Rationale.....	48
1.6 Aims and Objectives	49
1.6.1 Aim	49
1.6.2 Objectives.....	49
Chapter 2. General materials and methods.....	50

2.1	General materials	50
2.1.1	Phosphate Buffered Saline (PBS)	50
2.1.2	Lubricant- New born calf serum.....	50
2.1.3	PMMA Bone Cement.....	50
2.1.4	Bovine, porcine and human tissue.....	50
2.1.5	Femoral Component - PFC Sigma.....	51
2.1.6	Microset replicating compound.....	51
2.1.7	AccuTrans replica moulds	51
2.2	General equipment	52
2.2.1	Linear Variable Differential Transformer (LVDT)	52
2.2.2	Micro Computed Tomography (Micro-CT).....	53
2.2.3	SolidWorks	53
2.2.4	Image-Pro Plus	53
2.2.5	Alicona optical surface metrology unit	53
2.2.6	Single station knee simulator (SSKS).....	54
2.3	Methodology for the preparation of natural tissue samples.....	56
2.3.1	Patello femoral joint dissection	56
2.3.2	Obtaining osteochondral plugs.....	56
2.4	Mechanical characterisation of cartilage	57
2.4.1	Indentation rig.....	57
2.4.2	Indentation test.....	59
2.4.3	Cartilage thickness measurement.....	61
2.4.4	Deriving the mechanical properties using an FE model.....	63
2.5	Methodologies for wear study	65
2.5.1	Calculating wear area using flexible film method.....	65
2.5.2	Validating Accutrans for obtaining cartilage replicas	66
2.6	Methods for statistical analysis.....	69

Chapter 3.	Geometry of the patello-femoral joint	70
3.1	Introduction.....	70
3.2	Materials and methods	70
3.2.1	Dissection of the patello-femoral joint	70
3.2.2	Dimensions of the joint.....	72
3.2.3	Area of patella.....	73
3.2.4	Radius of curvature of the patello-femoral groove	73
3.3	Results	78
3.4	Discussion	80
3.5	Conclusion	83
Chapter 4.	Material properties of the porcine patello-femoral cartilage	84
4.1	Introduction.....	84
4.2	Materials and methods	84
4.2.1	Osteochondral plugs	84
4.2.2	Method to determine the equilibrium elastic modulus and permeability	86
4.2.3	Method to determine the thickness of the cartilage.....	86
4.3	Results	86
4.4	Discussion	91
4.5	Conclusion	97
Chapter 5.	Characterisation of the human patello-femoral joint.....	98
5.1	Introduction.....	98
5.2	Materials and methods	98
5.2.1	Materials	98
5.2.2	Dissection of human PFJ	98
5.2.3	Determining the geometry of human PFJ	99
5.2.4	Obtaining the osteochondral plugs.....	100
5.2.5	Determination of material properties of the cartilage	101

5.3	Results	102
5.3.1	Observations during dissection.....	102
5.3.2	Size of the human patello-femoral joint	106
5.3.3	Material properties of the human PFJ cartilage	106
5.4	Discussion	108
5.5	Conclusion	115
Chapter 6.	Contact point study.....	116
6.1	Introduction.....	116
6.2	Materials and methods	117
6.2.1	Determination of contact point	117
6.2.2	Estimating the contact point using the Microset method	119
6.2.3	Theoretical model	120
6.3	Results	123
6.3.1	Determination of contact point	123
6.3.2	Microset method.....	126
6.3.3	Theoretical model	127
6.4	Discussion	128
6.5	Conclusion	130
Chapter 7.	Developing the methodologies for investigating the biotribology of the porcine patello-femoral joint.....	131
7.1	Introduction.....	131
7.2	Materials and Methods	132
7.2.1	Modifying a Single Station Knee Simulator	132
7.2.2	Setting up the porcine PFJ sample	138
7.2.3	Wear study	144
7.3	Results	147
7.3.1.	ICRS grading and wear area	147

7.3.2.	Surface analysis using Alicona IF G5	148
7.4	Discussion	149
7.5	Conclusions.....	154
Chapter 8.	Contact mechanics of the porcine patello-femoral joint.....	155
8.1.	Introduction.....	155
8.2.	Materials and methods	155
8.2.1	Porcine PFJ	155
8.2.2	Tekscan sensors.....	155
8.2.3	Calibration	156
8.2.4	Setting up the test.....	159
8.2.5	Running the test.....	160
8.2.6	Analysing the contact mechanics recordings.....	162
8.3	Results	163
8.3.1	Gait cycle study	163
8.3.2	Fundamental study	165
8.4	Discussion	170
8.5	Conclusions.....	175
Chapter 9.	Overall Discussion and Conclusions	176
Bibliography	184

List of Figures

Figure 1-1: Bony anatomy of the right patello-femoral joint (Gray, 1918)	1
Figure 1-2: Patello femoral joint movements along different axes and planes (a) medial-lateral translation (b) medial lateral tilt (c) internal-external tilt (Leal et al., 2015)	3
Figure 1-3: Six degrees of freedom of the knee with 3 rotational and 3 translational motions (Komdeur et al. 2002)	3
Figure 1-4: Contact area and position of patella at different degrees of flexion (Maquet, 1990)	5
Figure 1-5: Hierarchical structure of articular cartilage (Mow et al. 1992)	10
Figure 1-6: Zonal arrangement in articular cartilage showing the cellular organization (A) and collagen fibre architecture (B) (Newman 1998)	11
Figure 1-7: Tensile properties of articular cartilage (Sophia Fox et al. 2009)	16
Figure 1-8: Examples of compression tests	18
Figure 1-9: Creep response of cartilage under constant compressive load (Mow et al. 1980)	19
Figure 1-10: Partial and full thickness defects (Kelc Robi, 2013)	26
Figure 1-11: Area of wear in patella (left) and femur (right). The medial side of each patella and femur is on the right side of the diagram (Gorniak, 2009)	27
Figure 1-12: Stages in a tissue engineered osteochondral substitution technique (Adapted from Maioregen® (Fin-Ceramica Faenza Spa 2013))	33
Figure 1-13: Types of lubrication regimes (Akkok 2013)	35
Figure 1-14: Average roughness of profile (Ra)	40
Figure 1-15: Maximum peak height (Rp), Maximum valley height (Rv), Maximum peak to valley height (Rt)	40
Figure 1-16: Schematic of a pendulum device (Radin and Paul, 1971) and pin-on-plate device (Furey and Burkhardt, 1997)	44
Figure 2-1: Press fit condylar sigma design femoral component used as the positive control	51
Figure 2-2: Simplified diagram of the single station knee simulator for the patello-femoral joint	55
Figure 2-3: Coring tool from the Smith and Nephew mosaicplasty kit	56
Figure 2-4: A fully prepared osteochondral plug for the cartilage characterisation study ...	57
Figure 2-5: Indentation rig (Taylor, 2012)	58

Figure 2-6: Calibration graph for the piezoelectric force transformer	59
Figure 2-7: Calibration graph for the LVDT	59
Figure 2-8: Indentation set up with the osteochondral plug under the indenter	60
Figure 2-9: From left to right- Stainless steel bath, O ring to fix the collet in place, the collet and flat indenter	60
Figure 2-10: The needle attached to the Instron is positioned just above the cartilage.....	62
Figure 2-11: Schematic of how cartilage thickness was determined from needle indentation (adpated from Fermor, 2013)	63
Figure 2-12: Finite element model of an osteochondral pin	64
Figure 2-13: Experimental curve and curve produced by the finite element model	65
Figure 2-14: Measuring the area of patella cartilage (a) Images of the patella for measurement (b) flexible film over the patella (c) image of the film for calculation	66
Figure 2-15: : Patella cartilage scan from Microset	67
Figure 2-16: : Patella cartilage scan from AccuTrans.....	67
Figure 2-17: Roughness standard used to measure the Ra for 0.8 μ m	68
Figure 2-18: Surface roughness of the actual standard, measured standard on Talysurf, measured from AccuTrans replicas and Microset replicas	68
Figure 3-1: Dissection of a bovine knee joint to separate the patella and the patello-femoral groove. Left to right: Bovine femur with intact PFJ, Soft tissues removed to obtain the patella, patello-femoral groove exposed.....	71
Figure 3-2: Porcine femoral groove (left) and patella (right) with all the soft tissues removed	71
Figure 3-3: Typical size of the bovine (left) and porcine (right) patello-femoral grooves respectively	72
Figure 3-4: Dimensions of the femoral groove and patella.	73
Figure 3-5: Taking the measurements from the sample using the Vernier Calliper.....	74
Figure 3-6: Diagram explaining the radius of curvature calculation in equation 1	74
Figure 3-7: Sample set up for LVDT study: Left- LVDT equipment, Right- LVDT needle on the sample surface.	75
Figure 3-8: Movement of LVDT tracking the groove (left) and the output from the LVDT (right).....	75
Figure 3-9: The displacement from the LVDT plotted against the reference line and an arc of known radius drawn	76

Figure 3-10: Micro-CT image showing the slice containing the crystals and a circle of known radius drawn connecting the crystals using ImagePro Plus.....	77
Figure 3-11: Mean lengths of the two condyles of bovine and porcine PFJ	78
Figure 3-12: Sizes of bovine and porcine femoral grooves. Data is presented as the mean (n=6) ± 95% confidence limits.....	79
Figure 3-13: Sizes of bovine and porcine patella. Data is presented as the mean (n=6) ± 95% confidence limits	80
Figure 3-14: Labelled Micro-CT image of the porcine patello-femoral groove	81
Figure 3-15: The sizes of patella from bovine, porcine and human** (Baldwin & House 2005)	82
Figure 4-1: Locations of plugs obtained from the femur (left) and patella (right)	85
Figure 4-2: Permeability of cartilage in the porcine patello-femoral joint. The data is presented as the mean (n=6-12) ± 95% confidence limits. Data was analysed by one way analysis of variance which revealed no significant variation in the data (p= 0.074).....	87
Figure 4-3: Permeability of cartilage in the porcine patello-femoral joint.....	87
Figure 4-4: Equilibrium elastic modulus of cartilage in the porcine patello-femoral joint. The data is presented as the mean (n=6-12) ± 95% confidence limits. Data was analysed by one way analysis of variance followed by the Tukey test (p<0.05) which revealed a significantly higher equilibrium elastic modulus (*) in location E (patella inferior/ lateral) compared to locations A (patella superior medial) and 3 (superior femoral groove).	88
Figure 4-5: Equilibrium elastic modulus of cartilage in the porcine patello-femoral joint....	88
Figure 4-6: Thickness of cartilage in the porcine patello-femoral joint. The data is presented as the mean (n=6-12) ± 95% confidence limits. Data was analysed by one way analysis of variance followed by the Tukey test (p<0.05).	89
Figure 4-7: Thickness of cartilage in the porcine patello-femoral joint.....	89
Figure 5-1: Human knee with the soft tissues and patella removed.....	99
Figure 5-2: Dimensions of the left human patello-femoral groove and patella (n=6)	100
Figure 5-3: Location of osteochondral plugs from the left human PFJ (n=6)	101
Figure 5-4: ICRS grading of cartilage wear	102
Figure 5-5: The sizes of bovine, porcine and human patella from this study.....	109
Figure 5-6: The sizes of bovine, porcine and human patello-femoral groove from this study	109

Figure 5-7: Dimensions of the human patella from this study (n=6) compared to other studies from the literature. Baldwin (n=92), Osterhoff (n=24)	110
Figure 5-8: The overall material properties of the human PFJ and porcine PFJ	112
Figure 6-1: Fixture holding the porcine leg at 20 degree angle	117
Figure 6-2: Tracing the outline of the patella and placing it on the femur with respect to the drill holes made as a guide. Left: Position of patella at 20 degrees, Right: Position at 40 degrees of knee flexion	119
Figure 6-3: Left: Microset applied to the patella cartilage and placed over the femur using the drill holes as guide. Right: The Microset impression from the patella made on the femur representing the contact point.	120
Figure 6-4: Dynamics of the patella in a right knee (Herrmann et al., 2012). The figure illustrates how the patella travels on the femur from 0-120 degrees of flexion	120
Figure 6-5: 3D anatomical model of the femoral groove and patella contact mechanics (Akbar et al., 2012). The highlighted regions shows the contact between the patella and femur at 0-50 degrees of flexion.	121
Figure 6-6: Contact area between the patella and femoral groove (Kittl, Schmeling and Amis, 2015). The marked regions shows the contact between the patella and femur at 0-135 degrees of flexion.....	122
Figure 6-7: Position of patella at 20 degrees knee flexion for the 6 samples. The outer marking of the patella traced on the femur shows the relative position of the patella with respect to the femur when the knee is flexed at 20 degrees	124
Figure 6-8: Position of patella at 40 degrees knee flexion for the 6 samples. The outer marking of the patella traced on the femur shows the relative position of the patella with respect to the femur when the knee is flexed at 40 degrees	125
Figure 6-9: The contact point between the patella and femur obtained from the Microset study. Left – contact points on the patella and femur at 20 degrees. Right- contact at 40 degrees.....	126
Figure 6-10: Left- Medial View of the SolidWorks model representing the sample set up at the starting point in the simulator, Right – Lateral view of the SolidWorks model at starting point	127
Figure 6-11: Left- Anterior View of the SolidWorks model, Right – Posterior view of the SolidWorks model showing the whole articular surface of the femoral groove	128

Figure 7-1: Image of the SSKS displaying the 6 axes for the PFJ for a right knee with the polarities	133
Figure 7-2: Flow chart explaining the steps followed for the calibration of the machine ..	134
Figure 7-3: A typical graph following load calibration showing the relationship between the axial load cell and the load at the bearing surface	135
Figure 7-4: Left: Fully assembled patella fixture. The rectangular sample space is marked with the depression side for reference in yellow. Right: Manufactured Delrin PFJ fixture with the sample.....	137
Figure 7-5: Left- porcine PFJ assembled in the simulator within its fixtures.	138
Figure 7-6: Patella placed inside the cutting jig	139
Figure 7-7: Left- Full patella with curved base, Right- Dissected patella with the flat base	139
Figure 7-8: The desired shape and size of the femoral sample. Left- Side view of the femoral sample cut from the femur. Right- Top view of the femoral sample and patella showing its articular cartilage	140
Figure 7-9: Steps taken to cut the femoral groove sample from the femur	140
Figure 7-10: Left- Alignment of the patella at the centre of the fixture.....	141
Figure 7-11: Diagram of the patella in the mount at superior and anterior view of the simulator	142
Figure 7-12: Cementing the patella and femur at the same position as its alignment at the starting point of the gait cycle	142
Figure 7-13: Porcine patello-femoral gait cycle.	143
Figure 7-14: ICRS grading of cartilage wear	144
Figure 7-15: Impression of the patella made from AccuTrans mould	145
Figure 7-16: The area scanned using Alicona IF G5	145
Figure 7-17: The S/I reference points from an S/I scan	146
Figure 7-18: 3D model of a S/I scan	146
Figure 7-19: Surface profile extracted from the S/I scan at 800 μ m cut off wavelength	147
Figure 7-20: The area of deformation caused by the wear study is marked in red.....	148
Figure 7-21: Roughness values from positive and negative control, mean (n=6) \pm 95 % CL, where p1 is the S/I and p2 is the M/L scan.....	149
Figure 8-1: Left– A Tekscan sensor connected to the handle, Right – Labelled diagram of a Model 4000 sensor	156

Figure 8-2: Tekscan sensor was placed between two rubber sheets and compressed between two metal plates in the Instron during calibration.....	157
Figure 8-3: Tekscan verification curves from the Instron pre and post study with regression lines	158
Figure 8-4: Output from external load cell and Tekscan compared to the input from the SSKS before and after the contact mechanics study	159
Figure 8-5: Porcine patello-femoral gait cycle. HS= Heel strike, TO= Toe off.....	161
Figure 8-6: Marking the location of patella on the pressure map	162
Figure 8-7: Pattern type 1 with larger contact area showing the 5 stages (as indicated in Figure 8.6) in the gait cycle	163
Figure 8-8: Pattern type 2 with smaller contact area showing the 5 stages in the gait cycle	163
Figure 8-9: Mean contact area over a gait cycle . Data is presented as the mean (n=6) \pm 95% confidence limits	164
Figure 8-10: Mean contact pressure over a gait cycle. Data is presented as the mean (n=6) \pm 95% confidence limits	164
Figure 8-11: Mean peak pressure over a gait cycle .Data is presented as the mean (n=6) \pm 95% confidence limits	165
Figure 8-12: Pattern type 1 (left) and pattern type 2 (right) showing the change in contact mechanics with respect to SI (left to right) and FE (top to bottom).....	166
Figure 8-13: Effect of flexion on the contact area at different loads and displacements (Mean (n=6) \pm 95% confidence limits)	167
Figure 8-14: Effect of flexion in the contact pressure at different loads and displacements (Mean (n=6) \pm 95% CL).....	167
Figure 8-15: Contact area at 300N (Mean (n=6) \pm 95% confidence limits)	169
Figure 8-16: Contact pressure at 300N (Mean (n=6) \pm 95% confidence limits).....	169

List of Tables

Table 1-1: Elastic modulus and permeability of cartilage in the knee and the various techniques used by other researchers.....	20
Table 1-2: Thickness of cartilage in the knee and the various techniques used by other researchers.....	22
Table 1-3: ICRS grading of cartilage lesions (ICRS, 2016).....	25
Table 1-4: Tissue engineered products for osteochondral repair (Nukavarapu & Dorcemus 2013)	32
Table 1-5: Typical roughness values of articular cartilage	42
Table 1-6: Artificial patello femoral simulator studies	46
Table 3-1: Dimensions (mm) of the porcine and bovine patella and patello-femoral groove. Data is presented as the mean (n=6) ± 95% confidence limits	78
Table 4-1: The location of each plug marked in Figure 4.1.....	85
Table 4-2: Overall (mean ± 95% CL) material properties of cartilage in the porcine femoral groove and the patella	91
Table 5-1: Table describing the location of osteochondral plugs taken from the human patello-femoral joint	101
Table 5-2: Observation made on the 6 human samples	104
Table 5-3: Size (mm) of the human patella femoral samples	106
Table 5-5: Elastic modulus of cartilage in each sample	107
Table 7-1: Design requirements for the SSKS fixtures	136
Table 7-2: Change in Ra in healthy porcine cartilage with respect to cut-off frequency	148
Table 8-1: Parameters for the fundamental study	162

Chapter 1. Literature Review

Advances in technology and regenerative medicine have improved the lifestyle of people but the need for better treatments for the ageing population is in greater demand. As people live longer the healthcare system demands a better way of improving the quality of life for older people, in order to reduce the cost of public health care. Therefore, it is ever more important to have earlier interventions to improve the health of the ageing population.

Osteoarthritis (OA) is a degenerative joint disease caused by the gradual loss of articular cartilage in the synovial joint leading to joint stiffness and pain. It is the leading cause of disability among people over 65 and knee OA in particular can greatly reduce the mobility of the patient and compromise their quality of life. Although OA might be common in the elderly, damage to cartilage affects the young active population as well as the elderly. Chondral defects have a variety of causes. This study focuses on improving the in- vitro testing methods for early intervention therapies to treat osteochondral lesions in the patello-femoral compartment of the knee joint.

1.1 Patello-femoral joint

The knee is the largest synovial joint and arguably the most complex joint in the body. It facilitates major locomotion in a person whilst supporting several times body weight (Al-Turaiki, 1990). The knee is a tri-compartmental joint consisting of the tibia, femur and patella. This makes up the medial and lateral tibio-femoral joint (TFJ) and the patello-femoral joint (PFJ). The bony anatomy of the patello-femoral joint is shown in Figure 1.1.

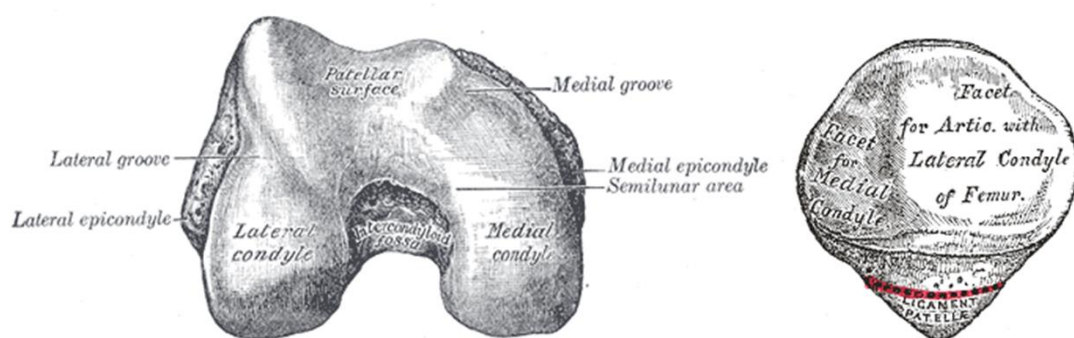


Figure 1-1: Bony anatomy of the right patello-femoral joint (Gray, 1918)

1.1.1 Biomechanics

The patello-femoral joint (PFJ) consists of the patella and distal femur; it is the most complex compartment in the knee as a result of the tracking mechanism of the patella (Dhafer and Kahn, 2002). The geometry of the articulating surface of a synovial joint has a significant impact on its contact mechanics. Considering the curvature of its articular surface, the geometry of PFJ can be classified as a saddle joint. The articulation within the tibio-femoral joint (TFJ) is a combination of rolling and sliding of the femoral condyles along the tibial plateau whereas the articulation in the PFJ consists of the patella sliding over the patellar femoral groove. The area of the intercondylar groove of the femur with the adjacent anterior aspect of the condyles is known as the femoral groove, trochlea or intercondylar fossa (Al-Turaiqi 1990; Dhafer & Kahn 2002; Gorniak 2009).

The patello-femoral joint consists of the patella and the femur which are tightly held together by the soft tissues. The patella is the largest sesamoid bone (small round bone formed in a tendon where it passes a joint) in the body (Maquet, 1990). The cartilage on the vertical central ridge of the patella is the thickest in the body and can be up to 7 mm thick (Koskinen 1993; Grelsamer & Weinstein 2001). The cartilage in the condyles which is approximately 3.5 mm thick becomes thinner towards the lateral and medial borders (Koskinen, 1993).

Cartilage helps the patella to glide smoothly over the groove located between the superior medial and lateral femoral condyles. The PFJ has a concave intercondylar groove and a convex patellar surface geometry. There is slight projection in the lateral femoral condyle and the retropatellar surface is also larger on this lateral side. This feature prevents the lateral dislocation of the patella (Walker *et al.*, 1968; Brien, 2001). The PFJ movements along different axes and planes are shown in Figure 1.2 (Leal *et al.*, 2015).

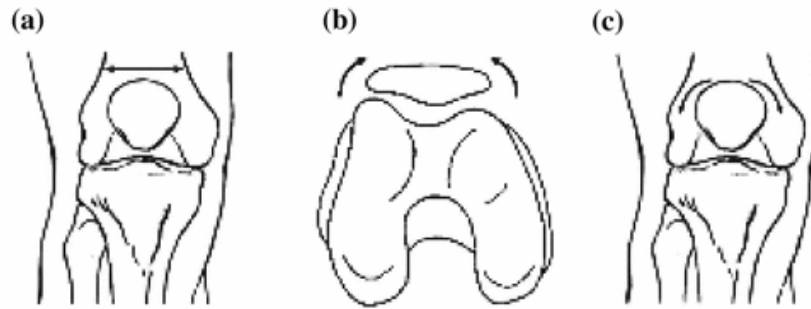


Figure 1-2: Patello femoral joint movements along different axes and planes (a) medial-lateral translation (b) medial lateral tilt (c) internal-external tilt (Leal *et al.*, 2015)

The patello-femoral joint allows flexion, extension and rotation. The 6 degrees of freedom with respect to the tibia and femur are shown in Figure 1.3.

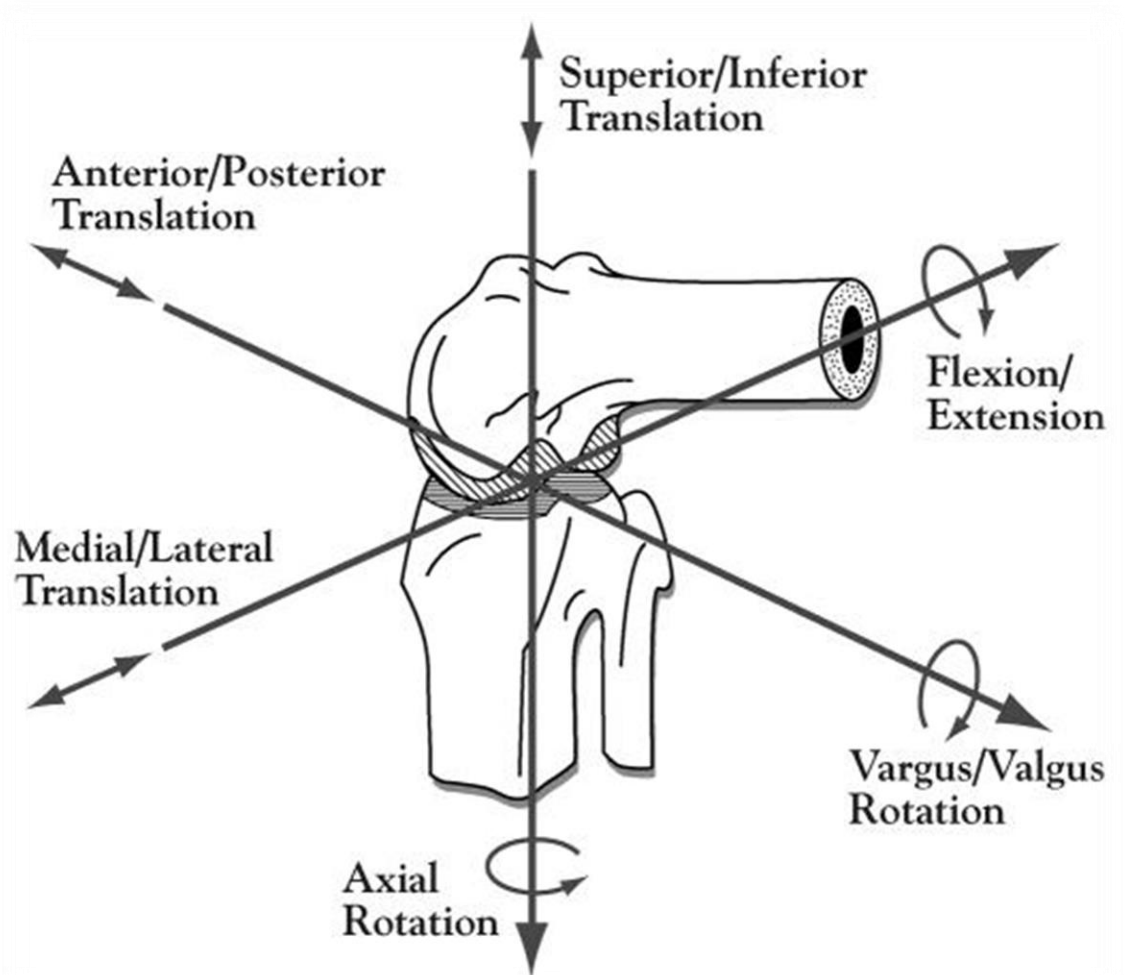


Figure 1-3: Six degrees of freedom of the knee with 3 rotational and 3 translational motions (Komdeur *et al.* 2002)

At 0° the knee is fully extended and as the flexion increases the angle becomes larger (Al-Turaiki, 1990). The patella ligament is attached to the proximal tibia and the quadriceps

tendon joins the quadriceps muscles that attach to the proximal femur (Koskinen 1993; Mason et al. 2008; Gorniak 2009).

The articulation of the joint and the tracking of the patella is controlled by the function of the quadriceps and hamstring muscles. The quadriceps tendon and the patellar tendon form the quadriceps mechanism that straightens the knee by tightening the quadriceps muscles to pull the tendons. As the leg straightens, the vastus medialis obliquus and vastus lateralis control the position of the patella in the femoral groove (Brien, 2001).

The quadriceps exerts an oblique pull on the patella that forms a laterally obtuse angle known as the Q angle or quadriceps angle; the angle between the quadriceps muscles and the patella tendon. The Q angle is 10°-15° during extension and lies between the lines of action in the frontal plane. In flexion, the femur rotates laterally and the Q angle becomes zero (Brien, 2001). Women have a larger Q angle than men. Typically the Q angle in men is 14° and 17° in women due to their greater physiological valgus at the knee and wider hips (Maquet, 1990).

When the quadriceps contract, the patella moves proximally to the groove. Due to the lack of side support in this region the height of the patella to the groove determines the kinematics of the patella (Zaffagnini *et al.*, 2016). The patella improves the biomechanical function of the knee by playing a major role in the extensor mechanism. It produces anterior displacement of the quadriceps tendon throughout the entire range of motion. This reduces the force required as the patella lengthens the moment arm and centralises the resultant forces. Without the patella, the force needed for extension could increase by up to 13% at 90° flexion and 31% at full extension (Reilly & Martens 1972; Dowson 1981; Nordin & Frankel 2001).

The patella increases the contact area between the patellar tendon and the femur. This distributes the compressive stress on the femur and reduces the patello-femoral contact stress. The low coefficient of friction of the articular cartilage helps the patella to transmit the quadriceps power over the distal femur to the tibia while the patella protects the anterior aspect of the joint from trauma. The patella also prevents the additional wear of the quadriceps tendon and improves cosmesis (Hungerford & Barry 1979; Koskinen 1993; Ellison 2007; Maiti 2012).

The patello-femoral joint reaction force (PFJR) is caused by the muscular activity of the knee during flexion and extension. It changes with the angle of knee flexion and magnitude of the quadriceps force. During level walking, the reaction force in PFJ can be up to 0.5 times the body weight whereas in the TFJ it is 3 times the body weight (Reilly and Martens, 1972).

The PFJR increases with increasing angles of flexion. The angles are low during walking and therefore the quadriceps forces are lower. In deep knee bend activity the angle is higher and therefore the quadriceps forces and patellar tendon forces will also increase in order to equilibrate the PFJR. At these conditions the PFJR has been calculated to be 7.6 times body weight (Reilly and Martens, 1972). This is why patients with patello-femoral problems often experience pain when stair climbing and descending. They compensate by the push-off with the unaffected leg to decrease the muscle force during the stair walking (Wallace *et al.*, 2002; Besier *et al.*, 2005; Eckstein *et al.*, 2005; Chinkulprasert, Vachalathiti and Powers, 2011; Suzuki *et al.*, 2012).

1.1.2 Contact mechanics

Many researchers have investigated the contact mechanics of the PFJ (Matthews, Sonstegard and Henke, 1977; Hungerford and Barry, 1979; Maquet, 1990; Brien, 2001; Nordin and Frankel, 2001; Herrmann *et al.*, 2012; Kittl, Schmeling and Amis, 2015; Zaffagnini *et al.*, 2016). The contact area and position of the patella at different degrees of flexion is shown in Figure 1.4.

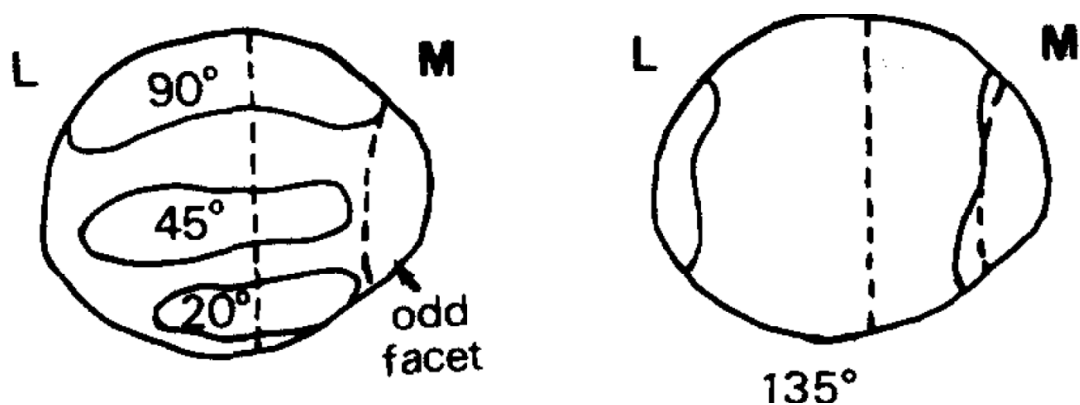


Figure 1-4: Contact area and position of patella at different degrees of flexion (Maquet, 1990)

The earliest patello-femoral contact area study was conducted by Aglietti *et al.* (1975) on patella retrieved from cadavers. They found that the contact area increases with increasing flexion up to an angle of 60° after which it remains almost the same up to 90°. This increase in contact area occurs as the patella slides down in the patella femoral groove during the

flexion to achieve congruency in the joint. Over 90° flexion the area starts to decrease until 120° and then shows a slight increase at 120 to 135 degrees. At any angle of knee flexion the contact area of the PFJ is considerably lower compared to other synovial joints such as the TFJ and hip. Hence the contact stress on the PFJ can be considerably higher (Ahmed et al. 1983; Besier et al. 2005).

A recent literature review carried out on the biomechanics of the PFJ also concluded that the contact area in the patella moves from distal to proximal where-as that of the groove moves against the patella from proximal to distal. At full extension the patella is rarely in contact with the femur. However, at 135° there are two contact points in the femoral groove which articulate against the odd facets of the patella (Kittl, Schmeling and Amis, 2015). The entire retropatellar surface is never in full contact with the femur. The contact area increases with increasing level of flexion moving proximally on the patella through the increasing pull of quadriceps muscles. From full extension at 0° to full flexion at 135°, the patella descends vertically about 7 cm to the intercondylar notch (Hungerford & Barry 1979; Nordin & Frankel 2001; Brien 2001).

1.1.2.1 Contact mechanics study

The contact area and contact pressure have been investigated by many researchers (Ahmed, Burke and Yu, 1983; Heino *et al.*, 1999; Clark, Herzog and Leonard, 2002; Hsieh *et al.*, 2002; Lee, Morris and Csintalan, 2003; Besier *et al.*, 2005; Bachus *et al.*, 2006; Merkher *et al.*, 2006; Li *et al.*, 2011; Jansson *et al.*, 2013; Leichtle *et al.*, 2014; Padalecki *et al.*, 2014; Geeslin *et al.*, 2015; Lorbach *et al.*, 2016; Kim *et al.*, 2016) to understand the load distribution and pathology of diarthroidal joints.

Various methodologies have been recorded in the literature to investigate the contact mechanics in diarthroidal joints. Different methods use a variety of tools for measuring contact area; in- vitro studies using pressure sensitive films such as Tekscan and Fuji films, as well as invivo studies using MRI scans and the use of computational methods are also common. Pressure sensors are often inserted into the joints arthroscopically and fixed in place using sutures. This technique ensures adequate and constant fixation of the sensors in each sample. Studies have documented reduced resistance during motion and comparable positioning of the sensors in every sample (Lorbach *et al.*, 2016).

Many studies have used Fuji films to investigate the contact mechanics in the PFJ (Ahmed, Burke and Yu, 1983; Liggins, Hardie and Finlay, 1995; Lee *et al.*, 2001; Clark, Herzog and Leonard, 2002; Bachus *et al.*, 2006). Fuji film was used on a custom made loading apparatus designed by Ahmed *et al.* (1983) to measure the contact area in cadaveric knees at 0° to 130°. The mechanical system consisted of a brass cap attached outside the patella from which five strings representing the five quadriceps muscles were attached as a pulley system to a transducer. The ratio of contact area to the total surface area at various knee flexion angles was measured. They found that even when the quadriceps force was doubled, the contact area only increased by 25%. This shows the influence of the congruency of the joint in the contact mechanics. For the same normal force, the PFJ contact stress was larger than even a meniscectomised TFJ. The average contact stress at the PFJ was twice as much as the TFJ during the walking down-ramp and climbing up and down the stairs.

Clark *et al.* (2002) used feline PFJs to measure the contact area and pressure using Fuji films. They observed an exponential increase in contact area with force and a linear increase in mean and peak contact pressures. As the contact load increased, the contact area increased to keep the contact pressure constant. This could be an indication why in osteoarthritic joints the contact areas are significantly increased to reduce the peak contact pressures. By increasing the contact area the joint can regulate the pressures on the cartilage as the applied forces are increased.

MRI is another method that can be used to investigate the contact mechanics. Besier *et al.* (2005) used MRI imaging to compare the contact area in men and women at 0°, 30° and 60°, under loaded and unloaded conditions. Under load bearing conditions there was a 24% increase in contact area, and a 34% larger contact area in men than in women. Except at full extension, the unloaded contact area was significantly higher in men with a maximum at 60° flexion. When results were normalised by patellar dimensions there was no significant difference between the two groups. This was influenced by the finding that 78% of the variation in patellar size is due to the positive correlation between patellar area and subject height.

MRI is a non-invasive technology that can also be used in patients for diagnostic purposes. Whereas pressure sensitive films such as Fuji film and Tekscan sensors can only be used for in- vitro investigations. Although MRI cannot be used to assess contact pressure, it can be

used to measure contact area. Since there is a substantial amount of research data available for Fuji studies compared to MRI, it is clear that comparing the two could demonstrate the effectiveness of MRI for measuring contact area. Importantly, a study conducted by Heino and colleagues compared the contact area in cadaveric knees using MRI and the Fuji film method. Results showed a 95% correlation between the two methods, suggesting MRI as a non-invasive method to measure contact area that is comparable to the Fuji film method (Heino *et al.*, 1999).

The contact area measured by Besier *et al.* (2005) using MRI was 5.20 cm² in men and 3.96 cm² in women. However, the contact area measured by Heino *et al.* (1999) from Fuji film was 3.04 cm² and from MRI was 2.94 cm². This variation could be due to various reasons. Besier *et al.* measured the area in 8 men and 8 women whereas Heino *et al.* reported measuring just 6 cadaveric samples. There was a large variation between these samples, ranging from 1.4 – 4 cm² in Fuji film and 1.5 – 4.5 cm² in MRI. This could be due to the small sample size or the influence of gender as shown by Besier *et al.*

Males have a larger patella and contact area compared women as they are generally larger than women and the surface area of their patella may be almost 20% greater (Clark, Herzog and Leonard, 2002; von Eisenhart-Rothe *et al.*, 2004). A larger contact area allows improved load distribution which can reduce the peak stress and thereby reduces wear (Besier *et al.*, 2005; Gorniak, 2009).

Studies conducted using pressure sensitive films often attempt to use minimal dissection techniques to allow the film to be inserted between the joint without disrupting the surrounding tissue and keeping the joint intact as much as possible. This allows the muscle forces to be applied appropriately to replicate the in- vivo contract mechanics. Tekscan is one of the most successful and commonly used techniques to study the contact mechanics of the knee joint in- vitro (Bachus *et al.*, 2006; Jansson *et al.*, 2013; Leichtle *et al.*, 2014; Padalecki *et al.*, 2014; Geeslin *et al.*, 2015; Wang *et al.*, 2015; Kim *et al.*, 2016; Lorbach *et al.*, 2016).

Application of Tekscan to study the effect of contact mechanics in different pathological conditions is very common. Wang *et al.* (2015) investigated the contact pressure on the tibial plateau at various meniscal conditions using Tekscan pressure sensors. They observed a site dependent variation in all conditions and specimens, suggesting the influence of the

geometry of the joint. Padalecki et al. (2014) have investigated the effect of meniscal tear in the cadaveric human TFJ and found significant decrease in contact area and increase in contact pressure at such conditions.

Leichtle et al. (2014) investigated the effect of total knee replacement (TKR) on the PFJ contact mechanics. They noticed that the PFJ peak pressure increased up to 3 times in knees with TKR compared to normal knee. They also observed a wider area pattern for the patello-femoral contact point in the normal knees. The contact area decreased in TKR knees and with a dotted pattern on a TKR joint and a line-shaped pattern with a resurfaced patella.

Contact mechanics studies on cadaveric knees using Tekscan have shown a contact area up to 7.21 cm² in the normal patella whereas the area in chondromalacia patellae reduced to 6.35 cm² (Kim *et al.*, 2016). This small sample size of 10 human knees and the difference in test conditions makes it difficult to compare this contact area to the results found from the Fuji film and MRI studies by other authors. A comparison study was carried out by Bachus et al. (2006) using an Instron material testing machine to compare the contact area and pressure results from Tekscan and Fuji film sensors. They showed that either of the techniques was accurate to $\pm 5\%$ of a known value and Tekscan was comparatively more accurate than Fuji film. However, the application of these techniques in natural joints might not necessarily show the same results. It could be less accurate in natural joints where there could be a substantial influence of the complexity of joint curvatures.

1.2 Articular cartilage

Articular cartilage is a biphasic viscoelastic tissue with exceptional mechanical properties. It is a weight-bearing, load distributing and lubricating connective tissue that can withstand large compressive forces. The hierarchical structure of articular cartilage is shown in Figure 1.5. The complex and unique structure and composition of articular cartilage gives the tissue an extraordinary mechanical durability which allows specialised biomechanical functions. It provides a lubricating bearing surface with a low coefficient of friction which makes it ideal for synovial joints. Its ability to distribute load can minimise the peak stress on subchondral bone and protect it from high compressive loading (Haberth, 2002; Scott, 2011).

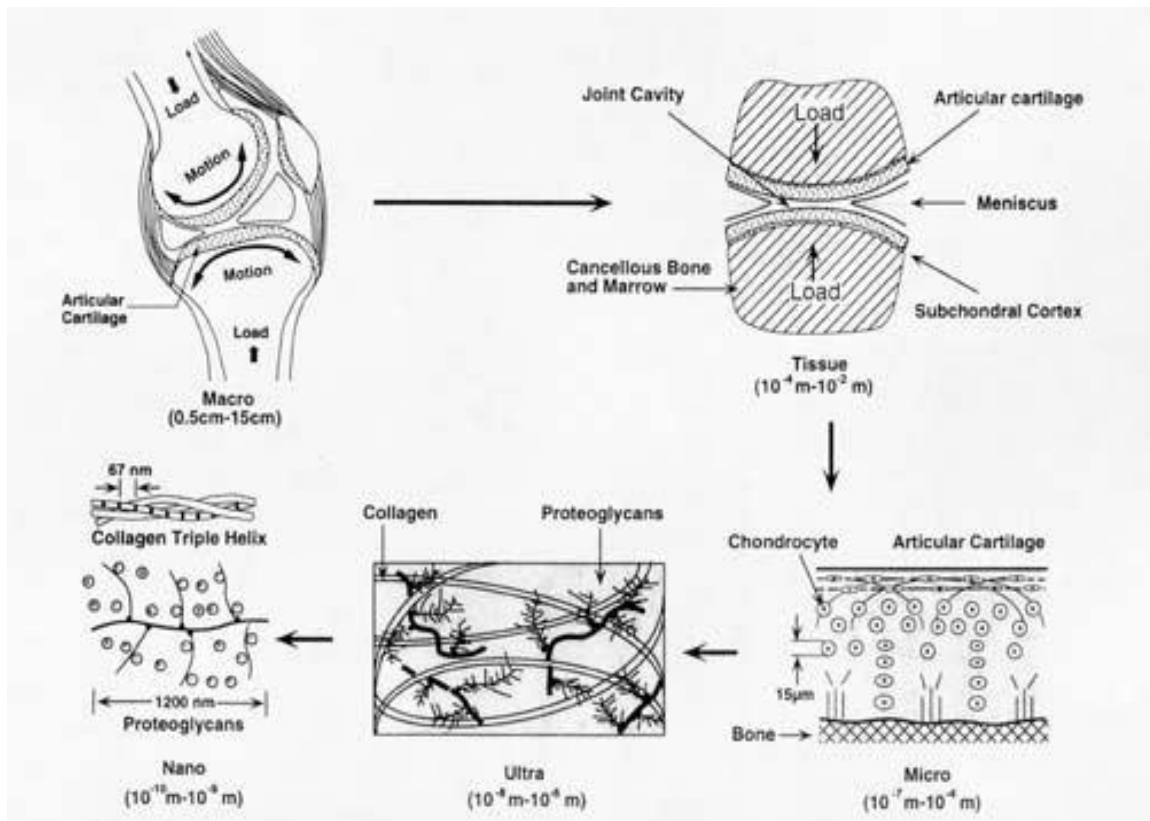


Figure 1-5: Hierarchical structure of articular cartilage (Mow et al. 1992)

At heel-strike the pressure in the fluid film deforms the articular surface. As the surfaces glide over each other, this increases the surface area as well as reducing the escape of fluid between the surfaces. Articular cartilage has the ability to distribute loads so that the subchondral bone does not deteriorate under peak stresses (Newman 1998).

1.2.1 Structure

Articular cartilage can be divided into four distinct zones as shown in Figure 1.6. The structure and composition of the components change with the zone. Water content decreases from 80% in the superficial zone to 65% in the deep zone and the proteoglycan concentration increases with depth (Mow *et al.*, 1990).

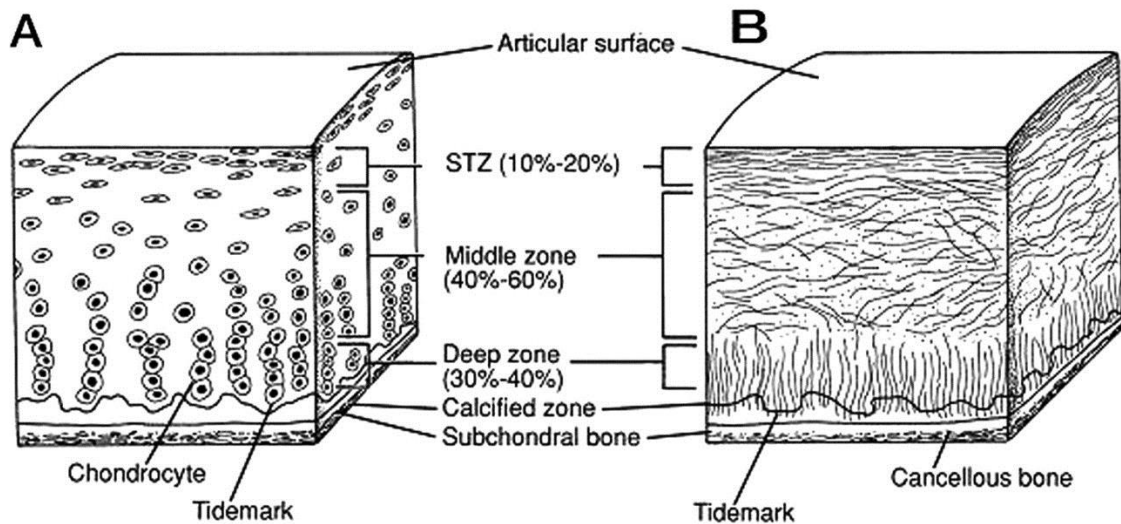


Figure 1-6: Zonal arrangement in articular cartilage showing the cellular organization (A) and collagen fibre architecture (B) (Newman 1998)

The outermost and the thinnest layer is called the *superficial zone*. It has the lowest coefficient of permeability and mainly contains horizontally oriented type II collagen which gives great resistance to shear. The cells are flat and elongated but these less active cells have a low healing potential. In this zone, the cells synthesise an extracellular matrix (ECM) with high collagen concentration and low proteoglycan concentration compared to the other zones.

The middle zone is also known as the *transition zone* as its morphology and composition is a transition from the superficial and deep zone. The chondrocytes in this zone have a much more rounded morphology and are much more active than in the superficial zone and the collagen fibres are also larger. The high concentration of collagen arranged perpendicular to each other gives good resistance to compression.

The deep zone also known as the *radial zone* has the largest concentration of proteoglycans. The cells are oriented in a columnar manner perpendicular to the surface. It has mainly type II collagen which is vertically oriented and has the largest collagen fibres. These fibres pass into the *tide mark*, which is a faint line seen under a microscope that separates the calcified zone from the uncalcified zones. The *calcified zone* acts as a barrier to cellular invasion. The cells mainly synthesise type X collagen and calcify the ECM. It has a very sparse population of cells and they are almost inactive.

Even though the connection between the articular cartilage and the underlying bone is strong its nature is not well known. The role of subchondral bone is critical in supporting the

structure and function of cartilage. The subarticular tissues include calcified cartilage, which provides a transition between the stiff subchondral bone and the compliant articular cartilage. The subchondral bone can be further classified into the subchondral bone plate and the trabecular bone. The subchondral bone plate is the bone layer that separates the calcified cartilage from the marrow spaces (Li & Aspden 1997; Kawcak et al. 2001; Day et al. 2004). The subchondral bone is vascular and contains marrow spaces. None of the vessels of the bone pass into the articular cartilage as they terminate in its immediate vicinity. Vascular channels connect the marrow spaces of trabecular bone with the calcified cartilage layer, thus nourishing the deeper cartilage layers including the osteocytes in the subchondral bone plate that cannot be nourished by synovial fluid (Kawcak *et al.*, 2001).

There is evidence to indicate that initial damage to the subchondral bone may trigger changes in the overlying articular cartilage which may lead to osteoarthritis (Grynpas *et al.*, 1991; Amir *et al.*, 1992; Li and Aspden, 1997; Li *et al.*, 1999; Bobinac *et al.*, 2003; Coats, Zioupos and Aspden, 2003; Mrosek *et al.*, 2006; Castañeda *et al.*, 2012). Radin et al popularised the view of osteoarthritis progress over the initial damage of subchondral bone rather than damage to the cartilage itself (Radin and Paul, 1971; Radins and Paulq, 1972; Radin and Rose, 1986). Rabbit legs were tested by stiffening the subchondral bone to test this hypothesis. These studies suggested negative results for treatments such as micro fracture. A study by Muraoka et al. (2007) on guinea pigs with progressive osteoarthritis has shown an increased thickness of osteochondral bone plate. Changes in the subchondral bone can alter the stiffness of the bone which could affect the mechanical properties of the articular cartilage.

Cartilage is an avascular tissue that relies on the synovial fluid for nutrients. Synovial fluid is a dialysate of blood plasma without clotting factors. It contains high molecular weight hyaluronate and also other glycosaminoglycans (GAGs) in minute amounts. Hyaluronate and lubricin are believed to be responsible for the viscosity and low coefficient of friction of cartilage (Northwood, 2007).

Synovial fluid plays a very important role in the biotribology of articular cartilage. It not only provides nutrients but also acts as a lubricant in reducing friction and wear. It reduces the shear stress on the joint surface as the shear occurs within the lubricant. This reduces wear and provides smooth movement for a longer durability (Dowson, 1981). It is a non-

Newtonian fluid which decreases the viscosity with increasing shear. In arthritic joints the fluid is less viscous and hence less efficient at reducing the shear stress on the cartilage resulting in a higher wear. Normal synovial fluid has the highest viscosity followed by the fluid from the osteoarthritic joint and the fluid from rheumatoid joints has the lowest (Wright and Dawson, 1976).

Visco-elastic properties of the synovial fluid have been studied to understand the biomechanics of the joint. At high shear rates of 1000/s the fluid is 10 times more viscous compared to lower rates of 0.1/s showing the non-Newtonian nature of synovial fluid (Cooke, Dowson and Wright, 1978). Several studies (Approach 1969; Graindorge et al. 2005; Liang 2008) have been carried out on the lubricating properties of the joint, especially with regards to hyaluronan and lubricin. In a normal healthy joint the viscosity of synovial fluid is twice that of water. Unlike normal serum, several proteins such as fibrinogen and prothrombin are absent in the synovial fluid to prevent clotting.

1.2.2 Composition

Articular cartilage consists of 20% solid and 80% fluid with the solid phase consisting of 50-73% collagen and 15-30% proteoglycan. The fluid phase has 58-78% water and the remainder is the dissolved electrolytes including sodium, calcium, chloride and potassium ions. It has cells known as chondrocytes that maintain and remodel the ECM (Mow *et al.*, 1990; Hussainova, 2007).

Water is the major constituent of articular cartilage representing 65-85% of the wet weight. 70% of this water is trapped in proteoglycan and the rest is contained in the intra-fibrillar space of collagen. The interaction of water with the matrix has significant influence on the mechanical properties of the tissue. It helps to provide lubrication and aids diffusion of nutrients from the synovial fluid. It has a significant role in creating the osmotic pressure which contributes to the mechanical properties of the tissue. The inorganic ions dissolved in water balances the fixed charges on proteoglycans and generates a swelling pressure (Mow *et al.*, 1990).

Chondrocytes are the one and only cell type in articular cartilage. Even though they account for only approximately 5% of the total tissue volume, they are highly specialized mesenchymal cells responsible for the synthesis and maintenance of the tissue (Ateshian and Hung, 2006). The shape and distribution of chondrocytes varies with depth. Mature

chondrocytes are spherical in shape with scalloped edges reaching up to 24,000 cells/ mm³. The cell numbers decrease with age, reaching their lowest in a 30 year old adult (Mow *et al.*, 1990; James and Uhl, 2001; Haberth, 2002).

Collagen is a protein formed from the triple-helical structure of three polypeptide chains (Balasubramanian *et al.*, 2013). Two-thirds of the dry weight of cartilage is contributed by the different types of collagen in its ECM. Articular cartilage primarily contains type II collagen which accounts for 90% of the collagen content of the tissue and the rest is collagens III, VI, IX, X, XI, XII and XIV. The helical structure assembles to form collagen fibrils which then aggregate to form collagen fibres. Each fibril is linked to each other and to the other components in the ECM by cross linking (Haberth, 2002). The mechanical integrity of cartilage is influenced by this extensive cross-linking and the changes in its fibrillar construction in different zones. The swelling pressure generated by the proteoglycans is resisted by the network of fibrils formed by the collagen (Eyre, 2002).

Proteoglycans (PG) are polysaccharides of proteins constituting about 5-10% of the wet weight of cartilage. They consist of several negatively charged GAG chains covalently attached to a link protein. The large high molecular weight PG aggregates by binding to a hyaluronan backbone stabilised by a globular link protein. This link can be lost during tissue degeneration due to the depolymerisation of hyaluronan (Mow *et al.*, 1990).

The elasticity and stiffness provided by the aggrecan gives cartilage its high compressive strength. The hydrophilic nature of PG attracts water to form aggregates and this swelling property of PG gives cartilage its compressive mechanical behaviour. The negatively charged GAGs repel each other which results in an open structure and is space filling (Hauser, 2009). The common GAGs in cartilage are chondroitin sulphate, keratan sulphate and hyaluronic acid (HA) or hyaluronan. The viscous but rigid structure of cartilage is due to the ability of chondroitin sulphate to hold large quantities of water (Mow, 1969).

1.2.3 Biphasic theory

The biphasic theory introduced by Mow *et al.* provides a convincing explanation of the mixed phase behaviour of articular cartilage. It assumes that cartilage has an immiscible and intrinsically incompressible solid matrix phase and interstitial fluid phase (Mow *et al.*, 1990).

Lai et al. (1991) considered the electromagnetic interactions between the charged ions in the matrix to incorporate an ionic phase and also developed a triphasic model.

Under the biphasic theory the load is initially carried by the fluid phase and then transferred to the solid phase. The fluid phase reduces friction and protects the underlying cartilage surface by shielding the solid phase from high levels of stress (Setton, Zhu and Mow, 1993).

In a biphasic material the load is shared between the solid and fluid phase depending on the porosity of the tissue. Cartilage has a high proportion of fluid and the porous permeable solid ECM which allows water to be excluded from the cartilage when a load is applied. This creates a pressure gradient called the interstitial fluid pressurisation which is responsible for the load bearing capacity of articular cartilage. This pressure protects the solid matrix from most of the biomechanical loading and prevents cartilage degeneration. Hence the variation in cartilage permeability can be an indication of why some patients are susceptible to some joint disease rather than others (Little, Bawolin and Chen, 2011).

1.2.4 Mechanical properties

Due to the inhomogeneity of the tissue caused by the varying structural arrangement of the collagen, cartilage behaves as an anisotropic material. Being a visco-elastic, anisotropic and non-homogeneous tissue, it is necessary to make assumptions while creating any model for cartilage. A biphasic model assumes cartilage has a solid and fluid phase while a triphasic model includes a third ionic phase (Ateshian *et al.*, 2004).

The mechanics of the joint have to be considered as a composite structure, with the thin compliant cartilage layer integrated to the stiffer and stronger subchondral substrate. The nerve endings in the outer layer of the joint capsule are sensitive to the mechanical stimuli and have been shown to sense the rate and direction of joint movement. Studies have shown that mechanical stimulation is necessary to maintain healthy cartilage. Cyclic loading of cartilage exerts a pumping action on the interstitial fluid that enables the circulation of products to and from the chondrocytes (Levangie and Norkin, 2011).

1.2.4.1 Tensile property

The anisotropic behaviour of cartilage makes it difficult to predict the deformation and reaction to loading and direction. Due to non-homogeneous nature, each non-calcified

zone in the cartilage shows different properties. This difference from zone to zone arises from the difference in composition and organisation in each zone. Therefore, each zone will respond differently in different directions although the load is applied at the same point. This happens due to the way the collagen fibres are organised, resulting in obliquely isotropic or orthotropic behaviour in the superficial zone. A greater resistance to tensile strength is displayed along the direction in which the collagen fibrils are arranged (Sophia Fox et al. 2009; Mow et al. 1992).

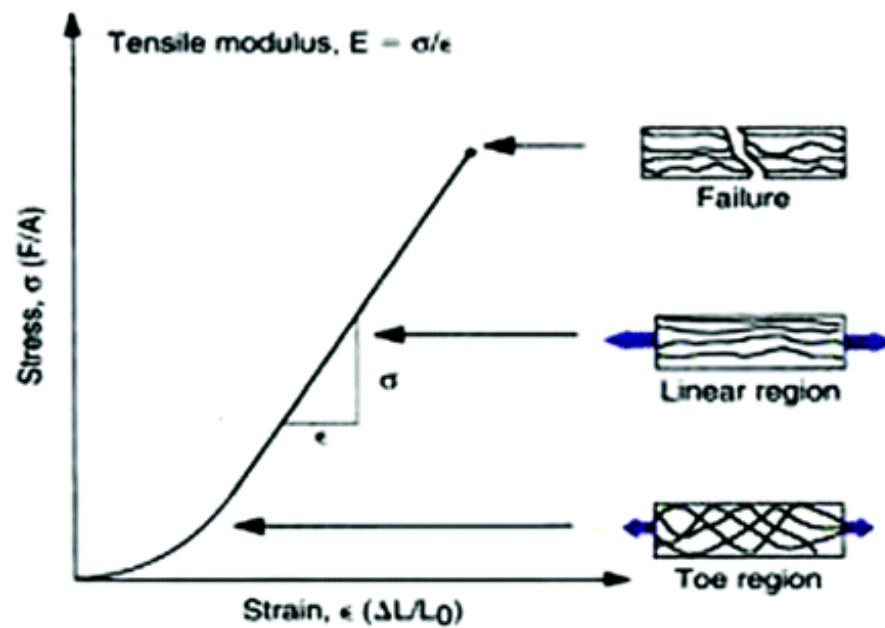


Figure 1-7: Tensile properties of articular cartilage (Sophia Fox et al. 2009)

At the initial phase of tensile stress, the collagen fibers are undergoing realignment or “uncrimping”, which marks the toe region. The collagen fibers are stretched at the next phase and the straightened collagen fibers marks the linear region. The final stage is when the collagen fibers cannot withstand more tensile forces and the fibers breaks to mark the failure region (Sophia Fox et al. 2009; Nordin & Frankel 2001).

The tensile modulus of cartilage depends on the depth of the tissue and the zonal arrangement of collagen fibers. At physiological strain levels the tensile modulus of human cartilage range from 5 to 10 MPa(Nordin & Frankel 2001). The equilibrium tensile modulus of osteoarthritic cartilage was found to be around 1.36 MPa. In normal bovine cartilage it ranges from 0.2 to 13.4 MPa (Mow & Huiskes, 2005) and in porcine it is from 10-24 MPa (Macbarb et. al. 2012).

1.2.4.2 Viscoelastic properties

The visco elastic property of cartilage is provided by the linearly charged HA (Mow et al. 1992; Balazs 1982). The negatively charged sulphates in PG attract cations that attract water molecules to minimise the difference in osmotic pressure. This gives PG, its gel like consistency that makes them capable of absorbing shock and withstanding pressure. Degeneration disintegrates the aggrecan structure and loses its water holding capacity which breaks down the collagen meshwork (Haberth, 2002). Shear behavior of cartilage is an interaction between the PG network and the collagen fibers. One way of understanding the viscoelastic behavior of the solid matrix is through pure shear tests under small torsional displacements of cylindrical samples. Collagen fibers can stretch and deform under these shear forces. The equilibrium shear modulus have shown to vary from 0.05 to 0.25MPa in humans (Abbot et al. 2003). At high shear rates of 1000/s the fluid is 10 times viscous compared to lower rates of 0.1/s showing the non-Newtonian nature of synovial fluid (Cooke, Dowson and Wright, 1978). Porcine condylar tissue shows dynamic shear modulus of 0.3 to 0.5 MPa and bovine showed 1.0 to 3.0 MPa (Nordin & Frankel 2001).

1.2.4.3 Compressive property

Articular cartilage is loaded under compression in vivo and hence it is particularly important to understand the biomechanics of the tissue under compressive loading. Elastic modulus and permeability are the main properties that are determined to define the compressive properties of cartilage. The elastic modulus of a solid material can be defined as the resistance to the change in its length (Serway and Jewett, 2012) . It is the ratio of its stress to the resulting strain i.e., (stress ÷ strain). Permeability is the measure of the ability of a material to transfer a fluid under a pressure difference. In cartilage it can be defined as the ability of the interstitial fluid to move through the ECM across a pressure gradient. It may depend on the pressure applied, viscosity of the fluid and the pore size of the material (Little, Bawolin and Chen, 2011).

The compressive properties of cartilage vary with depth. This is because deeper zones have more PG concentration and the high negative charge of PG makes the molecules repel each other leading to an expansion of the PG network and therefore limiting the free flow of interstitial fluid. This increases the compressive stiffness (McCann, 2009).

There are three main types of compressive testing as shown in Figure 1.8; Confined compression, unconfined compression and indentation. Typically, in confined compression, a circular cartilage sample is placed inside a cylindrical container and compressed with a piston of the same diameter that prevents lateral expansion. However, in unconfined compression the cartilage sample is typically compressed between two plates with larger diameters to the sample, allowing for lateral expansion.

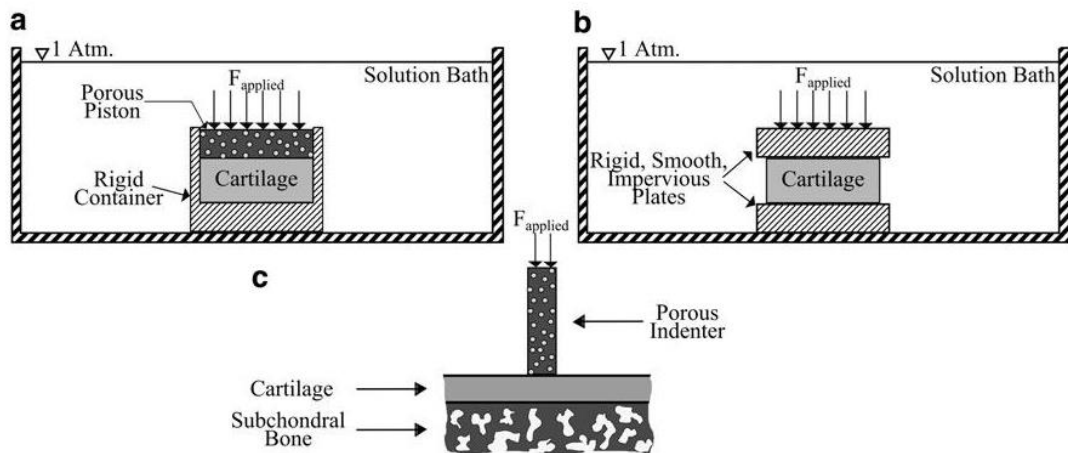


Figure 1-8: Examples of compression tests

(a) confined compression (b) unconfined compression (c) indentation (Little, Bawolin and Chen, 2011)

Under compression, the interstitial fluid flows out of the matrix and the fluid flows back in when the load is taken away. Cartilage has a low permeability which ensures that the fluid is not quickly pressed out hence protecting the solid part in the matrix (Newman, 1998). Creep deformation studies are carried out by applying a constant compressive load to the cartilage and maintaining it for a period of time. Unconfined compression provides a free-draining condition and creep deformation occurs until equilibrium is reached. At this stage the load is entirely carried by the solid matrix (Pawaskar, 2006).

1.2.4.4 Indentation

In Indentation, the load is applied through an indenter several times smaller in diameter than the sample itself. Unlike the cartilage samples in confined and unconfined compression, indentation samples are cylindrical plugs of cartilage attached to the subchondral bone (in situ). Therefore, indentation resembles a closer physiological environment which allows accurate measurements. In all 3 types of compression tests, a step force is applied and the displacement is measured over time. The sample set up is the major difference.

Indentation can be used to measure the permeability, elastic modulus and Poisson's ratio of the cartilage. It is important to maintain constant measurement of conditions as the material properties could change in different conditions such as hydration of the sample, size and shape of the indenter, rate and magnitude of the loading (Wang and Peng, 2015).

When a constant load is applied through an indenter, the exudation of interstitial fluid occurs. This causes creep indentation which reaches equilibrium when the interstitial flow ceases and the load is completely supported by the solid phase (Mow *et al.*, 1980). This creep response of cartilage is shown in Figure 1.9.

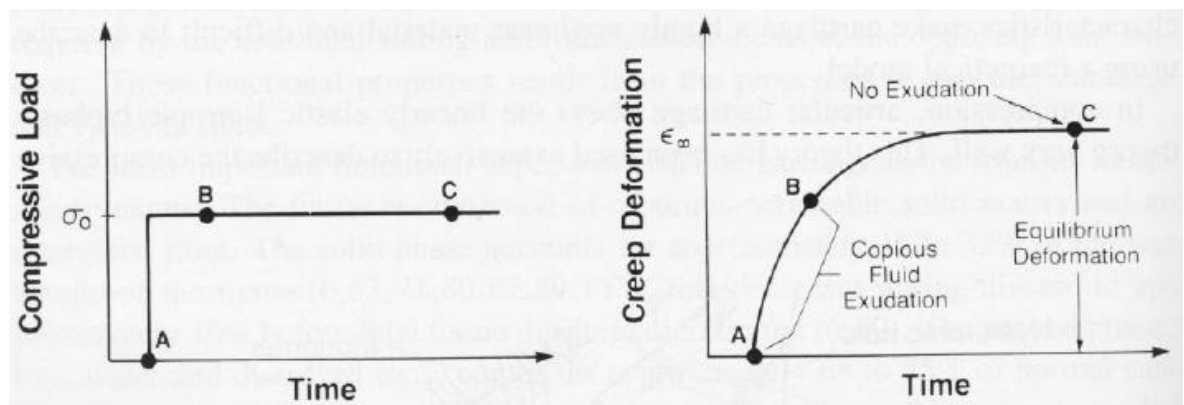


Figure 1-9: Creep response of cartilage under constant compressive load (Mow *et al.* 1980)

There are several arguments about the results from indentation tests compared to confined and unconfined compression testing. The elastic property of the tissue is dependent on the type of test. While the Poisson's ratio is independent of the test applied, elastic modulus can be affected by the type of tests. Korhonen *et al.* have shown that the Young's modulus from confined and unconfined compression could be up to 79% lower compared to the indentation method (Korhonen *et al.*, 2002). This could be due to the damage that occurs to the fibrous tissue during sample preparation for the confined and unconfined tests.

The typical Poisson's ratio is under 0.4 and often could approach zero. Previously, cartilage was considered as an incompressible material as cartilage mostly constitutes to water and water is incompressible. Therefore the Poisson's ratio was assumed to be 0.5. As cartilage is biphasic material, the fluid flows out of the cartilage when it is loaded and therefore making it compressible. The elastic modulus and permeability of cartilage in the knee joint is summarised in Table 1.1. Human cartilage has been shown to have higher elastic modulus than bovine or porcine cartilage (Athanasίου *et al.*, 1991; Taylor, 2012; Fermor, 2013; Nebelung *et al.*, 2016). The difference in results could be due to various reasons. The type of

indenter used for the test has an effect on the values obtained, especially on the permeability of the tissue. The permeability obtained from a 3 mm hemispherical indenter (Taylor, 2012; Fermor, 2013) was up to 30 times higher than the permeability through a 1.5 mm flat indenter (Athanasίου *et al.*, 1991). This could be because with a hemi-spherical indenter the contact stress on the cartilage is much higher, which resists the interstitial fluid flow to reduce permeability. The assumptions made on the finite element model for the analysis can also contribute to the results.

Table 1-1: Elastic modulus and permeability of cartilage in the knee and the various techniques used by other researchers

Sample	Elastic modulus (MPa)	Permeability ($10^{15}m^4/Ns$)	Technique	Author
Bovine femoral condyle	0.9	0.43-0.45	1.5mm flat indenter	Athanasίου et al. 1991
Bovine femoral condyle	1.17	40.49	3mm hemispheric indenter	Fermor 2013
Bovine femoral head	1.84	30.03	3mm hemispheric indenter	Taylor 2012
Bovine groove	0.86	63.3	3mm hemispheric indenter	Fermor 2013
Bovine groove	0.47 ± 0.15	1.42±0.58	1.5mm flat indenter	Athanasίου et al. 1991
Porcine femoral condyle	0.74	71.8	3mm hemispheric indenter	Fermor 2013
Porcine femoral head	1.15	55.3	3mm hemispheric indenter	Taylor 2012
Porcine groove	1.04	44.9	3mm hemispheric indenter	Fermor 2013
Human femoral condyle	0.70-0.59	1.18-1.14	1.5mm flat indenter	Athanasίου et al. 1991
Human femoral condyle	4.48	-	3mm hemispheric indenter	Taylor 2012
Human femoral condyle	4.48 -5.96	-	1.5mm flat indenter	Nebelung et al. 2016
Human groove	0.53 ± 0.094	2.17 ±0.73	1.5mm flat indenter	Athanasίου et al. 1991

1.2.4.5 Thicknesses

Cartilage is several millimetres thick depending on the area and the patella cartilage is the thickest in the body. There are several methodologies to measure the thickness of cartilage which include using Vernier Calipers, microscopes, histology and ultrasound measurements (Kempson *et al.*, 1971; Fermor, 2013; Nebelung *et al.*, 2016; Robinson *et al.*, 2016). However,

the needle probe method is the most common technique used to measure the thickness of articular cartilage (Athanasίου *et al.*, 1991; Shepherd and Seedhom, 1999; Taylor, 2012; Nebelung *et al.*, 2016).

The indentation test introduced by Hori and Mocros used a blunt needle attached to a standard depth micrometre to measure the thickness. This technique was later improved by (Hoch *et al.*, 1983) who used a sharp needle attached to a load transducer to measure the thickness by piercing through rabbit cartilage at 20 $\mu\text{m/s}$ (Hori and Mockros, 1976; Hoch *et al.*, 1983). The thickness from the needle probe method is calculated from the resistance of the needle piercing through the cartilage - as the distance between resistance in initial contact and the steep increase in resistance when the needle touches the much stiffer bone.

Nebelung *et al.* (2016) measured the thickness of femoral cartilage using needle probe, MRI and histology methods. Although all methods showed a large variation across the samples there were no significant differences ($p=0.063$) between the methods. Studies conducted by McLure (2012) in the same lab with the same equipment and conditions have also validated the use of the needle probe method. The method principle was validated by creating a dummy specimen of a known thickness and measuring it using the needle probe method. This showed no significant difference ($p=0.046$) in thickness between the actual and calculated values. The method was also validated against recognized methods such as the Shadowgraph method (Nikon profile Projector) and Micro-CT method. The Shadowgraph results were significantly higher than those calculated from the needle probe and Micro-CT method. There was no significant difference between the needle probe and Micro-CT method.

Froimson *et al.* (1997) carried out an indentation test using a penetrating needle probe on human patella and femoral regions that were in contact with each other at 30° and 90° of knee flexion. They observed that the patellar cartilage was more permeable and thicker than the other regions. They showed a 30% lower compressive aggregate modulus in the patellar region compared to the opposing cartilage on the femoral trochlea region.

The thickness of cartilage in the knee joint is summarised in Table 1.2. Human cartilage is comparatively thicker than the porcine, ovine and bovine cartilage. Ovine cartilage is the thinnest ranging from 0.6- 0.86 mm whereas human cartilage is 1.08- 3.57 mm. The age of the species is also a factor that affects the thickness of the cartilage. Studies have shown that

cartilage becomes thinner with age (Fermor, 2013). The region where the samples are obtained is another factor. Cartilage from the patello femoral groove is comparatively thicker than the cartilage in the hip or ankle.

Table 1-2: Thickness of cartilage in the knee and the various techniques used by other researchers

Sample	Technique	Thickness (mm)	Author
Bovine condyle	Histology	1.28±0.17	Fermor 2013
	Needle Probe	1.19-0.94	Athanasίου et al. 1991
Bovine groove	Histology	1.6 ± 0.85	Fermor 2013
	Needle Probe	1.52	Shepherd & Seedhom 1999
	Needle Probe	1.38 ± 0.19	Athanasίου et al. 1991
Bovine hip	Needle Probe	1.32±0.13	Taylor 2012
Human condyle	Needle Probe	2.31-2.21	Athanasίου et al. 1991
	Histology	2.2 ± 0.3	Robinson et al. 2016
Human femur	Needle Probe	2.77	Nebelung et al. 2016
	MRI	2.6	Nebelung et al. 2016
	Histology	2.82	Nebelung et al. 2016
Human groove	Needle Probe	1.76-2.59	Shepherd & Seedhom 1999
	Needle Probe	3.57±1.12	Athanasίου et al. 1991
Human hip	Needle Probe	1.82±0.18	Taylor 2012
	Needle Probe	1.08-2.40	Shepherd & Seedhom 1999
Ovine (mature) groove	Histology	0.6 ± 0.20	Fermor 2013
	Needle Probe	0.63	Shepherd & Seedhom 1999
Ovine (young) groove	Histology	0.8 ± 0.10	Fermor 2013
	Needle Probe	0.86	Shepherd & Seedhom 1999
Porcine condyle	Histology	2.23±0.20	Fermor 2013
Porcine groove	Histology	2 ±0.70	Fermor 2013
	Needle Probe	2.04	Shepherd & Seedhom 1999
Porcine hip	Needle Probe	1.22±0.05	Taylor 2012

1.3 Pathology and treatments

1.3.1 Patello-femoral disorders

Patello-femoral problems affect nearly a quarter of the population and remain a common cause of knee replacement revision surgery. Even though it is the most common contributor to knee pathology, it still remains one of the most neglected and least understood areas in terms of proper diagnosis and treatment. The complexity of the joint articulation is the main factor which contributes to these limitations, and pathology commonly occurs in young adults, especially women and those active in sports (Draper et al. 2011; Fitzpatrick et al. 2011; Leal et al. 2015).

According to Merchant, PFJ disorders can be classified into trauma, patello-femoral dysplasia, idiopathic chondromalacia patellae, osteochondral lesions and osteochondritis dissecans (Merchant, 1988). Damage to cartilage tissue which also extends into the underlying bone is a challenging case to treat. Cartilage has poor healing capacity and some treatment techniques for the full thickness cartilage lesions often lead to the formation of fibro cartilage which has inferior biomechanical properties compared to articular cartilage.

Any abnormalities in the anatomy for specific species can have an adverse effect on the biomechanics and pathology of the joint. The anatomy varies between the species depending on their functional needs. Animals that walk on their toes are called unguligrades. Species such as pigs, sheeps and cows are unguligrade quadrupeds. They require slightly different anatomical features for their appropriate biomechanics compared to the bipedal humans. Sheep have been shown to have narrower intercondylar notch. This feature coupled with the ligaments helps them with the correct functioning of the joint. However, humans with a narrower intercondylar notch do not allow the proper functioning of the joint. This will cause a continuous pinching of the anterior cruciate ligament which will result in higher cartilage wear (Osterhoff *et al.*, 2011).

1.3.1.1 Patella instability

The movement of the patella in the femoral groove is known as patella tracking. Patella instability is caused by abnormalities in the morphology of the patella that leads to dislocation or mal-tracking. Normally, the forces passing through the patella onto the front of the knee are dissipated evenly. With lateral patellar maltracking the joint loading forces

will be greater on the lateral PFJ, which can lead to pressure overload on the lateral side of cartilage (Ateshian and Hung, 2005). People are born with various anatomic variations in the joint that may cause patellar dislocation. This is a serious condition where repeated dislocation may lead to rapid degeneration of the PFJ.

Abnormally large Q angle: This is a condition in which there is a greater than normal angle where the femur and the tibia come together at the knee joint. The patella normally sits at the centre of the Q angle within the femoral groove. When the quadriceps muscle contracts, the Q angle decreases, pushing the patella to the outside of the knee. Where the Q angle is larger than normal, the patella tends to shift outwards with greater pressure. So, as the patella slides through the groove, it shifts to the outside, which in turn creates a greater pressure on one side of the cartilage (Ellison, 2007).

Trochlear dysplasia: This is a condition which can lead to patellar dislocation. Van Haver et al developed a statistic shape analysis to describe the geometrical complexity of this condition. By comparing joints with and without dysplasia, they showed that the medial lateral width and the notch width were smaller in dysplastic femurs compared to the controls. They also discovered that the femoral groove could be shifted to the anterior/proximal/ lateral direction in this condition (Van Haver *et al.*, 2014).

Uneven patello-femoral condyles: This causes medial-lateral dislocation. This condition can create a situation in which the lateral groove is too shallow, causing the patella to slip sideways out of the groove, resulting in a patellar dislocation. This is not only painful but can also damage the articular cartilage underneath the patella (Mehl *et al.*, 2014).

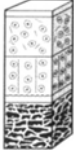
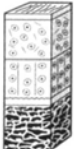



Patella alta: This is superior inferior dislocation. The patella sits high on the femur where the groove is very shallow. The sides of the femoral groove provide only a small barrier to keep the high-riding patella in place. A strong contraction of the quadriceps muscle can easily pull the patella over the edge and out of the groove, leading to a patellar dislocation (Zaffagnini *et al.*, 2016).

1.3.1.2 Osteochondral lesions

According to Mehl et al. (2014) patella cartilage lesions are more challenging to treat and have less chance of healing, compared to damage in the femoral condyles. Anatomical features such as patellar height, shape of the patella and trochlear groove, and patellar tilt can all influence the direction and magnitude of PFJ forces. Any abnormalities in these features could contribute to the damage to the PFJ cartilage.

Osteochondral lesions are a major problem in the knee affecting more than 9 million Americans with over 2 million undergoing surgical procedures. The International Cartilage Repair Society (ICRS) grades the severity of these lesions as described in Table 1.3.

Table 1-3: ICRS grading of cartilage lesions (ICRS, 2016)

Grade	Description
 GRADE 0	White glossy cartilage
 GRADE 1	Superficial rubbing and discolouring on the cartilage
 GRADE 2	Scratches propagating to under half the thickness of the cartilage
 GRADE 3	Scratches propagating to over half the thickness of the cartilage, just before it reaches the subchondral bone
 GRADE 4	Full thickness that goes beyond the cartilage damage and expose the underlying bone as shown in Figure 1.10.

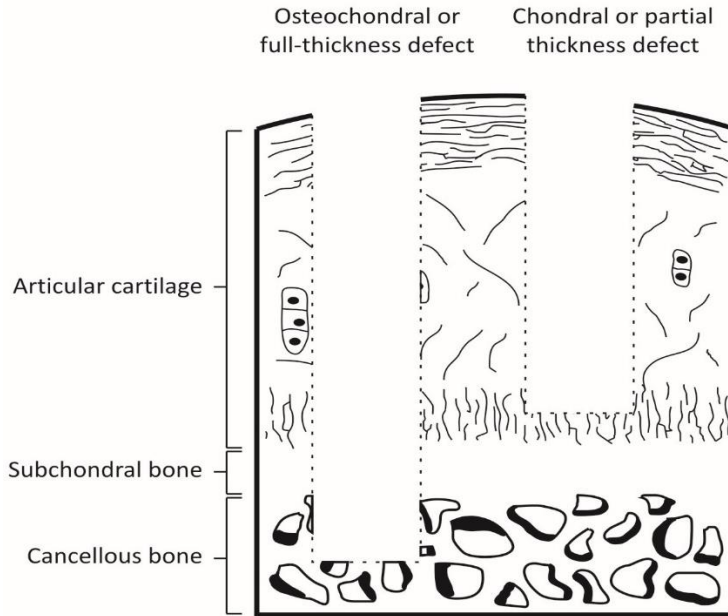


Figure 1-10: Partial and full thickness defects (Kelc Robi, 2013)

Osteoarthritis (OA) is a degenerative disorder that occurs as a result of biochemical breakdown of the cartilage which can harmfully change the articular cartilage as well as the underlying bone. Secondary osteoarthritis, as seen in young adults, is due to the gradual degeneration of synovial joints resulting from situations such as trauma, which eventually affects the articular cartilage and the underlying subchondral bone. Due to the limited healing capacity of the tissue, even minor cartilage damage could progress into OA. Primary osteoarthritis, seen in the elderly, arises spontaneously in intact joints without any clear initiating factor. This is due to the alteration in the structure and composition of collagen fibres and proteoglycans that decrease the tensile strength of the articular cartilage. The nutrient supply to the cartilage also reduces with age (Wyndow *et al.*, 2016).

Osteoarthritis is more common in the PFJ than in the TFJ, even in patients under the age of 50. Patello femoral disorders often result in the progression of OA (Hinman *et al.* 2014; Wyndow *et al.* 2016). A recent literature survey showed that 44% of the patients were affected by OA in both PFJ and TFJ. 25% of those affected had isolated OA in the PFJ only but isolated TFJ cases were very uncommon. 63% of the patients were affected by OA in both the medial and lateral PFJ (Hinman *et al.*, 2014).

With age, the repetitive motion of a specific joint may lead to the degeneration and wear of its articular surfaces. Gorniak (2009) observed this specific pattern in 50 patallae and 50

distal femurs from 13 male and 13 female cadavers of mean age 73 and 85 respectively. The patella and femoral condyle wear patterns found from this study are shown in Figure 1.11.

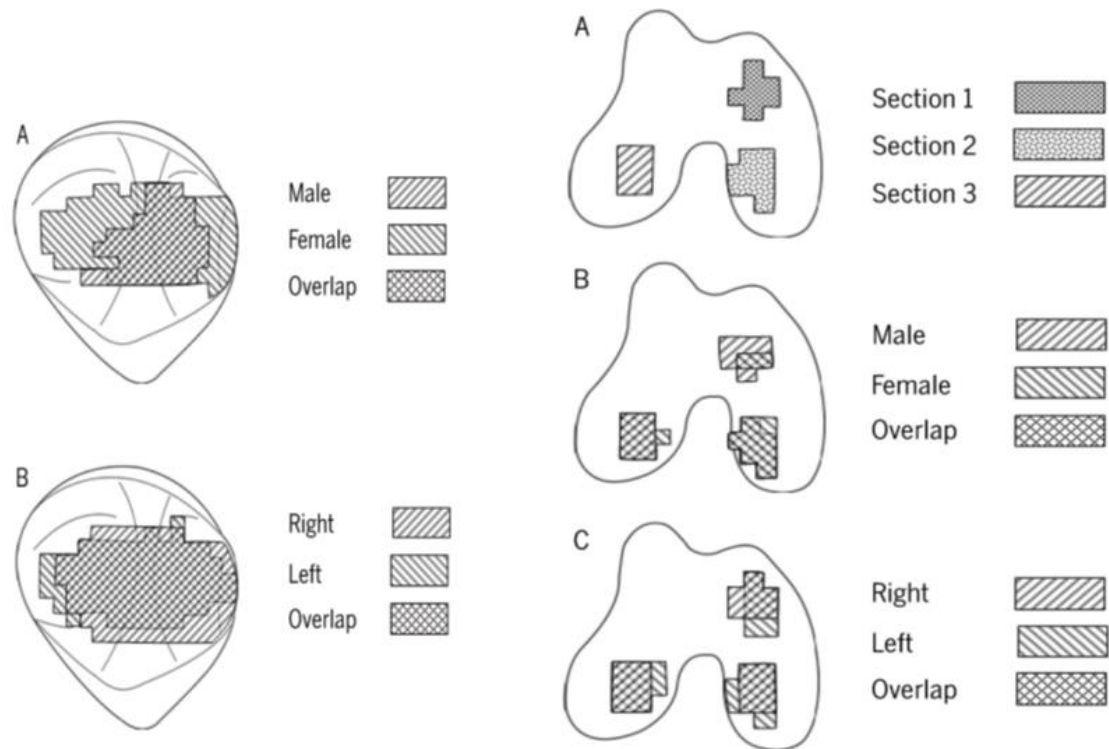


Figure 1-11: Area of wear in patella (left) and femur (right). The medial side of each patella and femur is on the right side of the diagram (Gorniak, 2009)
Patella: (A) Area of wear in male and female cadavers, (B) right and left patella
Femur: (A) Three common wear sections on the anterior and posterior medial condyle and the posterior lateral condyle,
(B) Superimposed wear for males and females showing wear in that section, (C) Superimposed wear for right and left sides for cadavers with wear in that section

The most prevalent patellae wear area were the long continuous horizontal wear in the middle. Wear scars in both genders were mainly confined to the horizontal medial side of the patella. The lateral, medial and odd facets in females were more affected than in men. The wear area was smaller in men compared to women which relates to the finding of Besier et al. (2005) which shows a larger contact area in males compared to females. A larger contact area can distribute the applied load more evenly and reduce the peak stress to reduce the wear.

The appearance of areas of common wear for the patellar facets and the femoral condyles supports the concept that each joint may have a joint-specific wear pattern (Gorniak, 2009). High patello-femoral joint reaction force corresponds to this common patellar facet wear. There is greater medial patellar facet and odd facet wear than lateral facet wear, suggesting

higher medial than lateral patello-femoral joint reaction force. High odd facet wear may result from medial patellar facet thinning, producing a change in patello-femoral mechanics over time. The wear area on the patella also matched the contact area between the PFJ at 45-90 degrees of knee flexion discussed in Section 1.1.2.

1.3.2 Treatment options

Although most patello femoral disorders can be treated non-operatively depending on the severity of the condition, joint replacements are the common end stage solution for severe osteochondral damage. However, there are minimally invasive surgical interventions that can be performed at the earlier stages to delay the need for artificial joints. There are several treatments including micro fracture (MF), autologous chondrocyte implantation (ACI) and osteochondral autograft transplantation (OAT). Suitable repair and restoration techniques should be able to replace the damaged area with hyaline-like or hyaline cartilage that can improve function (Berta *et al.*, 2015).

Micro fracture is one of the most popular reparative techniques which allows the entry of mesenchymal stem cells and growth factors into a chondral defect to induce the formation of fibro cartilage (Lewis *et al.* 2006). Autologous chondrocyte implantation (ACI) is a cartilage restorative procedure in which a concentrated solution of chondrocytes is inserted into a periosteal flap fixed around the defect. This procedure is another widely used surgical procedure for the restoration of damaged cartilage (Tuan 2007). It is often only used as a last resort when the other procedures have failed and is ideally used in defects where the subchondral plate is intact. The cost effectiveness of this method and its ability to produce hyaline-like cartilage is still controversial. Using a combination of different techniques has proven effective in cases in which using a single technique is not suitable or has failed (Duif *et al.*, 2015).

All marrow-stimulating techniques such as microfracture lead to the formation of fibro cartilage which is inferior compared to the mechanical function of articular cartilage. Therefore a technique is essential to create hyaline like cartilage that can provide a more durable surface than that of the fibro cartilage. In 1996, Laszlo Hangody introduced the use of cylindrical plugs in osteochondral surgery and this has been an established surgical procedure ever since (Hangody *et al.*, 1997). This is widely known as osteochondral autograft transplantation (OAT) or mosaicplasty.

The efficiency of the different treatment options are often evaluated from short term and long term clinical follow up studies to rate the success of the procedures. The clinical outcomes are assessed through various approaches such as patient reported outcomes and functional outcomes, clinical scoring systems, appearance of the lesion through radiological evidence, coverage of hyaline cartilage and its properties through histological evidence as well as need for re operations or the occurrence of post-operative complications (De Caro *et al.*, 2015; Lynch *et al.*, 2015). There are a range of clinical scoring systems used in various follow up studies and hence there are limitations (De Caro *et al.*, 2015).

1.3.2.1 Osteochondral transplantation

Mosaicplasty is a surgical treatment introduced by Hangody to repair osteochondritis dissecans. It involves obtaining small cylindrical plugs of bone with healthy hyaline cartilage on the surface (Hangody *et al.*, 1997). To treat the lesion in the high load bearing regions such as femoral condyles, grafts are taken from a minimal load bearing surface such as the patella femoral groove and transferred to the prepared defect site. OAT is the only technique that can restore the structure of the articulating surface with autologous material with the least fibro cartilage fill. It is particularly useful in full thickness lesions involving damage to the cartilage as well as the underlying subchondral bone. It can be used for predominantly large defects that cannot be treated or that have failed other procedures (Ahmad *et al.*, 2001; Scott, 2011; De Caro *et al.*, 2015; Lynch *et al.*, 2015)

There are several clinical follow up studies that have compared the success of OAT to other techniques. A 4 year follow up study on paediatric patients showed significantly healthier cartilage from OAT compared to MF (Gudas *et al.*, 2005). A 10 year study in athletic patients showed quicker recovery and functionality from OAT than MF (Gudas *et al.*, 2012). A 9.8 year follow up study on a randomised patient population observed no significant difference in the two procedures but found a larger occurrence of re-operations after MF (Ulstein *et al.*, 2014). Horas *et al.* (2003) recorded improved clinical scores and faster recovery time in patients with OAT treatment compared to AC from short term biopsy studies. Although there was no significant difference in these clinical scores 2 years post recovery, upon histomorphological evaluation it was observed that the cartilage formed from ACI mostly consisted of fibro cartilage. This study was limited by its small sample size and short term follow up. A 10 year follow up by Bentley *et al.* (2003) found improved clinical scores in ACI and a higher failure

rate in OAT patients. However, the quality of cartilage produced through the procedures was not investigated. Gudas et al. (2012) observed that more OAT patients with lesions smaller than 2cm² returned to sports than those with lesions larger than 3 cm². They also reported a higher incidence of failures in the patellar region compared to the condyles.

Despite the effectiveness of the procedure in most defects that fails other treatment, significant limitations causes this technique to be inaccessible to certain cases. Larger lesions and those damages extending to the subchondral bone often need allografts rather than autografts. The outcome of the treatment depends on the cell viability in the allografts and the biomechanical properties of the ECM. Preserving the features of the allografts from harvesting, during storage and while testing before being released by the tissue bank is a significant challenge. This is why autografts are preferred over allografts and are more successful (De Caro *et al.*, 2015). Therefore, alternative solutions such as tissue substitutions are required to meet patient needs and demands.

1.3.2.2 Osteochondral substitutions

With the PFJ being a low weight bearing joint, the femoral groove is often used as a donor site for these treatments. Previously following donation from the femoral groove the donor site was left untreated. However, these are now filled by other osteochondral substitutes. Therefore, there is a requirement for osteochondral substitutions in the patello-femoral region either to treat these donor sites or when the patello-femoral region itself is affected (Garretson 2004; Nho et al. 2008; Nishida et al. 2012).

Advances in tissue engineering have introduced various biomaterials as bone and cartilage scaffolds. They require specific material properties for the cells to integrate with the new scaffold and produce their extra cellular matrix (ECM). An appropriate scaffold for osteochondral tissues will be bi-phasic as it allows improved reconstruction of both bone and cartilage. In these scaffolds one material represents bone and the other cartilage. Multiphasic scaffolds will have an additional interphase which marks the transitional area from the cartilage to the subchondral bone (Nukavarapu and Dorcemus, 2013).

Autografts has shown significantly high success rates compared to allografts. However, donor site morbidity is a major disadvantage. Allografts and xenografts can trigger immune response and cause the body to reject the graft (Hangody, 2008). Tissue substitutions are

acellular and the lack of genetic material reduces the risk of immune response. These grafts can provide a scaffold that give the mechanical stability while the host cells populate the grafts and integrate into the surrounding tissue. However, depending on the design of the implant and the surgical procedure there are still complications and failures associated with it (Bowland, 2015; Farr et al. 2016).

Biomechanics and stability of osteochondral grafts contribute to the success and failure of these techniques. Differences in the congruency between the host and graft and its lack of integration are also limitations. Integration may require a longer recovery time and partial integration may lead to detachment of the graft from the donor site (Kon et al. 2014). Inappropriate placement of grafts can induce abnormal stress-strain distribution which can cause loosening or breakage of grafts within the host site that leads to failure. There is a larger failure rate when the graft length is shorter than the defect depth. Therefore, availability of correct sizes for each defect is an important factor. The ease implantation during surgery is also essential as placing the graft at an angle could effect the contact pressure within the joint (Koh et al. 2006; Wu et al., 2002; Bowland et al., 2015).

Currently there are no pre-clinical testing carried out to investigate the difference in design or surgical technique used for these substitutions. However, there is clear evidence that these factors does have an effect on the success rates of the implants and this shows a gap in the research.

1.3.2.2.1 Synthetic approaches

Hydrogels are one of the common and earliest cartilage substitutions (Freeman *et al.*, 2000; Northwood and Fisher, 2007; Ma *et al.*, 2010). Due to the biphasic nature of the material it has an advantage towards the lubrication side and its structure can be engineered to mimic the material properties of cartilage (Baykal, 2013). Osteochondral composites engineered by seeding patient's own cells in 3D porous scaffolds are a promising technique. As the cells produce the ECM for the tissue the scaffold slowly degrades at a defined rate. Collagen, gelatin and fibrin are commonly used as natural biomaterial scaffolds (Benders *et al.*, 2013).

A substantial amount of work has been done on developing synthetic grafts and there are many making their way to clinical trials. Some of the recent ones are detailed in Table 1.4.

Table 1-4: Tissue engineered products for osteochondral repair (Nukavarapu & Dorcemus 2013)

Product name	Company	Material
Agili-C Bi-phasic Implant	Cartiheal LTD	Bone phase composed of aragonite and trace elements such as strontium and magnesium, and a cartilage phase composed of modified aragonite and polymers
Bi-phasic osteochondral composite	National Taiwan University Hospital	Autologous chondrocyte-laden biphasic cylindrical plug of DL-poly-lactide-co-glycolide, with lower body impregnated with tricalcium phosphate as the osseous phase
Cartilage repair device	Kensey Nash Corporation	Bioresorbable scaffold with two layers, one collagen fibrils and the other calcium mineral held together by biodegradable polymer material
MaioRegen®	Fin-Ceramica Faenza Spa	Biomimetic nanostructured osteochondral scaffold consisting of deantigenated Type I equine collagen and magnesium enriched-hydroxyapatite

MaioRegen is a multi-layered scaffold that includes a tide mark layer between the usual cartilage and subchondral layer design. The cartilage layer is made up of type I collagen whereas the subchondral layer mainly consists of magnesium-enriched hydroxyapatite (Mg-HA). The unique intermediate layer is composed of Mg-HA and collagen to reproduce the tide-mark. A 6 month study in a sheep model showed promising results including evident cartilage and trabecular bone development in both MaioRegen plugs and cell seeded MaioRegen (Kon *et al.*, 2012; Fin-Ceramica Faenza Spa, 2013).

TRUFIT™ CB Plug, a synthetic resorbable biphasic osteochondral substitute from Smith & Nephew is another product. It is made with Smith & Nephew POLYGRAFT™ technology to mimic the mechanical properties of the surrounding tissue and consists of polylactide-co-glycolide copolymer, calcium sulphate and polyglycolide (Williams and Gamradt, 2008). Unlike MaioRegen that comes as a rectangular piece which is then cut to shape, Trufits are cylindrical plugs that come with a delivery device and trimming knife (Smith and Nephew, 2013). Therefore, Trufit is placed at an advantage as an easier to use product.

1.3.2.2 Tissue engineering approaches

The stages in a tissue engineered osteochondral substitution technique are shown in Figure 1.12. The damaged site is prepared and an implant site is made. The osteochondral graft is implanted and the cells populate the scaffold. The tissue engineered substitute integrates with the recipient tissue.

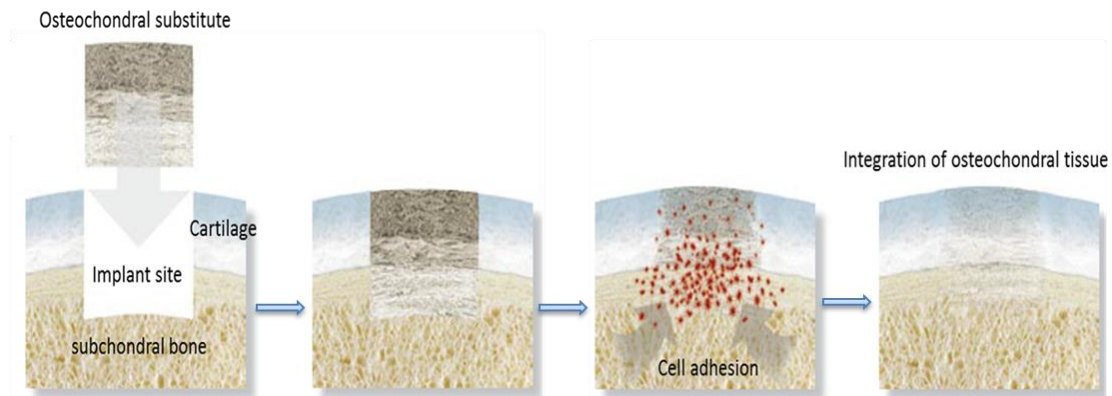


Figure 1-12: Stages in a tissue engineered osteochondral substitution technique (Adapted from Maioregen® (Fin-Ceramica Faenza Spa 2013))

1.3.2.3 Decellularised osteochondral grafts

Using biodegradable scaffolds to grow chondrocytes in-vitro often takes considerable time and expense. Even when tissue engineered cartilage is successfully achieved, the integration of this new cartilage tissue with the underlying subchondral bone remains a challenge (Redman, Oldfield and Archer, 2005; Ohba, Yano and Chung, 2009; Zhang, Hu and Athanasiou, 2009).

Clinical trials using decellularised tissues have been successful in creating natural tissues such as dermis, bladder, peripheral nerves and heart valves that have compatible biomechanical and material properties (Andrus and O'Rourke, 2007; Bolland *et al.*, 2007; Bannasch *et al.*, 2008; Luo *et al.*, 2011; Rössner *et al.*, 2011; Crapo, Gilbert and Badylak, 2011; Joda *et al.*, 2011; Khorramirouz *et al.*, 2014; Chian, Leong and Kono, 2015; Coakley *et al.*, 2015; Greaves *et al.*, 2015; Greco *et al.*, 2015). Decellularisation has vast potential to create non-immunogenic xenogeneic tissue substitutes which will solve the limitations of donor tissue. There are several promising attempts to decellularise osteochondral grafts, many of which are moving towards clinical trials (Elder, Eleswarapu and Athanasiou, 2009; Kheir *et al.*, 2011; Fermor, 2013; Fermor *et al.*, 2015).

Schwarz et al. (2012) used their unique techniques to decellularise various bovine and porcine cartilages. Although the shape and size of the scaffolds were maintained, SEM analysis showed denatured collagen. Micro-CT analysis demonstrated that the porosity was greatly increased which led to higher linear modulus. Using the same decellularisation technique, analysis showed different scaffold strength depending on the source of cartilage (Goldberg-bockhorn *et al.*, 2012). Osteochondral decellularisation is more challenging as the same technique must work on both cartilage and bone.

Porcine chondrocytes were seeded using a novel centrifuging technique into decellularised porcine osteochondral grafts from which even the proteoglycans were removed. The cell seeded constructs were cultured in a bioreactor for up to 3 weeks. Histological analysis showed the ability of the decellularised scaffold to sustain cell viability at all-time points. DMMB assay supported the ability of the scaffold to sustain the accumulation of ECM produced by the cells. There was an overall increase in proteoglycan concentration, especially at weeks 2 and 3 suggesting that the cells were recovered from the stressful new environment. There was a high rate of cell proliferation and increased cell density (Scanlon, 2012). These results could be promising if the cells could be equally distributed, as currently cell distribution is limited to the superficial layer.

Kheir et al. (2011) used a different technique for decellularising porcine osteochondral grafts. Analysis showed the absence of cells and also revealed near to complete DNA removal. Although the GAG content was reduced, there was minimal disruption to the collagen network. The decellularised cartilage showed a significant change in the elastic modulus and permeability compared to native tissue. Cytotoxicity assays showed favourable in vivo and in vitro compatibility of the decellularised tissue. This study was the first in this research area to have achieved complete removal of cells from an osteochondral tissue.

The process of decellularisation varies with the research group by the use of different freeze-thaw cycles and then the use of different chemicals for washing. More research and careful selection of decellularisation techniques are needed to fully make the grafts non-immunogenic while maintaining the biomechanical integrity of the tissue constructs.

1.4 Biotribology

Tribology is defined as 'the science and technology of interacting surfaces in relative motion and the practices related to it' (Czichos, 1978). Biotribology is the study of wear, friction and lubrication in a biological system. Articular cartilage provides a lubricating surface with a low coefficient of friction which reduces the wear of the cartilage itself.

1.4.1 Lubrication

Lubrication provides a low coefficient of friction which is an important factor in the natural functioning of synovial joints. It is a major challenge in articular cartilage as it needs to carry high loads over a long period of time. In the lifetime of a person a major synovial joint will have to withstand about 10 times the body weight on cartilage over a surface area of about 3 cm², articulating about a million cycles per year (Hussainova, 2007). The schematic of the three main types of lubrication regimes are shown in Figure 1.13 and are described in the following sections.

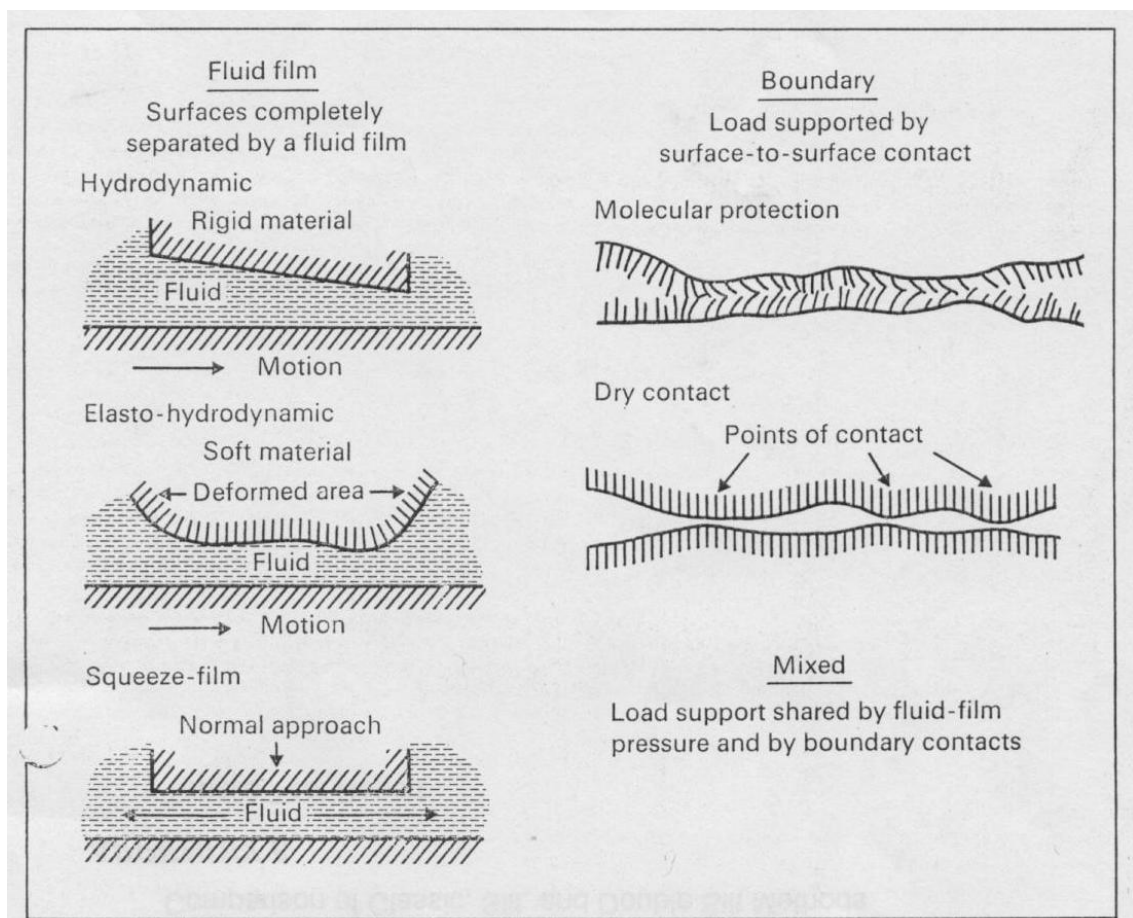


Figure 1-13: Types of lubrication regimes (Akkok 2013)

1.4.1.1 Fluid film lubrication

The motion of bearing surfaces draws in a layer of the lubricant between the surfaces. Fluid-film lubrication occurs when the lubricant prevents contact between the bearing surfaces. The load is supported by the pressure in this fluid film. This will reduce the friction and wear of the surfaces to a minimum. The characteristics of this type of lubrication depend upon the viscosity of the fluid, shape and thickness of the film and the velocity of movement in the joint (Wright and Dawson, 1976; Hamrock, 1984).

There are different forms of fluid film lubrication. *Hydrodynamic lubrication* is caused by the tangential movement of two non-parallel surfaces that are completely separated by a cohesive fluid film. The converging wedge that forms during motion creates a lifting pressure between the surfaces. This type of lubrication is capable of carrying low loads with relatively high speeds between bearing surfaces. It can provide a much lower coefficient of friction than boundary lubrication (Hamrock, 1984).

When the cartilage surface deforms under the high hydrostatic pressure, *elastohydrodynamic lubrication* occurs (Walker *et al.*, 1968; Wright and Dawson, 1976). When the bearing surface separated by the fluid film moves perpendicular to each other at high velocity, it gives rise to *squeeze film lubrication*. The viscosity of the fluid between the surfaces produces pressure which forces the lubricant out. This system is capable of carrying very high loads for a short period of time. As the fluid is forced out, the layer of fluid lubricant becomes thinner and the joint surfaces come into contact (Wright and Dawson, 1976; Hussainova, 2007; Stewart, 2010).

1.4.1.2 Boundary lubrication

With excessive joint reaction force, the fluid film is overcome and boundary lubrication occurs. Certain substances in the lubricating fluid migrate to the solid boundary forming a protective layer which prevents contact between surfaces. The absorption of glycoprotein from the synovial fluid makes the cartilage act as a low shear modulus material. This gives it the boundary lubrication where the load is said to be carried by the surface asperities rather than by the lubricant. Boundary lubrication happens when the speed of joint movement is very low with a low viscous lubricant under a very high load (Bosman, 2010, 2011).

1.4.1.3 Mixed lubrication

Mixed lubrication is a transition lubrication system in which there is a mixture of fluid film and boundary lubrication occurring simultaneously. Sometimes the surface is partially separated by the fluid film and where this fluid film lubrication discontinues there is some contact between the asperities. Although this contact area is affected by boundary lubrication, there will be an increase in friction. This is where the mixed lubrication comes in to play (Stewart, 2007; Reddi, 2008). In this system the load is carried by both the pressure in the fluid film and by the boundary lubricated contacts. Weeping and boosted lubrication are the two types of mixed lubrication regimes proposed for articular cartilage (Callaghan, 2003).

Lewis and McCutchen were the first to suggest a '*weeping lubrication*' created by the release of interstitial fluid from the ECM. Due to the high water content, cartilage is lubricated through a '*weeping*' behaviour where the water exudes to the surface like a compressed sponge when a load is applied. Fluid builds between the surfaces creating a fluid film that increases the hydrostatic pressure that can support the load applied. As long as this hydrostatic pressure remains high enough, it can maintain a lower coefficient of friction (Accardi, Dini and Cann, 2011; McNary, Athanasiou and Reddi, 2011).

Articular cartilage is a porous and permeable tissue that allows water and small solutes to pass through. When the joint is loaded, the high pressure reduces the thickness of the fluid film which causes the water in the synovial fluid to permeate the cartilage. This increases the concentration of hyaluronic acid and high molecular weight proteins in the synovial fluid and viscous gel of lubricating layer is formed. This *boosted lubrication* layer protects the cartilage when fluid film lubrication breaks down (Walker *et al.*, 1968; Callaghan, 2003; Accardi, Dini and Cann, 2011).

1.4.1.4 Lubrication of cartilage

Lubrication theories are developed through friction testing and in vitro compression testing. To reduce friction in weeping lubrication the majority of the load is shown to be carried by the interstitial fluid pressurisation (Mccutchen, 1962). Cartilage has a low permeability which helps to resist the fluid flow to create large drag forces. This may contribute to its ability to maintain this high fluid pressurisation (Ateshian and Wang, 1995).

The introduction of biphasic lubrication has emerged as an important mechanism in explaining the biotribology of cartilage. In a biphasic material the load is shared between the solid and fluid phase depending on the porosity of the tissue. Cartilage has a high proportion of fluid and the porous permeable solid matrix which allows water to be excluded from the cartilage when a load is applied. This creates a pressure gradient called the interstitial fluid pressurisation which is responsible for the load bearing capacity of articular cartilage. Under this biphasic theory the load is initially carried by the fluid phase and then transferred to the solid phase. The fluid phase reduces friction and protects the underlying cartilage surface by shielding the solid phase from high levels of stresses (Setton, Zhu and Mow, 1993).

As it is dependent on time dependant biomechanical conditions and loading, it has become critically important in fully simulating the biomechanics fully. A finite element model created by Graindorge et al. showed increased effectiveness in the lubrication of BSAL under cyclic loading compared to static loading (Graindorge *et al.*, 2005). Most of the load was supported by the surface layer itself and was greater than that supported by the fluid in the bulk of the cartilage. This could be due to the much less solid content of the thin BSAL which hence improved efficiency of its load carrying capacity. An earlier study by Malcom (1976) investigating the effect of static and dynamic loading on the lubrication and friction supports this theory. This pin on plate study on bovine cartilage showed considerably low friction in dynamic loading compared to static loading which implies a more effective lubrication.

Recent research has proposed a biphasic surface amorphous layer (BSAL) covering the surface of healthy articular cartilage that could explain the low friction coefficient. This layer is 2 -200 μm thick and has a low elastic modulus. Unlike the superficial layer of cartilage, BSAL is a non-collagenous layer mainly consisting of proteoglycan molecules. It is not a distinct separate layer but just a continuation of the superficial layer itself. As the BSAL is softer than the underlying cartilage it can maintain a high fluid pressure for a long period of time (Graindorge *et al.*, 2005). This allows it to transfer the load more effectively and support up to 90% of the external load. This results in less solid to solid contact to reduce the coefficient of friction and this kind of fluid support tends to increase between congruence surfaces.

There are theories suggesting the change in lubrication regime with the various stages in gait cycle. Wright & Dowson (1975) used a simple pendulum machine to study human cadaveric

hip joints lubricated with synovial fluid. They concluded that there was squeezed film lubrication at heel strike which then became elasto- hydrodynamic followed by squeezed and boundary condition; and the free swing at the end of the gait cycle was hydrodynamic. This agrees with the earlier finding of Walker et al. who observed fluid film lubrication in the swing phase. Pin on plate studies using human femoral cartilage over glass on a dry joint resulted in a reduction in friction at increasing speed. The friction was reduced as the fluid was squeezed out of the cartilage to enable elasto-hydrodynamic lubrication (Walker *et al.*, 1968; Wright and Dawson, 1976). It is to be noted that the load in each of these test conditions was different and may have influenced the results.

1.4.2 Friction and wear

Friction plays an important role in the proper functioning of a synovial joint as it is a measure of resistance to the sliding experienced by the articular cartilage when the knee is in motion. A co-efficient of friction (CoF) can be measured to quantify friction between two surfaces; the higher the CoF, the larger the friction. Human joints tend to have extremely low CoF as low as 0.02 (Katta et al. 2008; Stewart 2007; Schmidt & Sah 2007; Graindorge et al. 2005). Low friction helps synovial joints to glide over easily. Difficulty in moving the joints is caused by higher friction which releases heat energy and causes swelling in joints (McCutchen, 1962; Furey and Burkhardt, 1997).

Wear can be described as the progressive loss of material from the surface as a result of relative motion at the surface. In tribological studies of artificial joints the material can be weighed to determine the amount of materail lost due to wear. It has been shown that wear of an artificial joint can lead to osteolysis and loosening of the implant (Abu-Amer, Darwech and Clohisy, 2007; Revell, 2008)

Wear can be influenced by a number of factors and studies have been carried out to investigate the parameters that affect the wear of cartilage (Lipshitz, Etheredge and Glimcher, 1975, 1980; Lipshitz and Glimcher, 1979; Furey and Burkhardt, 1997; Russell, 2011). It is influenced to varying extent by the load, friction, contact area, lubrication regime, properties and characteristics of the materials and its surfaces as well as the mechanism by which the wear occurs.

Measuring the surface roughness is one of the main ways of assessing wear in natural and artificial joints. Gravimetric measurements of wear are possible in artificial joints but that is not always possible with natural joints. Therefore, measuring the surface roughness of the cartilage can give an indication of the damage made on the cartilage in a wear test.

Some typical measurements of thoroughness are R_a , R_p , R_v , R_t , R_z and R_{max} . R_a , R_p , R_v and R_t are illustrated in Figure 1.14 and 1.15. R_z is the mean peak to valley height of a roughness profile whereas R_{max} is the maximum peak to valley height of roughness profile within a sampling length (L_c).

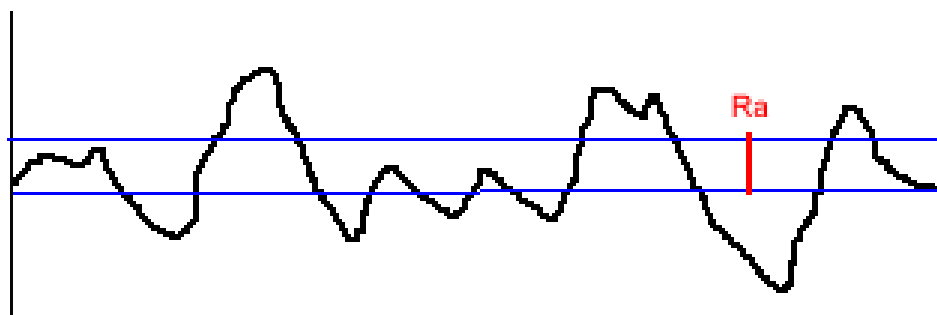


Figure 1-14: Average roughness of profile (R_a)

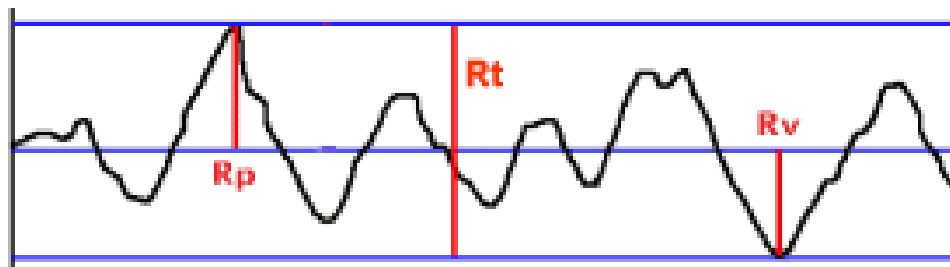


Figure 1-15: Maximum peak height (R_p), Maximum valley height (R_v), Maximum peak to valley height (R_t)

While R_a is the arithmetic average of the 2D roughness, P_a and S_a are the averages of the unfiltered raw profile and the 3D roughness respectively. Depending on the cut off wavelengths applied during analysis, these values change. The larger cut off wavelength includes the waviness and a smaller cut off wavelength reduces the waviness.

Various techniques including MRI, scanning electron microscopy (SEM), atomic force microscopy (AFM), stylus profilometry, ultrasound and interferometry have been used to measure the surface topography of cartilage (Park, Costa and Ateshian, 2004; Saarakkala *et al.*, 2009; Russell, 2010; Ghosh *et al.*, 2013; Brill *et al.*, 2015; Wang and Peng, 2015; Nebelung *et al.*, 2016).

The typical roughness values of articular cartilage measured using various techniques is shown in Table 1.5. The results in the table show the variation between measurements techniques used in cartilage surfaces. This could indicate that the surface roughness can vary depending on the technique used. Therefore, for comparison purposes it is important that the same technique and measurement parameters such as magnification and cut off wavelength are used.

Ghosh et al. (2013) showed that the roughness values increased linearly with magnification using the SEM method. Smyth et al. (2012) showed significant difference in roughness values at different locations. These could be an indication of differences in joint lubrication and how the cartilage in each joint is adapted to its function.

The roughness obtained by Ghosh et al. (2013) from SEM stereoscopic imaging was comparatively higher than those obtained from AFM. However, the AFM values obtained by Moa-Anderson et al. (2003) were 5 times larger than those from Ghosh et al. (2013) and Peng & Wang (2013). Moa-Anderson et al values were closer to the values obtained by Russell (2010) using Talysurf method.

AFM is capable of high resolution roughness measurements at submicron levels. It is widely used for frictional and mechanical measurements of cartilage. Wang & Peng (2015) used AFM to measure the roughness of cartilage wear particles and showed an increase in Sa values with the progression of OA. However, this technique requires a very long scanning time and is only capable of scanning small areas up to 25,000 μm^2 . Therefore, it is impractical for quantitative analysis of the surface topography of cartilage for larger areas (Shekhawat *et al.*, 2009; Peng and Wang, 2013). Although widely used, SEM does not provide quantitative measurements of the surface topography (Shekhawat *et al.*, 2009). It is mainly used to investigate the ECM arrangement within cartilage. The method is time consuming and difficult as the samples needed to be dried and gold plated before the SEM analysis (Gan *et al.*, 2013). The samples could be subject to undesired dehydration and deformation that could potentially affect the results.

Table 1-5: Typical roughness values of articular cartilage

Sample	Technique	Roughness (μm)	Reference
Healthy Bovine cartilage	AFM	Ra= 0.083-0.114	(Ghosh et al., 2013)
Healthy Bovine cartilage	AFM	Sa= 0.086-0.136	(Ghosh et al., 2013)
Fresh bovine cartilage	AFM	Ra= 0.450	(Moa-Anderson et al., 2003)
Frozen bovine cartilage	AFM	Ra= 0.495	(Moa-Anderson et al., 2003)
Human knee cartilage Grade 0	AFM	Sa= 0.068	(Peng and Wang, 2013)
Human knee cartilage Grade 1	AFM	Sa= 0.110	(Peng and Wang, 2013)
Human knee cartilage Grade 2	AFM	Sa= 0.111	(Peng and Wang, 2013)
Human knee cartilage Grade 3	AFM	Sa= 0.119	(Peng and Wang, 2013)
Horse Mid carpal	Dektak 150 Stylus Profilometer	Ra= 2.29 \pm 1.48	(Smyth et al., 2012)
Horse Radiocarpal	Dektak 150 Stylus Profilometer	Ra= 1.60 \pm 0.69	(Smyth et al., 2012)
Horse Carpometacarpal	Dektak 150 Stylus Profilometer	Ra= 1.65 \pm 0.91	(Smyth et al., 2012)
Bovine trochlear groove	Interferometry	Ra= 1.15 \pm 0.4	(Shekhawat et al., 2009)
Bovine condyles	Interferometry	Ra= 0.60 \pm 0.1	(Shekhawat et al., 2009)
Human talar cartilage Grade 0	Interferometry	Ra= 0.80 \pm 0.3	(Shekhawat et al., 2009)
Human talar cartilage Grade 1	Interferometry	Ra= 1.00 \pm 0.3	(Shekhawat et al., 2009)
Human talar cartilage Grade 2	Interferometry	Ra= 1.70 \pm 0.9	(Shekhawat et al., 2009)
Natural human cartilage	Optical coherence tomography	Ra= 2.5	(Saarakkala et al., 2009)
Degenerated human cartilage	Optical coherence tomography	Ra= 18.5	(Saarakkala et al., 2009)
Healthy Bovine cartilage	SEM	Ra= 0.165-0.175	(Ghosh et al., 2013)
Healthy Bovine cartilage	SEM	Sa= 0.183-0.261	(Ghosh et al., 2013)
Healthy bovine cartilage	Talysurf Stylus Profilometer	Ra= 0.43	(Russell, 2010)
Cartilage on cartilage wear	Talysurf Stylus Profilometer	Ra= 0.52	(Russell, 2010)
Cartilage on steel wear	Talysurf Stylus Profilometer	Ra= 1.80	(Russell, 2010)
Natural human cartilage	Ultrasound	Ra= 9	(Saarakkala et al., 2004)

1.4.2.1 Friction and wear studies on cartilage

Friction and wear studies of cartilage have shown an increase in the CoF from change in sliding velocity, type of lubrication used and; the level and duration of load (Forster and Fisher, 1999; Krishnan, Mariner and Ateshian, 2005; Katta, 2007; Katta *et al.*, 2009; Chan *et al.*, 2011)

Studies have looked at the effect of static and dynamic loading on friction (Forster *et al.*, 1995; Katta *et al.*, 2007; J Katta *et al.*, 2008). The CoF have been shown to increase when a static load was applied for a prolonged period of time. However, there was a reduction of CoF upon the retrieval of this static load as the cartilage was allowed to rehydrate itself. Katta *et al.* (2008) showed an increase in friction at high contact stresses. This may have been due to the reduced fluid load support caused by the dehydration of cartilage. Under dynamic loading conditions, increasing the stroke length helped to reduce the CoF even at a higher level of stress. This is because even at higher stress the longer stroke length will give time for the cartilage to recover. However, a longer period of preload did not allow the cartilage to rehydrate and hence the friction was higher. Therefore, the contact mechanics have been shown to have an effect on the CoF due to the lubrication regime.

Lipshitz *et al.* carried out wear studies of cartilage articulating against metal plates of known roughness profiles (Lipshitz and Glimcher, 1979). They found the wear to be linear to the sliding speed, contact pressure and time. The wear rate of pins articulating on a smooth surface decreased with time and reached a plateau when at a given surface pressure. The chemical index was made by measuring the hydroxyproline content in the lubricant after wear test. Schwartz and Bahadur (Schwartz and Bahadur, 2007) used osteochondral pins for wear studies using an in-house dual axis wear simulator. Wear rates of cartilage pins subjected to multi-directional sliding on a stainless steel surface were compared with the wear rates against a polymeric material. The wear rates on stainless steel were more than twice that of the polymeric counterface after 10,000 cycles under 39 N. This difference could have been due to the variance of contact pressure between the two types of material. To estimate contact pressure, they measured the storage and loss moduli in each case. For a frequency of 0.1 to 10 Hz, the storage modulus changed from 470 to 1010 kPa and the loss modulus changed from 176 to 249 kPa.

1.4.3 Tribology models for assessment of cartilage wear and friction

Tribological studies have used using simple geometrical configuration sliding devices like pin-on-plate systems and pendulum devices like arthrotripsometers as shown in Figure 1.16. In the sliding devices a pin and/or plate made of cartilage, metal and/or glass slide against each other. In pendulum devices, the joint acts as a fulcrum where one surface rocks over the other (Northwood, 2007).

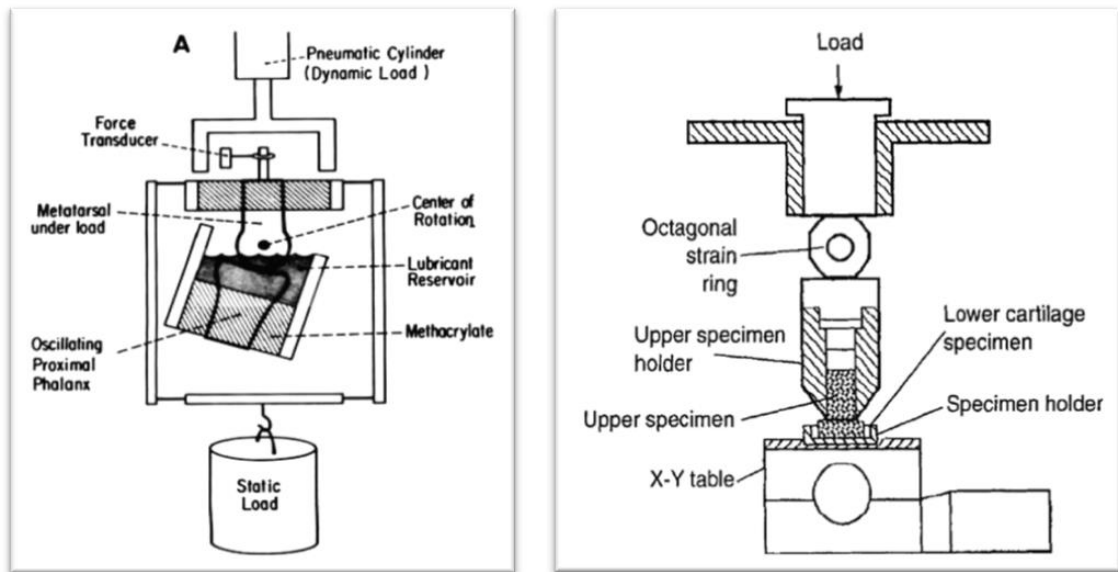


Figure 1-16: Schematic of a pendulum device (Radin and Paul, 1971) and pin-on-plate device (Furey and Burkhardt, 1997)

Lipshitz & Glimcher (1979) studied the wear properties of bovine osteochondral pins worn against stainless steel plates of different surface profiles. This type of pin on plate system became a common method in future tribological studies (Anon 1975; Lipshitz et al. 1980; Northwood & Fisher 2007; Lipshitz & Glimcher 1974; Krishnan et al. 2005; Kock et al. 2008). There are many studies that have measured the CoF using cartilage-on-ceramic, cartilage-on-metal and cartilage-on- cartilage using both animal and human tissue.

A pin on plate system is the most common and simple system used for cartilage tribology studies. It consists of a pin (made of cartilage or other material) articulating against a flat plate (made of cartilage or other material). The Pin-on-plate set up allows the calculation of contact areas between the articulating surfaces which could be used as a function of load. Although this approach does not reflect in- vivo conditions, it is possible to vary the factors independently to study the effect of each factor under in- vitro conditions (Taylor 2013; Russell 2010; Katta et al. 2008).

Due to the complexity of designing experiments for biological tissues, the literature on the wear of natural tissues is not as vast as the studies on friction tests. Most wear tests are done on cartilage-on-metal (J Katta *et al.*, 2008; Russell, 2010; McNary, Athanasiou and Reddi, 2011; Shi, Sikavitsas and Striolo, 2011; Taylor, 2013). Protein absorption in pin-on-plate systems is a common cause of change in friction. Albumin is a protein present in synovial fluid which can be absorbed by materials such as glass and form a layer that affects the frictional properties of these materials. Therefore, tribological models that use glass may have significant limitations in their studies (Jay, 1992; Roba *et al.*, 2010).

Although pin on plate systems can provide relevant results for hemi-arthroplasty implants, they do not replicate the behaviour in a natural synovial joint. The pin-on-plate apparatus are followed by joint simulators which are also used for wear assessments where the machine simulates the movement in a joint for several million cycles. The wear rate and other assessments can then be followed.

Joint simulators are also used to generate wear particles from different materials used in joint replacements. For testing a whole joint, a joint simulator is essential. The advantage of testing a whole joint is that it allows the contact geometry of the joint to remain intact to achieve the in vivo lubrication flow dynamics. It also helps to simulate the physiological biomechanics which control the biphasic lubrication.

One of the challenges is in measuring the wear of cartilage, which cannot be done gravimetrically, as in artificial joint replacement wear tests. Several techniques such as measuring the hydroxyproline content in the lubricant and measuring the change in cartilage thickness have been established to assess the wear of cartilage-on-cartilage specimens. The load, type of lubrication and sliding velocity have all shown to have an effect in the wear (Lipshitz, Etheredge and Glimcher, 1975; McGann, Vahdati and Wagner, 2012).

Assays developed by Woessner and Farndale *et al* to measure the concentration of GAG and hydroxyproline can be used to assess the cartilage wear through the lubricating fluid (McGann, Vahdati and Wagner, 2012). Studies by Katta *et al* and Lipshitz *et al* have used this technique to quantify the amount of wear of cartilage samples (Lipshitz and Glimcher, 1979; Lipshitz, Etheredge and Glimcher, 1980; Katta *et al.*, 2007; J Katta *et al.*, 2008).

Wear testing of animal joints in joint simulators has shown changes in the morphology of wear particles and visible damage in the cartilage surface. Wear particles obtained from healthy and arthritic patients has shown that the shape of the wear particles can be used as an indication of the degree of osteoarthritis (Kuster, Podsiadlo and Stachowiak, 1998).

Quantification of the wear rate in vitro is now considered an essential step in the development of new joint replacements prior to clinical trials. In vitro simulator testing of hip and knee (tibiofemoral joint—TFJ) prostheses has been common practice for over two decades. Little research exists around in vitro simulation of wear in the patello-femoral joint (Ellison *et al.*, 2008). Although not as common or extensive as the TFJ studies, researchers have investigated the wear in artificial PFJs. Studies differ in their load and kinematic inputs as well as their wear assessments. Some of these studies are summarised in Table 1.6. Different scenarios were tested to investigate various physiological conditions such as walking and stair climbing. The degrees of flexion, constrained of each parameter and loading conditions were all factors that influenced the test settings.

Table 1-6: Artificial patello femoral simulator studies

Author	Inputs	Wear assessment	Comments
(Hsu and Walker, 1989; Burroughs <i>et al.</i> , 2006)	Flexion Extension (F/E), Anterior Posterior (AP) load	Fuji films and grading methods	Limited to two degrees of freedom in the PFJ and assessment was based only on visual examination
(Ellison, 2007)	F/E, Adduction/Abduction (A/A), Axial load S/I and M/L displacement	Gravimetric measurements	M/L displacement was constrained. Maximum S/I was 10 mm. Patella tilt was left unconstrained and monitored
(Korduba <i>et al.</i> , 2008)	Controlled and uncontrolled M/L displacement (patellar shift), F/E, patellar compressive force (Axial load)	Gravimetric measurements	Constrained M/L showed higher wear compared to passive M/L
(Maiti, 2012; Maiti <i>et al.</i> , 2014)	Axial load passing through the centre of the patella, F/E, M/L rotation and tilt, M/L and S/I displacement	Gravimetric measurements	M/L displacement was unconstrained. Maximum SI was 20 mm. Higher kinematics with ML rotation $\leq 4^\circ$ and physiological scenario with $\leq 1^\circ$ were tested

Knee joint simulator studies have been developed to study the wear of artificial patello femoral replacements in human joints. The active motions were gathered from the gait cycle published by Ellison (2007) and Maiti (2012). They investigated the wear in artificial patello femoral joints using the Leeds hip simulator and six station knee simulators respectively. Their gait cycle represented a human patello-femoral gait cycle to test their artificial implants (Ellison, 2007; Ellison *et al.*, 2008; Maiti, 2012).

Van Haver et al. (2013) used a knee rig to investigate the kinematics of the cadaveric PFJs. This system applied flexion and extension under 700 N body weight and a force of up to 2700 N on the quadriceps tendon. They showed the contact area on 20-60° knee flexions moving from distal to proximal in the patello femoral region. They observed the mean contact area increase from 80.2 ± 3.3 at 20° to 349.5 ± 10.1 mm² at 60°. The contact pressure also increased from 0.9 ± 0.2 to 5.9 ± 0.7 MPa. However, the repeatability of the tests in this rig was only tested on two knee joints with four repeats of flexion extension. Hence the validation of this system and its methodologies need to be further analysed in order to apply this system for investigating further research questions.

1.5 Rationale

Patello-femoral problems can affect nearly a quarter of the population and remain a common cause for revision surgery in total knee replacements (Hinman *et al.*, 2014; Maiti *et al.*, 2014; Wyndow *et al.*, 2016). Joint replacement seems to be the final solution for improving the quality of life for patients suffering from final stage osteoarthritis. Minimally invasive interventions such as osteochondral transplantation are promising alternatives that could prevent or delay the need for such replacements (Nho *et al.*, 2008; Draper *et al.*, 2011; Fitzpatrick *et al.*, 2011). Autologous osteochondral transplantation can be a successful treatment but is limited to the treatment of small osteochondral defects due to donor site morbidity. Large defects treated with the same technique require allografts which may have the risk of immunological rejection (Freeman *et al.*, 2000; Northwood and Fisher, 2007; Ma *et al.*, 2010).

Decellularisation is a process by which the cells are removed from a tissue, leaving only its ECM scaffold which can then be implanted into the recipient site to be populated with the recipient's cells. The University of Leeds have developed an acellular porcine cartilage bone matrix that can be used as an osteochondral substitute. This has the potential to be used in the treatment of osteochondral defects of any size. These decellularised grafts have been shown to be biocompatible in both in- vitro and in- vivo studies (Kheir *et al.*, 2011). Currently there are no in- vitro studies developed for the pre-clinical testing of these grafts. The tribology and wear of these grafts need to be investigated before they can be approved for clinical trials. Hence there is a scope for an in- vitro model that can help to translate these substitutions from lab to the market.

This research develops a tribological knee simulator for the natural PFJ that can result in the advances in the understanding of the tribology and biomechanics of the joint that can serve as a simulation platform for investigating conditions such as osteochondral substitutions. The methodology developed has the potential to become the standard for the in- vitro study of any osteochondral substitutions that can be used in a PFJ. It could be used to assess the suitability of the product before it is used for clinical trials.

1.6 Aims and Objectives

1.6.1 Aim

The overall aim of the project was to develop and validate a design specification for the pre-clinical testing of the human patella-femoral joint.

1.6.2 Objectives

1. Determine a suitable animal model for the development of the method

The geometry of the bovine and porcine PFJs will be investigated to establish a suitable animal model that closely replicates the human PFJ. Cartilage from the chosen model and human cadaveric joints will be characterised to compare the material properties. The elastic modulus, thickness and permeability of the joints will be determined to make the comparison.

2. Develop an animal model to investigate the biomechanics and wear of the PFJ using a single station knee simulator (SSKS)

This stage will define the biomechanical simulation cycle to replicate the kinematics of the natural PFJs. The SSKS will be modified to accommodate the animal model and to apply the patello-femoral gait cycle. A methodology will be developed and validated to set up the animal model for the simulator study.

3. Develop a simulator study to investigate the contact mechanics in the PFJ

A consistent and repeatable method will be developed to investigate the contact mechanics in the natural PFJ. The contact area and contact pressure will be measured using a Tekscan pressure sensor for different conditions.

4. Develop a simulator study to investigate the wear in natural joints

The SSKS will be used to generate wear on the negative (cartilage on cartilage) and positive (metal against cartilage) controls. The wear will be assessed by grading the wear on the cartilage, measuring the wear area on the cartilage and the surface roughness of the cartilage. There must be significant difference in the measured wear on the negative and positive control.

Chapter 2. General materials and methods

This chapter describes the generic materials, instruments and calibration, and the methodologies used throughout this thesis. Any methodologies developed for specific studies in this project are discussed in the respective chapters.

2.1 General materials

2.1.1 Phosphate Buffered Saline (PBS)

PBS was used for storage, rinsing and hydration of tissue throughout the study. It is an isotonic solution and is non-toxic to cartilage tissue. It was prepared by dissolving 10 tablets of PBS (MP Biomedicals, US) in 1L of distilled water. Cartilage surfaces were always kept hydrated by wrapping in PBS soaked tissue. PBS was used instead of water because the cartilage will swell due to the ionic charge effect of the water.

2.1.2 Lubricant- New born calf serum

New born calf serum (NBCS) (Gibco, Life Technologies, New Zealand) was diluted with PBS to make the lubricant. A concentration of 25% (v/v) NBCS was used to obtain similar protein level in the lubricant as observed physiologically in the synovial fluid. The protein in the lubricant contributes to the boundary layer to reduce friction in the joint (Saikko, 2003; Wang, Sharkey and Tuan, 2004).

2.1.3 PMMA Bone Cement

Polymethyl methacrylate (PMMA) bone cement was used to secure the tissue samples into the correct position and orientation in the knee simulator fixtures. The cement, consisting of a cold cure solid powder and a liquid monomer (WHW Plastics, Hull, UK), was prepared according to the manufacturer's instruction. It was mixed at a 2:1 solid to liquid ratio in a fume cabinet.

2.1.4 Bovine, porcine and human tissue

The bovine tissue was obtained from 18 month old bovine femurs with an intact and untampered patello-femoral groove. The porcine tissue was taken from the right legs of 6 month old Large White pigs obtained from the abattoir within 48h of slaughter. The average weight of the pigs was 76kg.

Human tissue was obtained from 6 donors after ethical approval from Leeds West Research Ethics Committee [REC number 11/YH/0025]. Six fresh-frozen human knees (5 left knees and 1 right knee,) were obtained from 4 female and 2 male donors of an age range of 52-85, with an average age of 64.5 years.

2.1.5 Femoral Component - PFC Sigma

A PFC sigma (press fit condylar sigma design) femoral component for a right knee as shown in Figure 2.1 was used for the positive control in the wear study described in chapter 7. This component was manufactured (PFC Sigma, DePuy, Warsaw, Indiana) from Co-Cr-Mo alloy. It had a surface roughness (Ra) of 0.02 μm (ASTMF75-01, 2001), which is within the accepted orthopaedic implants surface finish of $<0.1 \mu\text{m}$ (ISO 7207-2:2011). It had a 7° angulation on the trochlea to replicate the geometry of the natural joint.



Figure 2-1: Press fit condylar sigma design femoral component used as the positive control

2.1.6 Microset replicating compound

Microset 101RF silicon compound (Nuneaton, Warwickshire, UK) is designed for producing high resolution 3D replicas. It is a mixture of two part polymer in a cartridge that is dispensed as a semi-viscous liquid. The cartridge and gun system allows quick and easy dispensing. The Microset compound produces flexible replicas with a resolution of more than 0.1 microns that sets within 5 min and can be easily peeled from the surface without any trace. It was used to mark the contact points as discussed in Chapter 6.

2.1.7 AccuTrans replica moulds

This was a low-viscosity casting silicone from AccuTranss® (AccuTranss®, Switzerland). Its time dependent shear thinning property can be used to obtain detailed impressions of surfaces (Goodall, 2015). This elastic compound can be used in smooth, textured and rough

surfaces. These flexible but accurate moulds are even perfect for curved surfaces, horizontal or vertical planes. They are long lasting and the moulds are permanent upon removal from the sample. Therefore there is no risk of smudging the material and producing inaccurate surface profiles. They are non-toxic and have no side effects or reaction to the samples. These are available in a range of colours and this study used the brown colour for the wear study replicas (AccuTrans, 2015).

Unlike other replica mixtures, AccuTrans is a compound and does not require any mixing. It takes less than 4 min to set at room temperature. The main advantage of this over the Microset is that as the AccuTrans moulds are firmer compared to Microset molds the prints are permanent upon removal from the sample. This allows the replicas to retain the shape of the samples.

2.2 General equipment

2.2.1 Linear Variable Differential Transformer (LVDT)

An LVDT (RDP D5-200H; ElectroSense, PA, USA) was used in this study to determine the radius of curvature of the femoral groove of knee joints and also in the indentation rig for measuring the displacement of the indenter tip from the cartilage surface. LVDT, also known as a linear variable differential transformer, is a type of transducer used to measure linear displacement. It converts the linear displacement from a reference point into a proportional electrical signal containing phase (for direction) and amplitude (for distance).

The LVDT was calibrated using standard stainless steel slip gauges (Broomfield Carbide Gauges, UK). The indenter tip of the LVDT was placed on a flat platform of height 7.5 cm and this was taken as the zero position. The voltage on the A2D indicator connected to the LVDT was recorded. Slip gauges of known thickness (starting from 1 mm) were placed between the zero point and the indenter. The voltage was recorded at each increment of slip gauge and a spirit level or bubble level was used to ensure that the LVDT was perpendicular to the slip gauges. Once the slip gauges reached up to 2 mm, the height was reduced and the change in voltage was again recorded for each height until it reached the zero point. Linear regression was used to fit a line to the calibration data to convert these output voltages into displacement in millimetres.

2.2.2 Micro Computed Tomography (Micro-CT)

A Micro-CT (XtremeCT, Scanco, Switzerland) was used to scan the femoral samples to measure the radius of curvature of the femur. It is an efficient, non-destructive and accurate imaging technique. It takes high resolution X-ray images at angular views while the sample rotates. A computer stacks the slices of images and the user can scroll through the cross sections along different planes and inspect the images to study the microarchitecture of the specimen (Bruker, 2013; B-cube, 2016).

2.2.3 SolidWorks

SolidWorks (Dassault Systèmes, Waltham, MA, USA), a solid modelling CAD software, was used to create all the design drawings for all components manufactured throughout this project. It was also used to create a theoretical model of the patello-femoral contact for the contact point study described in Chapter 6. Additionally, it was also used to design the angle fixtures for the contact point study, the fixture manufactured to cement the patella for obtaining osteochondral plugs and the fixture for the simulator studies.

2.2.4 Image-Pro Plus

Image-Pro Plus 7.0 software (Media Cybernetics, Silver Spring, USA) is an image analysis tool used to count, measure and classify objects through the images. Images were captured with a Canon SLR camera with x20 lens for quantification. The images were exported to the Image pro software and the images were calibrated using the reference scale in the pictures. The inner boundary of the marking was traced and a mask was applied. The area covered by the mask was calculated by the software and this was recorded as the value for the area. This software was also used to calculate the radius of curvature of the femur from the Micro-CT images, to find the areas of the samples from the images and to locate the position of the patella on the Tekscan in the contact mechanics study.

2.2.5 Alicona optical surface metrology unit

Infinite Focus G5 (Alicona, Austria) is an optical device for 3D surface measurements. The small depth of focus of the optical system and the vertical scanning capability of the device combines to provide the topographical data at variation of focus. A set of algorithms then reconstructs this topographical data into a 3D image. It has objectives of different magnification ranging from 2.5 x to 100 x and has a vertical resolution as low as 20 nm.

At higher magnification, an improved axial and lateral resolution is possible. However, this will reduce the area that can be reconstructed in a single scan. ISO conforming measurements for 3D models require at least a length of 4 mm. The ImageField functionality in Alicona IF G5 can provide large enough measurements to comply with the ISO standard. This ImageField functionality can provide 3D models for large measurements that can be used to analyse volume changes. The device reconstructs multiple 3D models by stitching together several single 3D models that are made to overlap slightly with each other. Based on the colour and topographical information, this technique is able to form large 3D models through several smaller 3D models.

2.2.6 Single station knee simulator (SSKS)

A single station knee simulator (SSKS) is an electro-mechanical dynamic testing rig used in this project to study the biotribology and biomechanics of the porcine PFJs. A simplified diagram of the simulator is illustrated in Figure 2.2. The calibration and the application of the SSKS in this project will be discussed in detail in Chapter 7.

The simulator (Simulator Solutions, Stockport) has six degrees of freedom and was used to apply the gait cycle in the wear studies and the loads and displacements for the contact mechanics study. It has the potential to facilitate the testing of different conditions, new tissue substitutions and various interventions under a wider range of gait scenarios.

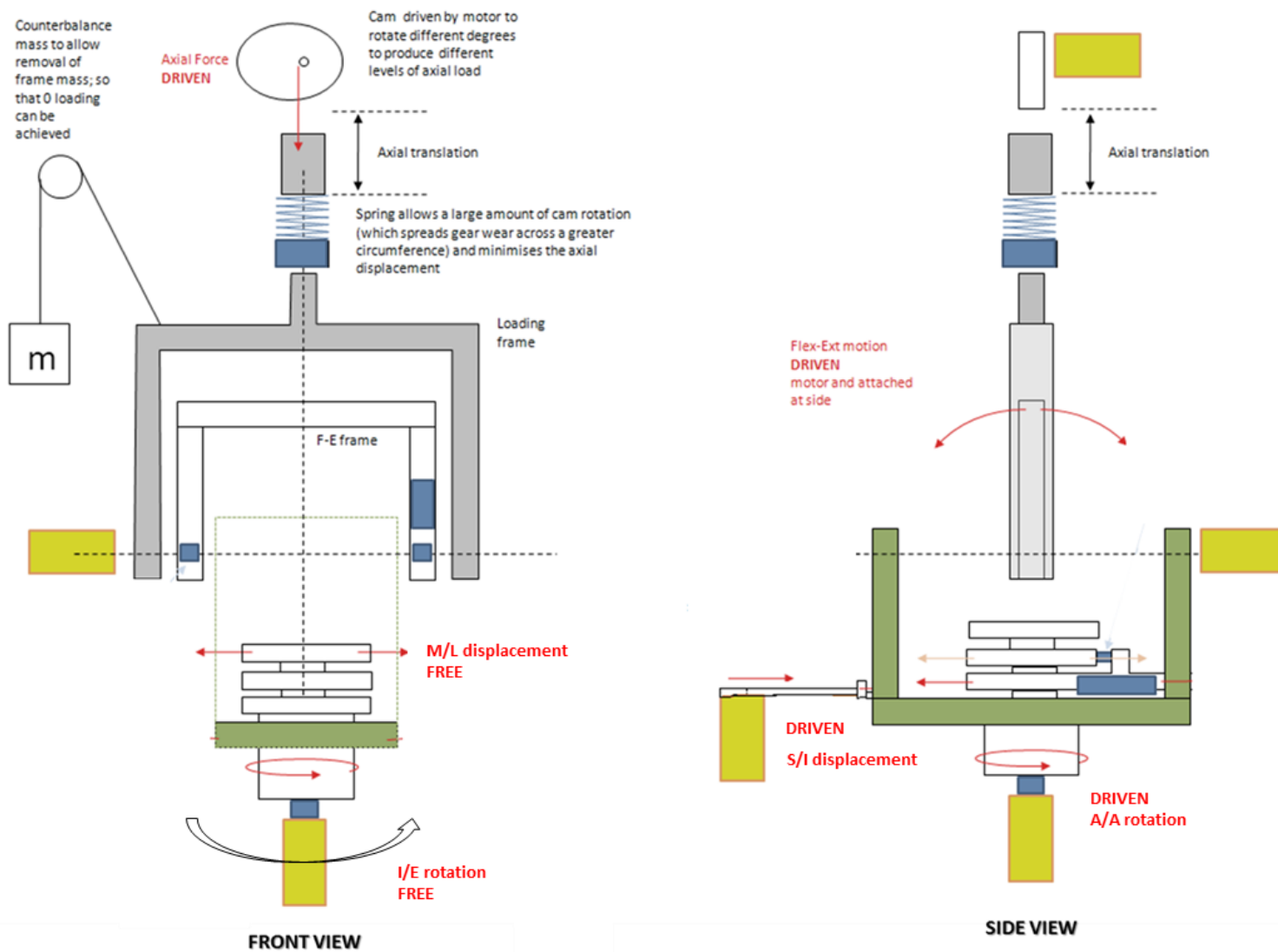


Figure 2-2: Simplified diagram of the single station knee simulator for the patello-femoral joint

2.3 Methodology for the preparation of natural tissue samples

This section discusses the procedure used to prepare the natural tissue samples from bovine, porcine or human knee joints. Once the tissue had been prepared, the samples were stored appropriately depending on when the samples were used for the test. Samples were either refrigerated at 4°C for a short time of up to 6h or frozen at -20°C up to a maximum of 6 months. Frozen tissues were thawed at room temperature or thawed overnight at 4°C, for a maximum of 3 freeze-thaw cycles.

2.3.1 Patello femoral joint dissection

The dissection of the porcine and bovine PFJ is described in Chapter 3 Section 3.2.1 and the dissection method for the human PFJ is described in Chapter 5 Section 5.2.2. Chapter 7 further discusses the methods used to prepare the samples for the simulator studies.

2.3.2 Obtaining osteochondral plugs

Osteochondral plugs were cylindrical grafts of subchondral bone with the articular cartilage attached to it. These were used to characterise the material properties of the articular cartilage.

An 8.5mm diameter coring tool from a mosaicplasty kit (Smith & Nephew, Andover, MA) as shown in Figure 2.3 was used to extract the osteochondral plugs. The markings on the end of the coring tool identified the depth when the tool was inserted into the bone. Each plug was extracted to a depth of 10 mm. The specific height was chosen to fit the collets used to hold the plugs during testing and also to ensure consistency.



Figure 2-3: Coring tool from the Smith and Nephew mosaicplasty kit

Once the patello-femoral joint was separated from the knee, the femur was clamped down with the cartilage surface of the joint extended from the table. Initial outlines for the plugs were marked by pressing the coring tool against the cartilage surface until it reached the

subchondral bone. This procedure helped to position the coring tool during the extraction process and avoided slippage during hammering.

Once all the plugs were correctly marked, the coring tool was placed over each plug and hammered in to a depth of 10 mm (using the markings on the coring tool). The plugs were removed with a swift sharp motion to break off the plug. Once the coring tool was detached, the plug came with it and was removed by inserting a rod into the bony end of the sample. The bone end of the plug was flattened using a file. An image of the osteochondral plug is shown in Figure 2.4.

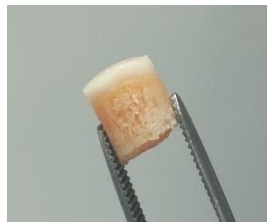


Figure 2-4: A fully prepared osteochondral plug for the cartilage characterisation study

It was necessary to grip the patella while taking the plugs; however, it was not possible to secure the patella straight into the vice without damaging the sample. The patella was therefore fixed in PMMA cement and then secured in the vice. The plugs were then obtained as described above.

2.4 Mechanical characterisation of cartilage

Mechanical creep indentation was conducted on osteochondral plugs to determine the elastic modulus and permeability of the cartilage specimens.

2.4.1 Indentation rig

A custom made indentation rig (Abdelgaied *et al.*, 2015) was used to study the time dependant behaviour of articular cartilage as shown in Figure 2.5. It consisted of an aluminium shaft to which the indenter was attached; which together applied a total load of 24 g on the cartilage. The motion was steered by a linear bearing to reduce friction within the apparatus. To avoid the impact of the indenter on the cartilage, the release velocity of the shaft was controlled by a dashpot filled with silicon oil.

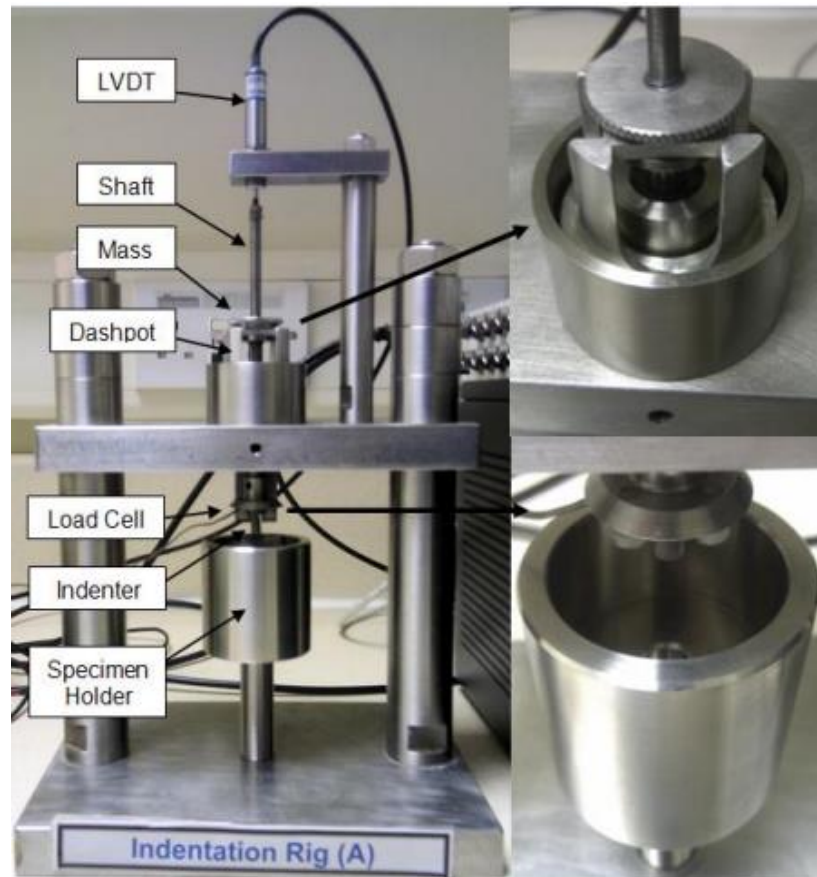


Figure 2-5: Indentation rig (Taylor, 2012)

A linear variable differential transducer (LVDT) as described in Section 2.2.1 measured the displacement and a piezoelectric force transformer measured the resistance force in the indentation rig. The LVDT (RDP D5-200H; ElectroSense, PA, USA) had a sensitivity of $0.4 \mu\text{m}$ at 10 mm range and 0.04 N at 2 N range for the piezo-electric force transformer (Part No: 060-1896-02, ElectroSense, PA, USA). The voltage output of these sensors was recorded using custom made Labview 8 software (National instrument, TX, USA).

The LVDT and the force sensor were calibrated to convert the voltage outputs to millimetres and Newtons respectively. Calibration for the LVDT is described in Section 2.2.1. To calibrate the piezoelectric force transformer, the indenter tip was placed on a flat platform without applying any load. Calibrated masses of 50 g were added incrementally and the change in voltage was recorded. Once it reached 200 g, the masses were removed one by one while still recording the decrease in voltage until the whole mass reached zero. This adding and removing of loads was carried out to characterise any hysteresis in the force sensor. A linear regression was used to fit a line to the calibration data to convert these output voltages into load in Newtons.

The calibration graph for the piezoelectric force transformer and the LVDT for the indentation test is shown in Figure 2.6 and 2.7 respectively

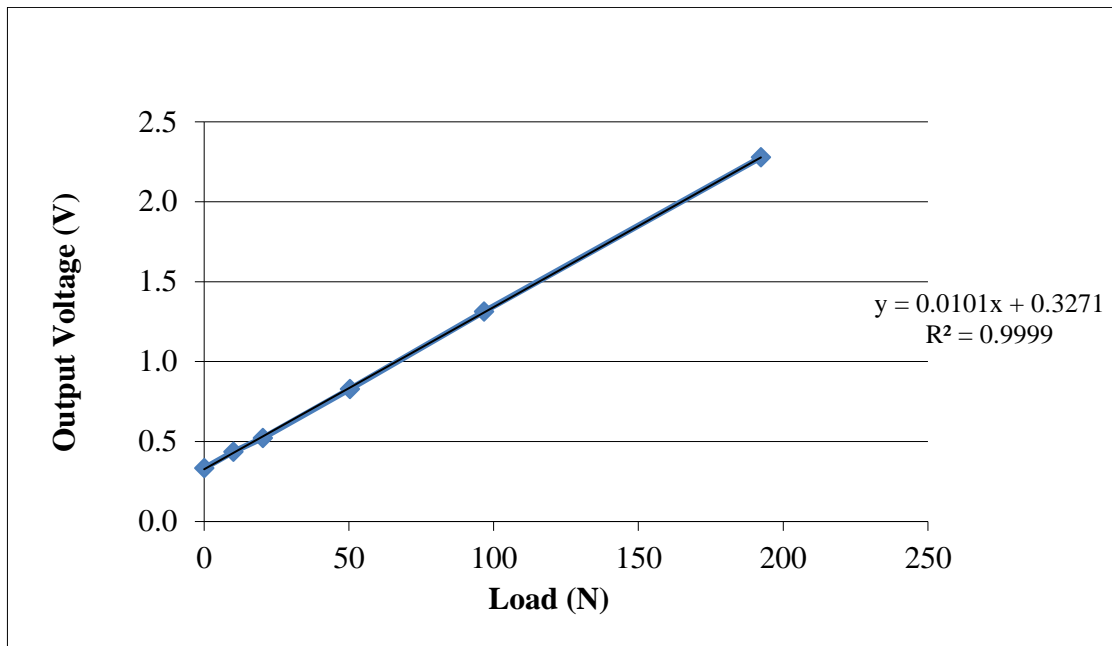


Figure 2-6: Calibration graph for the piezoelectric force transformer

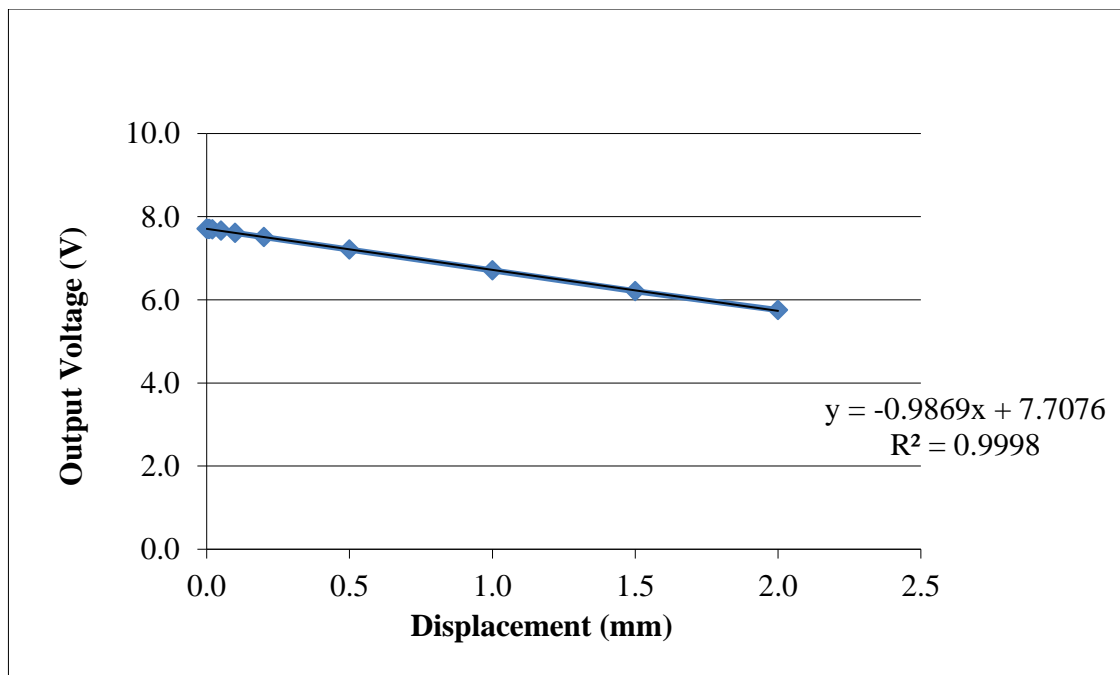


Figure 2-7: Calibration graph for the LVDT

2.4.2 Indentation test

Osteochondral plugs secured in a collet were fixed inside an O-ring to prevent motion during the test and were then placed within a stainless steel bath as shown in Figure 2.8. The bath

was filled with PBS to cover the surface to hydrate the cartilage. A flat rigid indenter of diameter 2.5 mm was positioned ~ 1 mm away from the cartilage surface. The stainless steel bath, O-ring, collet and the indenter are shown in Figure 2.9.



Figure 2-8: Indentation set up with the osteochondral plug under the indenter

As the osteochondral plugs used in this study provided a flat surface for indentation a flat indenter was used in this study instead of a hemi spherical indenter used in previous studies in the same lab (McLure, 2012; Taylor, 2012; Fermor, 2013). A flat indenter can provide a larger contact area between the indenter and the cartilage and hence reduces the contact stress at the surface.



Figure 2-9: From left to right- Stainless steel bath, O ring to fix the collet in place, the collet and flat indenter

When the indenter was released, a constant load of 0.24 N was applied through the indenter and the data was captured at a sampling frequency of 10 Hz for one hour to allow equilibrium deformation to be reached. On completion of the indentation test the plugs were removed and kept covered in PBS soaked tissue for one hour to rehydrate and recover, before the cartilage thickness measurements were carried out.

The impact speed was decreased by dropping the indenter shaft through a silicone oil filled dashpot. LabView 8 software (National Instruments, TX, USA) collected and stored the data from the LVDT (measured the indenter displacement) and the piezo-electric force transformer (measured the resistance force) to produce a cartilage deformation curve for the experimental data.

2.4.3 Cartilage thickness measurement

An Instron material testing machine (Instron 3365, Bucks, UK) was used to pierce the cartilage with a needle to measure its thickness. This method is known as the needle indentation or needle probe method (McLure, 2012; Taylor, 2012; Fermor, 2013). Once the osteochondral plugs were secured in the PBS bath, the needle attached to the Instron was manually positioned ~1 mm above the cartilage surface as shown in Figure 2.10. The needle was lowered into the cartilage at a rate of 4.5 mm/min and its resistance was measured using a 50 N load cell.



Figure 2-10: The needle attached to the Instron is positioned just above the cartilage

The thickness was calculated from the resistance of the needle piercing through the cartilage - as the distance between resistance in initial contact and the steep increase in resistance when the needle touched the much stiffer bone. A sampling frequency of >50 Hz enabled the force sensors to detect the moment when the needle touched the cartilage surface, pierced through the tissue or touched the bone surface. The thickness was calculated from the difference in deformation levels at these points as shown in Figure 2.11.

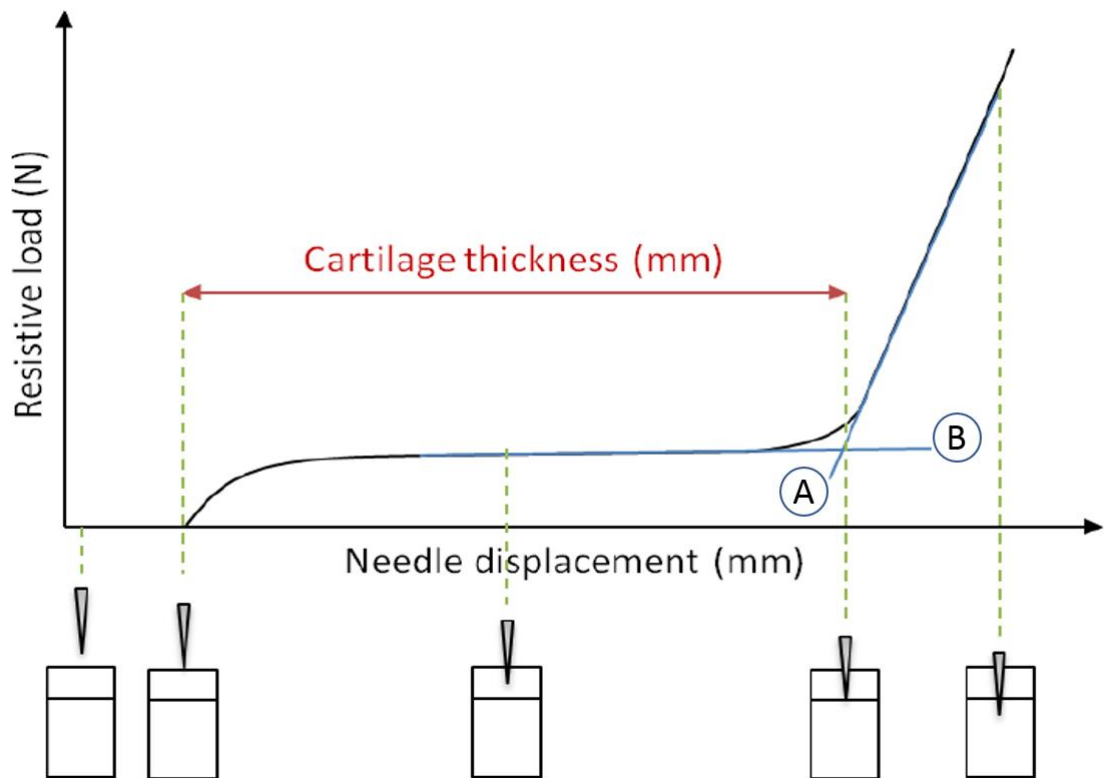


Figure 2-11: Schematic of how cartilage thickness was determined from needle indentation (adapted from Fermor, 2013)

In Figure 2.11, the equations for Line A and Line B is used to obtain the thickness values. The sample calculation is shown below.

$$\text{Line A} \rightarrow y = m_1x + c_1$$

$$\text{Line B} \rightarrow y = m_2x + c_2$$

$$\text{Thickness} = (c_2 - c_1) / (m_1 - m_2)$$

2.4.4 Deriving the mechanical properties using an FE model

An axisymmetric biphasic poroelastic finite element model (ABAQUS, version 6.9-1 Dassault Systemes, Suresnes Cedex, France) created and published by Pawaskar et al. (2010) was used to derive the elastic modulus and permeability. The model was a representation of how the data from the results were collected in the experiment.

Several boundary conditions were set as follows:

Poisson's ratio of cartilage = 0 (Jin et al., 2000)

Water content of cartilage = 74.7% (Elder, Eleswarapu and Athanasiou, 2009)

Thickness of cartilage = Thickness of each plug obtained from the needle probe study

Elastic modulus of subchondral bone = 1510 MPa (Mitton et al., 1997)

Poisson's ratio of subchondral bone = 0.3 (Shirazi, Shirazi-Adl and Hurtig, 2008)

The cartilage thickness measured for each plug provided the geometric information for the FE model to derive the properties from the cartilage deformation curves generated during indentation. The indenter was created in the model as an analytical rigid body with 2.5 mm diameter flat tip. The FE model created is illustrated in Figure 2.12.

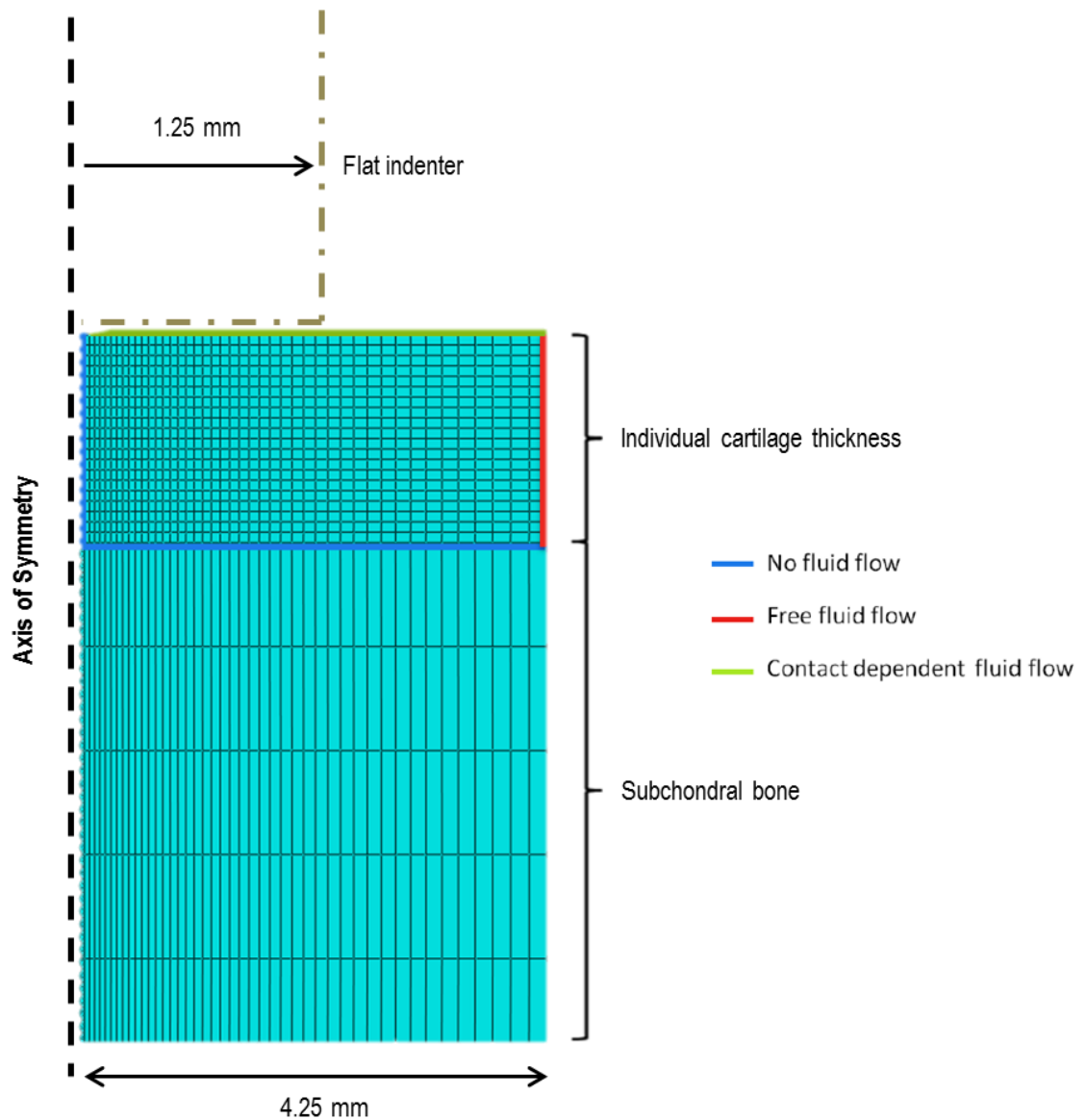


Figure 2-12: Finite element model of an osteochondral pin
 This schematic shows the axis of symmetry, and the imposed fluid flow restrictions

The deformation curve obtained through this FEM was matched with the curve created by the experimental data. A displacement vs time graph was produced by the FEM as shown in Figure 2.13. MATLAB (version 7.4, MathWorks Inc, Boston, MA, USA) was used to calculate the best fit between the final 30 % of FE curve and experimental curves. A curve fitting process was repeated until it reached the maximum squared error (R^2 value) by altering the input material properties. An R^2 value greater than 0.85 was accepted as significant for

biological tissues (Fermor, 2013). In the FE model, the inputs used as elastic modulus and permeability to give the highest R^2 values was recorded as the determined material properties for that sample.

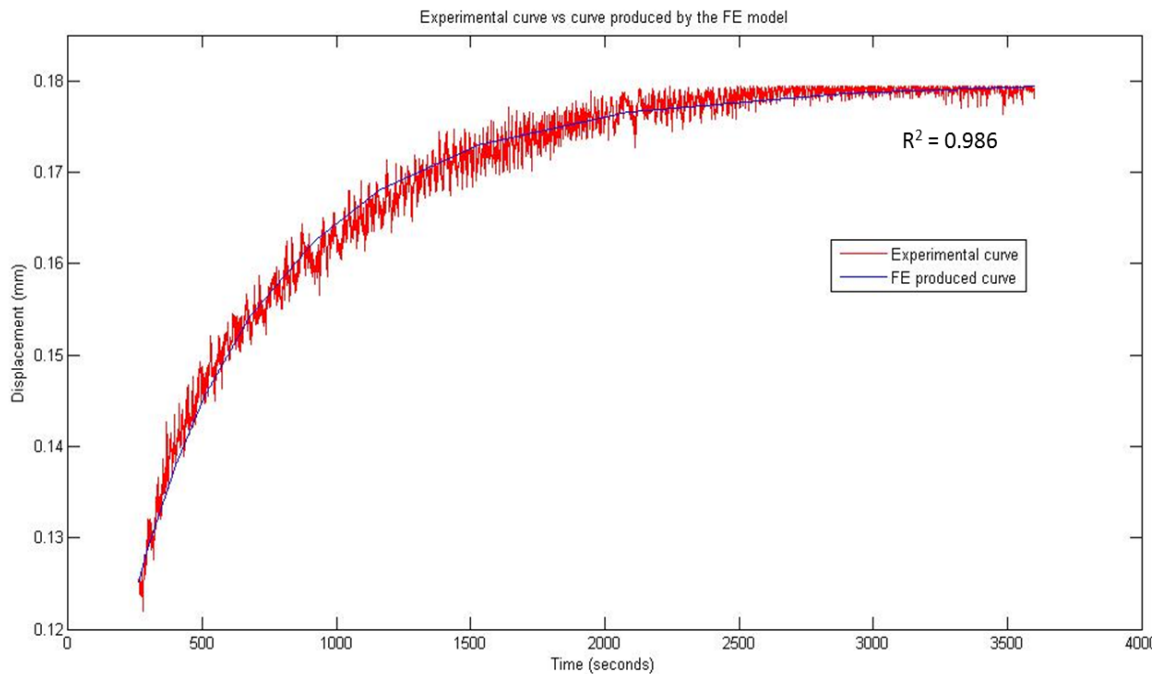


Figure 2-13: Experimental curve and curve produced by the finite element model

2.5 Methodologies for wear study

2.5.1 Calculating wear area using flexible film method

The flexible film method was used to measure the area of a surface (Lizhang 2010; Taylor 2012). In this project, this method was applied to determine the total surface area of the patella and the wear area on the cartilage.

A single layer of cling film was placed over the area to be measured, making sure that there were no air bubbles. The area was traced using a permanent marker as shown in Figure 2.14. The film was removed from the surface and carefully placed over a flat surface ensuring that the film was not stretched. A photograph of the marked film was taken with a ruler next to it. This procedure was repeated 3 times on the same area. The area inside the marked region was calculated using ImagePro Plus.

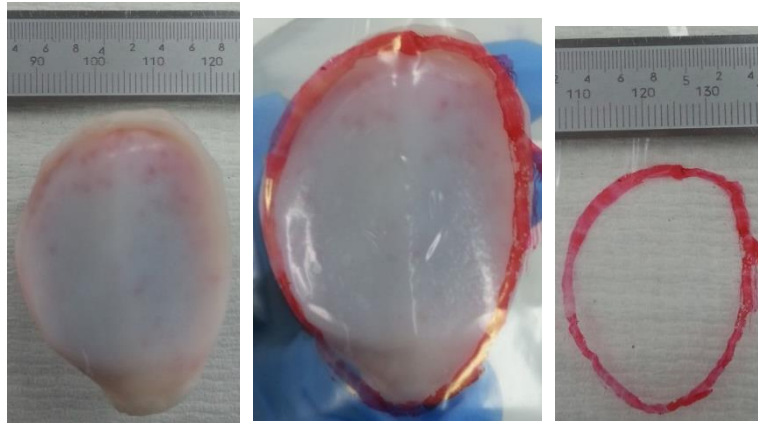


Figure 2-14: Measuring the area of patella cartilage (a) Images of the patella for measurement (b) flexible film over the patella (c) image of the film for calculation

A study by (Taylor, 2012) validated this method by measuring the area of a known defect on a custom made metal acetabular cup. The cup was designed in Solidworks and the defects were created using a laser sintering machine. The area known from the design was compared to the calculated area from the ImagePro Plus, which showed good repeatability and accuracy. For an actual area of 281.32 mm² the flexible film reading was 263.32 ± 10.39 mm².

2.5.2 Validating Accutrans for obtaining cartilage replicas

Microset was used to obtain replicas from the cartilage surface to measure the surface roughness using Talysurf. This thesis introduced the application of Alicona to measure surface roughness of the cartilage from the wear study. Microset was not compatible with the Alicona method due to various reasons and therefore AccuTrans molds were used to obtain the replicas.

AccuTrans moulds were firmer and the geometry of the replica was maintained when removed from the sample. Upon scanning both replicas in the Alicona IF G5, the results were much clearer using AccuTrans compared to Microset. The black glossy surface finish of the Microset caused reflections, which resulted in areas of missing data (Figure 2.15). AccuTrans with its brown colour and matt finish allowed better-quality image capture (Figure 2.16).

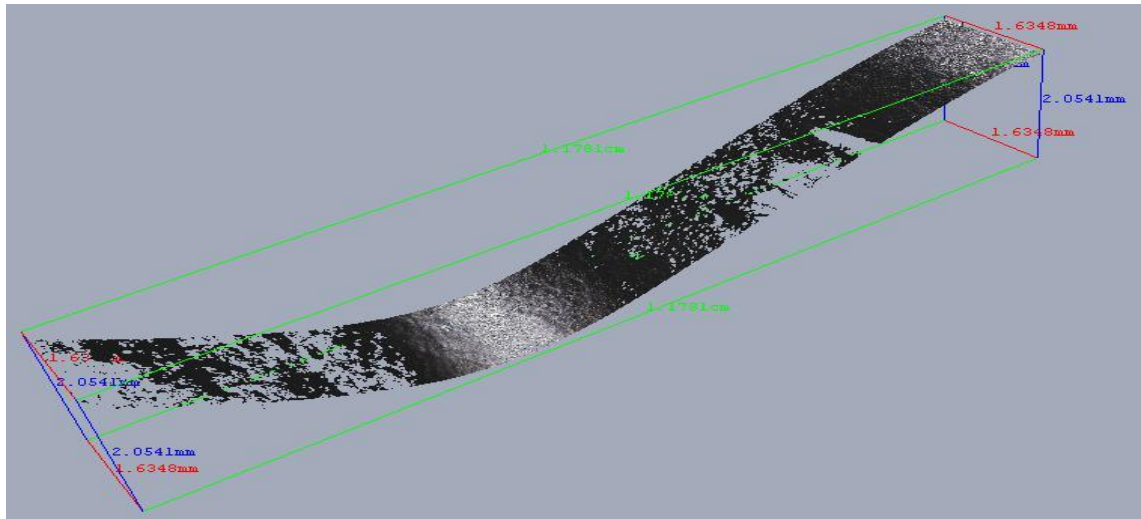


Figure 2-15: : Patella cartilage scan from Microset

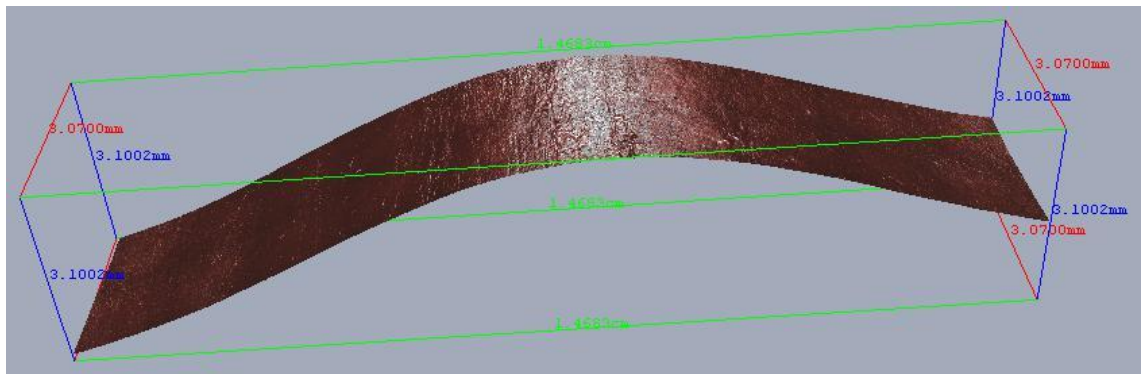


Figure 2-16: : Patella cartilage scan from AccuTrans

Therefore, it was concluded that AccuTrans was the most suitable material to make replicas for the natural joints. This section details the validation of the use of AccuTrans as the replica material.

Talysurf Surface profilometer was used to measure the surface roughness of a roughness standard with an Ra of 0.5 μm and another standard with an Ra of 0.8 μm (Figure 2.17) . This was compared to the Ra measured from the replicas of these standards taken using Microset and AccuTrans molds. Three lines each were taken for each measurements and three molds each were taken using each replica material. The mean roughness values and the 95% confidence limits for the measured standard and the replica molds are shown in Figure 2.18



Figure 2-17: Roughness standard used to measure the Ra for 0.8 μ m

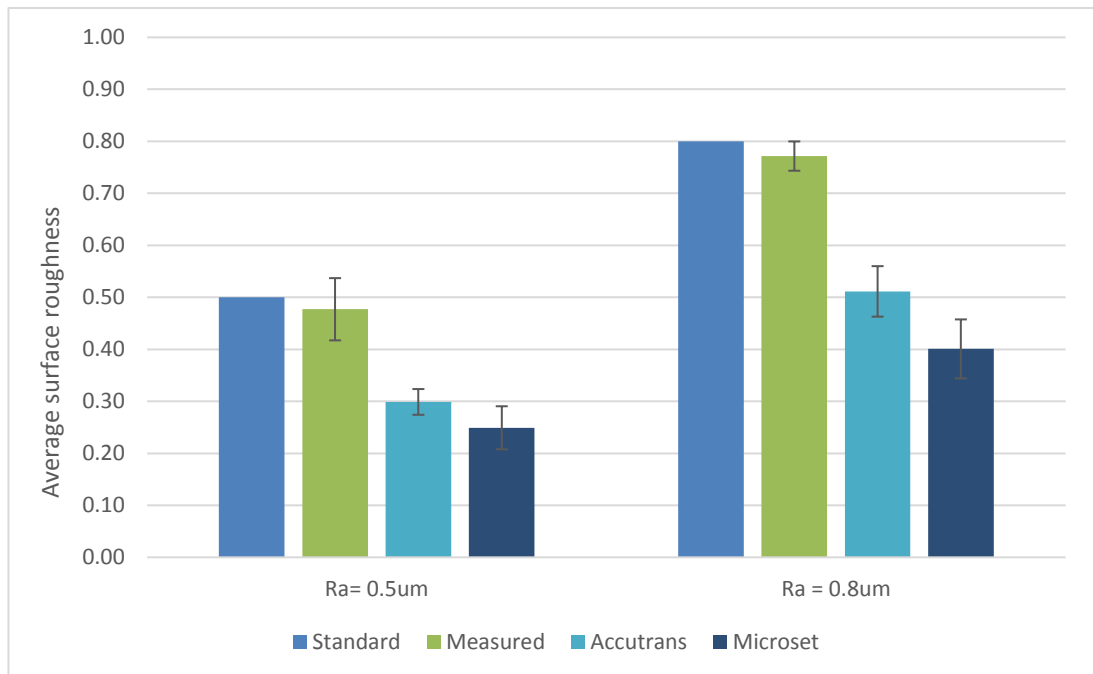


Figure 2-18: Surface roughness of the actual standard, measured standard on Talysurf, measured from AccuTrans replicas and Microset replicas

The surface roughness measured from the AccuTrans molds were closer to the roughness of the actual standard measured using Talysurf compared to the roughness measured using Microset molds. This shows that the AccuTrans is more accurate than Microset for replicating the surface and hence suitable for the purpose of this study. This method shows good repeatability as the error bars were small in both cases. But neither of them were accurate, as the readings were significantly lower than the measured roughness. However, as this is only used for relative comparison of roughness in pre and post wear study, this is still valid for the purpose of the study.

2.6 Methods for statistical analysis

For every experiment a minimum of 6 samples were tested and each measurement was taken at least 3 times for each quantity. Microsoft Excel (version 2010, Microsoft), SPSS version 21.0 (IBM Corp, 2012) and OriginPro version 8.5.1 (OriginLab; Northampton, MA) was used to analyse the numerical data in this project.

The results are presented as the mean ($n \geq 6$) \pm 95 % confidence limits. The descriptive statistics part in the data analysis package of Microsoft Excel was used to calculate the mean, 95% confidence intervals ($\alpha = 0.05$) and standard deviation.

$$95\% \text{ confidence limit} = \text{Mean} \pm t_{5\%}(n - 1) \times \text{standard error}$$

where, n is the sample size,

standard error = standard deviation / \sqrt{n}

when $n=6$, $t_{5\%}(n-1) = 2.447$

Student t-test was carried out using SPSS to compare the means of two groups of data. If there were more than two groups, One-way analysis of variance (ANOVA) was used to compare the means of these groups. A p-value under 0.05 was accepted as significant and those that showed a minimum significant difference (MSD) were further analysed using Tukey test. OriginPro was used to carry out the ANOVA and also a Tukey test as necessary.

Chapter 3. Geometry of the patello-femoral joint

3.1 Introduction

The aim of this project was to develop a methodology to investigate the biomechanics and wear of the natural patello-femoral joint (PFJ). Before commencing this it was essential to investigate an appropriate animal model of the PFJ and understand its characteristics. The purpose was to choose an animal model which had dimensions similar to that of the human joint. The animal model should have cartilage with similar material characteristics to the cartilage of the human tissue that would potentially require osteochondral transplantation. Availability, ease of dissection, repeatability and comparison to other methods were also factors that needed to be considered. Bovine and porcine PFJs were available as the possible alternatives for the animal model at this stage of methodology development.

This chapter describes the study undertaken to investigate the geometry of the bovine and porcine PFJ. This was important since the geometry of the articulating surfaces can influence the contact mechanics of the joint and hence the tribology. The dimensions of the patello-femoral sample, area of the patella and radius of curvature of the groove were determined to define the geometry of the joint. This chapter reports the methods, results and conclusions drawn from the studies carried out to characterise the bovine and porcine PFJs.

3.2 Materials and methods

Right knee joints from 6 month old Large White pigs and 18 month old cows (n=6) were used in this study. All the joints were healthy and had shiny, white and slippery cartilage with no visible defects.

3.2.1 Dissection of the patello-femoral joint

As shown in Figure 3.1, the bovine patella was separated from the patello-femoral groove by removing the soft tissues around it that kept the PFJ intact. The patella was then cleaned using a scalpel to remove all the soft tissues around it and making sure the cartilage was not damaged.

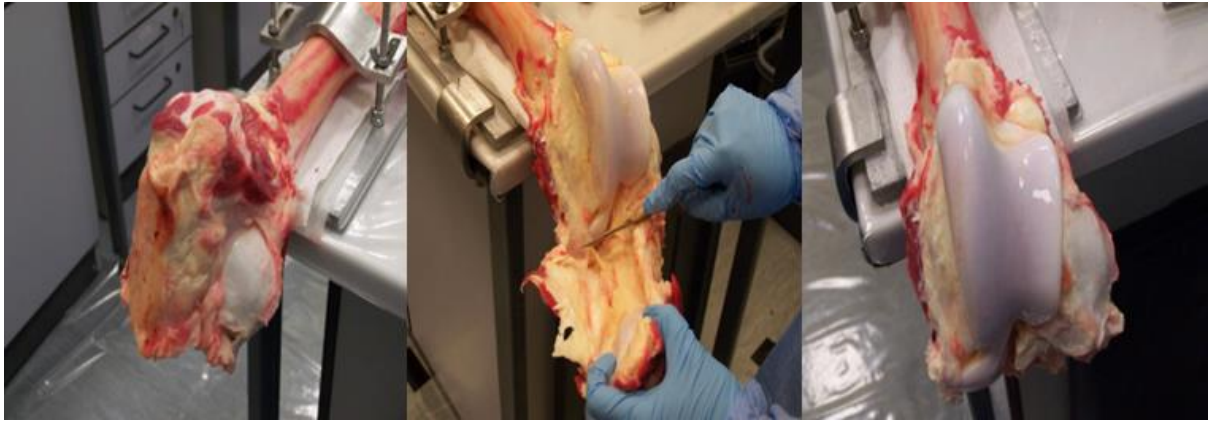


Figure 3-1: Dissection of a bovine knee joint to separate the patella and the patello-femoral groove. Left to right: Bovine femur with intact PFJ, Soft tissues removed to obtain the patella, patello-femoral groove exposed

In porcine dissection, the femur was separated from the tibia and hip. The soft tissue around the knee was removed using a scalpel to separate the tibia from the intact knee. To cut the femur from the hip, most of the soft tissues around the rest of the leg were removed and the femur was secured in a vice. The femur was cut using a hacksaw to remove the hip, leaving approximately half the length of the femur. The patella was removed from the femoral groove and both components were cleaned using a scalpel to remove any soft tissues around the bone without damaging the cartilage. A cleaned patella and femur are shown in Figure 3.2.



Figure 3-2: Porcine femoral groove (left) and patella (right) with all the soft tissues removed

3.2.2 Dimensions of the joint

The bovine and porcine PFJs were dissected to obtain the patella and groove as described in Section 3.2.1 and 3.2.2 respectively. The patello-femoral groove was cut from the femur ensuring all the cartilage surface of the groove was retained. The typical size of the bovine and porcine grooves is shown in Figure 3.3.

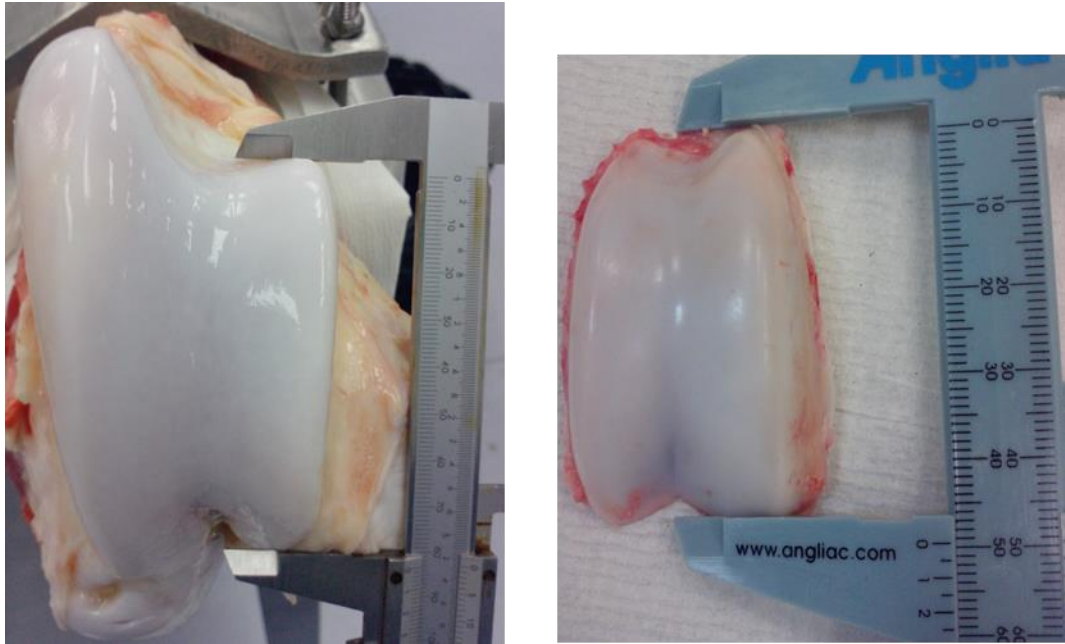


Figure 3-3: Typical size of the bovine (left) and porcine (right) patello-femoral grooves respectively

The measurements for the dimensions (height, length and width) of the patella and the groove were taken using a Vernier Calliper. Each measurement was taken 3 times for each of the 6 samples. The dimensions obtained for this study are illustrated in Figure 3.4 and described below:

- Patellar length ($L_{(p)}$): distance from the apex (inferior) to the base (superior).
- Patellar width ($W_{(p)}$): distance between the medial and lateral cartilage surface.
- Patellar height ($H_{(p)}$): distance from the articular surface to the retropatellar surface was measured by placing the Vernier Calliper at the middle of the patellar length.
- Patello-femoral length ($Lg_{(m)}$ and $Lg_{(l)}$): distance from the superior to the inferior edge of the articular cartilage on the medial and lateral side respectively.
- Patello-femoral width ($W_{(g)}$): distance between the medial and lateral side

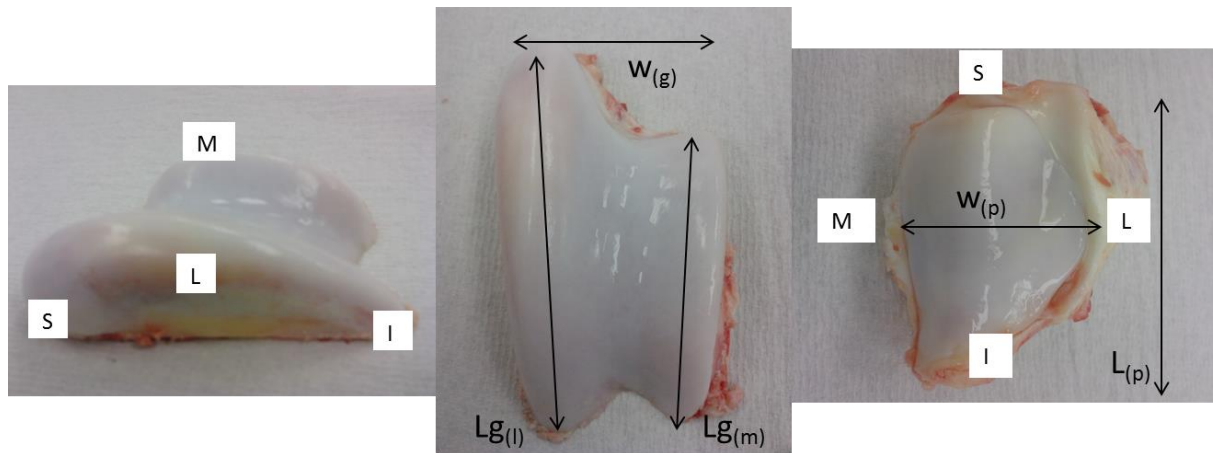


Figure 3-4: Dimensions of the femoral groove and patella.

M=medial, L=lateral, S=superior, I= inferior

Lg(l)= length of lateral groove, Lg(m)= length of medial groove, W(g)= width of the groove

L(p)= length of patella, W(p)= width of patella

3.2.3 Area of patella

The area of the articular surface of the patella was determined by overlaying the flexible film method described in Chapter 2 Section 2.5.

3.2.4 Radius of curvature of the patello-femoral groove

Three methods were investigated to measure the radius of curvature (RoC) of the patello-femoral groove using porcine samples. The first method used a Vernier Calliper to measure the dimensions of the sample from which the curvature was calculated. The second method used an LVDT to trace the curvature from which the radius was measured. The final method used a Micro-CT to scan the sample to show the curvature of the groove for each Micro-CT section. These methods were assessed and compared; and one was chosen for use in this study based on the accuracy and consistency of the method.

Porcine legs were dissected to obtain the samples as described in Section 3.2.1. The sample was fixed in PMMA cement such that the articulating surface of the femoral groove was parallel to the base of the cemented sample. Once the samples were prepared, they were refrigerated (4°C) or frozen (-20°C) until the measurement was carried out.

The same 6 samples were tested using the 3 methods to ensure consistency and reliability of data.

3.2.4.1 Vernier Calliper method

A Vernier Scale Calliper was used to measure the dimensions of the samples. The instrument was always verified using a known gauge block before each test. The height and length of the femoral groove were measured as shown in Figure 3.5.

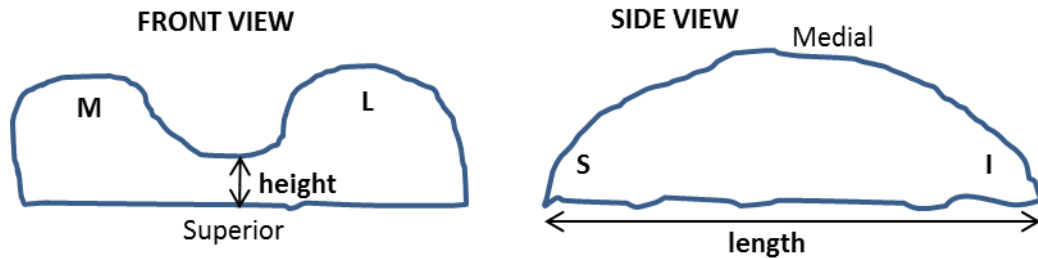


Figure 3-5: Taking the measurements from the sample using the Vernier Calliper.
Left: Femoral groove in the Frontal plane. Right: Femoral groove in the Sagittal plane

The length was measured from the superior end to the inferior end of the patello-femoral cartilage. The height was calculated by placing the sample between the Vernier Calliper such that the lower end of the Vernier touched the flat base of the sample and the top part rested on the midpoint of the patello-femoral groove (found using the previously measured length). Each measurement was taken 3 times for each sample.

Using the Pythagoras theorem, the RoC was calculated as shown in Equation 1 and as explained in Figure 3.6.

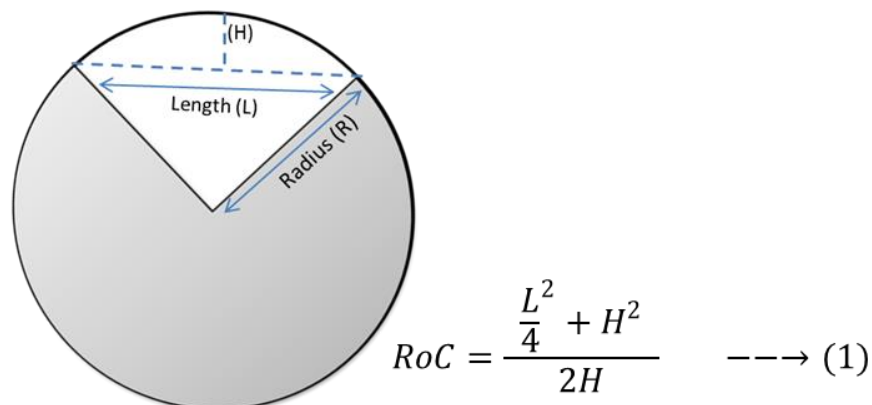


Figure 3-6: Diagram explaining the radius of curvature calculation in equation 1

3.2.4.2 LVDT method

A differential transducer was used to trace the curvature of the groove to determine the radius of curvature of the patello-femoral groove. The LVDT set up on the porcine samples

is shown in Figure 3.7. The position of the LVDT and its course of perpendicular displacement in the groove with respect to the reference line are shown in Figure 3.8.

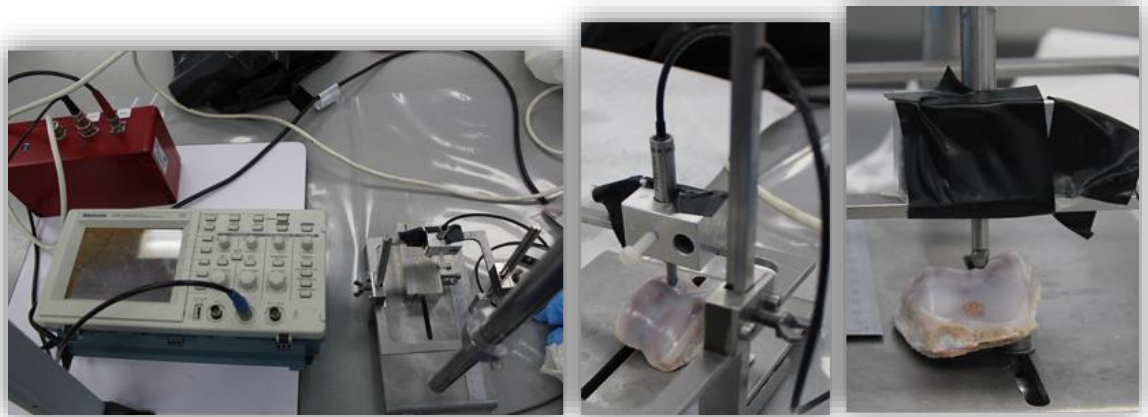


Figure 3-7: Sample set up for LVDT study: Left- LVDT equipment, Right- LVDT needle on the sample surface.

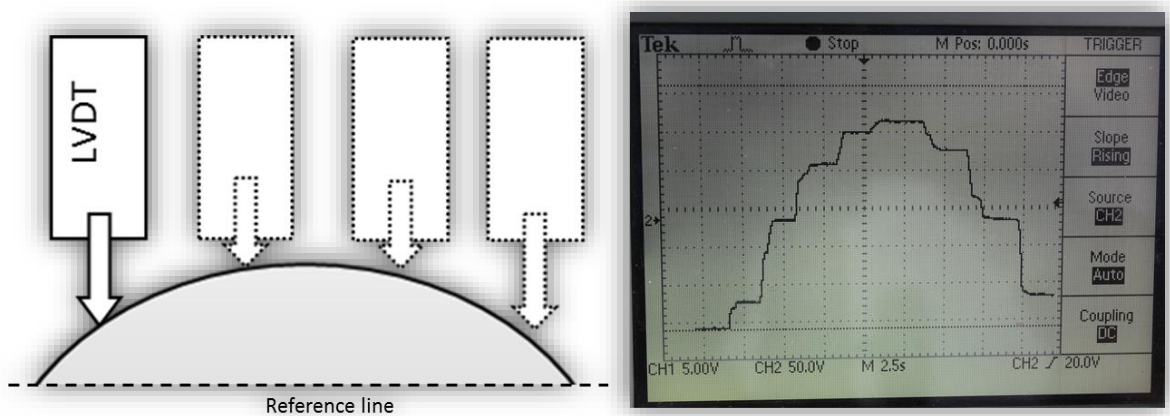


Figure 3-8: Movement of LVDT tracking the groove (left) and the output from the LVDT (right)

The LVDT consisted of a needle end (Figure 3.7, extreme right) which was positioned on top of the cartilage surface. The output from the LVDT tracked the course of vertical displacement of this needle from the reference point, which was the bottom of the sample (Figure 3.8, left), as it moved from the superior end to the inferior end of the patello-femoral groove. The LVDT recorded the distance between the tip of the needle and the bottom of the sample (reference line) every 5 mm. This was used as an input into SolidWorks as shown in Figure 3.9. An arc was drawn over the perpendicular lines (the height recorded by the LVDT) covering as many tips as possible. The radius of the arc, as shown in Figure 3.9, determined in SolidWorks, gave the RoC.

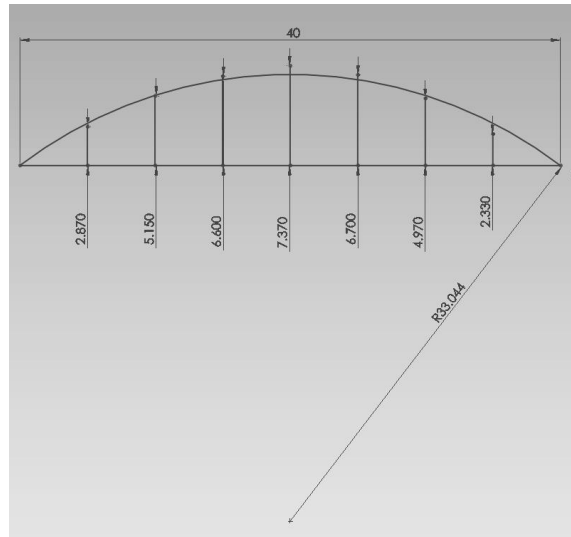


Figure 3-9: The displacement from the LVDT plotted against the reference line and an arc of known radius drawn

3.2.4.3 Micro-CT method

A Micro-CT as described in Chapter 2 Section 2.2 was also used to determine the RoC of the femoral groove. Two HDCs (high density crystals) were placed on either end of the patello-femoral surface to mark the radius of the groove. This helped to track the Micro-CT slice that marked the RoC of the groove from the stack of Micro-CT image slices for that sample.

The samples were thawed and placed inside a sealed bag ready to be scanned. The bag was then placed in a cylindrical container in such a way that the articulating surface was facing upwards. The specimens were then scanned using Micro-CT. A series of images were obtained along an orthogonal axis to the patello-femoral cartilage surface with an isotropic voxel dimension of 26 μm . 240 slices of each sample were taken and the slices that showed the HDCs were taken for analysis. ScanIP software environment (Simpleware Ltd, Exeter, UK) was used to perform the subsequent image processing and analysis.

The slices were analysed to select 3 slices with both visible HDCs. The Micro-CT slice/image is shown in Figure 3.10 and the bright white dots on the surface are the HDCs. These mark the curvature of the groove and hence a circle was drawn to connect the two crystals. These images obtained from the Micro-CT scanner had a 5 mm scale embedded in the image. This was used as a scale factor in Image Pro Plus to draw a circle of known radius using the software. The radius of the circle gave the RoC for the sample. The measurement was repeated 3 times on each image for each of the 6 samples.

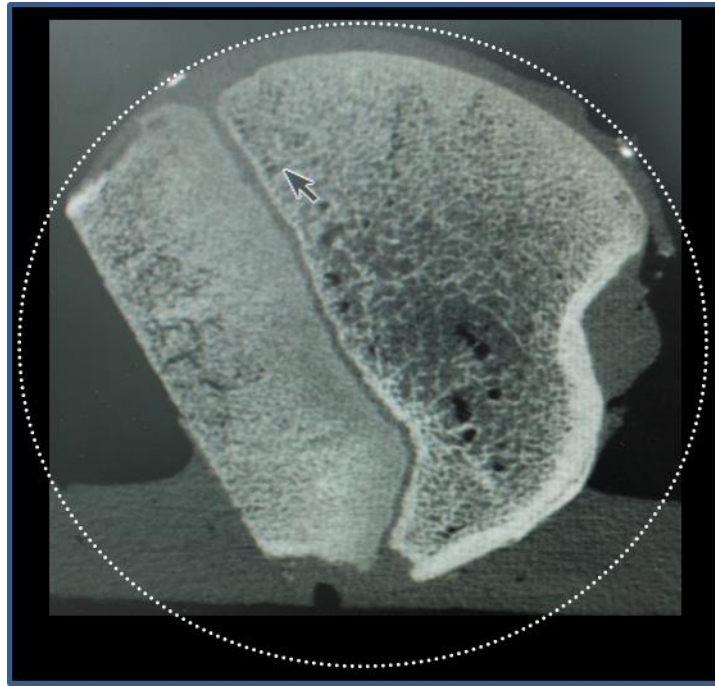


Figure 3-10: Micro-CT image showing the slice containing the crystals and a circle of known radius drawn connecting the crystals using ImagePro Plus

3.2.4.4 Evaluating the methodologies

The results (n=6) from these three methods were analysed to evaluate and compare the three methodologies. The average radii calculated using Vernier caliper, Micro-CT and LVDT were 27.61 ± 4.41 mm, 29.96 ± 1.29 mm and 30.90 ± 3.03 mm respectively.

Micro-CT technique was the most direct method, though there are inherent assumptions associated with image distortion. The 95% confidence limit shows the least variation in the results. Micro-CT also needed the minimal number of calculations; therefore the room for error was minimal. Therefore, the results were considered to be the most accurate amongst the three.

The radius of curvature for each sample was calculated 3 times using the Vernier and Micro-CT method but only once for LVDT. The LVDT method was also time consuming and complex; leaving more room for error. Therefore, this method was omitted and further analysis was carried to compare the Micro-CT and Vernier Calliper methods.

Analysing the Micro-CT and Vernier Caliper results using Student t-test showed no significant difference ($p=0.193$) in the RoC found between the two techniques. The Vernier Calliper method was less time consuming and unlike Micro-CT the measurements could be

taken straight after dissection. Therefore, the Vernier calliper method was used throughout the study to find the RoC.

3.3 Results

The dimensions of the bovine and porcine patellae and patello-femoral grooves are presented in Table 3.1 as determined by the Vernier Calliper method. Bar graphs representing the size of the bovine and porcine patello-femoral groove and patella are shown in Figures 3.12 and 3.13 respectively. The bovine groove was much deeper than the porcine groove and had a prominent anterior projection on its lateral condyle.

Table 3-1: Dimensions (mm) of the porcine and bovine patella and patello-femoral groove. Data is presented as the mean (n=6) ± 95% confidence limits

Mean ± 95% CL		
	Porcine	Bovine
Lg_(m)	49.2 ± 2.0	114.5 ± 9.4
Lg_(l)	46.5 ± 2.3	84.6 ± 7.2
W_(g)	31.6 ± 2.0	64.4 ± 6.0
H_(p)	27.9 ± 2.4	51.6 ± 10.2
L_(p)	38.8 ± 2.3	66.9 ± 10.9
W_(p)	28.1 ± 2.0	49.8 ± 11.5

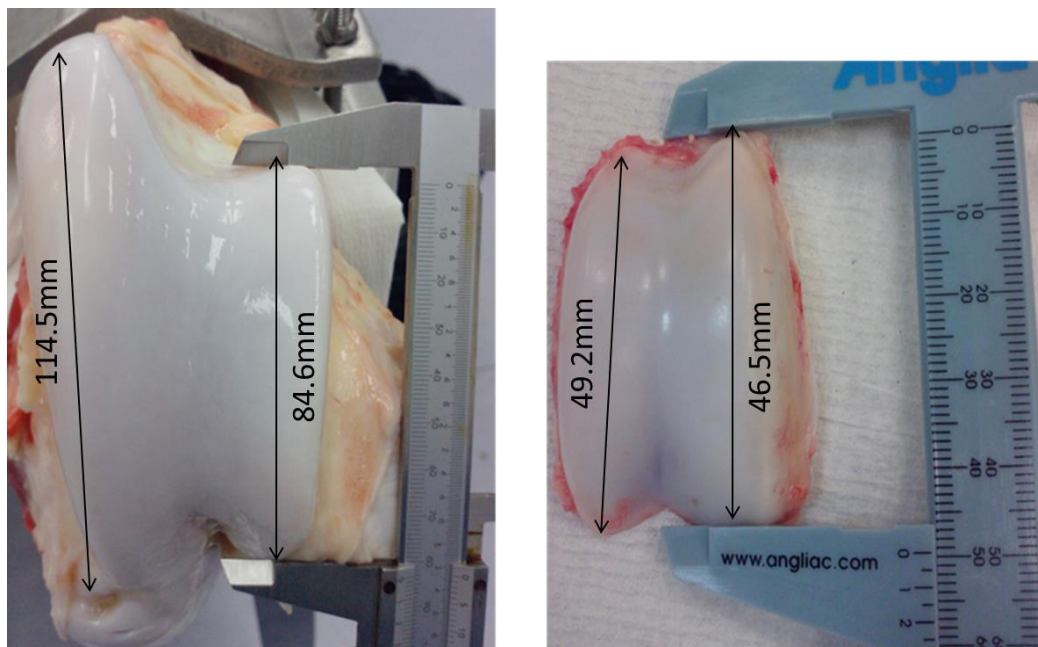


Figure 3-11: Mean lengths of the two condyles of bovine and porcine PFJ

The mean radius of curvature of the porcine groove and the true area of the patellar cartilage were 31.96 ± 2.7 mm and 878.0 ± 141.6 mm² respectively. The bovine patello-

femoral groove had a mean radius of curvature of 63.5 ± 5.4 mm and a patellar area of 2842.7 ± 299.42 mm². The elliptical shape of the femur increases the contact between the femur and the tibia and the radius of curvature of the condyles projects the patella anteriorly to increase the lever arm of the extensor muscles.

In order to compare the size of the bovine and porcine patello-femoral joint, the measurements were compared using Student's t-test. There was a statistically significant difference ($p < 0.05$) between all the dimensions. The results clearly showed that the bovine joints were twice as large as the porcine joints. The lateral condyles on the bovine joints were smaller than the medial condyles. The superior-inferior length of the articular surface of the medial condyle in the bovine groove was almost 30 mm longer than the length of the lateral articular surface.

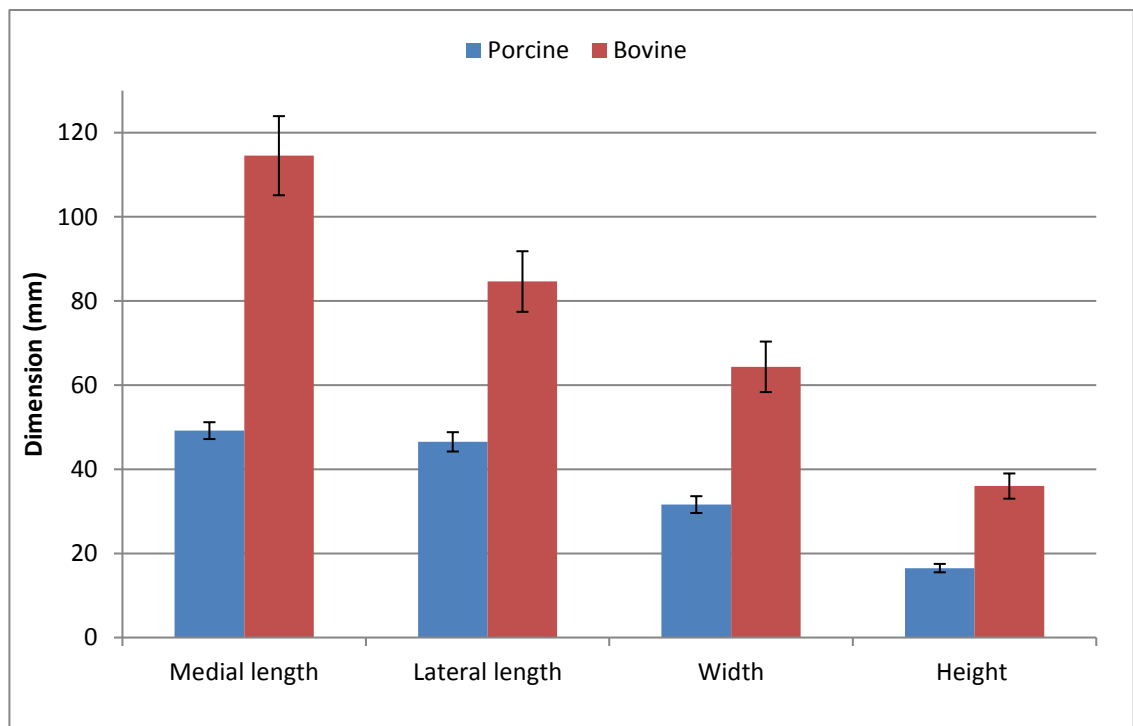


Figure 3-12: Sizes of bovine and porcine femoral grooves. Data is presented as the mean ($n=6$) \pm 95% confidence limits

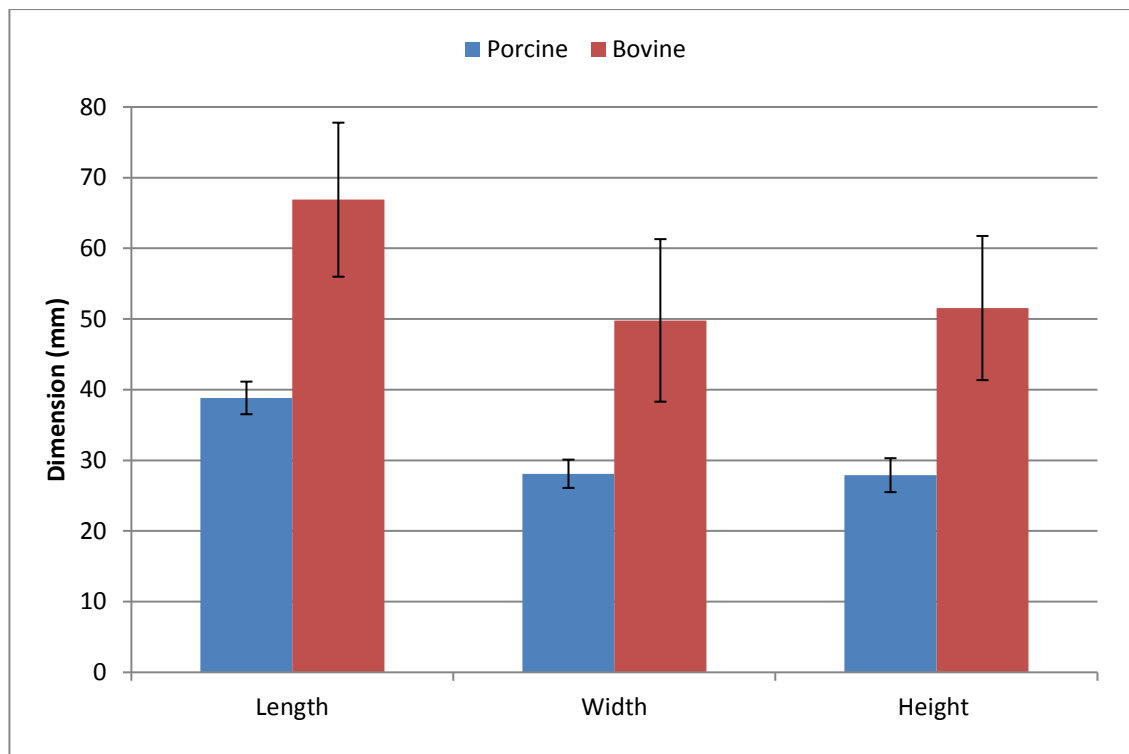


Figure 3-13: Sizes of bovine and porcine patella. Data is presented as the mean (n=6) ± 95% confidence limits

3.4 Discussion

The aim of this study was to investigate the geometry of the bovine and porcine PFJ to establish a suitable animal model that closely replicates the human PFJ in order to develop the whole PFJ tribological simulation model. The dimensions of the patella and the patello-femoral region were measured; the area of the patella and the RoC of the patello-femoral region were also calculated to define the geometry. In addition, the investigation of the geometry was also used to address the possibility of developing a simpler geometrical configuration as an interim step prior to developing the whole joint model.

Animal models are used to develop new methodologies and can be used to compare the effect of various abnormalities in the joint. Although it might not provide quantitative data that is directly comparable to humans, there is still the possibility to compare the level of damage caused by various abnormalities or change in parameters applied to a normal joint. This study was used to develop an animal model that was then used for the contact mechanics and wear studies in the single station knee simulator.

Porcine and bovine knees were dissected to study the anatomy of the joints and the dissection process was analysed. In terms of dissection, the porcine samples were easier to obtain compared to the bovine samples. As the bovine bones were much denser than

porcine bone, cutting the patellar groove was more difficult with the bovine knee. This was because the bovine joints were skeletally mature but the porcine joints were from young pigs which still had its growth plates. Figure 3.14 shows the Micro-CT image of a patello-femoral groove from a porcine joint used in this study. The growth plate in the bone is clearly visible in this image, which shows that the animal has not reached skeletal maturity.

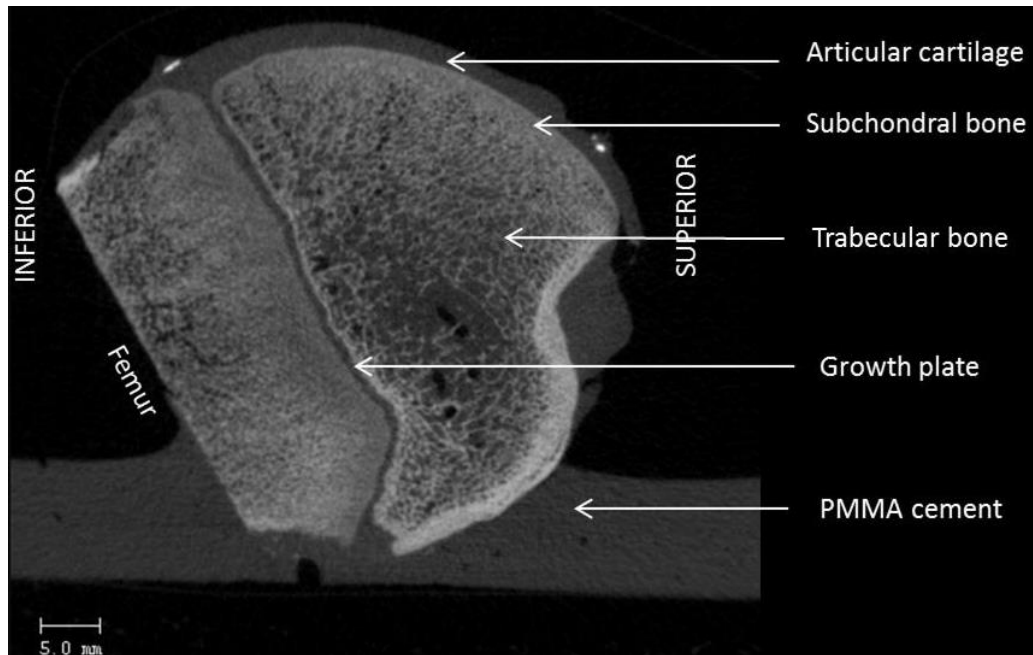


Figure 3-14: Labelled Micro-CT image of the porcine patello-femoral groove

Bovine joints were much larger compared to porcine joints and required different equipment for the dissection procedure. The porcine joints were much easier to handle during dissection and hence made the equipment more efficient as there were no issues of slipping or gripping while undertaking dissection. Overall, the porcine dissection took less time and effort; it was also possible to obtain more accurate sample geometry due to the ease of dissection.

The dimensions of the patella and the patello-femoral groove obtained from the bovine and porcine samples showed that the bovine joints were much larger than the porcine. These were compared to the anatomical dimensions in 92 human patellae obtained in a study carried out by Baldwin et al. They also calculated the dimensions using a Vernier calliper after the patellae were obtained from a total knee arthroplasty (Baldwin and House, 2005).

The dimensions of the tissues from the three species are shown in Figure 3.15. The length of human patella was 35.7 mm and that of porcine and bovine was 38.83 mm and 66.88 mm

respectively. The bovine patella was almost double the length of the human patella whereas the porcine was closer in length to the human patellae. Similarly, the height of the bovine tissue was higher than the porcine and human patella. The width of the human patella was 46.1 mm whereas that of the porcine and bovine was 28.1 mm and 49.8 mm respectively. This was the only dimension in which the bovine was similar to humans.

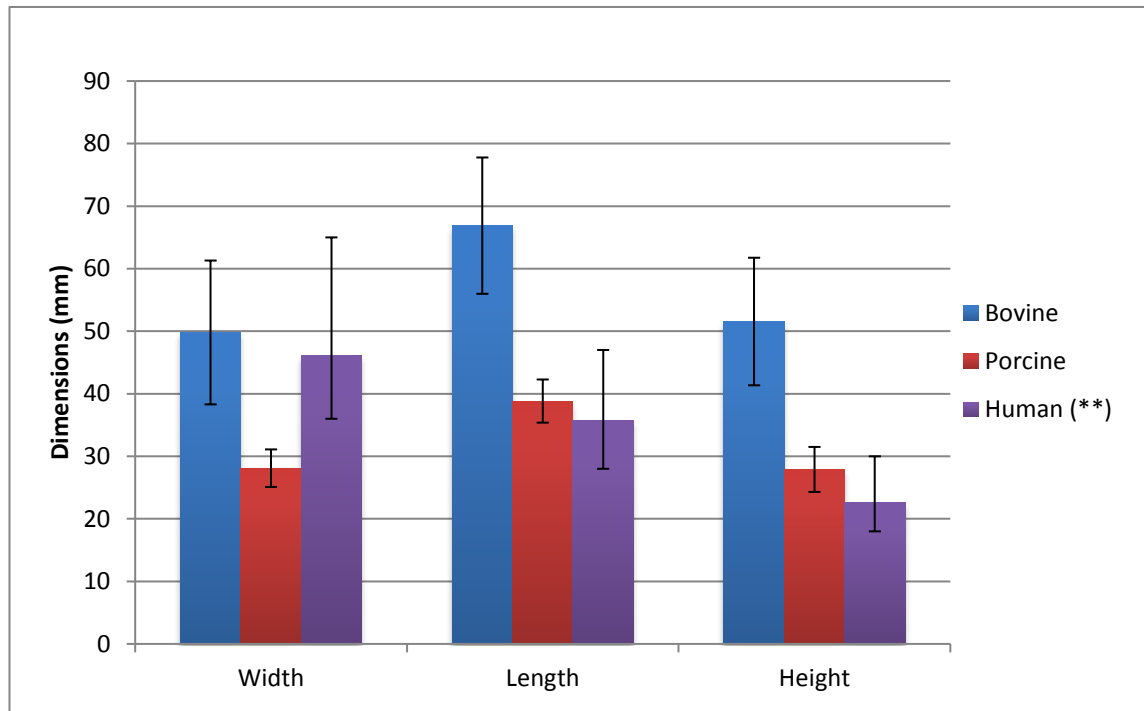


Figure 3-15: The sizes of patella from bovine, porcine and human** (Baldwin & House 2005)

The height of the porcine patella was 27.9 ± 2.4 and that of bovine was 51.6 ± 10.2 . The biomechanics of the PFJ requires the patella displacing the lever arm from the patello-femoral groove pivot point in order to reduce the quadriceps forces. A larger patella height reduces the work of the muscles that deals with the joint reaction forces (Sullivan *et al.*, 2014). The human patella was much closer in height to the porcine than to the bovine. Therefore, it would have shown similar biomechanics in the joint.

Vernier calliper, LVDT and Micro-CT were used to measure the RoC of the samples. The three methods were compared to validate the most repeatable methods for measuring the RoC. This method could also be used to find the centre of rotation of the femur when the PFJ is assembled in the simulator for contact mechanics and wear study discussed in Chapter 8 and 9 respectively.

The Vernier calliper method was the easiest and least time consuming technique. It could also be used to measure each sample before they are cemented in the fixtures. Reduced time ensured that the samples were less exposed to air and drying and hence had less chance of dehydration. Compared to the other techniques, the Vernier calliper method also enabled measurement with least risk of physical damage to the cartilage especially due to least handling time required.

The results supported the accuracy of the Vernier calliper method compared to the other two techniques. The Micro-CT method was the most accurate due to the least calculation requirements and least chance for error and the results using the Vernier calliper method were compared to the Micro-CT method results. There was no significant difference ($p>0.05$) between the results obtained using the Micro-CT and Vernier calliper methods.

A porcine model has previously been developed under similar conditions for investigating the tribology and biomechanics of the tibio femoral joint (Liu *et al.*, 2015). Therefore, using the same model for the PFJ study was also advantageous in terms of repeatability of tests and comparing the results between the two joints.

Investigating the geometry of the joint helped to establish an animal model and to consider the possibility of a pin-on-plate system for preliminary studies. The methods developed in this study such as measuring the RoC of the patello-femoral groove and calculating the area of the patella were also applied in other parts of this project. The RoC was also used to locate the centre of rotation of the femur while fixing the sample in the simulator. The method of calculating the area was used to measure the wear area in the samples after the wear tests.

3.5 Conclusion

Methodologies have been evaluated to determine the geometry of the PFJ and applied to the porcine and bovine joints. The geometry and size of the porcine joint was more comparable than the bovine joint, to the human joint. It was also more accurate to prepare the porcine samples for the tests than using a bovine joint. Therefore, the porcine joint was chosen as the animal model for this project.

Chapter 4. Material properties of the porcine patello-femoral cartilage

4.1 Introduction

The aim of this project was to develop a methodology to investigate the biomechanics and wear of the natural patello-femoral joint (PFJ). The geometry of porcine and bovine PFJs was compared in Chapter 3 to determine an appropriate animal model for this project. It was concluded that the porcine joint was more comparable to the human joint and hence, the porcine PFJ was investigated further in this part of the study.

This chapter describes the characterisation of the porcine patello-femoral cartilage. The aim of this part of the study was to characterise the material properties of various locations of the porcine patello-femoral cartilage by measuring the thickness, equilibrium elastic modulus and the permeability of the cartilage. The equilibrium elastic modulus is the resistance of a material to the change in its length and permeability is a measure of the ability of that material to transfer a fluid through it. The biphasic material properties of the cartilage from the various locations in the PFJ were then compared.

4.2 Materials and methods

Right knee joints from 6 month old Large White pigs (n=6) were used in this study. All the joints were healthy and had shiny, white and slippery cartilage with no visible defects. The PFJs were dissected as described in Chapter 3 Section 3.2.1.

4.2.1 Osteochondral plugs

Osteochondral plugs (n=6) obtained from the porcine femoral groove and patella were used to determine the material properties of the porcine cartilage. Osteochondral plugs ($\varnothing=8.5$ mm) were extracted from 8 locations in the femoral region and 5 locations in the patella as shown in Figure 4.1. The location of each plug marked in Figure 4.1 is described in Table 4.1.

The purpose of this study was to compare the material properties of cartilage in the femoral groove with that of the patella. Therefore, a number of locations were selected to cover most of the area in the joint.

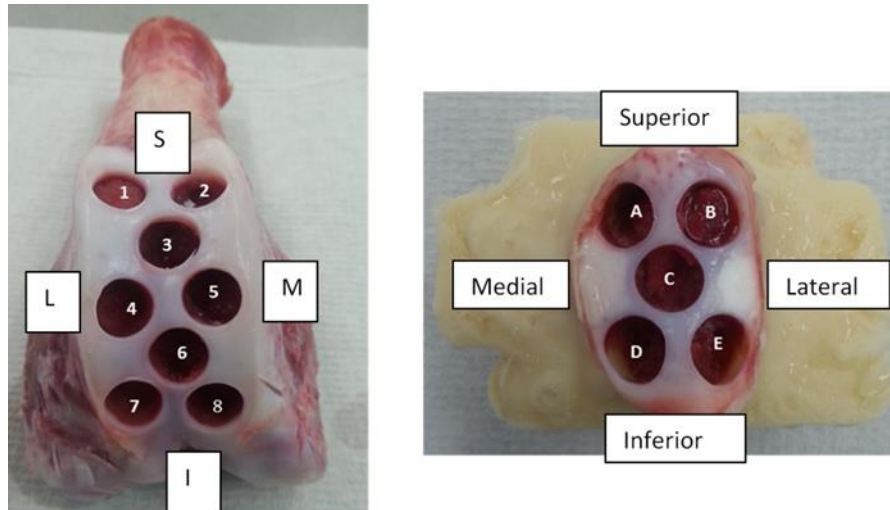


Figure 4-1: Locations of plugs obtained from the femur (left) and patella (right)
M/L = medial lateral, S/I = Superior Inferior

Table 4-1: The location of each plug marked in Figure 4.1

Label of plug	Location
Plug-1	Femur- Superior/Lateral
Plug-2	Femur- Superior/Medial
Plug-3	Femur- Superior/Femoral groove
Plug-4	Femur- Condyle/ Lateral
Plug-5	Femur- Condyle/ Medial
Plug-6	Femur- Inferior/Femoral groove
Plug-7	Femur- Inferior/Lateral
Plug-8	Femur- Inferior/Medial
Plug-a	Patella- Superior/Medial
Plug-b	Patella- Superior/Lateral
Plug-c	Patella- Centre Ridge
Plug-d	Patella- Inferior/Medial
Plug-e	Patella- Inferior/Lateral

Each plug was wrapped in a piece of tissue drenched with PBS and frozen in a labelled container at -20°C for up to 3 months, until further use. The frozen plugs were left at room temperature for up to 2h for thawing before each test. Once defrosted, a plug was tested the same day. Previous studies have shown that this freeze-thaw process does not affect the frictional properties (Forster and Fisher, 1996) or material properties (Athanasίου *et al.*, 1991) of the articular cartilage up to a maximum of two freeze-thaw cycles.

4.2.2 Method to determine the equilibrium elastic modulus and permeability

Indentation testing was carried out to determine the mechanical behaviour of the cartilage and to determine the equilibrium elastic modulus and permeability. A custom made indentation rig as described in Chapter 2 Section 2.4.1 was used for the mechanical testing of the osteochondral plugs. A flat rigid indenter of diameter 2.5 mm was used for the indentation tests. This gave an indenter to plug ratio of 1:3.2.

A finite element model was used to obtain the equilibrium elastic modulus and permeability using the experimental data obtained from the indentation tests and the thickness of cartilage from the needle probe tests as described in Chapter 2 Section 2.4. The FE model assumed that cartilage has a constant permeability. The deformation in the model was kept between 5-10% of the cartilage thickness. The weight of the indenter and the load applied to the cartilage can affect the deformation. The higher load causes a higher deformation and hence affects the FE model. This FE model (Pawaskar, Fisher and Jin, 2010) has been discussed in detail in Chapter 2 Section 2.4.4.

4.2.3 Method to determine the thickness of the cartilage

After indentation, the osteochondral plugs were rested for at least 1 hour before determining the thickness of the cartilage. The thickness was measured by the needle indentation method using an Instron, as described in Chapter 2 Section 2.4.3. Each osteochondral plug was pierced 6 times and the mean (n=6) for each plug was taken.

4.3 Results

The mean permeability, equilibrium elastic modulus and thickness of each location of plug are shown in Figures 4.2- 4.7. The labelling of the plugs and their location was shown in Table 4.1. Statistical analysis was carried out to compare the data between sample groups. Single factor ANOVA revealed no significant variation ($p=0.074$) between the mean permeability of any of the sample groups. However, there was significant variation amongst the groups for the equilibrium elastic modulus ($p=0.017$) as well as the thickness of the cartilage ($p=0.026$).

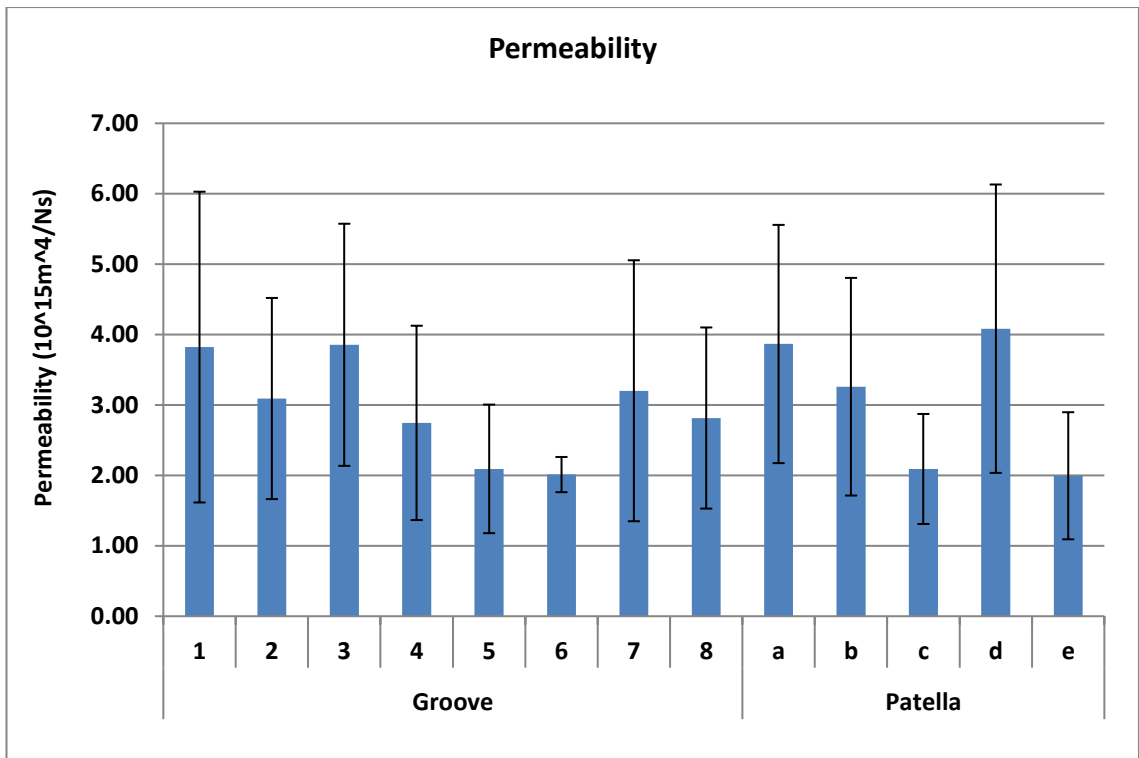


Figure 4-2: Permeability of cartilage in the porcine patello-femoral joint. The data is presented as the mean (n=6-12) ± 95% confidence limits. Data was analysed by one way analysis of variance which revealed no significant variation in the data (p= 0.074)

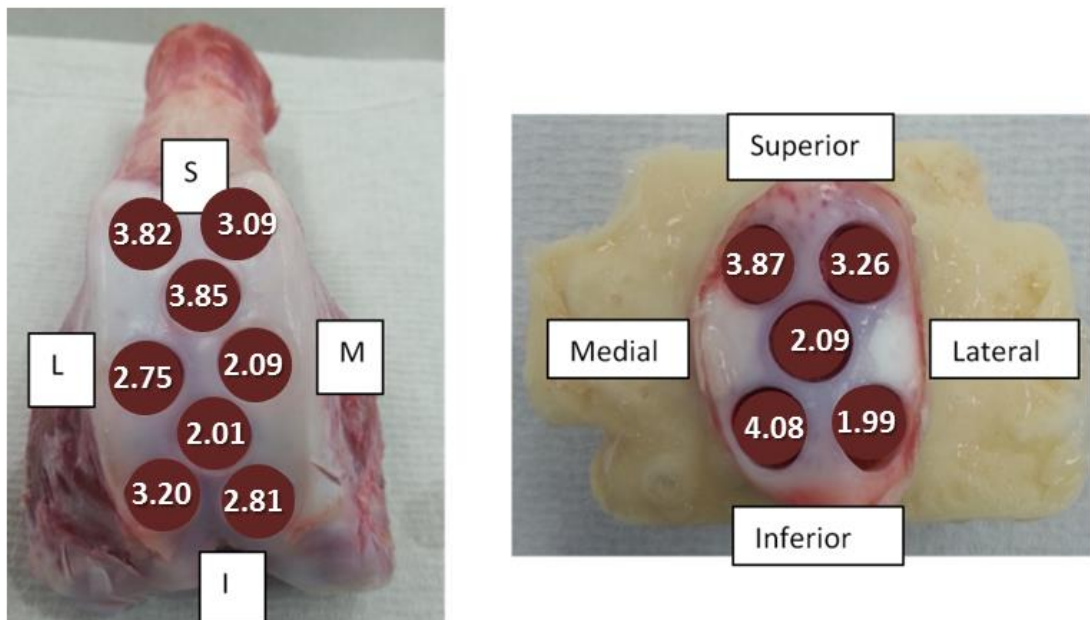


Figure 4-3: Permeability of cartilage in the porcine patello-femoral joint

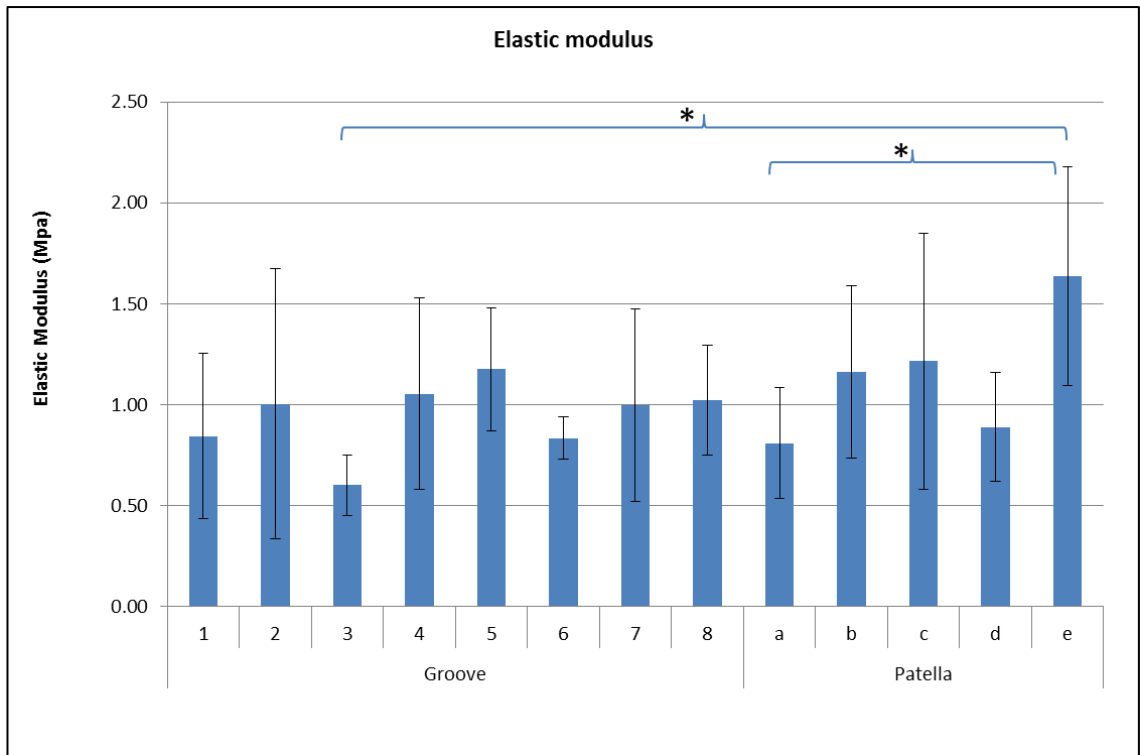


Figure 4-4: Equilibrium elastic modulus of cartilage in the porcine patello-femoral joint. The data is presented as the mean (n=6-12) ± 95% confidence limits. Data was analysed by one way analysis of variance followed by the Tukey test (p<0.05) which revealed a significantly higher equilibrium elastic modulus (*) in location E (patella inferior/ lateral) compared to locations A (patella superior medial) and 3 (superior femoral groove).

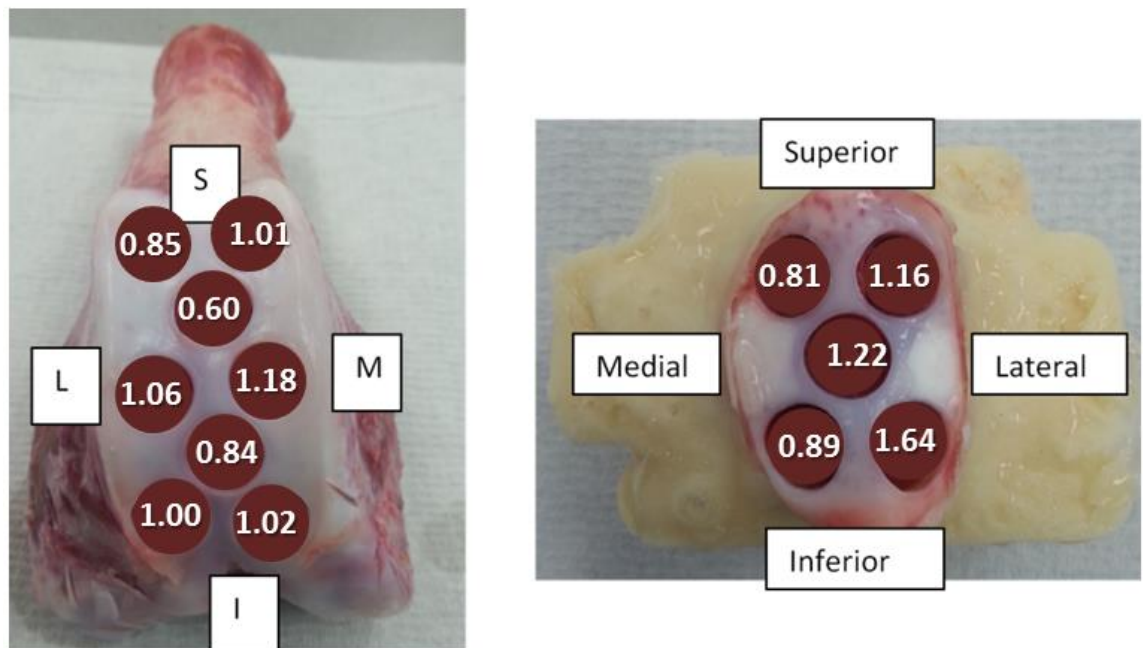


Figure 4-5: Equilibrium elastic modulus of cartilage in the porcine patello-femoral joint

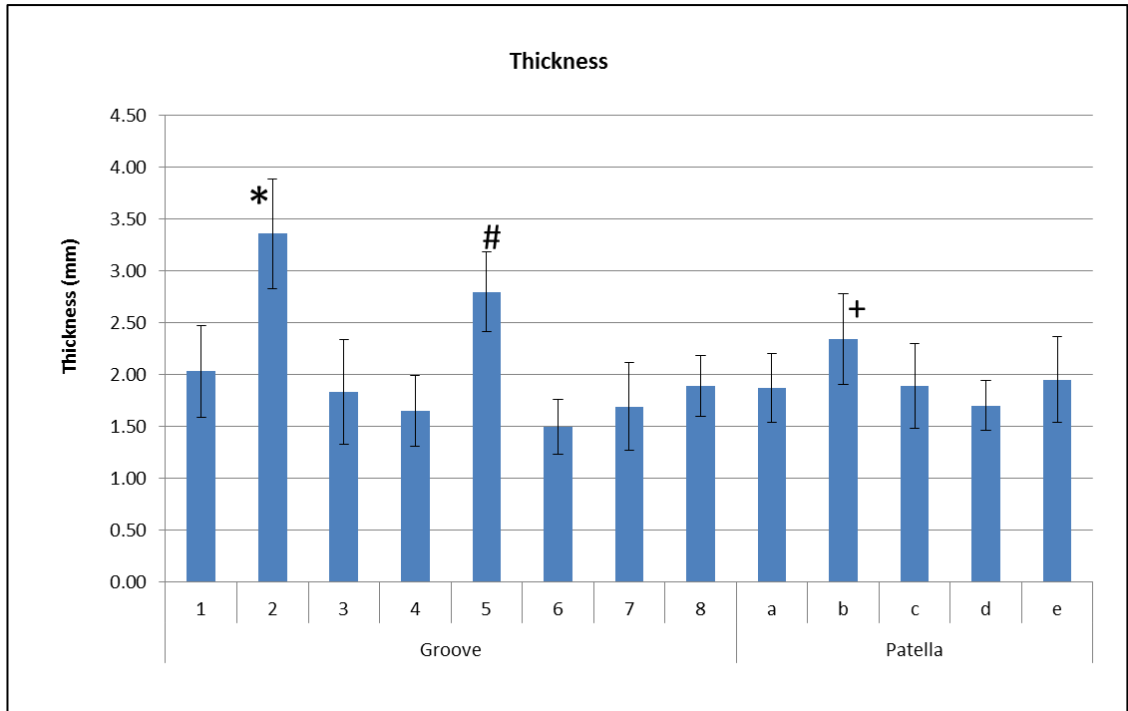


Figure 4-6: Thickness of cartilage in the porcine patello-femoral joint. The data is presented as the mean (n=6-12) ± 95% confidence limits. Data was analysed by one way analysis of variance followed by the Tukey test (p<0.05). It showed that the cartilage in Plug-2 (superior medial femur) was significantly thicker than others except Plug- 5 (medial femoral condyle), Plug-5 was significantly thicker than others except Plug- 1 (superior lateral femur), 2 (superior medial femur) and B (superior lateral patella); and Plug-B was significantly thicker than Plug- 6 (inferior trochlea).

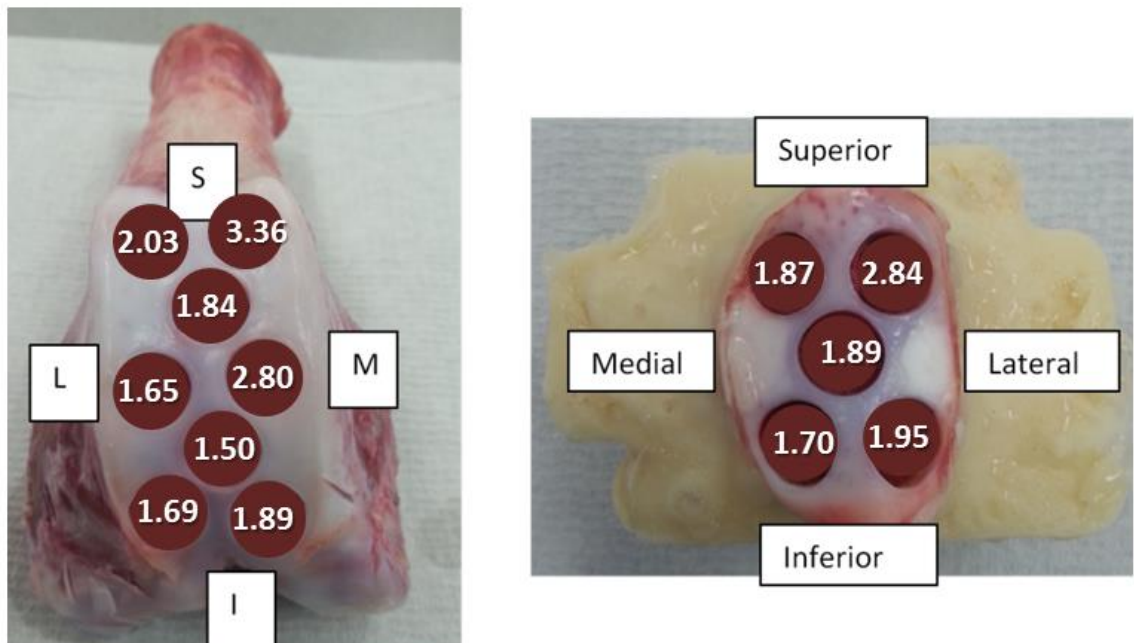


Figure 4-7: Thickness of cartilage in the porcine patello-femoral joint

The equilibrium elastic modulus of cartilage plugs from the groove ranged from 0.6 MPa in Plug-3 to 1.18 MPa in Plug-5 and in the patella the range was from 0.81 MPa in Plug-A to 1.64 MPa in Plug-E. The overall equilibrium elastic modulus in the patella (1.28 ± 0.36 MPa) was slightly higher than the equilibrium elastic modulus in the groove (0.96 ± 0.14 MPa). The mean permeability in the patella ($3.16 \pm 0.77 \times 10^{-15} \text{m}^4/\text{Ns}$) was similar to the permeability in the groove ($2.99 \pm 0.57 \times 10^{-15} \text{m}^4/\text{Ns}$). It ranged from $2.01 \times 10^{-15} \text{m}^4/\text{Ns}$ of Plug-6 to $3.85 \times 10^{-15} \text{m}^4/\text{Ns}$ of Plug-3 in the groove and $1.99 \times 10^{-15} \text{m}^4/\text{Ns}$ of Plug-E to $4.08 \times 10^{-15} \text{m}^4/\text{Ns}$ of Plug-D in the patella.

In the groove, the highest equilibrium elastic modulus was 1.18 MPa in Plug-5 which was from the middle of the medial condyle. Plug-4 from the middle of the lateral condyle had a modulus of 1.06 MPa which was also higher compared to the other locations. The lowest modulus was 0.60 MPa for Plug-3 from the superior end of the femoral groove, which was significantly lower than the modulus of Plug-E from the inferior end of the lateral patellar facet. The equilibrium elastic modulus of Plug-E was also significantly higher compared to Plug-A from the superior end of the medial patellar facet.

The thickness of cartilage in the groove ranged from 1.5 mm in Plug-6 to 3.36 mm in Plug-2 and in the patella the range was from 1.7 mm in Plug-D to 2.34 mm in Plug-B. Even though the overall thickness of cartilage in the groove (2.09 ± 0.33 mm) and the patella (2.06 ± 0.29 mm) was similar, the variation between the locations within the groove and the patella was noticeable in Figure 4.6.

In the groove, the highest thickness was 3.36 ± 0.53 mm for Plug-2 which was from the superior-medial location. Plug-5 from the middle of the medial condyle had a thickness of 2.8 ± 0.57 mm which was also larger compared to the rest of the sites. The thickness of Plug-2 was significantly higher than every other plug except Plug-5. The thinnest cartilage was 1.65 ± 0.47 mm on Plug-4 from the middle of the lateral condyle followed by the second thinnest for Plug-3 at 1.84 ± 0.50 mm from the central ridge on the superior femoral groove. The average thickness of the patella was 2.06 mm, with the thickest at 2.34 mm (Plug-B) and the thinnest location at 1.7 mm (Plug-D).

A Tukey test ($p < 0.05$) was carried out on the equilibrium elastic modulus and thickness of the cartilage to determine where the significant differences existed between the sample groups. The equilibrium elastic modulus of Plug-E on the patella was significantly higher

than Plug-A in the patella and Plug-3 in the femoral groove. The Tukey test also showed that the thickness of Plug-2 was significantly higher than all other plugs from the patella as well as the groove, except Plug-5. Similarly, the thickness of Plug-5 was significantly higher than all the other plugs except for Plug-1 and Plug-2 in the femoral groove and Plug-b from the patella. However, Plug-B had significantly thicker cartilage compared to Plug-6.

The overall material properties of the groove and patella samples are presented in Table 4.2. The 95% confidence limit shows that the variation in the data was greatest for the permeability compared to the other two material properties. There was no significant difference ($p < 0.05$) between the overall material properties in the patella and the patello-femoral groove.

Table 4-2: Overall (mean \pm 95% CL) material properties of cartilage in the porcine femoral groove and the patella

	Femoral groove	Patella
Thickness (mm)	2.09 \pm 0.33	2.06 \pm 0.29
Equilibrium elastic modulus (MPa)	0.96 \pm 0.14	1.28 \pm 0.36
Permeability ($\times 10^{-15} \text{m}^4/\text{Ns}$)	2.99 \pm 0.57	3.16 \pm 0.77

The overall thickness of the cartilage in the patello-femoral groove (2.09 \pm 0.33 mm) was similar to the cartilage thickness in the patella (2.06 \pm 0.29 mm). The difference between the permeability of the patella (2.99 \pm 0.57 $\times 10^{-15} \text{m}^4/\text{Ns}$) and the femoral groove (3.16 \pm 0.77 $\times 10^{-15} \text{m}^4/\text{Ns}$) was below 6%. However, the overall equilibrium elastic modulus of the femoral groove (0.96 \pm 0.14 MPa) was 25% lower than the patella (1.28 \pm 0.36 MPa).

4.4 Discussion

This study characterised the material properties of articular cartilage from the porcine PFJ by measuring the thickness, permeability and equilibrium elastic modulus of the cartilage. The needle probe method was used to measure the thickness of the cartilage and indentation tests were carried out to determine the equilibrium elastic modulus and permeability.

Osteochondral plugs were obtained from various locations in the patella and the femur. The position for each plug was marked on the PFJ sample before starting the extraction. This ensured that the plugs were consistently obtained from the correct location of each sample.

Indentation can measure the interstitial fluid flow through the extracellular matrix (permeability) and the deformations of this matrix (equilibrium elastic modulus) as a response to the pressure applied over time. This method is widely used for the study of cartilage biomechanics for various reasons (Lu and Mow, 2008). Firstly, it does not require complex techniques to prepare the samples. Secondly, as the method is non-destructive the same samples can be used for further analysis such as measuring the thickness of cartilage and histology studies. Finally, the biphasic material properties are determined in situ on the bone. This provides a more relevant result than any other technique as it closely resembles the physiological condition of the tissue. However, the assumptions in the finite element model used to determine the results may not reflect the in situ conditions as such. Cartilage is assumed to have constant permeability, and the cartilage is not homogenous or isotropic.

Unlike confined or unconfined compression, indentation resembles a closer physiological environment which allows correct measurements. Korhonen et al have shown that the young's modulus from confined and unconfined compression could be up to 79% lower compared to the indentation method (Korhonen *et al.*, 2002). This could be due to the damage that occurs to the fibrous tissue during sample preparation for the confined and unconfined tests.

During indentation, the load was applied perpendicular to the sample to ensure that the stress on the cartilage surface was uniform and it was axially symmetrical within the sample. Uneven contact could have led to higher stress concentration which in turn lead to tissue damage (Charles Swann, 1988).

In the current study, a 2.5 mm flat indenter was used, which gave an indenter to plug ratio of 1:3.2. Previous studies (McLure, 2012; Taylor, 2012; Fermor, 2013) conducted in the same lab by other authors used a 3 mm hemi-spherical indenter on porcine cartilage from the knee and hip. They used a 9 mm plug which gave an indenter to plug ratio of 1:3. They reported permeability in the order of $e-16m^4/Ns$ which was 10 times lower than that found in the current study. The equilibrium elastic modulus was also higher in these studies. These differences in elastic modulus and permeability can be due to the geometry of the indenter.

A hemi-spherical indenter can be beneficial for surfaces that are mostly curved as they require a small point of contact to obtain the correct results. With a hemi-spherical indenter the contact stress on the cartilage is higher, which resists the interstitial fluid flow to reduce

permeability. As the osteochondral plugs used in this study provided a considerably flat surface for indentation it was possible to use a flat indenter. A flat indenter provided a larger contact area between the indenter and the cartilage and hence reduced the contact stress at the surface. Higher contact stress can cause higher deformation which would have affected the validity of the FE model for this high deformation.

Equilibrium elastic modulus and permeability are affected by the load experienced by the cartilage within the joint. The equilibrium elastic modulus depends on the stress applied to the tissue and larger stress produces a higher equilibrium elastic modulus. Permeability allows the fluid to transport the nutrients across the tissue. It helps the tissue to withstand high compressive loads and maintain its fluid film lubrication, which ultimately reduces wear. Permeability decreases through the layers of cartilage across a pressure gradient (Landínez-Parra, Garzón-Alvarado and Vanegas-Acosta, 2012).

Due to the biphasic nature of cartilage, permeability is a primary factor when determining its deformation and visco-elastic properties. Previous studies (Lai and Mow, 1980) that have investigated the permeability of cartilage have shown a wide range of values on a very low scale (in the order of 10^{-15} to 10^{-16} m⁴N/s). The porosity of cartilage is very high, (20-30% solid content and 70-80% water content), therefore the low permeability and strong resistance to fluid flow is primarily due to the proteoglycan network's strong affinity for the water molecules. GAGs help to resist the interstitial fluid flow to reduce permeability (Maroudas 1968; Athanasiou et al. 1991; Setton et al. 1993).

Considering the biphasic nature of the cartilage, detecting the contact in the contact mechanics of a joint is an important factor for analysis. The boundary conditions of the fluid flow are dependent on the contact, which in turn affects the interstitial fluid pressurisation. During a creep indentation study, when the impermeable rigid indenter is applying a load to the cartilage, fluid flow cannot occur on the surface normal to the cartilage. On the other hand, in vivo flow will vary with the pressure difference across the two cartilage surfaces. Whether it is an experimental analysis with an indenter or the interface between two cartilage surfaces, there is a free flow in area with no contact (Pawaskar, Fisher and Jin, 2010).

Previous studies have shown that in the femoral groove the equilibrium elastic modulus is lower and the permeability is higher compared to the femoral condyles (Athanasiou *et al.*,

1991). In this study, the equilibrium elastic modulus of the femoral groove was 25% lower than the patella. A higher equilibrium elastic modulus would demonstrate stiffer cartilage which restricts the fluid flow. The patella had a higher equilibrium elastic modulus than the groove which means it was much stiffer than the cartilage in the groove. However, rather than showing a larger permeability in the groove the values for the patella and groove were very similar.

Greater stiffness leads to lower permeability and vice versa. Therefore, the region with a higher equilibrium elastic modulus normally shows lower permeability. Although the overall permeability was similar in the groove and the patella, at certain regions this difference was observed. Plug-E displayed the highest equilibrium elastic modulus and the lowest permeability. Plug-3 showed the lowest equilibrium elastic modulus and it had one of the highest levels of permeability as well.

After the indentation test was carried out, the osteochondral plugs were wrapped in tissue drenched with PBS and stored in the fridge for at least 1 hour before commencing the thickness measurements. This was carried out to allow the cartilage to recover to its normal state as the indentation would have deformed the cartilage (Fermor, 2013).

The 95% confidence limits showed that the variation of the thickness measurements was much smaller compared to the variation of the equilibrium elastic modulus and permeability. Therefore, there was a higher variation in the indentation results between each sample compared to the thickness measurements between the samples. This may be due to the sample itself or the methods used to measure these parameters. The samples were freeze-thawed which would have had a greater effect on the equilibrium elastic modulus and permeability rather than the thickness. The major effect could have been on permeability as there was significant variation between the location for the thickness and equilibrium elastic modulus but not on permeability.

The thickness of the cartilage in this study was measured using the needle probe method. There are other methods in the literature that are used to measure the thickness of cartilage in diarthrodial joints, as detailed in Section 1. 3.5. The needle probe method was compared to other methodologies by many researchers in the past (Pawaskar, Fisher and Jin, 2010; Abdelgaied Latif, Jin and Wilcox, 2012; McLure, 2012; Nebelung *et al.*, 2016). They applied

this methodology as it proved to be the most efficient method compared to the others with no significant difference in the results.

Nebelung et al measured the thickness of femoral cartilage using needle probe, MRI and histology methods (Nebelung *et al.*, 2016). Although all methods showed a large variation across the samples there were no significant differences ($p=0.063$) between the methods. Studies conducted by McLure (2012) in the same lab with the same equipment and conditions have also validated the needle probe method against recognized methods such as Shadowgraph method and Micro-CT method. This study is discussed in detail in Chapter 1 Section 1.2.4.3. These studies have shown the accuracy and reliability of the needle probe method in producing accurate values of cartilage thickness.

The Micro-CT method was most accurate due to having the least number of steps in the methods as well as fewer calculations and chances for human error. Although Micro-CT was shown to be the most accurate method of measurement as it takes a longer time it was not feasible for this study, especially due to the risk of the cartilage drying out.

In the current study, this needle probe technique was carried out using an Instron. This procedure carried out in a mechanical testing machine such as an Instron is a more accurate method compared to using a needle probe indenter. This is because the transition from the softer cartilage to the bone is much clearer in the Instron tests which make further measurement steps more accurate. Also, in a needle probe indenter the weight of the indenter has a significant role in characterising the thickness. A lighter weight will underestimate the thickness and a heavier indenter could indicate a higher thickness value. Abdelgaied Latif et al characterised the cartilage thickness of ovine facets and found that a weight of 3.5 N was necessary for that particular study to obtain the desired results (Abdelgaied Latif, Jin and Wilcox, 2012).

In the current study, the thickness measurement method involved piercing the cartilage and it was ensured that the holes were made as close to the centre of each plug as possible. This was done to avoid any errors caused by dehydration (if any, as it was continuously covered in PBS) or even excessive hydrophilic swelling (always wrapped in wet tissue rather than immersing in the liquid). Tissue closer to the centre was least likely to be affected by these factors.

Studies have shown that the thickness of cartilage decreases with age during skeletal maturity (Julkunen *et al.*, 2009; Fermor, 2013; Gannon *et al.*, 2015). There is also an increase in equilibrium elastic modulus with maturity which is mainly caused by the change in the arrangement of collagen fibres with age. There is evidence of differences in anatomical features and material properties between the joints of skeletally mature and young animals (Fermor 2013). The growth plate in the bone was clearly visible in the Micro-CT images taken from the samples used in this study, which shows that the animal has not reached skeletal maturity. In this study, the pigs were ~6 months old and the cartilage thickness was around 2 mm.

Cartilage thickness also varies with species. The thickness of the femoral groove in humans is ~3.57 mm (Athanasίου *et al.*, 1991), bovine is 1.37-1.52 mm (Athanasίου *et al.*, 1991; Fermor, 2013) and porcine is 1.7-2.4 mm (Fermor, 2013). The human cartilage is twice as thick compared to the other species. As humans have a bipedal posture unlike pigs and cows, there will be a larger load placed on human cartilage compared to the other species. This could be one of the reasons for the need of thicker cartilage in human knees.

The geometry of the joint can affect the characteristics of cartilage as the properties adapt to the appropriate functioning of the joint depending on its geometry. More congruent joints such as hips have thinner cartilage compared to less congruent joints such as a knee (Shepherd and Seedhom, 1999). Studies showed the presence of thinner cartilage in the hips compared to knees in porcine, bovine and ovine joints. The thickness in the hips (Taylor, 2012) were 1.22, 1.32 and 0.52 mm whereas that of the knees (Fermor, 2013) were 2.23, 1.28 and 0.71 mm respectively. Human cartilage was 80% thicker in the knees, bovine cartilage showed no difference and porcine cartilage was 37% thicker in the knees.

The structural composition of cartilage varies with depth. This will also contribute to the change in material properties. This study was limited to the surface layer of the cartilage whereas a number of other studies have shown a variation of properties across the layers (Ficat and Maroudas, 1975; Jurvelin, Buschmann and Hunziker, 1997; Treppo *et al.*, 2000; Chen *et al.*, 2001; Wang *et al.*, 2002). Boschetti *et al.* (2004) showed an increase in equilibrium elastic modulus and a decrease in permeability with depth. Studies have shown a higher permeability near the joint surface which helps create an improved fluid flow (Mccutchen, 1962; Maroudas and Bullough, 1968). However, the restricted fluid flow in the deep zone showed a lower permeability. This is supported by the tissue composition where

there is a higher collagen content and different orientation of its fibres in the deeper zone. Maroudas (1968) showed that this permeability is inversely proportional to the fixed charge density of the ECM.

Tissue composition plays a major role in the mechanical behaviour and functioning of the tissue. Ligaments acquire their tensile strength through collagen fibres that are orientated in the direction of stress whereas cartilage has cross-linked fibres that can withstand the swelling pressure of proteoglycans. Future studies could encompass histology studies to investigate the effect of various contents of the tissue and its effect on the properties of the cartilage.

4.5 Conclusion

This study characterised the porcine patello-femoral cartilage and determined its thickness, equilibrium elastic modulus and permeability. There were differences in properties within various regions in the patella and the femoral groove showing that the material properties can be location dependent. This data can be used to explain the suitability of this animal model as the surrogate for the actual human joint in the next chapter.

Chapter 5. Characterisation of the human patello-femoral joint

5.1 Introduction

The animal model developed during the course of this project aims to provide the basic information for future development of an in-vitro model using human cadaveric tissue for the pre-clinical testing of tissue substitutions in the PFJ. The work described in this chapter was carried out to characterise the human joint tissues by determining the geometry of the human PFJ and the material properties of its cartilage. The results from the studies of the human joint tissues were compared to the results obtained for the porcine and bovine joint tissues described in the previous chapter. This chapter compares the suitability of the animal model developed for this project.

5.2 Materials and methods

5.2.1 Materials

Six cadaveric human knees, 5 left knees and 1 right knee, were used for this study. The tissues were obtained with full ethical approval from Leeds West Research Ethics Committee [REC number 11/YH/0025]. The tissues were obtained from 4 female and 2 male donors with an age range of 52-85, with an average age of 64.5 years.

5.2.2 Dissection of human PFJ

The entire dissection process was carried out in a class II safety cabinet and any instruments in contact with the human tissue were specifically assigned for human tissue use only. The frozen samples were all defrosted overnight in a 4°C refrigerator before dissection.

A human knee with the soft tissue and patella removed is shown in Figure 5.1. The patella was separated from the femur using a scalpel. All tissues around the PFJ were removed. Observations such as the viscosity of synovial fluid, quality of the bone during cutting and the colour and condition of the cartilage were made for each sample during the dissection process and were recorded.



Figure 5-1: Human knee with the soft tissues and patella removed

5.2.3 Determining the geometry of human PFJ

The dimensions of the patella and patello-femoral groove were measured using a Vernier Caliper as described in Section 3.2.1. The area of the patella and the area of cartilage wear in the patello-femoral joint were measured using the flexible film method as described in Chapter 2 Section 2.5.

Dimensions of the patello-femoral groove and patella are illustrated in Figure 5.2. In the groove, $W_{(g)}$ is the width of the groove from one condyle to the other and $L_{(m)}$, $L_{(t)}$, $L_{(l)}$ are the lengths of the medial condyle, trochlea and lateral condyle respectively. These were determined with respect to the red line illustrated in Figure 5.2 which marks the beginning of the patello femoral groove from the main femoral condyles. In the patella, $W_{(p)}$ is the width measured from the most medial to the most lateral aspect of the patella of on its widest side and $L_{(p)}$ is the length of the patella covered in cartilage from the apex to base.

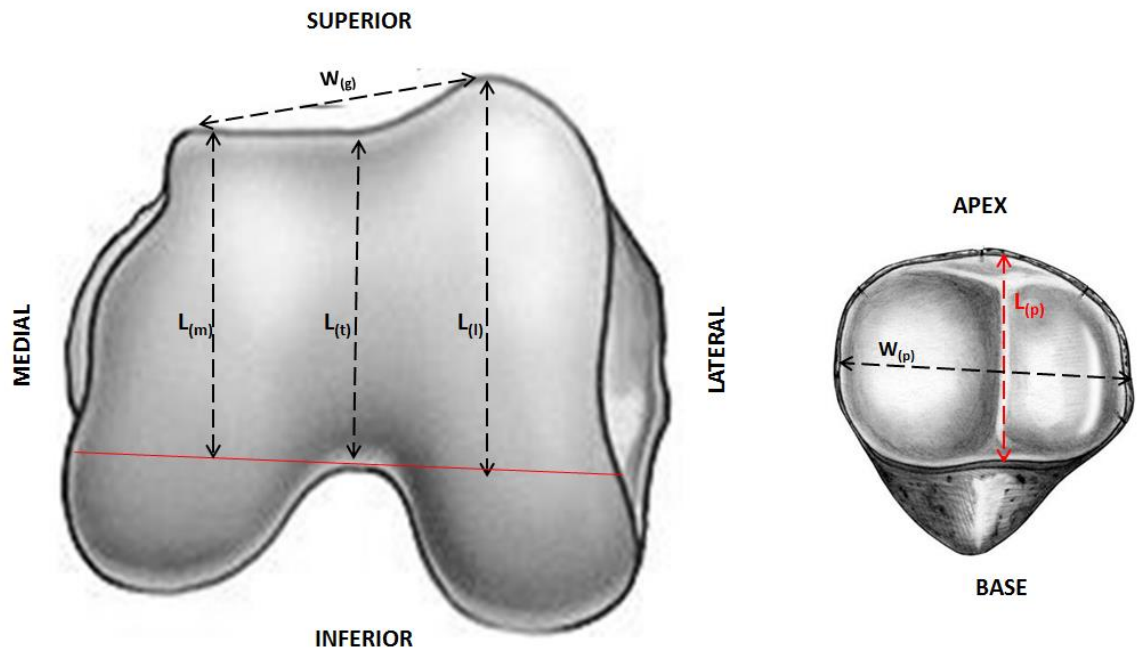


Figure 5-2: Dimensions of the left human patello-femoral groove and patella (n=6)

5.2.4 Obtaining the osteochondral plugs

The femur was held in a vice placed inside a class II safety cabinet. The entire osteochondral plug extraction process was carried out inside the safety cabinet. The patella was cemented into a metal tray using PMMA cement in order to secure it in the vice inside the cabinet for extracting the plugs. The plugs from the femoral groove were extracted on the same day as dissection.

Osteochondral plugs ($\phi=8.5$ mm) were extracted from 3 locations in the patello-femoral region and 2 locations in the patella. The location of plugs from the femur and patella is shown in Figure 5.3. The corresponding positions of the locations are explained in Table 5.1. Each plug was wrapped in a piece of tissue drenched with PBS and frozen in a labelled container at -20°C and was tested within a week.

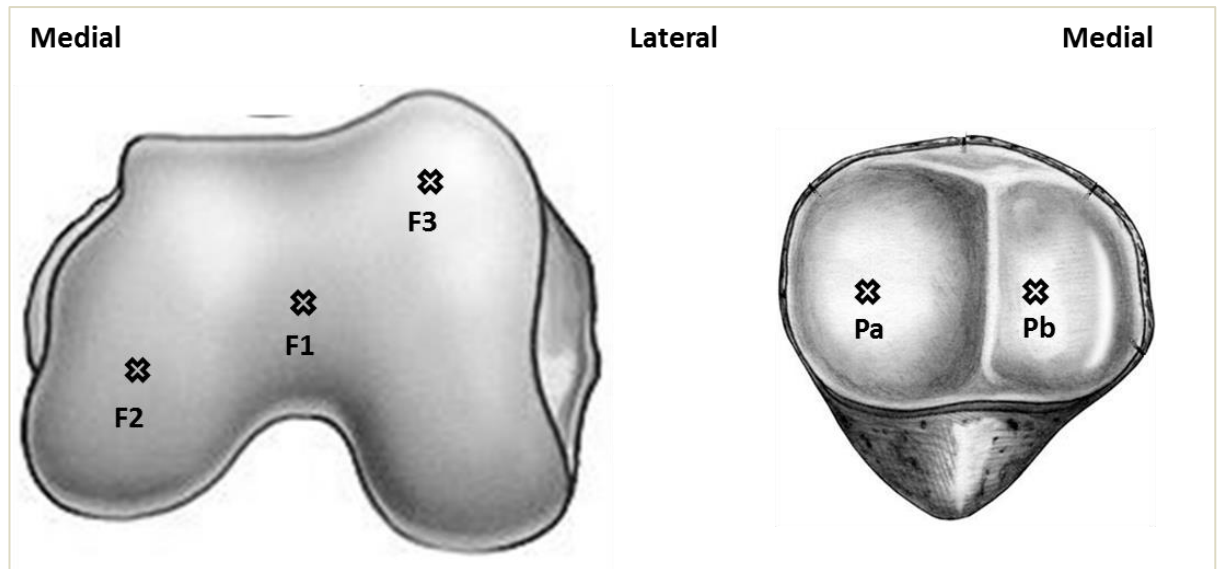


Figure 5-3: Location of osteochondral plugs from the left human PFJ (n=6)

Table 5-1: Table describing the location of osteochondral plugs taken from the human patello-femoral joint

Plug	Position
F1	Patello-femoral groove
F2	Medial patello-femoral condyle
F3	Lateral patello-femoral condyle
Pa	Lateral patella facet
Pb	Medial patella facet

5.2.5 Determination of material properties of the cartilage

The material properties of the human PFJ cartilage were determined using the osteochondral plugs. The thickness, equilibrium elastic modulus and permeability of the cartilage were measured as described in Chapter 4 Section 4.2. All instruments and equipment in direct contact with the human tissue was either made separately for the purpose of use with human tissue or autoclaved to be used for the purpose.

5.3 Results

5.3.1 Observations during dissection

The six human tissue samples used in this study were clearly very different from each other; in terms of age, gender, size and condition of the bone and cartilage.

The condition of the bone (bone quality) and the synovial fluid (viscosity and colour) was determined purely based on the visual observation during dissection and the ease of dissection. The cartilage was graded according to the ICRS grading system described in Chapter 1 Section 1.3.1.2 as shown in Figure 5.4. The area of wear in Grade 4 cartilage was determined using the cling film method described in Chapter 2 Section 2.5.

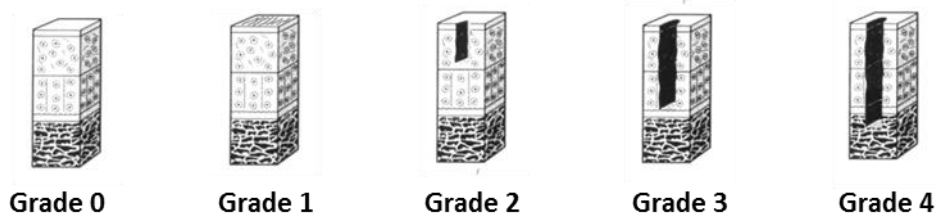


Figure 5-4: ICRS grading of cartilage wear


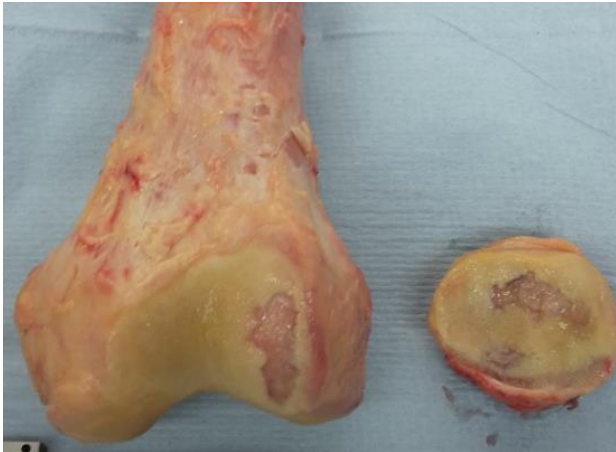
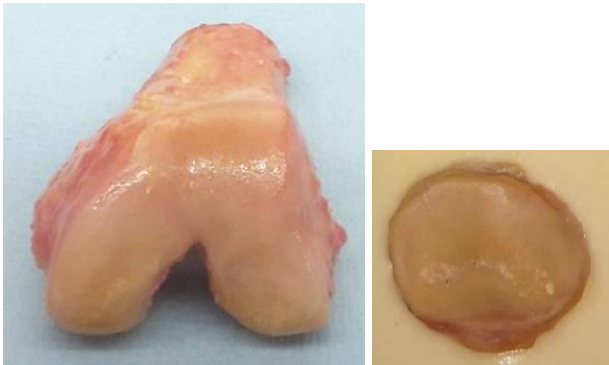
The visual inspection of the 6 knees revealed variation in appearance as shown in Table 5.2. Sample G10-14 was characteristically white and glossy in appearance whereas the other 5 knees had a yellow discolouration typically seen in age related changes. This can be due to the presence of advanced glycation end products (AGEs) seen in aged tissues. AGEs can induce collagen crosslinking which affects the mechanical properties of the cartilage by increasing the equilibrium elastic modulus (Fermor, 2013).

Sample G10-14 from a 52 year old female, appeared to have a healthy joint with clear synovial fluid and white glossy cartilage surface. However, sample G01-15 from an 85 year old male had visible cartilage damage. The femoral groove had a full thickness lesion of 388 mm² and the patella had a similar Grade 4 wear area of 561 mm². The synovial fluid was yellowish in colour and was observed to be less viscous compared to the fluid from sample G10-14.

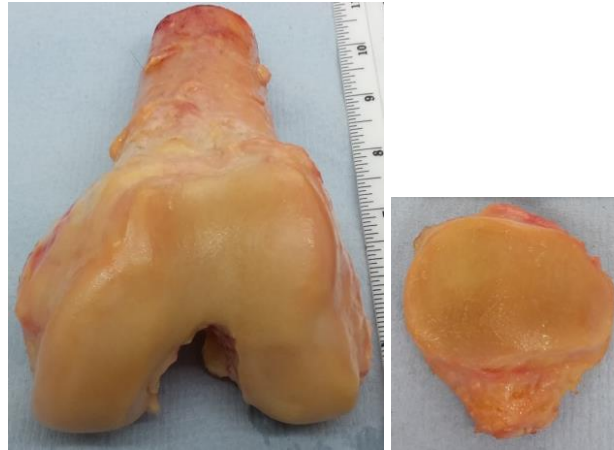
During dissection a difference in bone quality was also observed. Compared to these human joints, the porcine bones were relatively easy to cut through. The apparent softness in the porcine joints highlighted the skeletal immaturity of the tissues. Although the human joints

were skeletally mature and expected to have relatively harder bones, there were some exceptions. The three eldest joints were relatively easier to cut through as the bone was dry and crumbly. This could have been due to osteoporosis. The other two joints were easier to cut through due to their softer bone that released a large amount of fluid during the dissection. Sample G10-14 was relatively hard compared to all the others. The bone was not dry, not soft, with no crumbling and there was no significant fluid release compared to the others. This joint had a clear and viscous synovial fluid and the cartilage seemed almost bluish white. This was the healthiest of all the joints.

Table 5-2: Observation made on the 6 human samples

Donor	Sample	Observations
G01-12		<ul style="list-style-type: none"> • Age: 64 • Gender: Female • Left knee • ICRS grading (PFJ): Grade 1 • Bone quality: Very dense • Synovial fluid: Highly viscous, light yellow colour
G01-15		<ul style="list-style-type: none"> • Age: 85 • Gender: Male • Left knee • ICRS grading (PFJ): Grade 4 • Wear area (femoral groove) = 388 mm² • Wear area (patella) = 561 mm² • Bone quality: Very soft • Synovial fluid: Less viscous, dark yellow colour
G02-14		<ul style="list-style-type: none"> • Age: 70 • Gender: Female • Left knee • ICRS grading (femoral groove): Grade 1 • ICRS grading (patella): Grade 3 • Bone quality: Very porous, dry and crumbling • Synovial fluid: Highly viscous, light yellow colour

G04-13



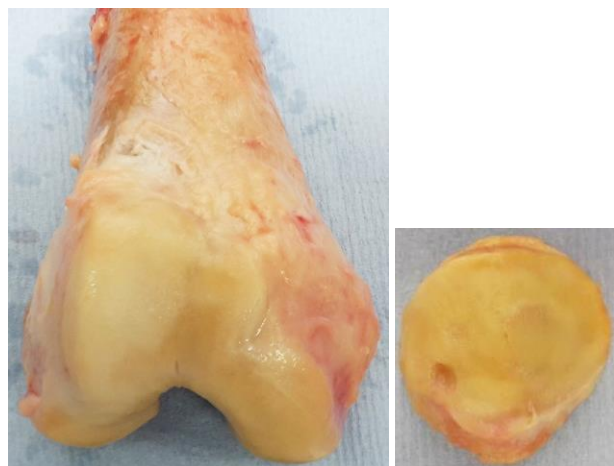
- Age: 62
- Gender: Male
- Left knee
- ICRS grading (femoral groove): Grade 1
- ICRS grading (patella): Grade 2
- Bone quality: Very porous, dry and crumbling
- Synovial fluid: Less viscous, yellow colour

G10-14



- Age: 52
- Gender: Female
- Left knee
- ICRS grading (PFJ): Grade 0
- Bone quality: Normal
- Synovial fluid: Normal, almost clear

G26-12



- Age: 54
- Gender: Female
- **Right knee**
- ICRS grading (femoral groove): Grade 3
- ICRS grading (patella): Grade 4
- Bone quality: Very soft
- Synovial fluid: Less viscous

5.3.2 Size of the human patello-femoral joint

The size of the human patella femoral groove and patella samples is shown in Table 5.3. $W_{(g)}$ is the width of the groove from one condyle to the other and $L_{(m)}$, $L_{(t)}$ and $L_{(l)}$ are the lengths of the medial condyle, trochlea and lateral condyle respectively. $W_{(p)}$ is the width of the patella on its widest side and $L_{(p)}$ is the length from the apex to base.

Table 5-3: Size (mm) of the human patella femoral samples

Sample	$W_{(g)}$	$L_{(m)}$	$L_{(t)}$	$L_{(l)}$	$W_{(p)}$	$L_{(p)}$
G01/12	35.09	30.13	32.91	35.42	23.75	24.82
G26/12	46.52	34.815	40.01	44.335	31.84	27.66
G02/14	47.24	42.47	46.53	55.62	30.08	35.01
G04/13	36.34	29.63	33.29	34.26	24.43	24.9
G10/14	54.97	36.38	42.17	50.16	37.02	28.75
G01/15	36.56	30.44	35.52	37.16	24.49	24.3

5.3.3 Material properties of the human PFJ cartilage

The material properties of the cartilage in the groove and patella of the 6 human samples were determined. The individual thickness, equilibrium elastic modulus and permeability of each location of plug is shown in Tables 5.4- 5.6.

As discussed in Section 5.3.1, there was a large variation in the condition of sample available for this study. They had different gender, age and pathological conditions. Therefore, it is not ideal to take the mean of all samples to determine the average material property of the region. The values obtained must be considered individually as each sample will demonstrate different material properties depending on its conditions. Therefore, it will be inconclusive to determine which factors have contributed to the certain material properties of the tissue.

In general, tissue with the lowest elastic modulus showed the largest permeability. This pattern was clear in all plugs from sample G10/14 which was the most healthiest samples out of the six. The poor bone quality of sample G02/14 and G04/13 made it difficult to obtain suitable sample height for indentation testing.

Table 5-4: Thickness of cartilage in each sample

	F1	F2	F3	Pa	Pb
G01/12	2.05	1.78	2.70	2.55	2.50
G26/12	3.34	2.62	1.97	1.80	4.05
G02/14	2.23	1.62	2.02	4.10	5.60
G04/13	2.94	2.20	2.05	2.51	3.07
G10/14	1.52	2.72	3.18	2.50	3.05
G01/15	2.63	3.02	2.88	3.04	2.90

Table 5-4: Elastic modulus of cartilage in each sample

	F1	F2	F3	Pa	Pb
G01/12	1.25	x	0.58	0.85	0.86
G26/12	1.42	1.40	0.55	0.42	x
G02/14	1.05	0.73	x	1.53	x
G04/13	x	0.30	0.24	x	0.58
G10/14	0.35	0.21	0.60	0.39	0.28
G01/15	1.81	2.22	0.19	9/491.65	x

Table 5-6:- Permeability of cartilage in each sample

	F1	F2	F3	Pa	Pb
G01/12	2.50	x	2.32	3.22	3.02
G26/12	1.21	1.20	3.15	2.19	x
G02/14	5.29	1.24	x	2.06	x
G04/13	x	2.73	1.52	x	9.65
G10/14	3.27	5.43	8.81	5.87	7.54
G01/15	5.73	1.82	2.14	1.01	x

5.4 Discussion

The aim of the study was to characterise the human PFJ in order to validate the animal model for the pre-clinical testing of tissue substitutions. By comparing the results from the animal joints obtained in Chapter 3 and 4, this chapter aimed to determine the major similarities and differences between the porcine model and the human joint tissue.

The dimensions of the patella and the femoral groove of 6 fresh-frozen cadaveric joints were measured. The cartilage was characterised by measuring its thickness, equilibrium elastic modulus and permeability.

Geometry of patello-femoral joints

The sizes of the bovine and porcine PFJ were determined in Chapter 3. These were compared to the size of the human PFJ in this chapter.

The size of the bovine, porcine and human patella is compared in Figure 5.50. The porcine patella is 32% narrower than human whereas the bovine is 22% wider than human. The bovine patella length is twice the size of the human patella but the porcine patella is only 15% longer than the human patella. The porcine patella is 33% thicker but the bovine patella is almost 2.5 times the height of the human patella.

The size of the bovine, porcine and human patello-femoral groove is compared in Figure 5.6. The porcine groove is 28% narrower than human whereas the bovine is 48% wider than human. The length of the bovine groove was significantly larger than the human grooves. The bovine medial groove is almost 3.5 times longer and the lateral groove is almost twice as long compared to the human grooves. However, the porcine lateral groove is almost the same length as the human and the human medial groove is just 32% smaller than the porcine medial groove.

Results showed that the bovine joints were significantly larger than the porcine and human joints. Although the porcine joints were slightly smaller than the human joints, the difference was not as large as the difference between the bovine and human joints. This was one of the reasons the porcine joints were chosen for the animal model as they were much closer in size to the human joints compared to bovine and hence more appropriate.

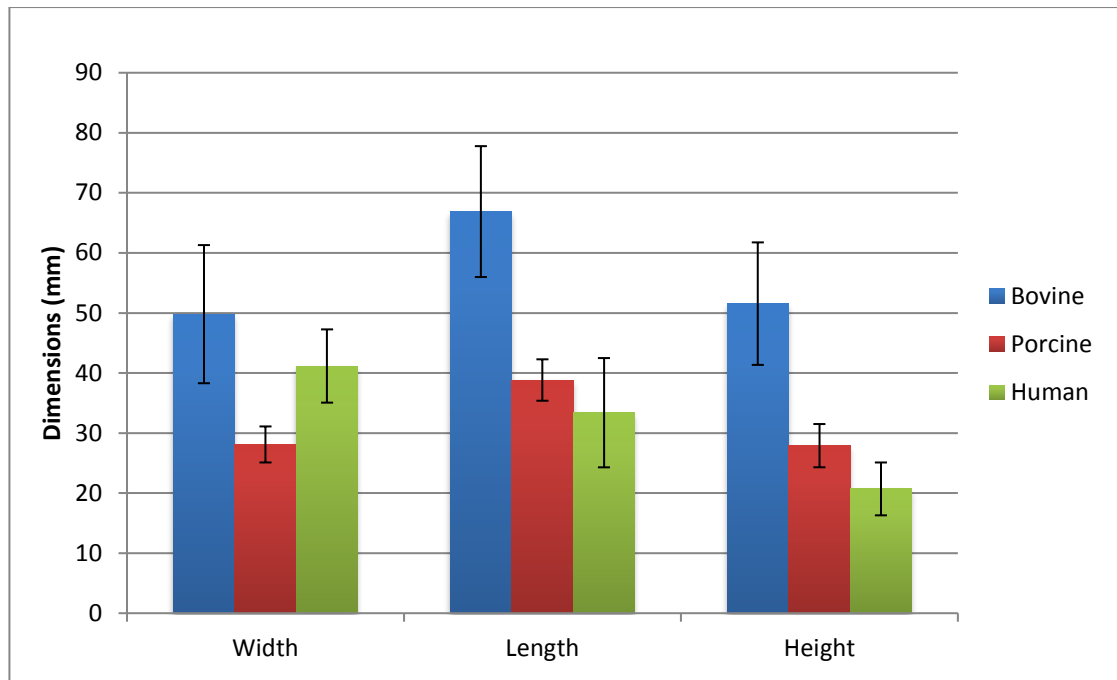


Figure 5-5: The sizes of bovine, porcine and human patella from this study

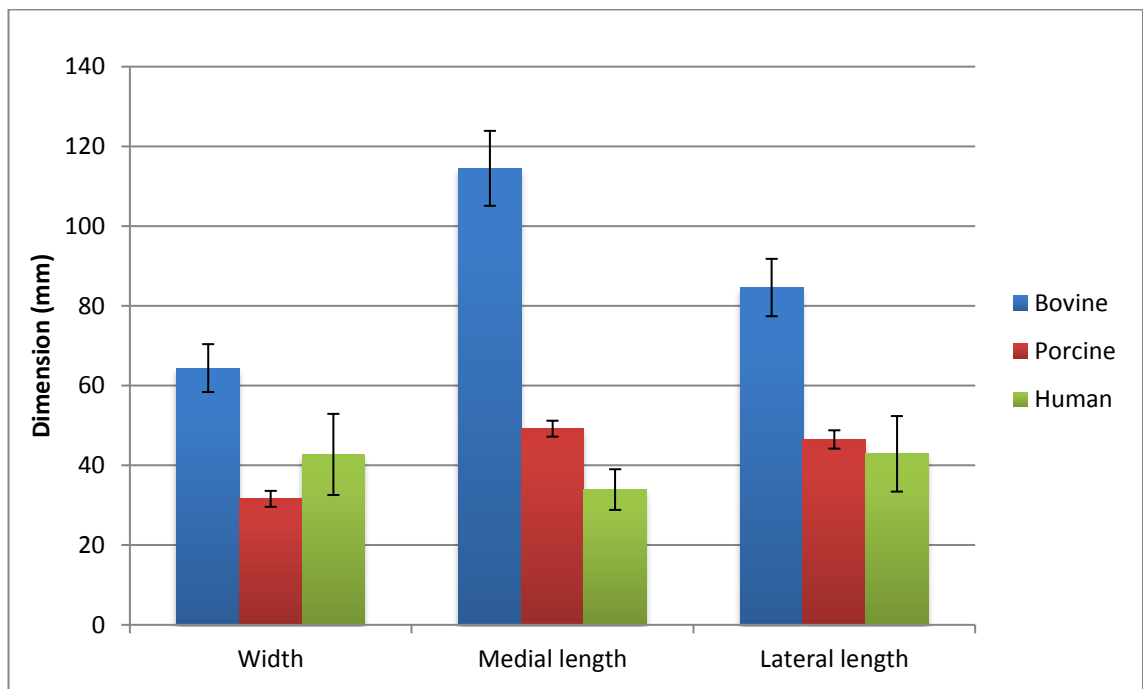


Figure 5-6: The sizes of bovine, porcine and human patello-femoral groove from this study

The size of human patella determined from this study was compared to other studies in the literature as shown in Figure 5.7. Overall, the results of the present study were consistent with the previous studies with a larger sample size (Baldwin and House, 2005; Osterhoff *et al.*, 2011).

The length of the patella from Osterhoff et al. (2011) was larger than the other two. This was because the current length and the length from Baldwin & House (2005) were both measured from the cartilage surface nearer to the apex to cartilage surface nearer to the base. However, Osterhoff et al. (2011) measured the length from the patella bone rather than the cartilage.

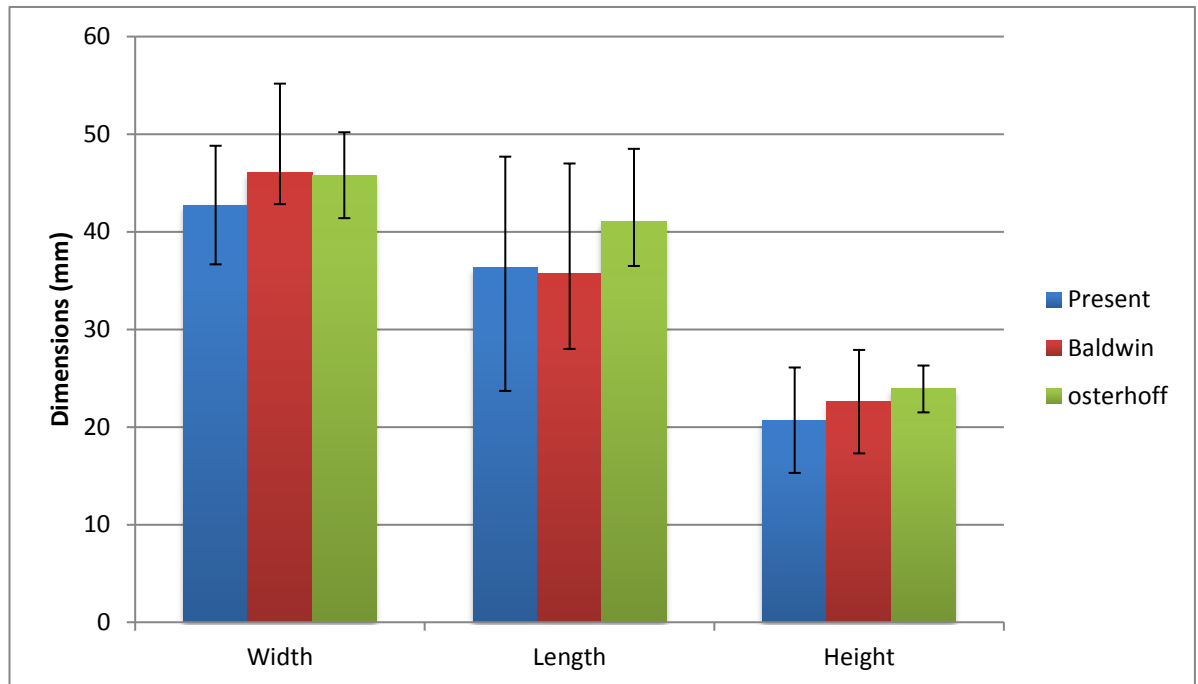


Figure 5-7: Dimensions of the human patella from this study (n=6) compared to other studies from the literature. Baldwin (n=92), Osterhoff (n=24)

There were many common features of the human PFJs observed in the current study. The femoral groove had a slight concavity on the medio-lateral direction that became more distinct towards the intercondylar notch. The ridge between the odd facet and the medial facet was more distinct in some patellae than the others. This was consistent with the literature as there were more patterns of anatomical features recorded in previous studies (Kwak *et al.*, 1997). Hence the various types of patello-femoral anatomies could affect the contact mechanics and wear study results.

According to the literature, the wear of the lateral patellar facet is the most prevalent. This may suggest that the lateral facet is mostly overloaded compared to the other facets (Fulkerson and Hungerford, 1990; Arendt, Fithian and Cohen, 2002; Saleh *et al.*, 2005). The lateral facet is larger than the medial facet and the patella is controlled by the lateral projection in the lateral patello-femoral condyles. In certain conditions, however where the pull of the ligament is weak, the patella could slip off the groove despite this projection. This

dislocation could also happen in joints with healthy ligaments if this lateral projection is not prominent enough for the patella to track the groove.

The lateral retropatellar surface in both human and bovine samples was larger than the medial side. The lateral femoral condyle of the femoral groove also showed a slight projection. These features contribute to controlling the lateral dislocation of the patella. This difference in the feature of the human trochlea was also observed by Osterhoff et al who compared human joints to ovine joints. However, this feature was not prominent in the porcine samples. This could be due to the skeletal immaturity of the joints and could develop further with age.

Pigs and cows are unguligrade (walk on their toes) quadrupeds (walk on four legs), which mean their knees experience different biomechanics compared to human knees. This could be why mature porcine, ovine and bovine grooves are more defined and deeper than human knees. Their patellae would need better positioning than the human patella that can glide over a shallower trochlea without dislocation (Osterhoff *et al.*, 2011).

Material properties of patello-femoral cartilage

The material properties of the human PFJ cartilage were characterised by measuring the thickness, equilibrium elastic modulus and permeability of the cartilage from the medial and lateral facet of the patella, medial and lateral condyles of the femoral groove and the trochlea. The overall material properties of the human cartilage were compared to the porcine cartilage discussed in Chapter 4 as shown in Figure 5.8.

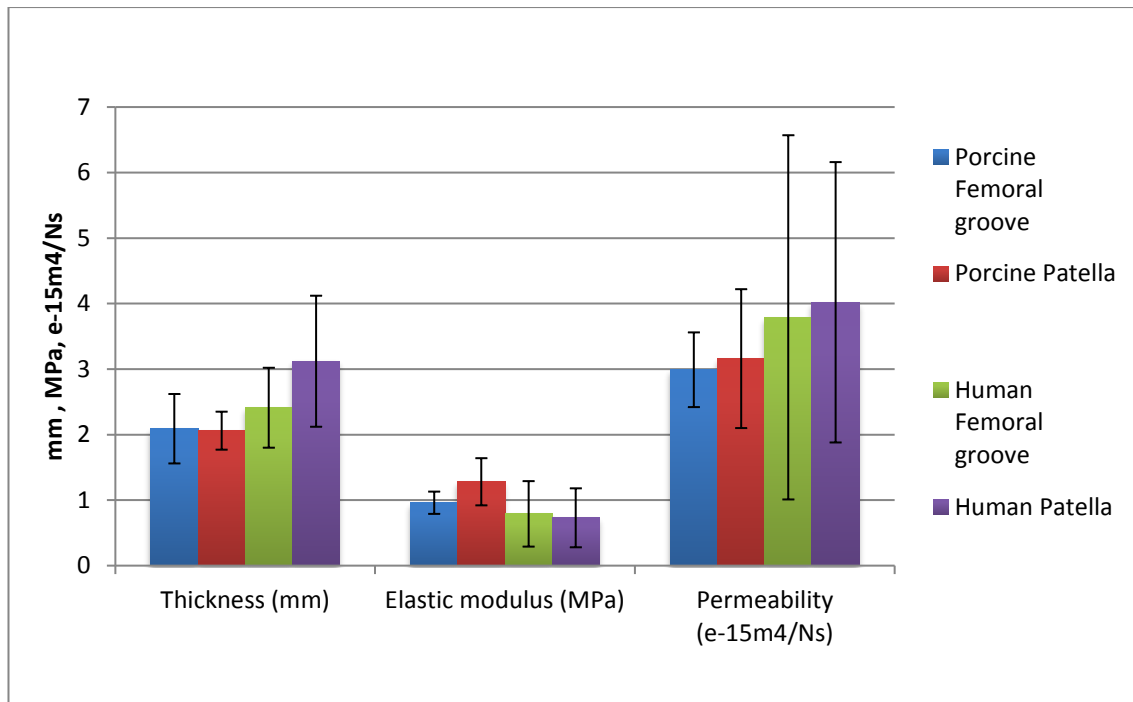


Figure 5-8: The overall material properties of the human PFJ and porcine PFJ

The porcine cartilage was 23% thinner and 21% less permeable than human cartilage. However, human cartilage was 30% less stiff compared to porcine cartilage. Although the same techniques and conditions were used to characterise both porcine and human cartilage, the 95% confidence limits on the human results were larger compared to porcine. This inconsistency in the results was almost certainly due to the type of samples available. The human samples were from adults of different age, gender and pathological condition whereas the porcine samples were obtained from 6 month old pigs with visible healthy cartilage.

The properties on opposing cartilage surfaces were shown to have differences. Athanasiou et al. (1991) demonstrated lower equilibrium elastic modulus and higher permeability in the human femoral groove compared to the condyles. In the current study, the equilibrium elastic modulus of the femoral groove cartilage was lower than the patella cartilage and the permeability of the patella cartilage was lower than the cartilage from the groove.

Like any tissue, articular cartilage deteriorates with age. Cartilage has been found to become stiffer and less permeable as the GAG content decreases and collagen content increases with age. Although the porosity of cartilage is very high, the proteoglycan network's strong affinity for water molecules and the ability of the GAGs present in the proteoglycan network resist the interstitial fluid flow to reduce the permeability. Reduction in GAG concentration

causes higher permeability which eventually causes the matrix to “wash out” into the joint cavity and hence, decreasing the overall stiffness (Ateshian *et al.*, 1997; Kwak *et al.*, 1997; Wang, Hung and Mow, 2001). This could be one reason why the porcine cartilage had a higher stiffness and lower permeability compared to the human cartilage.

The cartilage thickness varied across the species, with the human patella having the thickest cartilage. In the current study, the human patella cartilage was 51% thicker and the femoral groove cartilage was 16% thicker compared to the porcine cartilage. Several studies in the literature also support this species difference. The thickness of the femoral groove cartilage in humans is ~3.57 mm (Athanasίου *et al.*, 1991), in bovine it is 1.37-1.52 mm (Athanasίου *et al.*, 1991; Fermor, 2013) and in porcine it is 1.7-2.4 mm (Fermor, 2013). This could be due to various reasons such as the weight of the animal and the loading in the joint. Athanasίου *et al.* (1991) reported a greater thickness than the femoral groove cartilage thickness found in the present study. This could be due to several reasons such as the sample size, age of donors and the conditions of the cartilage. Athanasίου *et al.* (1991) analysed 4 healthy cadaveric knees with an average age of 34 whereas the current study analysed 6 knees from an average age of 64.5 with varying pathology.

Studies have shown an increase in cartilage thickness with body weight (Stockwell, 1971; Shepherd and Seedhom, 1999). This could explain why the cartilage is thicker in males than in females as males are generally heavier than females (Draper *et al.*, 2006). As humans have a bipedal posture unlike pigs and cows, there will be a larger load placed on human cartilage compared to the other species. These animals are unguligrade quadrupeds that walk on the tips of their toes. In addition, their knees are not capable of full extension (Osterhoff *et al.*, 2011).

The thickness of cartilage also varies with the joint which is related to the congruence of a joint. Congruent joints such as hips have thinner cartilage compared to incongruent joints such as the knee. Studies have reported a much lower thickness value in the hips compared to knees in human, porcine, bovine and ovine joints (Shepherd and Seedhom, 1999; Taylor, 2012; Fermor, 2013). The thickness of the cartilage in the hips was reported as 2.40, 1.22, 1.32 and 0.52 mm whereas that of the knees was 2.59, 2.23, 1.28 and 0.71 mm respectively. The location in the joint also has an effect. In the current study, the medial patello-femoral condyle cartilage was the thinnest (2.33 ± 0.58 mm) and the thickest cartilage was in the medial patellar facet (3.5 ± 1.27 mm).

The present study was limited to the material measured from the surface layer of the cartilage. The structure and composition vary through the depth of the articular cartilage and hence the material properties. A number of experimental studies have shown this variation in different species including human (Chen et al. 2001; Jurvelin et al. 1997; Treppo et al. 2000; Wang et al. 2002; Maroudas 1968; Gannon et al. 2015).

Boschetti et al. (2004) measured the permeability and equilibrium elastic modulus of cartilage from human cadaveric hip joints. Three consecutive layers of cartilage obtained from the osteochondral plugs were tested. The results showed that the equilibrium elastic modulus increased with depth whereas the permeability decreased with depth. A similar study conducted by Chen et al. (2001) showed the same trend in the material properties with depth. However, in the Boschetti et al study the permeability was determined through confined compression and equilibrium elastic modulus through unconfined compression.

Overall discussion

The current study was carried out to compare the species and find the appropriate model for the simulator study. Porcine joints were chosen as the animal model for the study as they were much closer in size to humans compared to bovine joints. The material properties of the porcine joints were 70% closer to the human cartilage.

Tissue composition plays a major role in the mechanical behaviour and functioning of the tissue. The joints used in the current study were from different donors with potentially different pathological conditions. In order to analyse the cartilage in each joint, measurement of biomechanical properties of the cartilage is not sufficient. To understand the disease process, it is essential to determine the biochemical composition of the tissue as well as its material properties. Therefore, to explain the determined mechanical properties, future studies should also encompass histology studies to investigate the effect of various contents of the tissue.

As the methods for both porcine and human cartilage were the same for the current study it is still valid for comparison. Therefore, the variation in properties across the layers of cartilage might not have a huge impact. The animal model will be created for short term wear study purposes. The histology studies will be useful in long term study where the composition of the tissue might change during the test.

Determining the geometry of the PFJ can contribute to the understanding of the biomechanics of the joint. The geometry of the PFJ investigated in this chapter and the previous chapter was limited to the length, width and height dimensions. Other measurements such as the sulcus angle, trochlea inclination, patellar tilt and displacement were not determined. These parameters can provide vital information regarding any abnormalities that could have influenced the results.

5.5 Conclusion

The geometry of the human PFJ and the material properties of its cartilage were determined. It was concluded that the geometry of the joint and its cartilage material properties varied with species. However, the porcine joints were closer in size to the human joints compared to the bovine joints. The material properties of porcine joints also showed strong similarities to the properties of the cartilage in the human joints. Therefore, the porcine joint is acceptable as an animal model for this study.

Chapter 6. Contact point study

6.1 Introduction

It was important to determine the position of the patella with respect to the femur as it was required to understand the starting position of the patella during the gait cycle. The starting point can be defined as the position of the patella with respect to the femur at the start of the gait cycle at full extension.

In similar in-vitro studies carried out on a tibio-femoral joint, the position of the tibia with respect to the femur was secured by placing a steel brace to fix the tibia and femur while the ligaments and tendons were holding the two bones in place (Liu *et al.*, 2015). With the patella-femoral joint (PFJ), however a more sophisticated method was required as the patella slipped while the braces were being fixed. The patella was also difficult to locate within an intact joint due to the large amount of associated tissue coverage.

Various methods were attempted and proved unsuccessful before the approach outlined below was taken. A nail was hammered through the patella while holding the whole leg at a certain angle (full extension). This was later carried out using a drill instead of the nail. The drill bit was left in the sample and the soft tissue around it was removed in order to fasten a set of braces to secure the patella in this position. This method was unsuccessful due to the following reasons. It required several pairs of hands since the leg needed to be held at a certain angle during the drilling. The process of holding the leg at a fixed angle was also not repeatable. The patella moved while drilling and the braces would not have held the patella in the correct position with respect to the desired angle.

The aim of the study discussed in this chapter was to determine the position of the patella with respect to the femur at 20 and 40 degrees in order to identify the neutral position of the sample set up in the simulator study. In the experimental model, the porcine leg was secured in a custom made fixture capable of holding the leg at the desired angle and the whole structure was frozen. A theoretical model was also built using SolidWorks to support this experimental data and to assist the analysis of the data.

6.2 Materials and methods

Materials included 6 porcine PFJs, Microset 101RF replicating fluid and the bespoke fixture used to hold the legs whilst freezing at a certain angle.

6.2.1 Determination of contact point

A bespoke fixture was designed and manufactured for this project to carry out the freeze-drill method. The relative position of the patella with respect to the femur was estimated using this method. . A labelled image of the fixture with the sample is shown in Figure 6.1. The fixture was designed to hold the porcine leg at 0, 20, 40 and 60° angles in order to determine the position of the patella with respect to the femoral groove. The design required the fixture to be capable of freezing the sample at any of these angles and therefore all the components were manufactured using stainless steel.

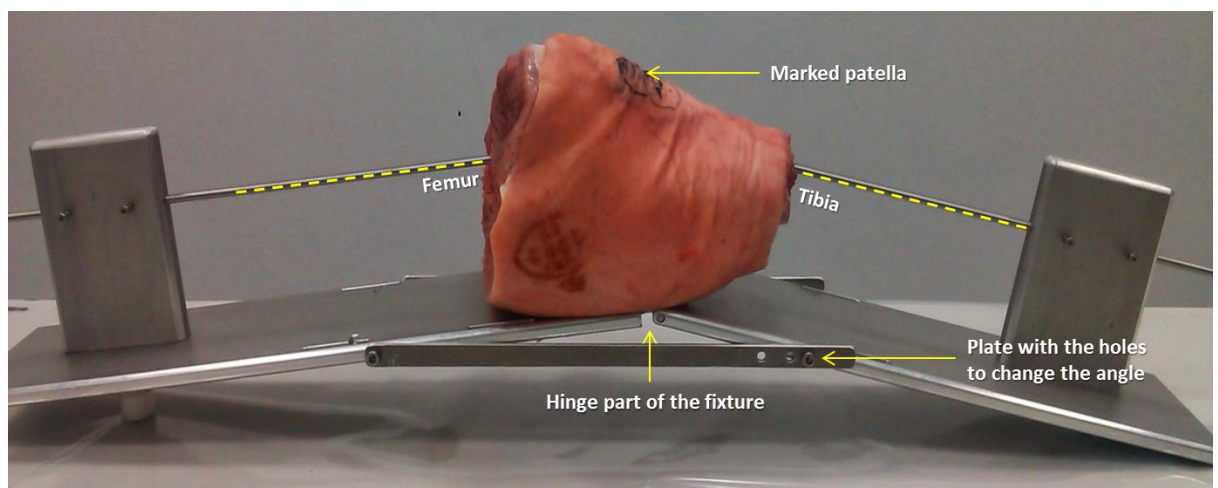


Figure 6-1: Fixture holding the porcine leg at 20 degree angle

The fixture consisted of two long rectangular plates with a small metal bar to which a 50 mm long rod was connected which had a diameter of 6 mm. The rectangular plates were held together by a screw that allowed it to move as a hinge joint. The angle between the plates was adjusted using two thin metal rods connected to the sides of the plates. These plates could be fixed at an angle of 0, 20, 40 or 60 degrees depending on the test. The legs were fixed by placing the metal rods through the bone canal which were connected to the two metal plates.

The leg was manoeuvred to locate the patella and was marked using a permanent marker pen. The ankle and femur were cut using a saw to expose the bone marrow. Two long thin

rods were inserted through either end of the bone through the marrow and the specimen was placed on top of the fixture. This ensured that the patella was assembled on top of the hinge part of the fixture. The two rods were fixed on the rectangular bars at the end of the fixtures. Plastic tape was wrapped around the specimen to ensure that it was secure while the whole assembly was placed inside a freezer. It was left for a minimum of 20 hrs freezing at -20° C.

While still frozen, a scalpel was used to pierce through the marking of the patella to locate the superior and inferior ends of the patella. A hand drill was used to drill two holes through the patella such that each hole lay at opposite ends. This identified the position of the patella on the femur after dissection. Once the drill markings were completed, the tissue was left to thaw for up to 4hrs before dissection. Patello-femoral dissection was carried out as described in Chapter 3 Section 3.2.1. Once the patella was separated from the femur, a photograph of the articular surface of the patella and femur was taken with a ruler for reference.

This study was carried out at 20° and 40° using 6 replicates for each. The 20° angle was chosen as this was considered as the neutral position for the porcine joints at full extension. The neutral position is the angle at the beginning of the gait cycle and unguligrade animals such as pigs have been shown to have a starting angle of 20 degrees (Liu *et al.*, 2015). The 40 degree angle was also tested to trace the kinematics of the patella. The PFJ gait cycle applied in the simulator study did not exceed 40 degrees flexion with respect to the femur and therefore angles beyond that were not investigated.

The outline of the patella and its holes were traced on the image and this was super imposed on the image of the femur. This would determine the position of the patella on the femur at that particular angle where the holes were created. An example of this process is shown in Figure 6.2.

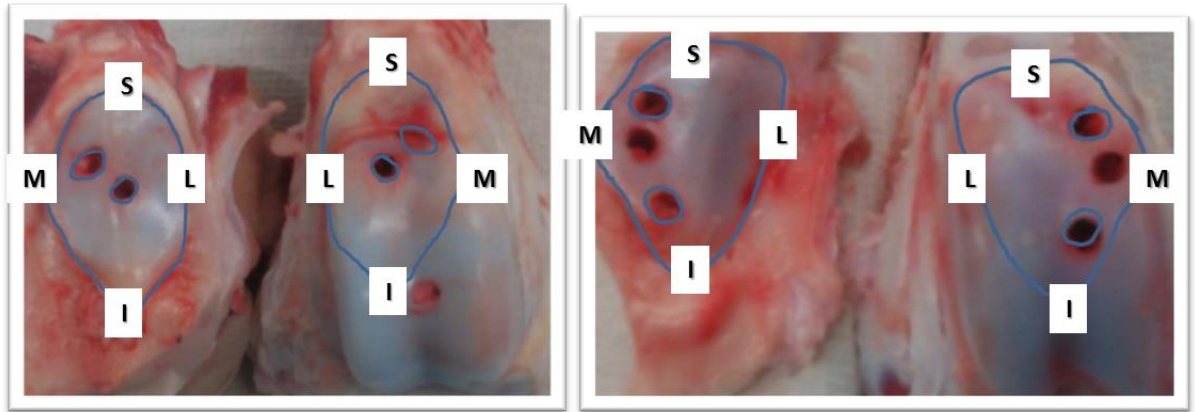


Figure 6-2: Tracing the outline of the patella and placing it on the femur with respect to the drill holes made as a guide. Left: Position of patella at 20 degrees, Right: Position at 40 degrees of knee flexion

6.2.2 Estimating the contact point using the Microset method

The contact point from the freeze drill method was better visualised using the Microset 101RF (replicating fluid) as a medium. Microset was applied to the same samples after the freeze-drill method. This made it easier to visualise the relative position of the patella on the femur.

The Microset silicon rubber replica black fluid was coated over the articular surface of the patella. The transparent part of the rubber replica was not allowed to mix with the black component of the mixture as this would have set the liquid rubber to the solid form. The patella was then carefully placed over the femoral groove such that the holes on the patella and femur made during the freeze-drill method were perfectly aligned. A nail was used to guide through the hole on the patella to reach the hole on the femur to ensure that the patella was placed on the correct position.

Once the position had been determined using the nail, the patella coated with the Microset was pressed against the femur, using hand pressure alone. When the patella was removed the Microset impression on the patello-femoral region showed the contact point at the specific angle at which the joint was frozen. An example of an image captured after the Microset impression is shown in Figure 6.3.



Figure 6-3: Left: Microset applied to the patella cartilage and placed over the femur using the drill holes as guide. Right: The Microset impression from the patella made on the femur representing the contact point.

6.2.3 Theoretical model

6.2.3.1 Literature data

A representation of the data from the literature that describes the dynamic interactions within the joint is shown in Figure 6.4, 6.5 and 6.6. This study was conducted to provide data to create the theoretical model described in Section 6.2.3.2

The model of a right knee created by Herrmann et al representing the dynamics of the patella is shown in Figure 6.4. The patella travels from the posterior to the inferior of the groove during knee flexion with respect to the femur (Herrmann *et al.*, 2012, 2013).

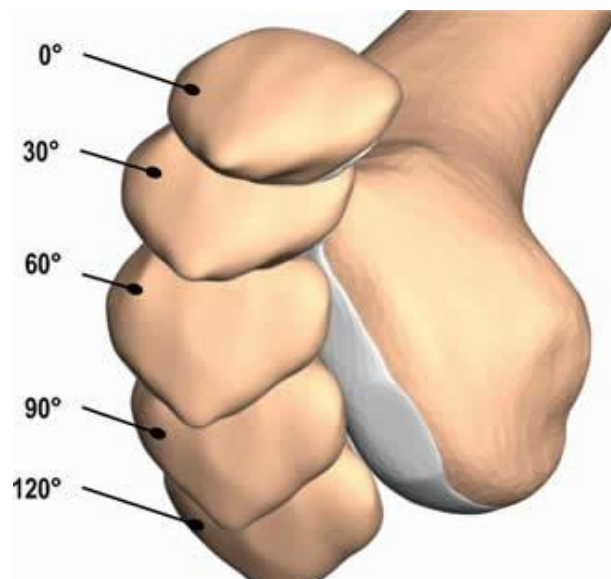


Figure 6-4: Dynamics of the patella in a right knee (Herrmann *et al.*, 2012). The figure illustrates how the patella travels on the femur from 0-120 degrees of flexion

The 3D anatomical representation displaying the contact mechanics in the knee joints at various degrees of flexion is shown in Figure 6.5. The geometrical data and the joint dynamics needed to create this computational model were obtained from the in-vivo experimental work carried out by the authors. MRI images of healthy knee joints at normal loading conditions were taken at 0-50 degrees of flexion. The contact mechanics pattern in the model showed close connections with their in-vivo experimental work. This was also consistent with the literature (Akbar *et al.*, 2012).

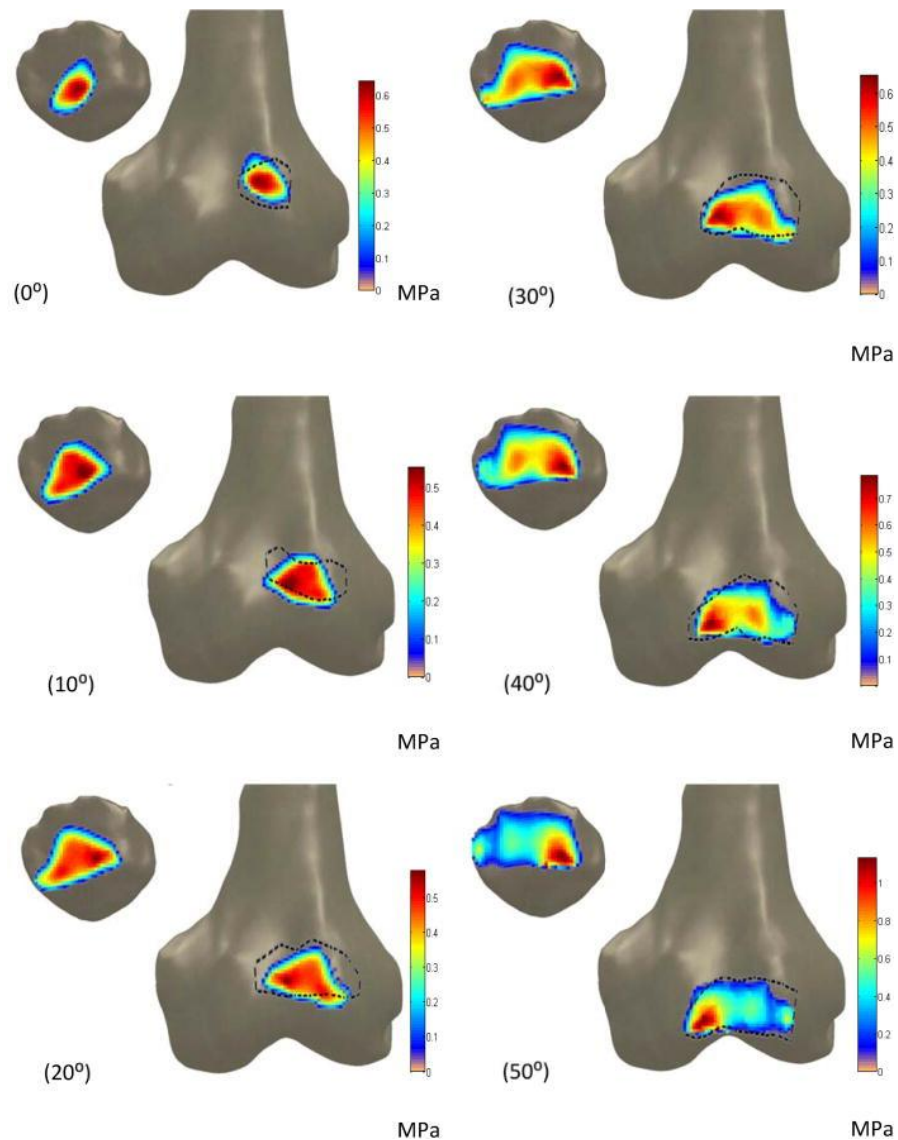


Figure 6-5: 3D anatomical model of the femoral groove and patella contact mechanics (Akbar *et al.*, 2012). The highlighted regions shows the contact between the patella and femur at 0-50 degrees of flexion.

A recent literature review was carried out on the biomechanics of the PFJ (Kittl, Schmeling and Amis, 2015). The contact data obtained from the literature survey is summarised by the image shown Figure 6.6. Kittl *et al.* concluded that the contact area in the patella moves

from distal to proximal, whereas that of the groove moves against the patella from proximal to distal. At full extension the patella is rarely in touch with the femur. However, at 135° there is a two point contact in the femoral groove which articulates against the odd facets of the patella.

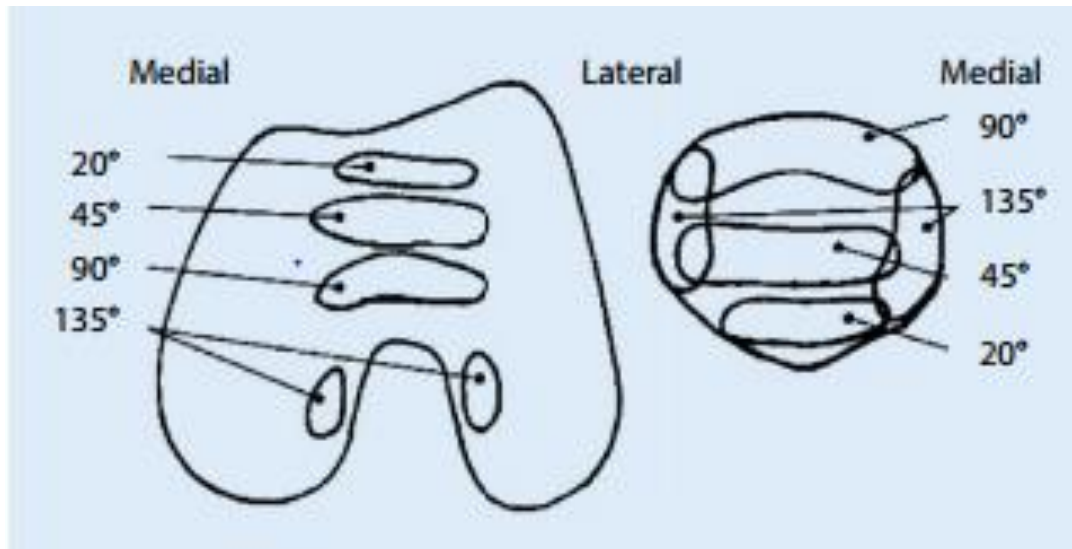


Figure 6-6: Contact area between the patella and femoral groove (Kittl, Schmeling and Amis, 2015). The marked regions shows the contact between the patella and femur at 0-135 degrees of flexion.

6.2.3.2 Creation of the model in SolidWorks

A simple model of the patella and femoral groove was created in SolidWorks using the dimensions obtained from the porcine samples in Chapter 3 and the position of the patella described in the literature (Akbar *et al.*, 2012; Herrmann *et al.*, 2012; Kittl, Schmeling and Amis, 2015) described in Section 6.2.3.1.

The model of the patella consisted of an oval patella with a ridge in the middle which created equal sized medial and lateral facets. The femoral component was modelled with condyles of constant radius. The lateral femoral condyle was made larger compared to the medial condyle. To maintain simplicity, the condyles were made parallel to each other without the natural lateral angularity of the trochlea.

The patella was allowed to tilt and move in S/I direction. The femur was fixed at its centre of rotation and was allowed to rotate in flexion and extension. The aim was to find the contact point at the starting position of the gait cycle. Therefore, the position was replicated for the 20 degrees of flexion.

The patella and femur were aligned according to the literature data gathered previously. According to the kinematics of the patella shown by Herrmann et al. (2012), the patella sits at the superior end of the femur at around 20°. So the femur was rotated to 20° and the patella was positioned to align it according to the position shown by Herrmann et al. (2012).

6.3 Results

6.3.1 Determination of contact point

The results for the determination of contact point using the freeze-drill method are presented in Figure 6.7 and 6.8. The outer marking of the patella traced on the femur shows the relative position of the patella with respect to the femur when the knee is flexed at 20 and 40 degrees respectively.

The patella was initially positioned at the superior end of the femur and closer to the lateral side of the condyles when the knee was flexed at 20 degrees. Increasing the angle of flexion to 40 degrees moved the patella towards the medial side of the condyles. The patella also travelled down the groove as the flexion increased and it also moved downwards from the superior end towards the middle of the groove.

Figure 6-7: Position of patella at 20 degrees knee flexion for the 6 samples. The outer marking of the patella traced on the femur shows the relative position of the patella with respect to the femur when the knee is flexed at 20 degrees

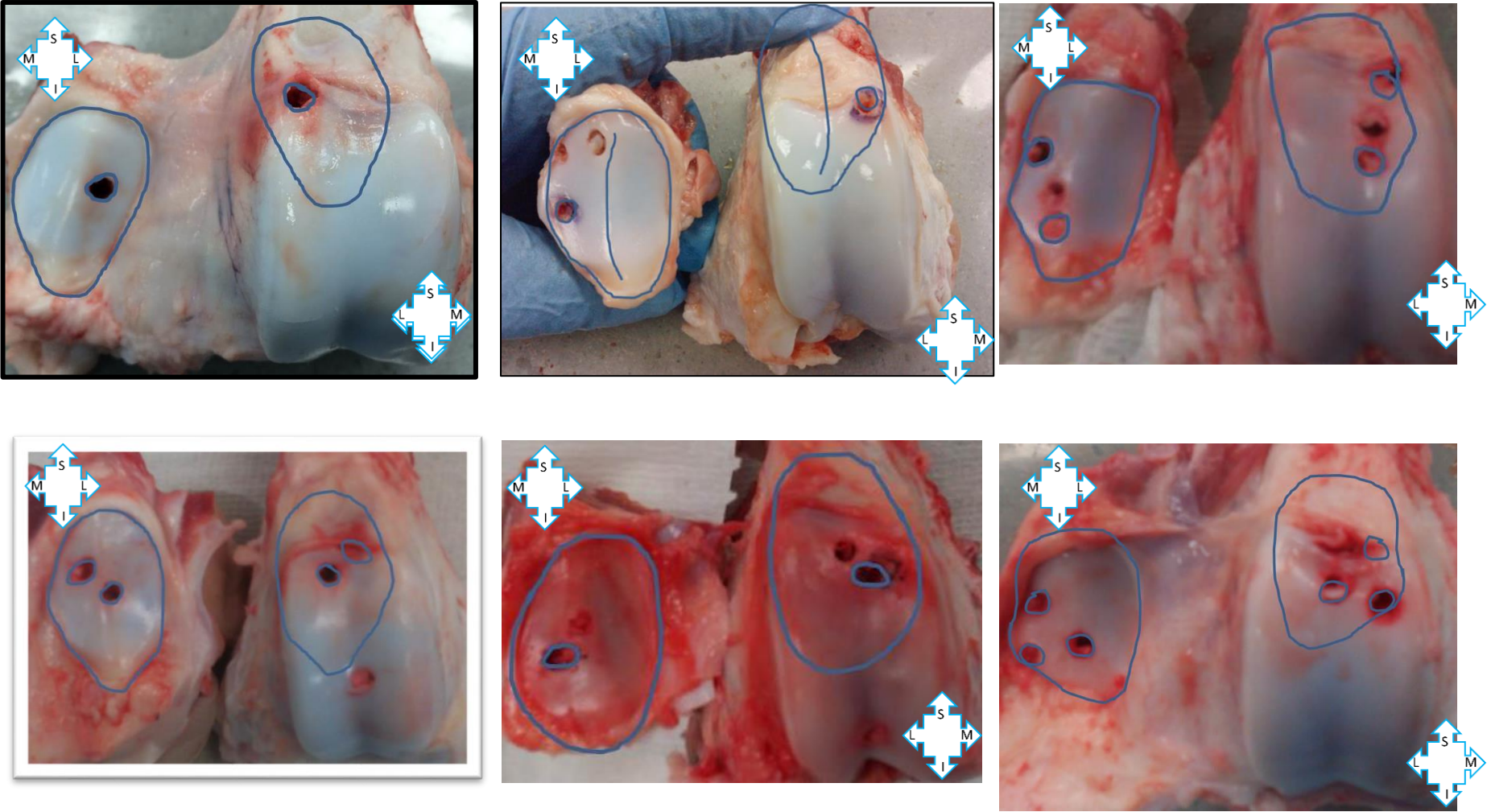
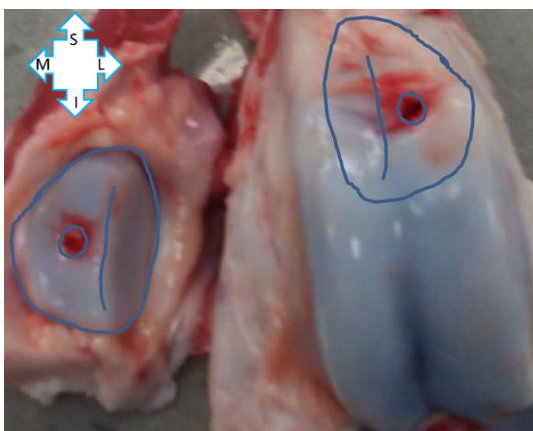
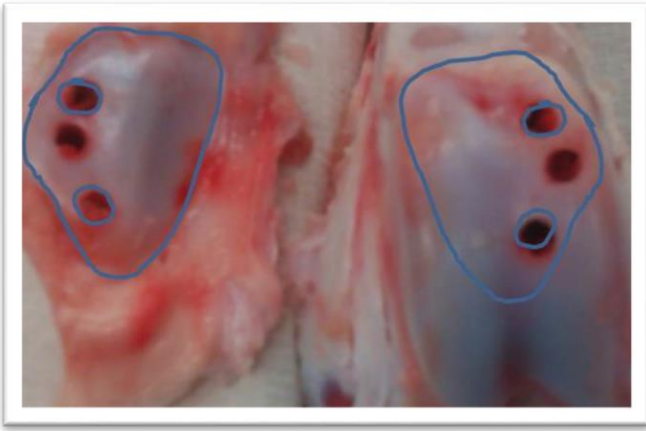
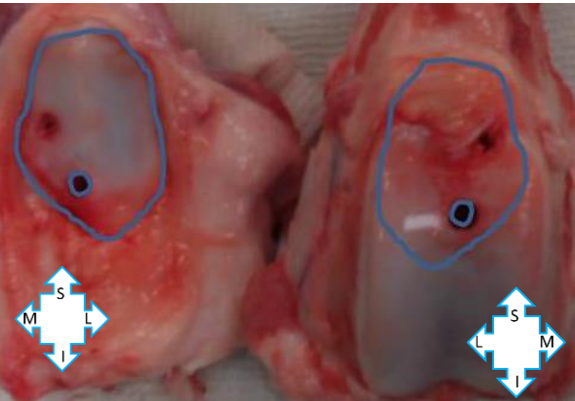
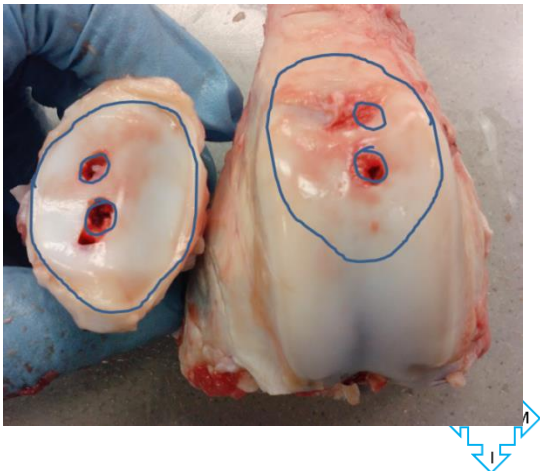
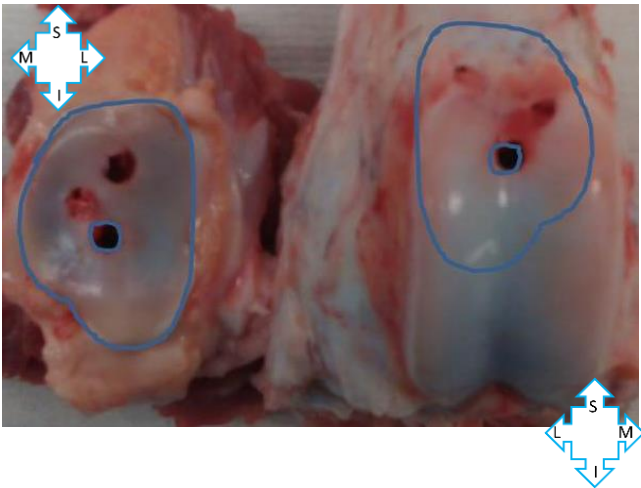
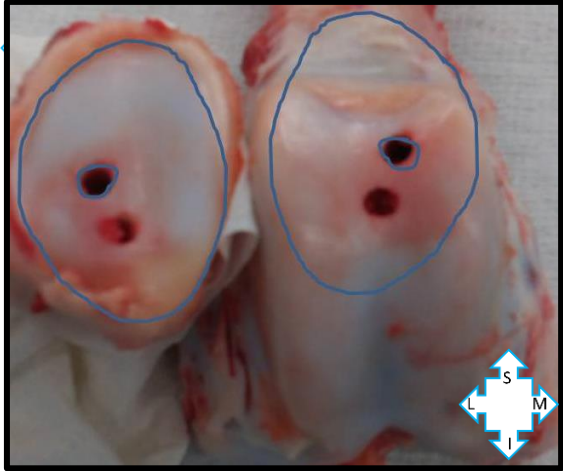


Figure 6-8: Position of patella at 40 degrees knee flexion for the 6 samples. The outer marking of the patella traced on the femur shows the relative position of the patella with respect to the femur when the knee is flexed at 40 degrees



6.3.2 Microset method

The drilled position from the freeze-drill method was kept during the Microset method by using the drilled holes as guides. During this step it was observed that the superior end of the femur was in contact with the inferior to middle portion of the patella. From the Microset markings, it was clear to see where this middle position was. The results from the Microset method are collated in Figure 6.9.

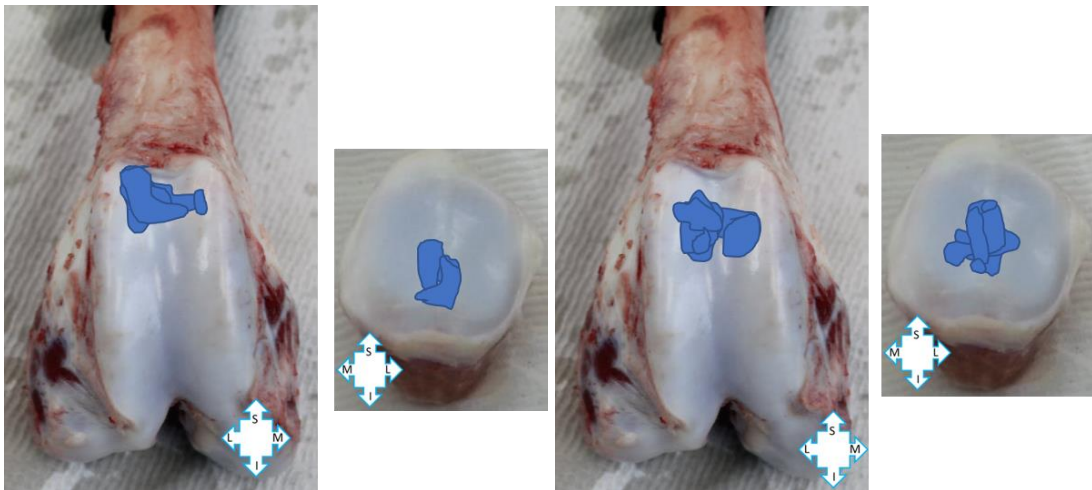


Figure 6-9: The contact point between the patella and femur obtained from the Microset study. Left – contact points on the patella and femur at 20 degrees. Right- contact at 40 degrees

This method made it easier to depict the contact point showing the main areas of contacts in the femur and patella. In the groove, the contact point lay on the superior end of the femur and it was also noticed that there was always a contact on the lateral side of the femur. In the patella, the contact point was mostly towards the middle of the patella in the medial/lateral as well as superior/inferior direction.

Although this method made the contact positions clearer, the Microset markings were not good enough to calculate the contact area. However, this method did help to position the patella from the freeze-drill results as it enabled visualisation of the contact on the patella and also the femur.

6.3.3 Theoretical model

The SolidWorks model assembly was created to support and present the experimental data in determining the contact points. The side view (Medial/ Lateral) and front view (Superior/ Inferior) of the model for a right knee. The contact points at 20 degree angle are shown in red markings in Figure 6.10 and 6.11. The computational model using SolidWorks showed contact points at the superior ends of the femoral condyles and the inferior of the patella.

The contact points from the Akbar et al and Kittl et al studies lay on the groove that follows the lateral tilt of the femoral groove. This was replicated on the 20 degree SolidWorks as shown in the Figures below, which reflected the contact point obtained from the experimental data.

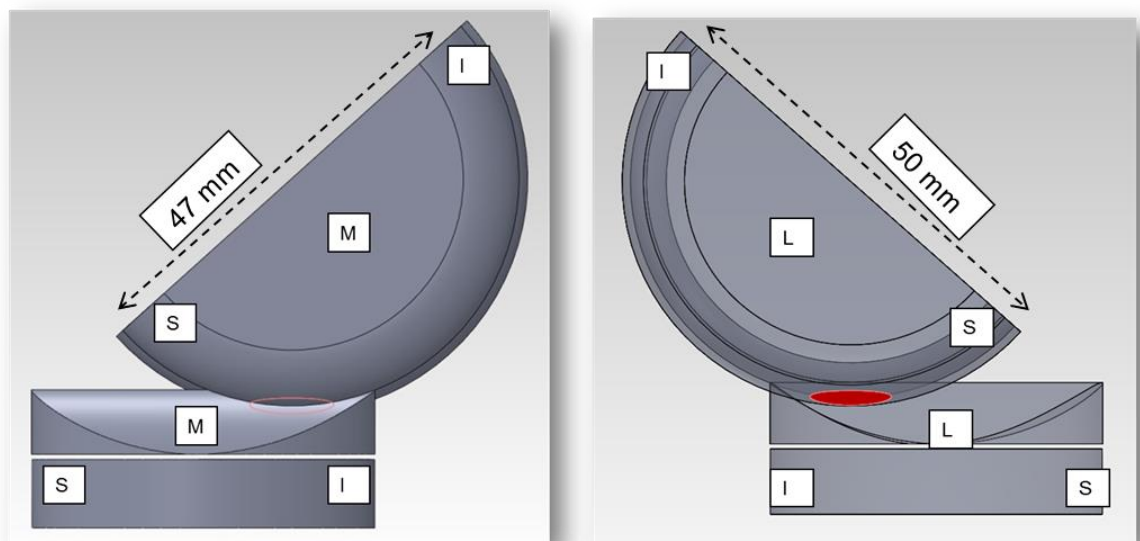


Figure 6-10: Left- Medial View of the SolidWorks model representing the sample set up at the starting point in the simulator, Right – Lateral view of the SolidWorks model at starting point

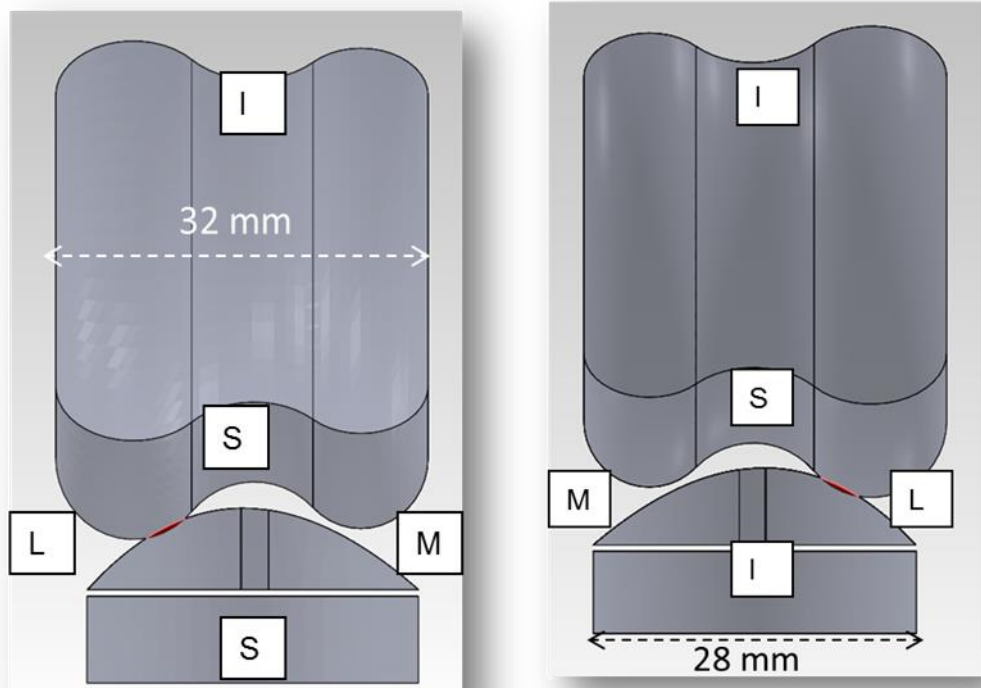


Figure 6-11: Left- Anterior View of the SolidWorks model, Right – Posterior view of the SolidWorks model showing the whole articular surface of the femoral groove

6.4 Discussion

It was important to understand the contact mechanics of the joint to better interpret the tribology. The contact point between the patella and femur was therefore a very important factor. It was also necessary to fix the samples in the neutral position when testing for contact mechanics and wear studies using the simulator. The aim of the study was to determine the contact point between the femur and patella to establish the neutral position.

An experimental model was first created which was then validated using a theoretical model created in SolidWorks using the data from the literature and results from Chapter 3.

The results from the experiments showed that the patella followed the femoral groove. At 20° the patella was placed higher and lateral compared to when it was at 40°. At the higher flexion it followed the groove downwards. The contact point shown in the Microset results also agreed with this finding and made this conclusion clearer.

It is worth noting that the contact area marked with the Microset was mostly situated in the central region for the patella and proximal for the femur. This showed that at lower angles

of flexion of 20-40° the central region of the patella is in contact with the proximal region of the femoral groove.

The theoretical model of the patella and femur was created in SolidWorks. The model was made from the dimensions obtained from the study in Chapter 3 and the patella was positioned using the data from the Hermann et al (2012) study. The contact point created through this model was identical to the data shown in Akbar et al (2012) and Kittl et al (2015) study. This matched with the results obtained from the experimental results.

The experimental results were similar to the theoretical model created from the literature data. It was comparable to other researchers' data from the literature. The kinematics of the patella recorded in the literature model agreed with the motion and positions replicated from the experimental model discussed in this chapter (Herrmann *et al.*, 2012, 2013). The positions of the contact points relating to these kinematics also showed similarities (Akbar *et al.*, 2012; Herrmann *et al.*, 2012; Kittl, Schmeling and Amis, 2015).

However, there were a few challenges that need to be considered. Under physiological condition, the load bearing leg will exert a higher force. In this situation, although the flexion angle was replicated, the loads on the leg would have been the same as when it would be in supine position at various angles.

The pressure applied during the Microset study to mark the contact point was carried out manually and hence would not have been consistent. Using a marker that does not spread with contact will give a better indication of the contact point and could even help to obtain quantitative data.

The process of removing the hips and ankle from the leg to secure the joint in the fixture could have damaged the soft tissues. However, the impact of this could not have caused any variations in the results as the study was focussed on low degrees of flexion.

The quadriceps muscles play a key role in stabilising the patella and preventing dislocation. They are only engaged in higher degrees of flexion where they pull the patella dorsally into the femoral groove. At lower degrees of flexion, however the patella normally does not engage with the femoral groove. The force at the medial patellar retinaculum is also the lowest at the beginning of flexion. It decreases from 210N at full extension to just 18 N at 20 degrees of flexion (Akbar *et al.*, 2012; Kittl, Schmeling and Amis, 2015).

According to Wiberg (1941), the displacement of the patella relative to the femur is about 5-7 mm. The current study attempted to obtain a qualitative indication regarding the contact point and did not measure the actual displacement of the patella. This was enough for the purpose of this study, as the maximum displacement of 7 mm would have only been achieved in full extension. However, the relatively small flexion angle in this study means that the displacement might not be even half as much, which would have needed a much more sophisticated methodology to measure. Nevertheless, future work could attempt to quantitatively measure the patella dynamics in order to obtain a more established validation on the positioning. This could include applying a constant pressure on the patella for the Microset method rather than using just hand pressure.

6.5 Conclusion

The overall results from the experimental methods and the theoretical model created in SolidWorks using the findings from the literature were used to cement the sample at the neutral position. The result from this study enabled positioning of the patella with respect to the femur. It was concluded that at the beginning of flexion the patella sits on the superior end of the femur and travels down wards as flexion progress.

Chapter 7. Developing the methodologies for investigating the biotribology of the porcine patello-femoral joint

7.1 Introduction

The aim of this study was to establish a wear model for the study of the natural patello-femoral joint (PFJ).

Initially, it was planned to use a pin-on-plate system for a preliminary study of the biotribology of the PFJ cartilage using the whole patella button. However, after due consideration this was not implemented. The pin-on-plate system could possibly have been used as a simpler system to study the biotribology of the cartilage surface before developing further using the more complex full joint simulation for wear testing. The porcine patello-femoral samples were however, larger than the available space on the current pin-on-plate friction rig; therefore it was not feasible to use the available rig. Design of a new friction rig was considered to accommodate the porcine PFJ model but this was not viable as discussed below.

Firstly, the friction rig would have needed to run with a stroke length of at least 20 mm to get significant data, assuming that the middle of that stroke length would pass through the contact area when the knee was at 45° flexion. This is because the simplest way of fixing the groove plate would have been to have a flat base for the groove. The patella would then have been articulating directly over the groove. This would have replicated the 45° flexion and any other degree of flexion would mean that the flat position of the groove was not possible. Alternatively, the patella could have been placed at an angle. However, this would have further complicated the friction rig design which was not considered to be a worthwhile option for a simple set up.

Secondly, the co-efficient of friction would vary according to the change in curvature of the groove. Consequently, the pin would have needed to move upwards to reach the middle of the sample and it would have been considerably easy for the pin to move down to the other half. This would have resulted in a change in co-efficient of friction as the first half would have had a larger co-efficient of friction in contrast to when the pin was effortlessly sliding down the other half. This was a further reason for not implementing the pin-on-plate study.

Developing the methodology to investigate the biotribology of the porcine PFJ was one of the most novel aspects of this project. A practical and consistent method was essential for mounting the porcine PFJ in the single station knee simulator (SSKS) in order to investigate the biomechanics and biotribology of the joint.

This chapter discusses the steps taken to consistently mount the PFJ on the simulator and run a wear study of the porcine PFJ using a SSKS. It also introduces the use of an Alicona IF G5 surface profilometer to assess the wear of cartilage in natural joints. A positive and negative control was used to establish the methods which can be used to compare the results for any future testing of cartilage substitution therapies. The positive control will be the worse case scenario that produces a higher wear. Cartilage articulating against healthy cartilage should have the least friction and hence produce least wear. Whereas, cartilage against metal is expected to show a greater friction resulting in higher wear and hence a larger roughness value.

7.2 Materials and Methods

The materials and equipment used for this study are detailed in Chapter 2. This chapter focuses on the novel methodologies developed for this part of the study. This section describes the methods developed using a SSKS to investigate the wear in a porcine PFJ under a normal gait cycle. A positive and negative control was also developed for porcine PFJs using the SSKS.

An artificial femur articulating against a porcine patella was the positive control and a natural patella articulating against a natural patello-femoral groove was the negative control. The artificial femur was a femoral component (PFC Sigma, Depuy) as described in Chapter 2 Section 2.1.5. Six samples were tested for each condition.

7.2.1 Modifying a Single Station Knee Simulator

The general description of the single station knee simulator (SSKS) is described in Chapter 2 Section 2.2.6. The SSKS used in this study has 6 degrees of freedom. An image of the SSKS showing the 6 axes for a PFJ with polarities is shown in Figure 7.1.

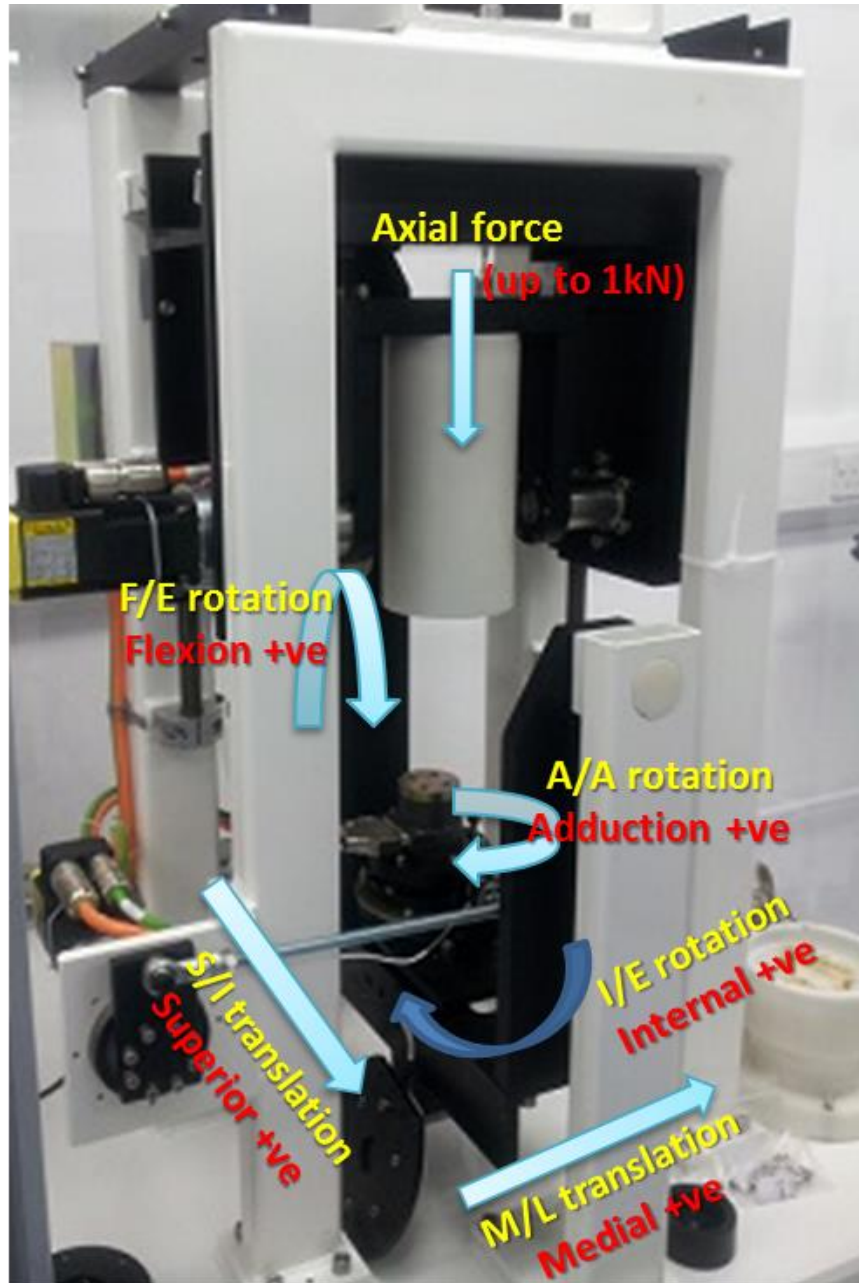


Figure 7-1: Image of the SSKS displaying the 6 axes for the PFJ for a right knee with the polarities

7.2.1.2 SSKS Calibration

The SSKS allowed 6 degrees of freedom. M/L displacement and I/E rotation depend on the geometry of the joint and hence these were left passive. Axial force (AF), SI displacement, flexion/extension and A/A rotation were driven.

The machine sensors were calibrated at the beginning and end of each series of tests. A flow chart explaining the steps followed for the calibration of the machine is shown in Figure 7.2.

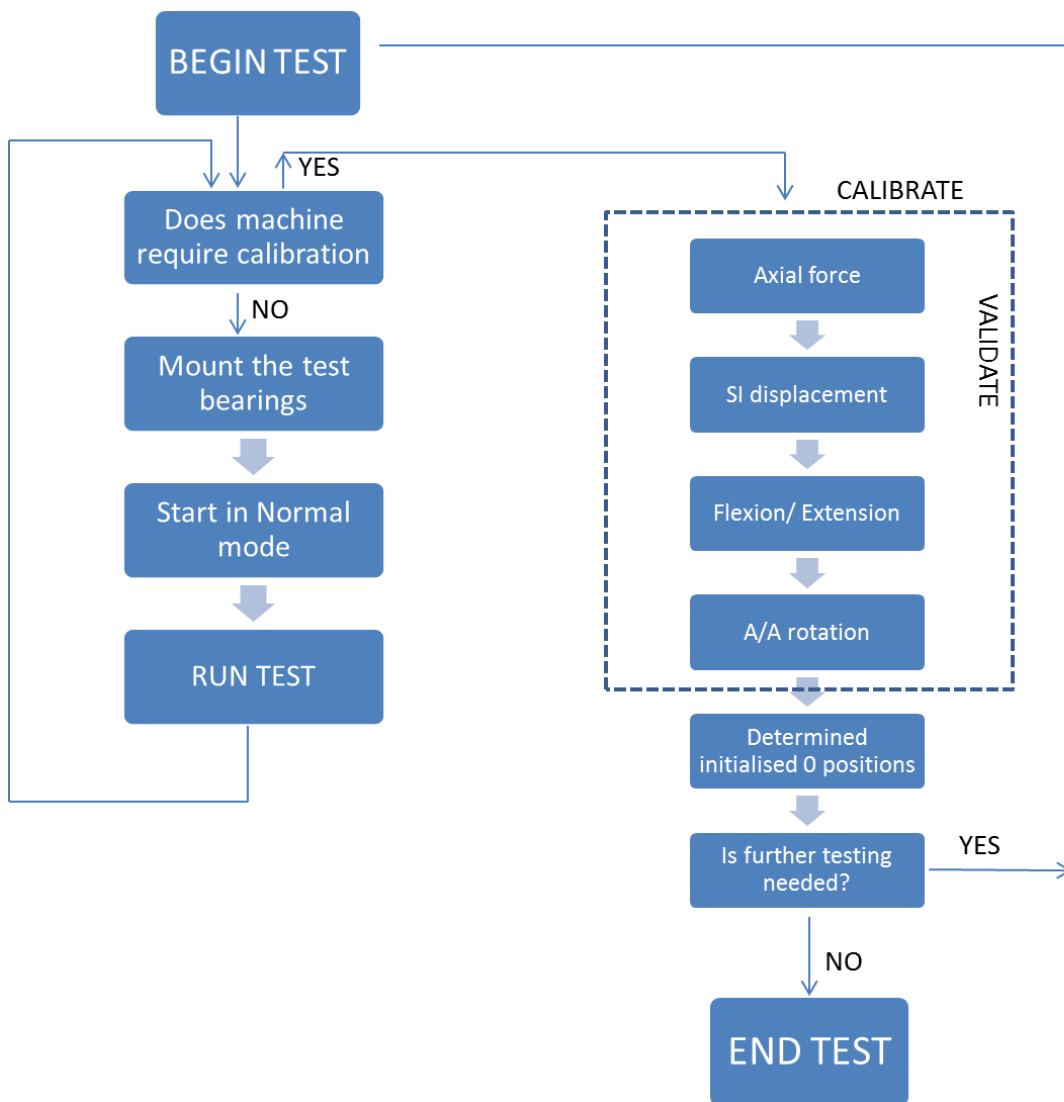


Figure 7-2: Flow chart explaining the steps followed for the calibration of the machine

Calibration ensured that the load and displacement sensors measured and produced the correct values. The calibration was performed by comparing the output values of the in-situ simulator sensors with the output values of external and independently calibrated sensors. Loads were monitored through the 6 axis load cell and motions were monitored through linear magnetic position sensors and optical encoders in the motors.

There was no calibration required for the ML displacement and IE rotation as these were left passive. There was no calibration procedure for the angular displacements such as FE and IE but they were validated against independent measurement gauges. The angular displacement was validated using a digital protractor and was monitored during the tests using gauges placed on each displacement axis. These were accurate to $\pm 0.5^\circ$. The main calibration was the axial force and SI displacement as discussed below.

AF calibration determined the relationship between the axial load cell and the load at the bearing surface as shown in Figure 7.3. This calibration was validated by repeating the procedures with a second load cell.

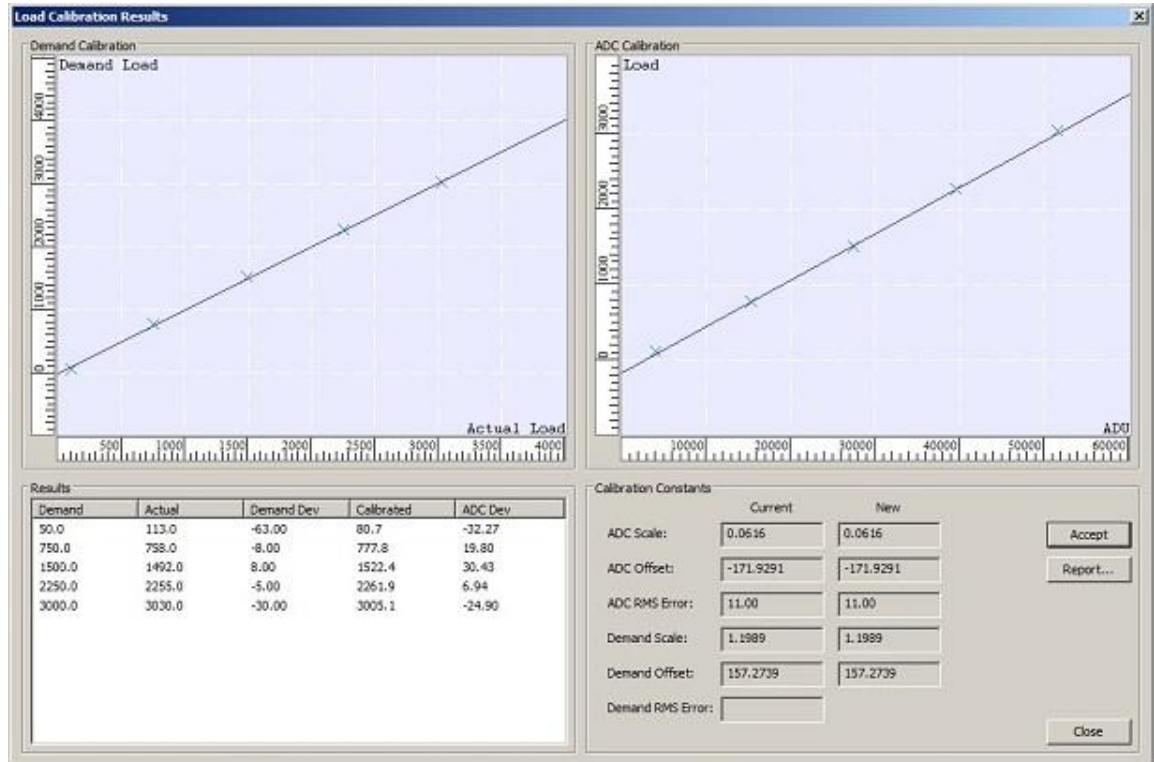


Figure 7-3: A typical graph following load calibration showing the relationship between the axial load cell and the load at the bearing surface

The linear displacement calibration was carried out using a set of slip gauges. SI displacement calibration was performed in 2 stages. Stage 1 determined the relationship between the sensor position and the actual distance positions. Stage 2 determined the relationship between the displacement sensor and the motor position. The polarity of the axis was such that superior was positive and inferior was negative. For SI axis calibration, SI motor demand position was calibrated against the actual position. The calibration was validated by repeating the procedure using a further set of slip gauges.

7.2.1.3 Fixtures for PFJ mounting

To design the fixtures to accommodate the natural PFJ in the SSKS, a design specification was produced. The aim of the design specification was to highlight the requirements for a fixture that could be used to carry out wear tests in a natural PFJ. The specific design requirements are given in Table 7.1.

Table 7-1: Design requirements for the SSKS fixtures

• Able to contain a porcine PFJ and allow a sample size of 50 by 50mm
• Able to fit into the SSKS with an allowed height of up to 90mm
• Able to attach the existing gaiters to contain the lubricant
• Able to withstand the dynamic forces applied (up to 1kN)
• Should have features that prevent it from rotating once fixed in SSKS
• Made from a material that is easy to handle and cleaned
• Need to be attached to the SSKS with respect to the axis of rotation
• Consider the CoR of the sample and how it is aligned with the simulator
• Made from a material that can be put into the freezer or a Micro-CT machine

The dimensions of the PFJ and the availability of sample space in SSKS were calculated to design the fixtures to accommodate the patello-femoral samples for the experiments. The fixtures were manufactured using Delrin polymer material and had ridges to attach the gaiters to contain the lubricant during the wear studies.

The fixtures were required to hold a porcine PFJ and it needed to be attached to the SSKS with respect to the axis of rotation. The dimensions of the sample obtained from Chapter 2 and the sample space in the SSKS were used to design the fixture in SolidWorks. It also took into account the centre of rotation of the sample and how it would be aligned with the simulator. A labelled diagram of the fixtures for the patella is shown in Figure 7.4 Left.

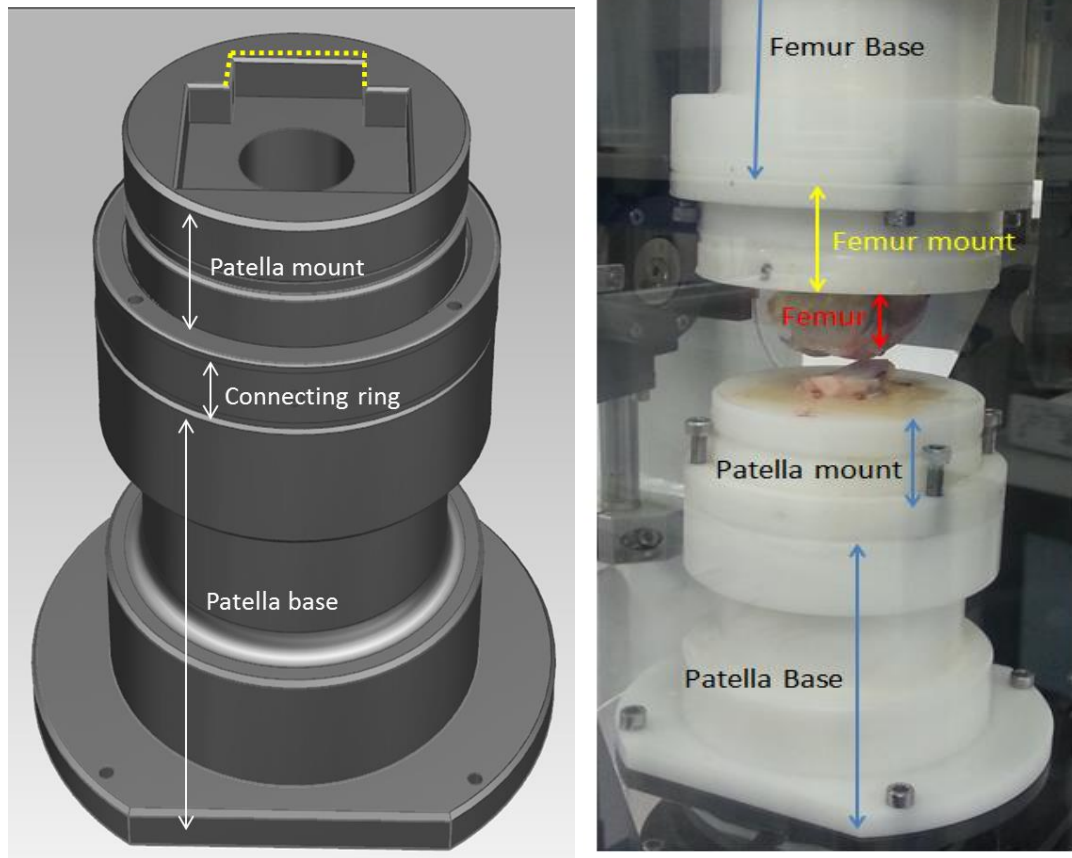


Figure 7-4: Left: Fully assembled patella fixture. The rectangular sample space is marked with the depression side for reference in yellow. Right: Manufactured Delrin PFJ fixture with the sample

The sample space was made rectangular with a depression at one end. The rectangular shape made sure that even if the cement was not attached to the Delrin, the sample did not rotate in the fixture. A dip at one side was made as a reference point so that the sample was always cemented with the superior side facing the dip end. The cylindrical hole also ensured that the sample and PMMA did not come loose from the fixture.

There were 4 main parts to the full patella-femoral fixture in the SSKS; these consisted of the patella base and mount and femur base and mount. The labelled assembly of the full PFJ fixtures in the simulator with the sample is shown in Figure 7.4 Right. The femoral sample was cemented in the femur mount and the patella was cemented in the patella mount. The base was the fixture connecting the mount to the simulator. It was designed

such that the mounts could be removed from the rest of the assembly and could be used separately to cement the sample into the fixture.

7.2.2 Setting up the porcine PFJ sample

Figure 7.5 shows the porcine set up in the fixtures, labelled with the forces and displacements applied by the simulator to show the 6 degrees of freedom.

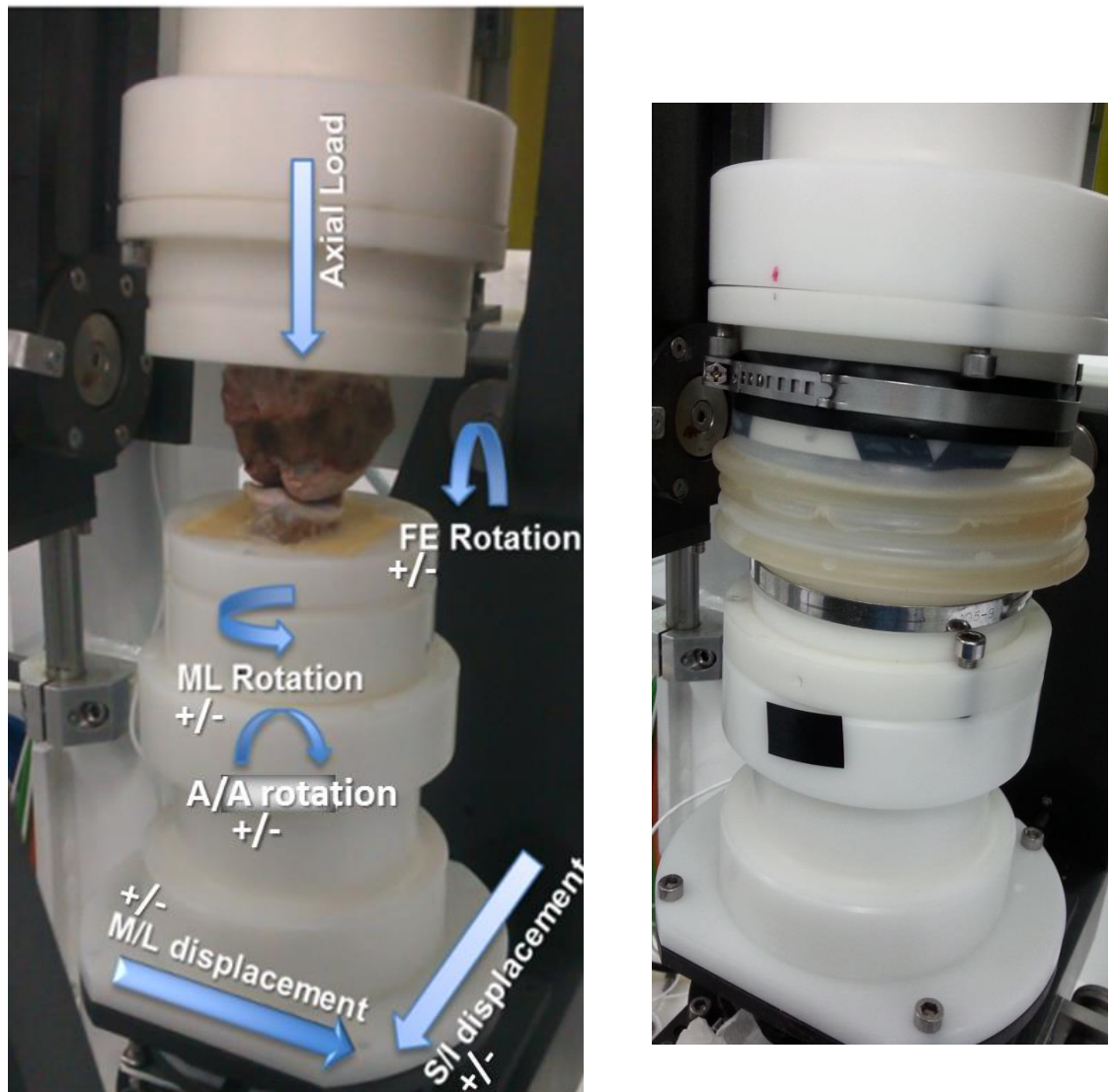


Figure 7-5: Left- porcine PFJ assembled in the simulator within its fixtures.

Right – sample with the serum contained within the gaiter.

7.2.3.1. *Preparing the sample*

The porcine PFJ was dissected as described in Chapter 3 Section 3.2.1. The patella component was then cut into the sample shape to provide a flat base using a custom made rectangular cutting jig as shown in Figure 7.6. The flat base ensured that the patella was cemented securely in the fixture and it allowed the patella to be at the correct position while following the femoral groove. The patella was placed inside the jig such that the cartilage faced the screw end although the screws were not tightened in order to avoid damaging patellar cartilage. The jig with patella was fixed in a vice grip and the patella base was cut using a hacksaw. The prepared patella samples are shown in Figure 7.7.

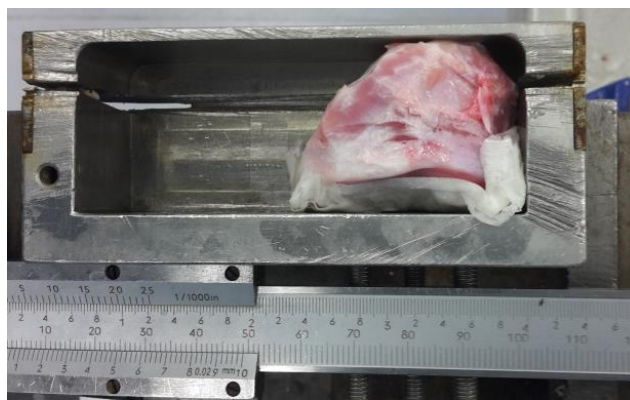


Figure 7-6: Patella placed inside the cutting jig



Figure 7-7: Left- Full patella with curved base, Right- Dissected patella with the flat base

The femur was placed in the vice grips and was cut into shape using a hacksaw. It was cut such that the entire cartilage surface was preserved for the testing and had a minimum height of 25 mm to allow the centre of rotation (CoR) to lie on the sample. The prepared femoral samples are shown in Figure 7.8 and the steps following to cut the sample are shown in Figure 7.9.

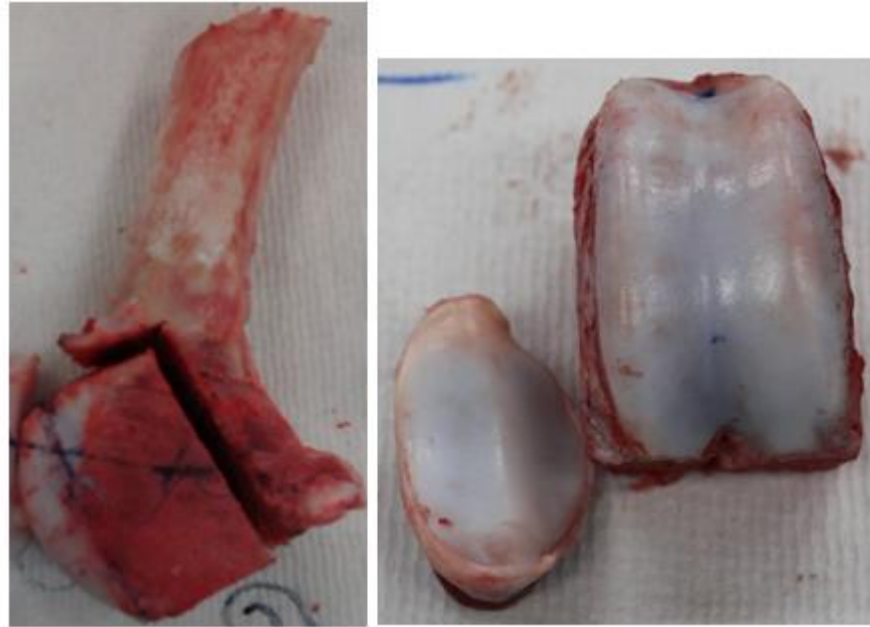
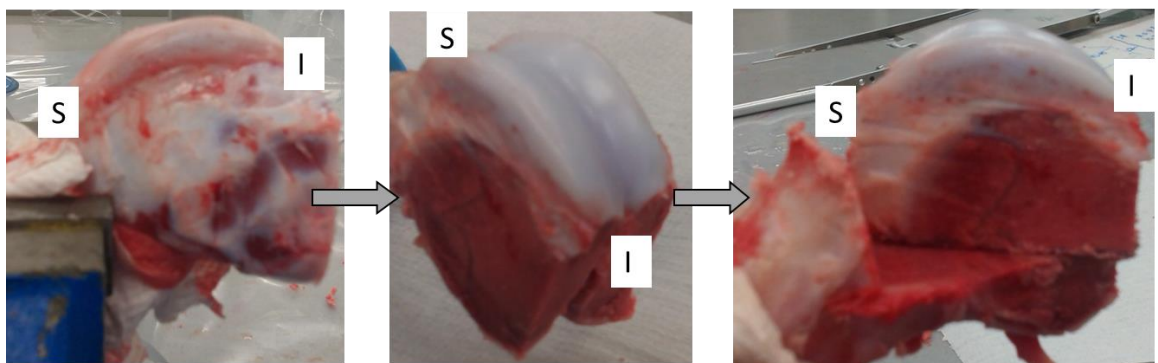


Figure 7-8: The desired shape and size of the femoral sample. Left- Side view of the femoral sample cut from the femur. Right- Top view of the femoral sample and patella showing its articular cartilage



The sample was held from the femur using the vice grips. The inferior ends of the femur was cut away from the transverse plane.

Similarly, the medial and lateral end of the bony part of the femur was cut away in the sagittal plane

Finally, the posterior end was cut away from the frontal plane, making sure all the cartilage surface was fully preserved for testing.

Figure 7-9: Steps taken to cut the femoral groove sample from the femur

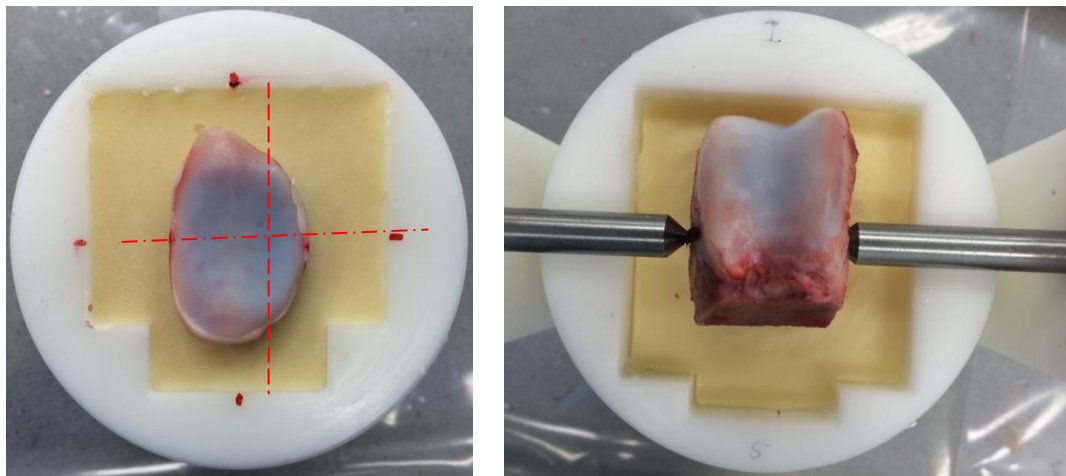
The artificial femur as described in Chapter 2 Section 2.1.5 was attached to a mount the same size as the natural femoral mount. Therefore, it was able to be attached to the femoral base component of the same SSKS fixture.

7.2.3.2. Sample mounting

The sample was cemented to the 'neutral' position. This is defined as the position of the patella with respect to the femur at the start of a gait cycle and with all axes in their zero positions. This was obtained through the contact point study discussed in Chapter 6. The

radius of curvature (RoC) of the femoral groove, determined as described in Chapter 3 Section 3.2.4, was used to mark the centre of rotation (CoR) of the femur on the sagittal plane of the femoral sample before cementing.

For cementing the femoral component, the femoral fixture was placed in the replica simulator frame. This frame consisted of a replica of the femoral frame that held the fixture in the simulator. It had a pin on either side that went through the femoral axis of rotation in the simulator. The femoral sample was placed on the fixture such that the CoR marked on the sample aligned with the pins on the frame as shown in Figure 7.10 Right.



**Figure 7-10: Left- Alignment of the patella at the centre of the fixture
Right: Alignment of the femoral component using CoR locating pins in the replica frame**

The patella was cemented on the fixture first. The diagram of the patella in the superior and anterior view from the simulator is shown in Figure 7.11. The superior view shows the patella mount and its centre. The centre of the patella was aligned with the centre of the patella mount as shown in Figure 7.10 Left and 7.11 Left.

When the patella mount was fixed in the SSKS, the assembly was locked in such a way that the patella was aligned to the M/L rotation (horizontal line) and the SI displacement (vertical line). M/L tilt occurs in the coronal plane as shown in Figure 7.12 Right. This was the reason the bottom of the patella was made flat during dissection. This aligned the patella in the coronal plane at an angle of zero degrees. The patella was aligned with the sagittal plane and was at the centre of the SI displacement as shown by the vertical lines on Figure 7.11 Left and 7.12 Left. As the simulator allowed movement about the z axis of the sagittal plane, the height of the patella during cementing was not significant.

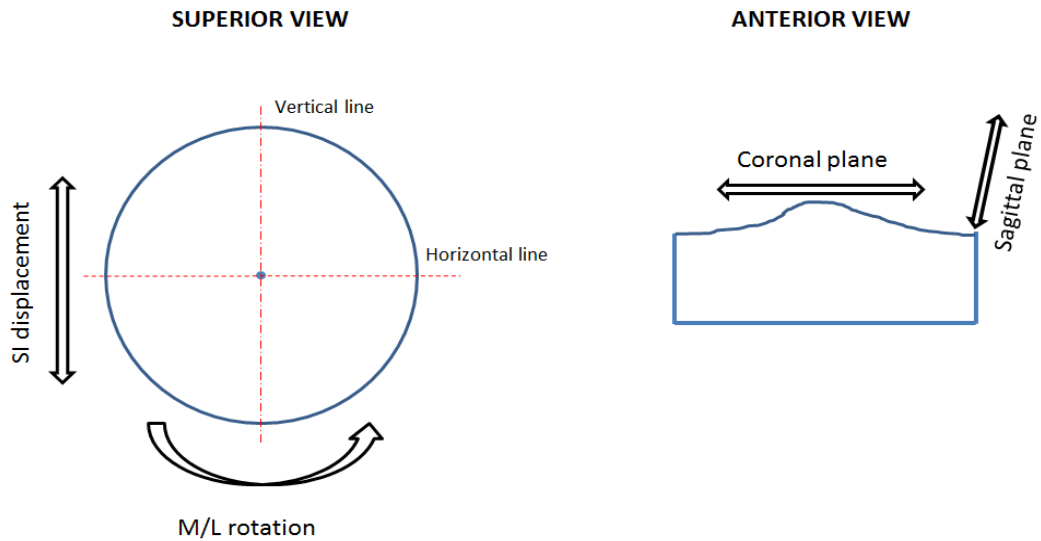


Figure 7-11: Diagram of the patella in the mount at superior and anterior view of the simulator

The position of cementing of the femur was determined by locating the position on the femur where its superior end had to be in contact with the inferior part of the patella as shown in Figure 7.12. The replica frame locating pins shown in Figure 7.10 Right were used to ensure that the CoR at the femur was correct. According to the contact point study discussed in Chapter 6, one third of the length of the patella from its inferior end needed to touch the femur at one-third of its superior end.

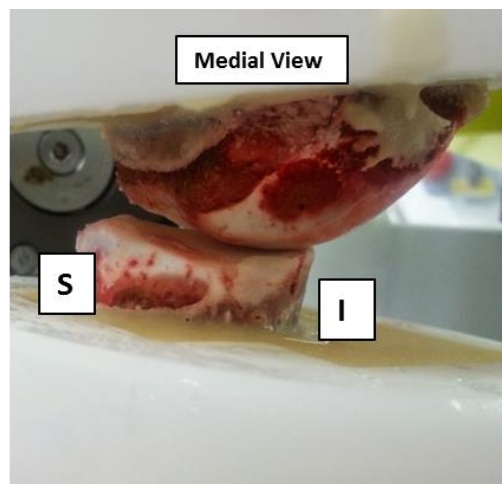


Figure 7-12: Cementing the patella and femur at the same position as its alignment at the starting point of the gait cycle

Once the sample was cemented into the fixture, the femoral fixture was secured into the simulator. A gaiter was used to encapsulate the joint and hold the lubricant. The 25% (v/v) calf serum lubricant was poured into the gaiter and the fixture containing the sample and lubricant was secured into the simulator.

7.2.3.3. Porcine PFJ Gait cycle

The SSKS was capable of applying 6 degrees of freedom. In this study the FE, SI, AA and AF were active and ML displacement and rotation were passive. The active motions were gathered from the gait cycle published by Ellison et al. (2008) and Maiti et al. (2014). They investigated the wear in artificial patello femoral joints using the Leeds hip simulator and six station knee simulators respectively. Their gait cycle represented a human PFJ gait cycle to test their artificial implants (Ellison *et al.*, 2008; Maiti *et al.*, 2014). In this project, their gait cycle was modified to the kinematic limits of a porcine PFJ as discussed below.

The patello-femoral gait cycle used in this study is show in Figure 7.13. The x-axis of the graph shows the stages of gait cycle which consisted of 128 input/ reference points for the SSKS. The input curves in the Maiti et al. (2014) gait cycle had sharp transitions which caused difficulty in the electromechanical simulator to achieve certain targets, especially the axial loads. Therefore, the curves were smoothed to allow the simulator to apply the inputs efficiently.

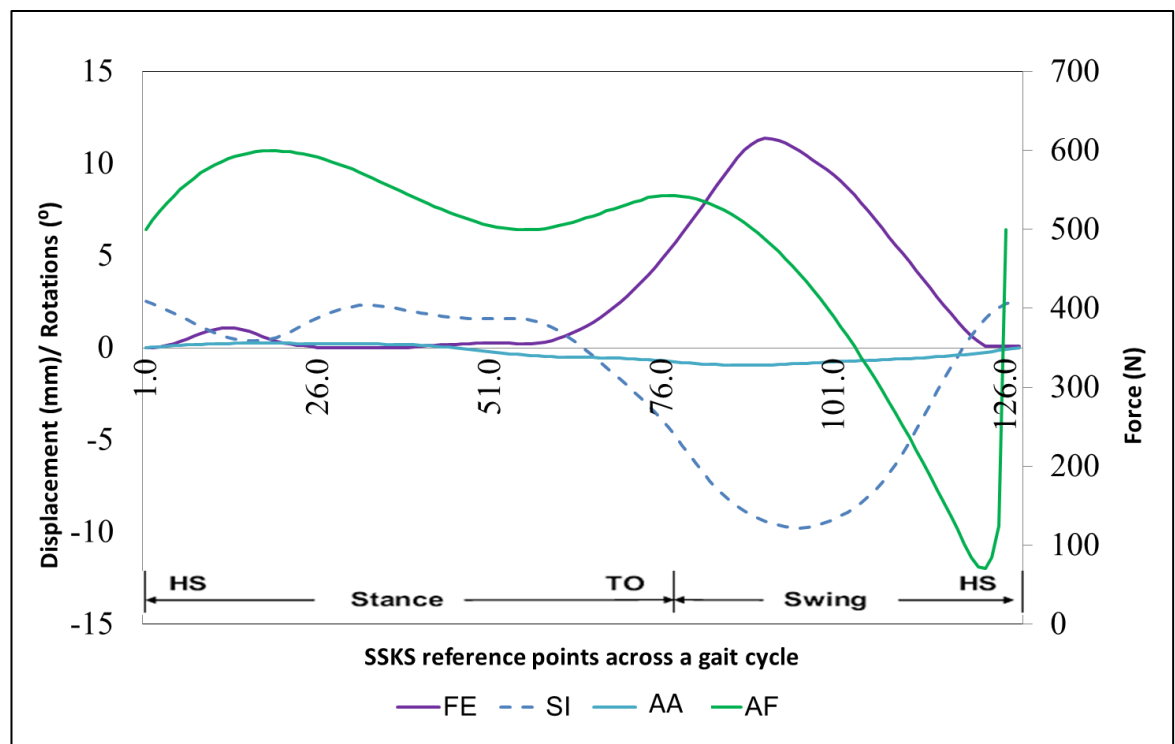


Figure 7-13: Porcine patello-femoral gait cycle.

FE= Flexion/Extension, SI= Superior/Inferior displacement, AA= Adduction/Abduction, AF= Axial Force

The major modification to this profile was the scaling factor that converted the values of the human gait cycle to the porcine joint. The axial force was divided in half. Since humans are

bipedal and pigs are quadrupedal the pigs will have a larger distribution of forces. The rest of the parameters were scaled down using a factor of 2.5 as established by Liu et al. for a porcine TFJ gait cycle. This TFJ model was used to investigate the biomechanics and biotribology of the joint using the knee simulator (Liu *et al.*, 2015).

7.2.3 Wear study

A standard porcine gait cycle as described in Section 7.2.3.3 was applied for 5 hours during the wear test with 25% (v/v) bovine calf serum as the lubricant. Two types of tests were carried out; one with a natural patella against artificial femur as the positive control and the other with a natural patella against natural femur as the negative control.

Once the test was finished, the sample was removed from the SSKS and the lubricant was separated. The cartilage was carefully dried with a tissue to take a replica mould for wear assessment. The patella wear area was measured using the flexible film method as described in Chapter 2 Section 2.5. The intensity of the wear on the patella and femoral groove was then graded using the ICRS grading system described in Chapter 1 Section 1.3.1.2, as shown in Figure 7.14.

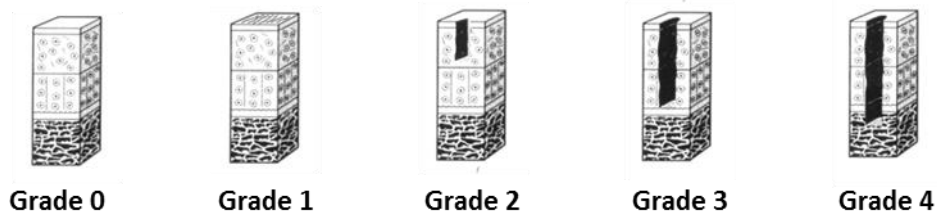


Figure 7-14: ICRS grading of cartilage wear

7.2.3.1. Sample preparation for surface analysis using profilometer

The samples for surface analysis were prepared by taking replicas of the natural patella. Due to the large curvature of the femoral groove it was difficult to obtain the replicas and scans from Alicona IF G5. Therefore, the roughness profiles of the femoral grooves were not considered in this study.

A thick layer of AccuTrans synthetic rubber replicating compound was spread over the articulating surface to make replicas. The replica of the cartilage surface was prepared pre and post wear test. AccuTrans was spread over the cartilage surface and left to set for 2 minutes and the patella was removed to leave the replica as shown in Figure 7.15.

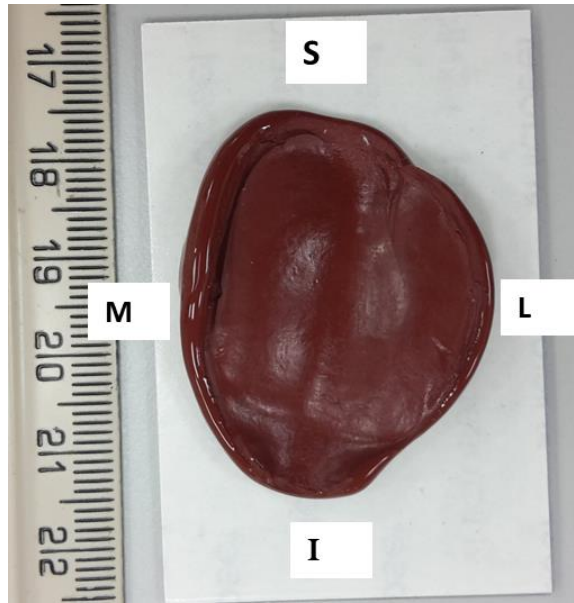


Figure 7-15: Impression of the patella made from AccuTrans mould

The Alicona Infinitefocus (IF) G5 surface profilometer as described in Chapter 2 Section 2.2.5 was used to evaluate the surface roughness of the cartilage. A vertical strip (red box of width 3 mm) from superior to inferior (S/I) and a horizontal strip (green box of width 5 mm) from medial to lateral (M/L) as shown in Figure 7.16 were scanned from each of the samples. The procedure in Alicona IF G5 implemented ISO 4287, 4288, 11562 and ASME B46 1-2002 for the process according to the profile lengths.

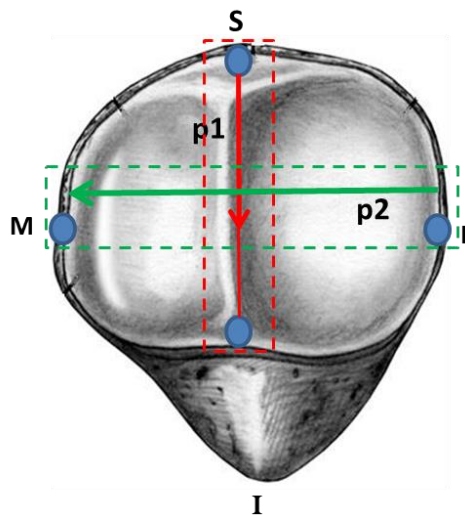


Figure 7-16: The area scanned using Alicona IF G5

Before the wear test, the 4 corners of the patella were marked using a 1 mm diameter drill bit. This allowed the AccuTrans to enter into the drilled holes and make reference points on the moulds. These were taken as the reference points during the Alicona IF G5 scanning. An S/I scan displaying the two reference points is shown in Figure 7.17. The reference point was

roughly at the middle of the S/I scan whereas the M/L reference points were more towards the Inferior end.



Figure 7-17: The S/I reference points from an S/I scan

7.2.3.2. *Obtaining results from Alicona IF G5*

The replicas were scanned in Alicona IF G5 surface profilometer at 10x magnification. The scanned data was then processed by the Alicona IF G5 software to provide a 3D image. The 3D model of the roughness standard reconstructed using this method is shown in Figure 7.18.



Figure 7-18: 3D model of a S/I scan

A line p1 and p2 was drawn with respect to the S/I and M/L reference points respectively. Line p1 was drawn from the centre of the S/I reference point whereas line p1 was drawn 3 mm superior to the M/L reference point. The surface roughness of these lines was then analysed. The reference points made sure that the same area was analysed pre and post wear study.

The surface profile extracted from the scan used for the measurement is shown in Figure 7.19. An 800 μm cut off wavelength was used to measure the surface roughness of cartilage in this study. This was because shorter wavelengths are better at capturing the finer irregularities seen in the early stages of cartilage damage (Brill *et al.*, 2015). Larger wavelengths of 2500 μm were used in previous studies which compared the roughness of cartilage against other artificial materials (Russell, 2010).

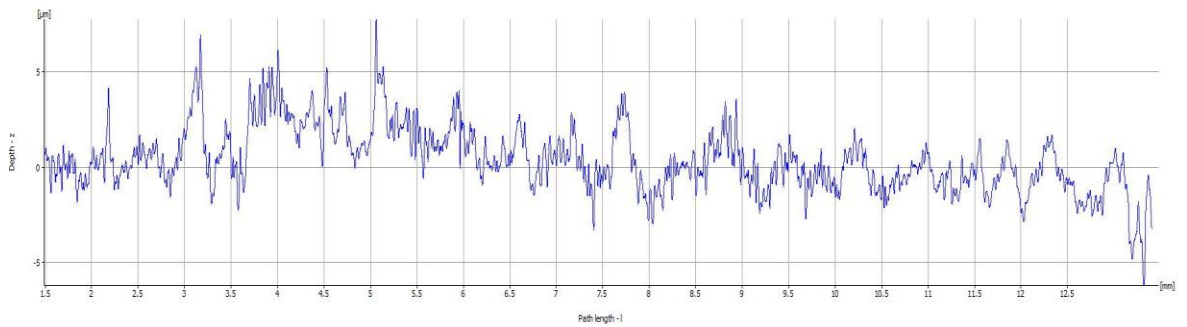


Figure 7-19: Surface profile extracted from the S/I scan at 800 μm cut off wavelength

The Ra values for each location were recorded pre and post wear study for the positive and negative control. Ra is the arithmetic average of the 2D roughness profile, measured as the average height of the peaks and valleys from the mean line calculated within the sampling length.

The mean \pm 95% confidence limits for the p1 and p2 locations of the 6 samples for negative and positive control were calculated for the pre and post wear tests. A Student's t-test was carried out to compare the roughness between the pre and post wear study in the two conditions.

7.3 Results

7.3.1. ICRS grading and wear area

In the negative control all 6 samples tested displayed Grade 1 wear. There was no visible damage to the cartilage but there was deformation on the cartilage surfaces that were in contact. The wear study caused the cartilage to compress and extrude water from the tissue at the point of contact and this was seen as the deformation. It was marked as shown in the femoral sample in Figure 7.20. This deformation was more visible directly on the sample compared to the deformation depicted in the photograph. The area was marked and calculated using the flexible film method.



Figure 7-20: The area of deformation caused by the wear study is marked in red

The positive controls displayed a larger deformation compared to the negative controls. However, Grade 1 wear occurred on all but one sample on which Grade 2 wear occurred. The deformation on the negative controls was no longer visible after the cartilage was allowed to rehydrate. However, only 2 femoral grooves from the positive controls were fully recovered after 2.5 hours of observation.

The area affected by the wear study in the positive control was $123.2 \pm 13 \text{ mm}^2$ in the patella (approximately 14% of the total patella area). In the negative control the patella area was $106.1 \pm 11 \text{ mm}^2$ (approximately 11% of the total patella area) and the femoral groove area was $178.7 \pm 42 \text{ mm}^2$.

7.3.2. Surface analysis using Alicona IF G5

Roughness values changes with change in cut off wavelength as shown in Table 7.2. The roughness of healthy cartilage (n=15) at various cut of wavelengths was recorded. The results showed that the roughness increased with increasing cut off wavelength.

Table 7-2: Change in Ra in healthy porcine cartilage with respect to cut-off frequency

Cut off wavelength (μm)	Ra (μm)
80	0.183 ± 0.04
250	0.368 ± 0.10
800	0.6855 ± 0.19
2500	3.2175 ± 0.93

The average surface roughness (Ra) obtained from Alicona IF G5 for the positive and negative controls, pre and post wear study, are shown in Figure 7.21.

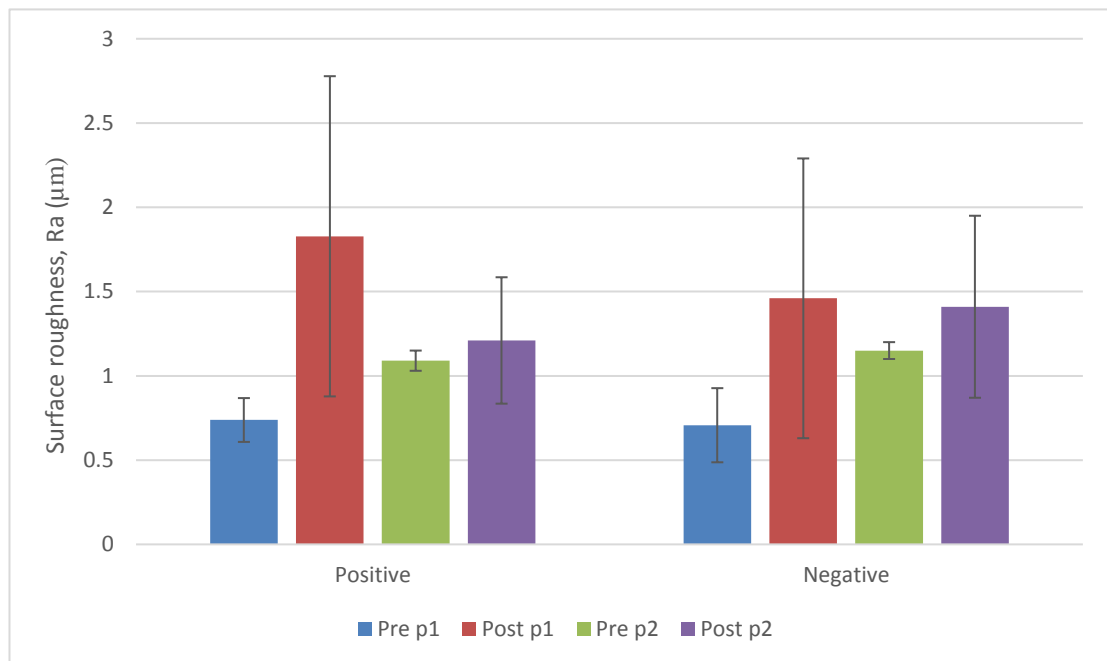


Figure 7-21: Roughness values from positive and negative control, mean (n=6) ± 95 % CL, where p1 is the S/I and p2 is the M/L scan

Although the post wear values were higher than the pre wear values in both conditions, there was no significant difference ($p > 0.05$) between the pre and post wear roughness. Therefore, the wear model established in this study was not enough to produce significant difference in wear.

7.4 Discussion

A method has been developed to apply physiological loading cycles to porcine PFJs to investigate the wear on natural joints. The wear area on the cartilage surface post wear test was calculated using the flexible film method and graded according to the ICRS grading standard. Replicas of the articular cartilage of the patellas were taken pre and post wear test. These replicas were analysed using Alicona IF G5 surface profilometer to measure the surface roughness of the cartilage pre and post wear study.

Developing the methodology to investigate the biotribology of the porcine PFJ was one of the most novel aspects of this project. A practical and consistent method was essential for mounting the porcine PFJ in the SSKS in order to investigate the wear. For the reproducibility of the tests it was necessary to maintain the same test conditions and follow the same procedure to prepare the samples.

Establishing a methodology to measure the radius of curvature (RoC) of the patello-femoral groove was essential to fix the samples in the SSKS. It was more accurate to develop a simple methodology to measure the actual RoC of each sample rather than assuming a constant RoC based on the literature as each sample had a large degree of variation in the shape and size.

There are several improvements that could be applied to increase the reliability and repeatability of this method. The validation of the methodology was the most limiting factor due to the lack of similar research carried out to date for comparison. If the biomechanics of the joint and kinematics of the patella is not replicated correctly, this could influence the model of lubrication in the cartilage that could affect the friction and the wear in joints. The assessment of wear particles could be used as an analysis to determine this change. This could happen in the absence of muscle compensation during joint kinematics, as seen in knee models that have soft tissues removed (Stachowiak and Podsiadlo, 1997).

The porcine gait cycle applied in this study was adapted from the human PFJ gait cycle used in the same lab to test artificial PFJs (Ellison *et al.*, 2008; Maiti *et al.*, 2014; Liu *et al.*, 2015). This could also be improved by combining the latest PFJ kinematic data from the literature. The adaptation and rescaling of the human gait cycle to the porcine gait cycle could have its limitations. However, this was the best option available as there was no existing data for the kinematics of porcine PFJs. Future studies on determining porcine kinematic data and patella position parameters will provide valuable data for validating these animal models for in-vitro simulations. However, this was not under the scope of the current project and hence the latest available data from the same laboratory was used for consistent comparative purposes.

A porcine model was used for the purposes of developing the method. There will be challenges when this method needs to be applied to human PFJs. There could be challenges in using human PFJ such as ethical approval, health and safety, tissue disposition and maintaining the tissue free of contamination by microbes. The size, cartilage properties, protein content in joint fluid, ligaments and material properties of the tissue can all contribute to the differences in the biomechanics of the joint.

Cartilage wear studies using pin on plate systems are carried out over a period of 24 hours (Russell, 2010). This usually involves a cylindrical plug reciprocating on a flat plate under constant loading conditions. Whole joint wear tests are usually limited to 2-4 hours

(Stachowiak and Podsiadlo, 1997; Taylor, 2012; Liu *et al.*, 2015) to reduce the damage caused by the gradual decomposition of the tissue. The current study was carried out for 5 hours in room temperature. Longer test duration needs to be explored to produce more wear but this will require the joint to be maintained for a longer period of time.

Even though it is was not fully under the scope of this project, the SSKS had special design features that allowed the testing of viable tissue over extended periods of time and under aseptic conditions. Compared to previous simulators, the test volume in the SSKS was significantly increased to permit the setup of a sealed test chamber under aseptic conditions, with direct temperature control. This will be a great asset for the future work that requires advanced control of certain parameters and will enable longer duration of wear tests.

There were no visible clearly defined wear patterns observed after the wear study. However, the deformation on the area of articulation on the cartilage was evident. This was more noticeable on the positive control than the negative. The area of deformation was marked and measured. The flexible film method used in this study allowed the 3D curvature of the sample to be considered while calculating the area. Hence this was a better method than calculating the area from the 2D direct image of the sample itself (Taylor, 2012). In the current study the wear was more visible directly on the sample than from a photograph. Therefore, assessing the wear using this method has been recognised to be more appropriate. The potential for error in this method will be in the area of human error when marking the boundary for the wear area.

ICRS grading can provide a qualitative analysis of the wear surface. However, in order to obtain a quantitative measure other sophisticated methods need to be implemented. Surface roughness has been shown to be a predictor of wear in many retrieval studies and it is true in the case of cartilage as well. A rougher surface creates higher friction and hence more chances of wear (Taylor, 2013). The roughness values vary across the literature depending on the techniques used. Alicona IF G5 is a non-contact method while for some of the others methods such as AFM and Talysurf is measured using a stylus. Currently, there is no study in the literature showing the roughness of cartilage using Alicona IF G5. Therefore, a direct comparison was not possible.

There is a large variation between measurements techniques and research groups. Some of the factors that could influence the results are the type of instruments used and the set up

applied for each method. The roughness obtained by Ghosh et al. (2013) from SEM stereoscopic imaging was comparatively higher than those obtained from AFM. However, the AFM values obtained by Moa-Anderson et al. (2003) were 5 times larger than those from Ghosh et al. (2013) and Peng & Wang (2013). The values obtained by Moa-Anderson et al were closer to the values obtained by Russell (2010) using the Talysurf method.

Parameters such as resolution, magnification and cut off wavelength chosen for each of the studies could be the other factors. For a direct comparison the same methods and testing parameters are required. Using an SEM, Ghosh and colleagues showed that the roughness values increased linearly with magnification Ghosh et al. (2013). The rough surface features are more prominent in longer cut-off frequencies and smaller features are elevated by shorter wavelengths. Studies have shown that shorter wave lengths were capable of capturing irregularities seen in the early stages of cartilage damage. Therefore a cut-off frequency of 800 μm was chosen for this study (Brill et al. 2015).

AFM is capable of high resolution roughness measurements at submicron levels. It is widely used for frictional and mechanical measurements of cartilage. However, this technique requires a very long scanning time and is only capable of scanning small areas. Therefore, AFM is impractical for quantitative analysis of the surface topography of cartilage for larger areas (Shekhawat *et al.*, 2009; Peng and Wang, 2013). Although widely used, SEM does not provide quantitative measurements of the surface topography (Shekhawat *et al.*, 2009). The method is also time consuming and difficult as the samples needed to be dried and gold plated before the SEM analysis (Gan *et al.*, 2013). The samples could have undesired dehydration and deformation that could affect the results.

Alicona IF G5 was used to measure the surface roughness of the cartilage. It can resolve roughnesses of up to 0.03 μm Ra value. The Alicona IF G5 is a non-contact measurement device unlike devices such as contacting Form Talysurf (Taylor Hobson, Leicester, UK) that uses a stylus which is dragged across the surface. Deflection of the stylus is picked up by a laser to recreate the surface topography. The stylus instruments require direct physical contact, which limits the measuring speed and are limited to the surface geometry of the material being measured and the measurements are 2D.

A pilot study was carried out using Talysurf and several difficulties were observed while measuring the roughness of the patella. The main problem was the inefficiency of the stylus to follow the steep curves in the patella. The steepness was too much for the slow speed of

the stylus to cover and this gave a few points where the stylus was not in contact with the material. In cases with large scars the stylus seemed to bend on contact whereas the non-contact Alicona IF G5 did not have any problem with the surface geometry and by individually adjusting the focus of the light and the brightness for each sample, the steep curves in the moulds were more easily captured.

Ferrography is a microscopic examination method that can be used to obtain wear particles from the lubricating fluid in a natural joint. This is widely used to qualitatively characterise the wear particles rather than quantitative wear volume measurements (Stachowiak and Podsiadlo, 1997). Modern particle counters have been claimed to detect wear volume as low as 0.02% of the total sample volume (Oungouliau *et al.*, 2012). Other methods of wear detection also exist that include the measurement of biomechanical assays for collagen and GAG measurement. However, the problem lies in obtaining the lubricating fluid that contain the wear particles. If all the fluid or particles are not collected from the joint, the measurement will not be accurate. Other debris such as the cement that is used to fix the joint or the bone and other tissues around the joint can also be collected along with the lubricating fluid. This migration can complicate the analysis.

There was no significant difference in roughness values between the negative and positive control. Therefore, the

The current study shows the potential of Alicona IF G5 in assessing wear in natural joints. A negative and positive control was used in this study to describe the methods. This could be applied to wear studies on joints with tissue substitutions such as osteochondral grafts to compare the tribology of the substitutions. Alicona IF G5 is able to scan large surfaces in 3 dimensions. It is much faster and easier than other instruments such as Talysurf. In future this feature could be used to explore the potential for volumetric measurements. This will enable the determination of the volume loss in natural cartilage.

Currently, there is no study in the literature showing the application of Alicona IF G5 in the assessment of wear in the articular cartilage. This will be the first of its kind. The method developed in this thesis can be applied to whole joints with osteochondral substitutions. This will allow investigating the wear patterns in the joints when these substitutions are implanted. This is a promising technique to compare the effect of different types of substitutions and their implant techniques.

7.5 Conclusions

This chapter established the methods for testing porcine PFJs in a SSKS. A positive and negative control was developed to apply different methods of measuring wear. The application of Alicona IF G5 was used to analyse the surface roughness at each test condition which showed that the roughness values in the positive control was larger than the negative control. However, there was no significant difference in the wear which implies that the wear model established in this study is not sufficient to produce significant wear.

Chapter 8. Contact mechanics of the porcine patello-femoral joint

8.1. Introduction

Contact area and pressure can be predictors of wear and failure in joint replacements (Hsieh et al. 2002; Clark et al. 2002; Lee et al. 2003; Bachus et al. 2006; Merkhher et al. 2006) and are also applicable to joint substitutions. Various in-vitro techniques have been used to study the contact mechanics in diarthrodial joints including Fuji film , Tekscan, piezoelectric transducers and dye injection methods (Liggins et al. 1995; Lee et al. 2001; Garretson 2004; Li et al. 2004; Bachus et al. 2006). However, the variations in parameters such as load, flexion and type of joint used for the testing can make direct comparison difficult. Therefore, the present study systematically investigated the effect of load, flexion and displacement on the contact mechanics of the porcine patello-femoral joint (PFJ) using Tekscan pressure sensors.

The aim of this study was to develop and apply a methodology to investigate the contact mechanics of PFJ using Tekscan in an SSKS. The contact mechanics of the joint were investigated by measuring the contact area and contact pressure at various points in a porcine PFJ gait cycle. The effect of constant load, flexion angles and displacement were determined to better interpret and understand the contact mechanics at these various points in the gait cycle.

8.2. Materials and methods

The materials included a single station knee simulator as described in Chapter 7, porcine PFJs and Tekscan sensors as described below.

8.2.1 Porcine PFJ

Right knee joints from 6 months old Large White pigs were used in this study. All the joints were healthy and had shiny, white and slippery cartilage with no visible defects. The patello-femoral samples were prepared as explained in Chapter 7 Section 7.2.2. Six samples were tested for each study; these consisted of the gait study and the fundamental study. The gait cycle study was carried out first followed by the fundamental study.

8.2.2 Tekscan sensors

A Tekscan sensor (Model 4000, saturation pressure 10.3 MPa) with the I-Scan software (Tekscan, Inc., South Boston, MA), as shown in Figure 8.1, was used to measure the contact

area and contact pressure between the patella and the femur under different conditions during the contact mechanics study. This particular Tekscan sensor was used because it was most suited for the load applied in this study as well as the area and geometry of the sample that was being measured.

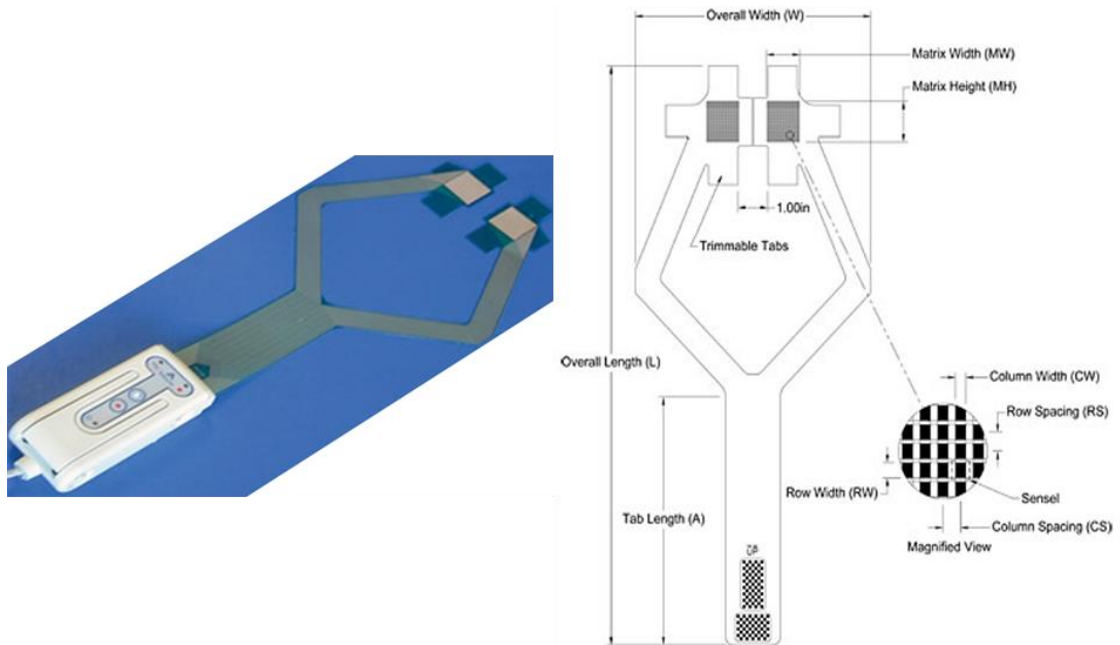


Figure 8-1: Left– A Tekscan sensor connected to the handle, Right – Labelled diagram of a Model 4000 sensor (Obtained from Tekscan®)

The proximal end of the sensor was attached to the handle with a USB connection to enable data connection to the computer. The dimension of each sensor was 27.9 mm (width) x 33 mm (length) x 0.1 mm (thick). It contained 572 sensel measurement points with a sensel density of 62 sensels per cm².

8.2.3 Calibration

The Tekscan sensors were calibrated using an Instron material testing machine (Instron 3365, High Wycombe, Bucks, UK) as shown in Figure 8.2. A 4 mm thick polyurethane sheet with an elastic modulus of ~0.7 MPa was placed on either side of the sensor during calibration to provide a similar compliance to cartilage. The sensors and the rubber sheets were of the exact same dimensions and these were compressed between metal plates on the Instron in order to produce an area of uniform pressure with 10 pre-conditioning cycles to 2 MPa.

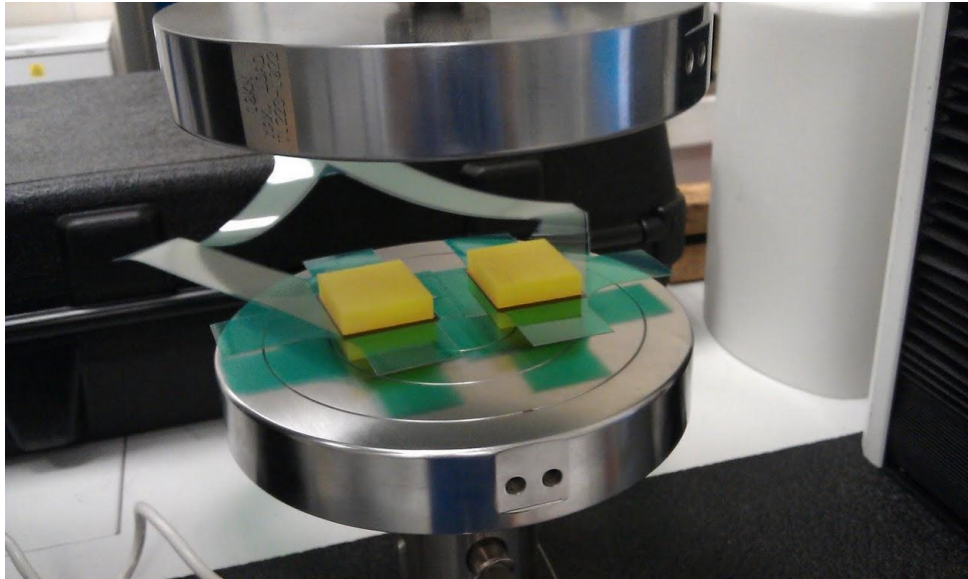


Figure 8-2: Tekscan sensor was placed between two rubber sheets and compressed between two metal plates in the Instron during calibration

Each sensor was calibrated individually as they were unique in terms of digital output. They were equilibrated to 10%, 50% and 90% of the maximum expected load for the study to normalise the readings and to ensure identical output for an applied uniform force. As readings were to be taken across the full range of the sensor, an identical two-point power law calibration was performed. This used two readings, taken at 20% and 80% of the peak expected loads, which were 250 N and 750 N respectively.

As it was the first time these sensors had been used, the response needed to be characterised. Therefore, the output load from the Tekscan was checked before and after the contact mechanics study by applying a known load using the Instron material testing machine. These Tekscan verification results are shown in Figure 8.3. The overall output force was higher compared to the applied load in both cases. Before the test, the Tekscan outputs were almost 5% higher than the Instron input and this increased to 13% after the test. Therefore, there was an 8% overall increase in the Tekscan output at the end of the contact mechanics study.

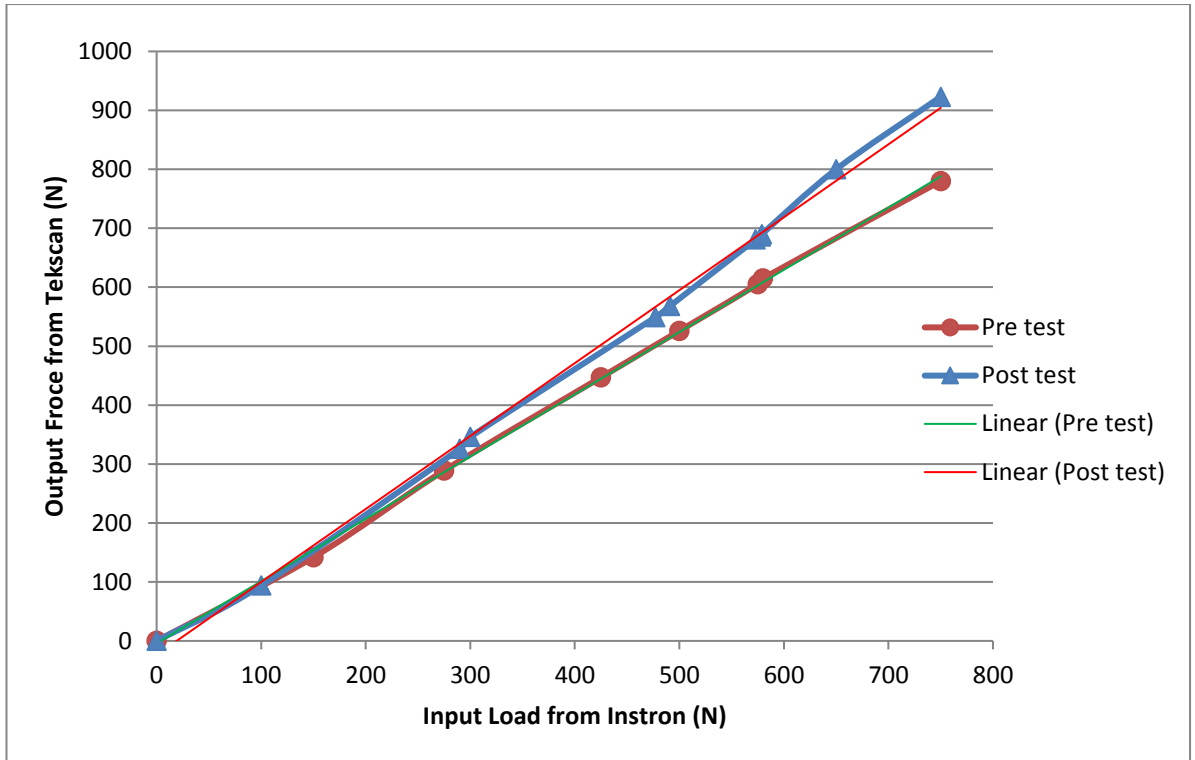


Figure 8-3: Tekscan verification curves from the Instron pre and post study with regression lines

Another set of verification tests were carried out to investigate the sensitivity to load in the input and output systems. The SSKS was used to apply the input loads and the output forces were measured using the Tekscan pressure sensors and an external load cell.

Pressure sensors were placed between the rubber sheets as before. This set up was fixed inside the SSKS dummies and a constant load of 100 N was applied through the SSKS for 10 seconds. The output was measured from the Tekscan sensors as well as from an external load cell, similar to the SSKS axial load calibration process. The process was repeated, increasing the load in increments of 100 N until it reached 1000 N.

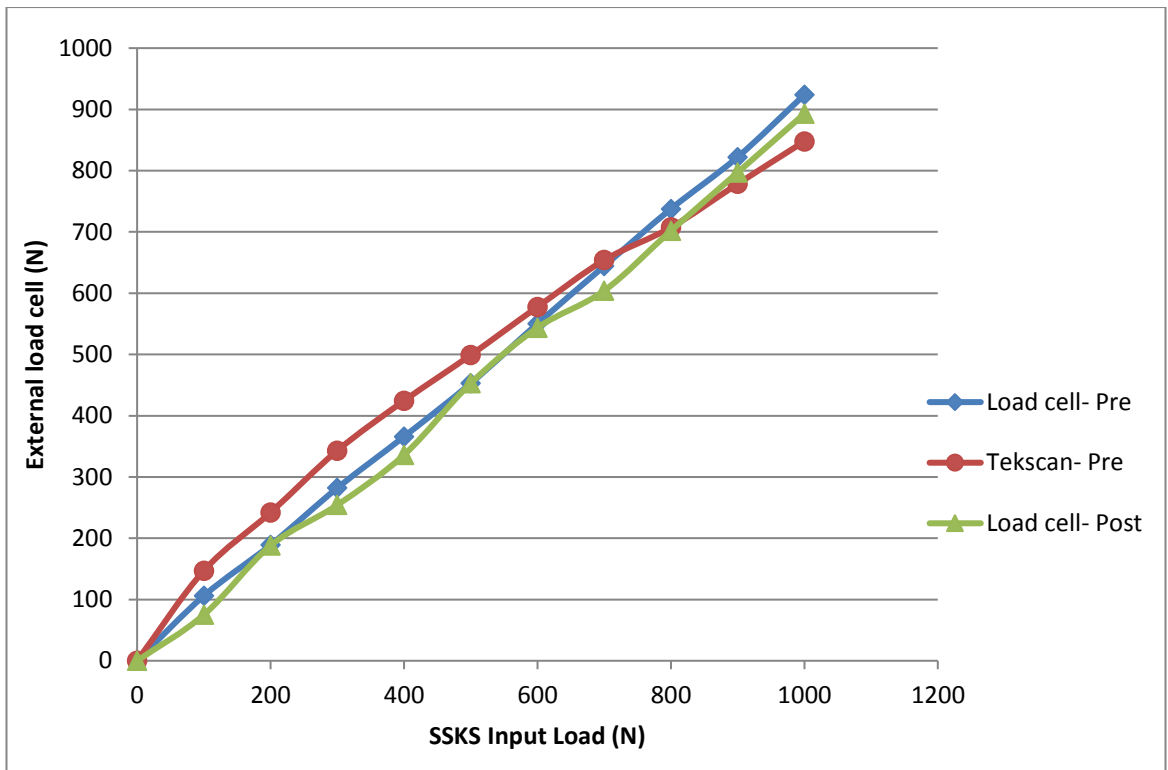


Figure 8-4: Output from external load cell and Tekscan compared to the input from the SSKS before and after the contact mechanics study

The Tekscan verification curves from the SSKS before and after the contact mechanics study is shown in Figure 8.4. The load cell results showed only minor differences pre and post-test, indicating that the SSKS was consistent in its load application. The Tekscan results were, however higher post study after a load of 400 N. In the previous verification curve (Figure 8.3), it was noticed that there was an 8% increase in the Tekscan results after the contact mechanics study. In the current verification curve, the overall Tekscan output force was also higher compared to the applied load in both cases. Pre-test, the Tekscan outputs were almost 4% higher than the SSKS input and this increased to 13% post-test. Therefore, there was a 9% overall increase in Tekscan output compared to the SSKS input load at the end of the contact mechanics study.

8.2.4 Setting up the test

The samples were prepared as described in Chapter 7 Section 7.2. The pressure mat on the Tekscan was placed over the patella, making sure that the patella was positioned on the centre of the sensor. Only one sensor was placed between each sample and was secured with vinyl electric tape around the edges. It was necessary to ensure that the sensor did not

move during the test as this could have interfered with the readings and also made it difficult to plot the relative position of the joint.

Pressure was applied to the medial, lateral, superior and inferior corners of the patella. This was used to determine the location of the patella on the pressure maps later. The contact mechanics were mapped with respect to the patella because as the pressure sensor was attached to the patella there was no angular displacement in the patella. Hence the four markers identified for each specimen would be the same throughout the test which maintained the repeatability of the study.

8.2.5 Running the test

In terms of the SSKS, A/A was fixed but the ML displacement was unconstrained to allow the PFJ to find its neutral position in these axis. The axis of the PFJ in the SSKS is discussed in Chapter 7 as shown in Figure 7.1. The sample with the Tekscan was placed inside the SSKS at the neutral position as established by the contact point study described in Chapter 6. The simulator and Tekscan were activated together and the contact mechanics was recorded for 10 continuous frames.

Two types of test were carried out; these consisted of the fundamental contact mechanics study and the contact mechanics at five different stages in the gait cycle. The gait cycle study was carried out on the sample first, and this was then kept hydrated for an hour before it was used for the fundamental study. This ensured that the cartilage was able to recover to its original state before the next test commenced. The same 6 samples were used for the two studies to ensure that the results from the fundamental study could be compared to the gait cycle study without any variation among samples within the two tests.

For the gait cycle study, 5 points were taken from the porcine PFJ gait cycle. The gait cycle marked with these 5 points is shown in Figure 8.5. The points were chosen such that the main points in the different stages in the gait cycle were covered. The first two points were in the stance phase, the third point was half way through the gait cycle and the last two points were in the swing phase. The corresponding load, flexion and SI displacement were applied to the joint.

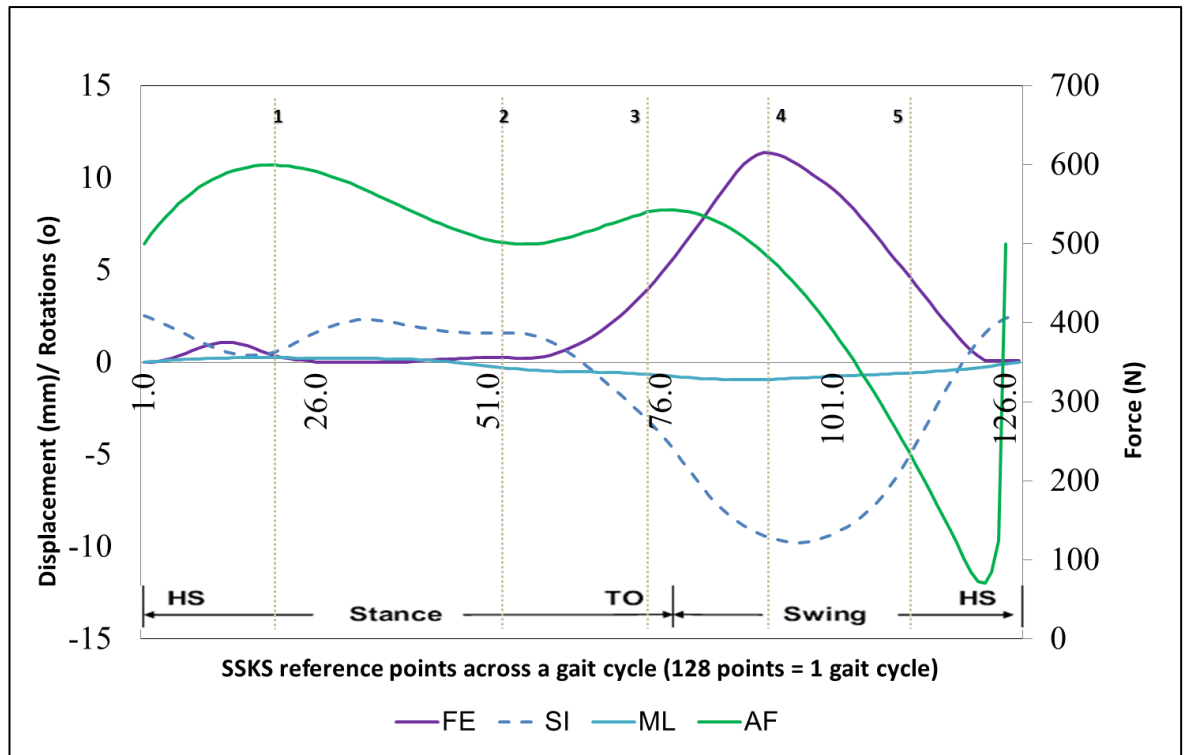


Figure 8-5: Porcine patello-femoral gait cycle. HS= Heel strike, TO= Toe off

FE= Flexion/Extension, SI= Superior/Inferior displacement, ML= Medial/Lateral rotation, AF= Axial Force

The fundamental study was then carried out to systematically investigate the effect of flexion, load and displacement. Flexion at 0, 5 and 10 degrees and load at 100, 300 and 600 N was used. Displacement at 5, 0, -5 and -10 mm (5 mm in superior direction, neutral position, 5 and 10 mm in inferior direction respectively) were also investigated.

The 36 test conditions carried out for the fundamental study are shown in Table 8.1. The 36 numbers in the Table correspond to the different conditions tested in this study. For example, for condition #1 the axial force was 100 N, 0 degree flexion and SI displacement was 5 mm. Similarly, for #36 the axial force was 600 N, 10 degree flexion and SI displacement was -10 mm.

Table 8-1: Parameters for the fundamental study

36 test conditions with varying Load (axial force, N), flexion (FE, degrees) and displacement (SI, mm)

	a	b	c
AA	Fixed/0		
ML displacement	unconstrained		
ML rotation	unconstrained		
Axial Force (N)	100	300	600
FE = 0	Condition Number		
SI=5	1	13	25
SI= 0	2	14	26
SI= -5	3	15	27
SI=-10	4	16	28
FE = 5	Condition Number		
SI=5	5	17	29
SI= 0	6	18	30
SI= -5	7	19	31
SI=-10	8	20	32
FE = 10	Condition Number		
SI=5	9	21	33
SI= 0	10	22	34
SI= -5	11	23	35
SI=-10	12	24	36

8.2.6 Analysing the contact mechanics recordings

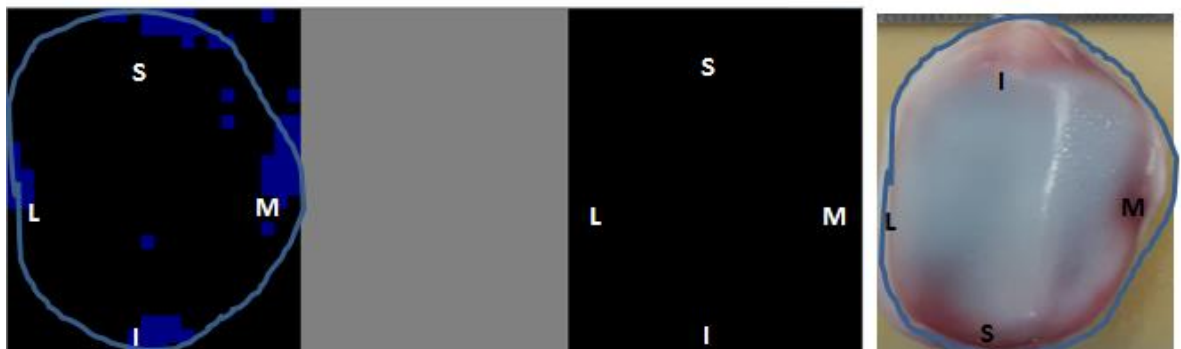


Figure 8-6: Marking the location of patella on the pressure map

The pressure map created from the Tekscan software for the reference points of the patella was exported to Image Pro plus along with the image of the corresponding patella. A photograph of the patella was taken using a Canon SLR camera with a ruler next to it. The dimensions of the Tekscan pressure mat and hence the Tekscan pressure map image was 33 mm by 28 mm. The size of the patella and the pressure map was used to calculate the

position of the patella using ImagePro Plus. This method was applied to trace the position of the patella on the contact mechanics results.

8.3 Results

Two typical recurring patterns of contact mechanics were observed. Out of the 6 samples tested, 2 samples showed type 1 pattern and 4 samples showed type 2 pattern. These patterns were the same in both tests. Pattern 1 had a larger contact area compared to pattern 2. Pattern 2 showed higher peak pressure compared to pattern 1.

8.3.1 Gait cycle study

The typical pressure maps for pattern 1 and 2 observed in the gait cycle study are shown in Figure 8.7 and 8.8. In type 1 pattern, the beginning of the gait cycle showed a larger contact area.

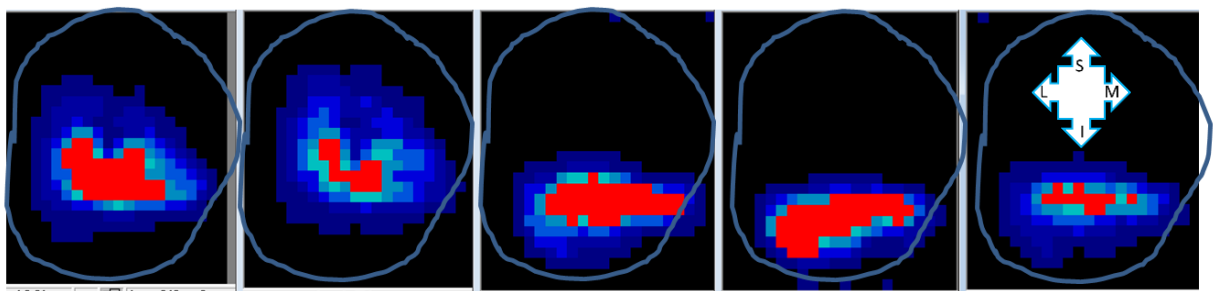


Figure 8-7: Pattern type 1 with larger contact area showing the 5 stages (as indicated in Figure 8.6) in the gait cycle

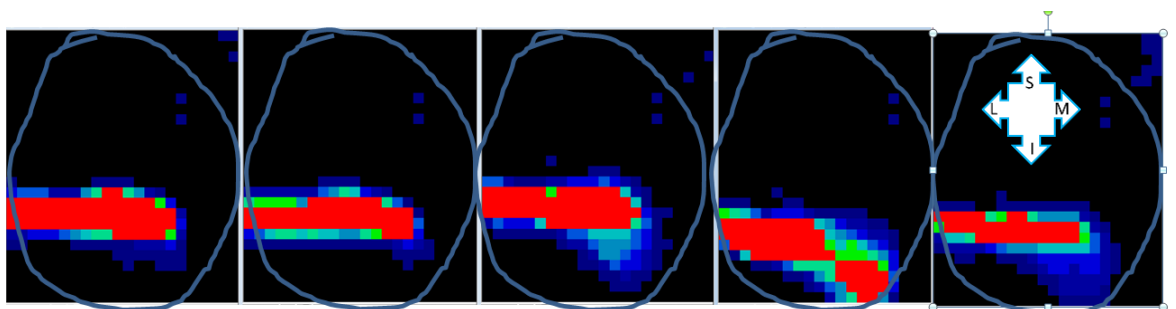


Figure 8-8: Pattern type 2 with smaller contact area showing the 5 stages in the gait cycle

The mean contact area for the 6 samples is shown in Figure 8.9. The contact area decreased across the different stages of the gait cycle. The area in the stance phase was larger compared to the contact area in the swing phase. The contact areas in stage #1 and #2 in the stance phase were very similar. One way ANOVA was carried out to compare the 5 stages in the gait cycle. There were no significant differences ($p > 0.05$) in the contact area between the stages.

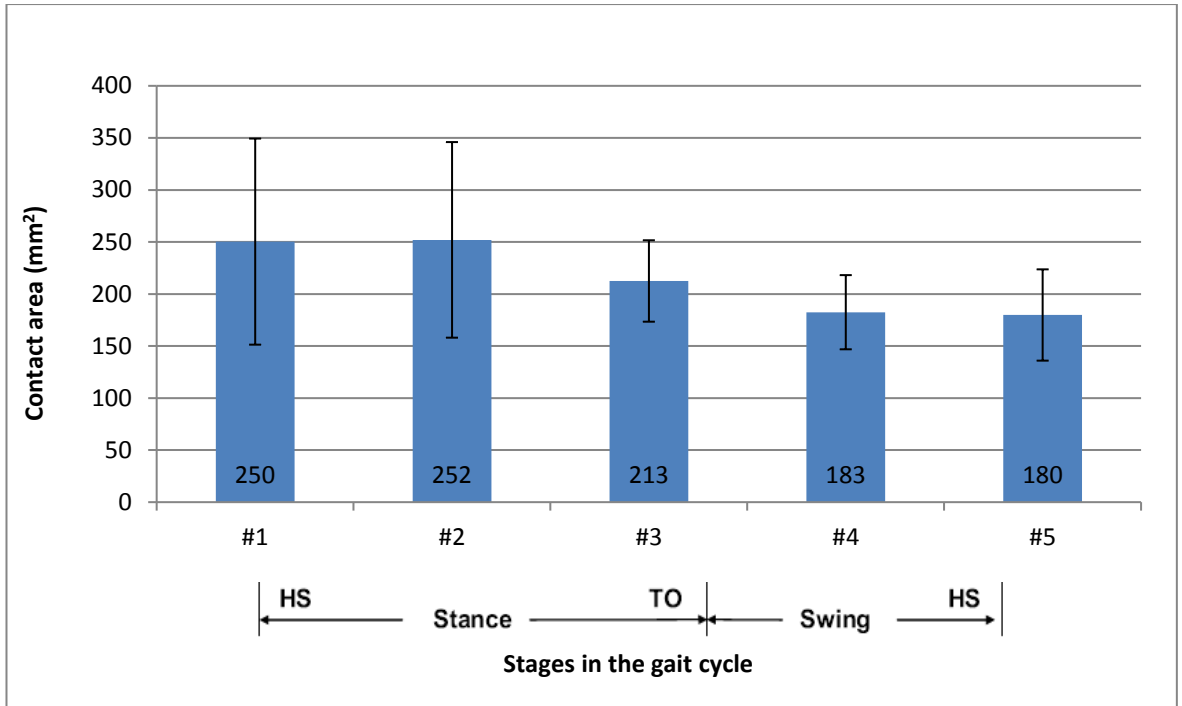


Figure 8-9: Mean contact area over a gait cycle . Data is presented as the mean (n=6) ± 95% confidence limits

The change in mean contact pressure and peak contact pressure during a gait cycle is shown in Figure 8.10 and 8.11 respectively. One-way ANOVA showed no significant differences (p>0.05) in the mean and peak contact pressures between the stages.

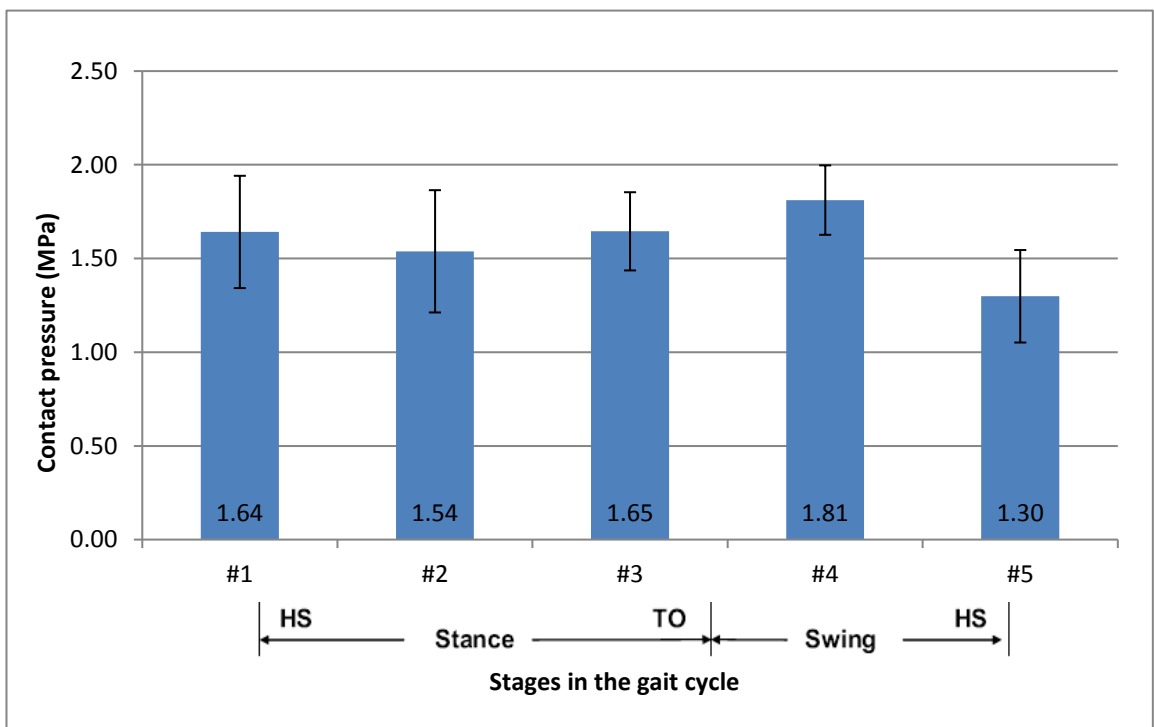


Figure 8-10: Mean contact pressure over a gait cycle. Data is presented as the mean (n=6) ± 95% confidence limits

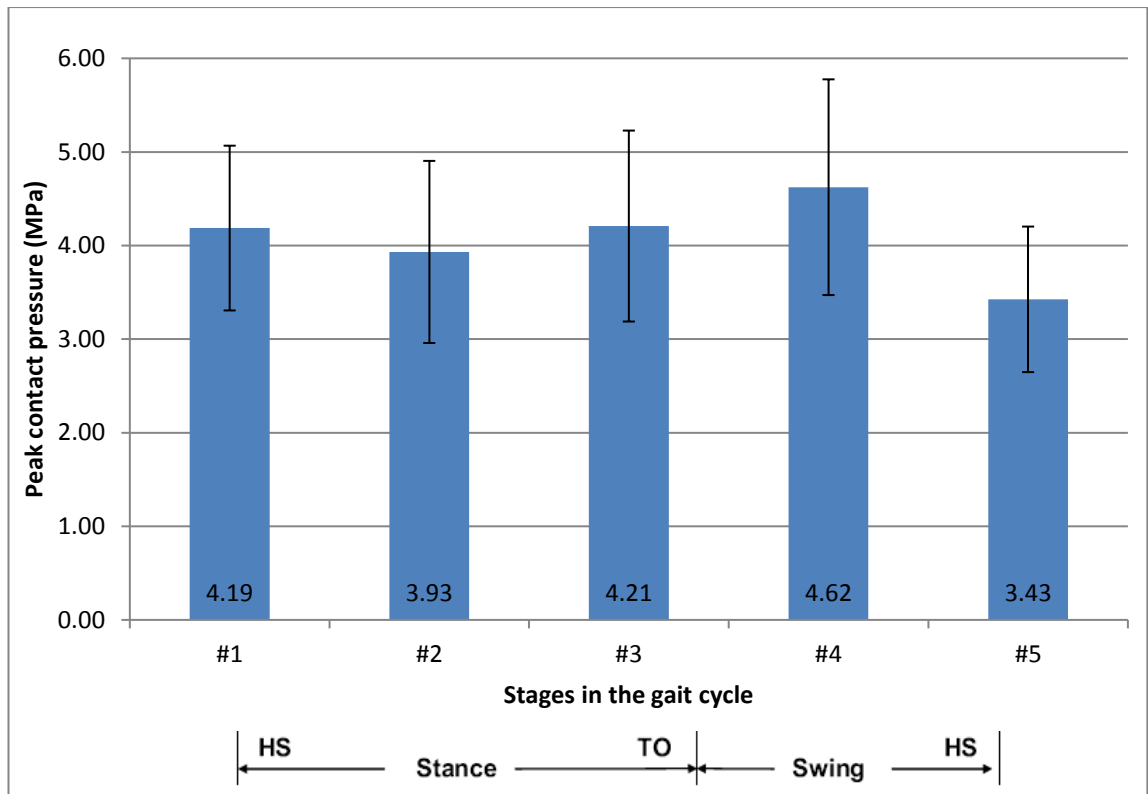


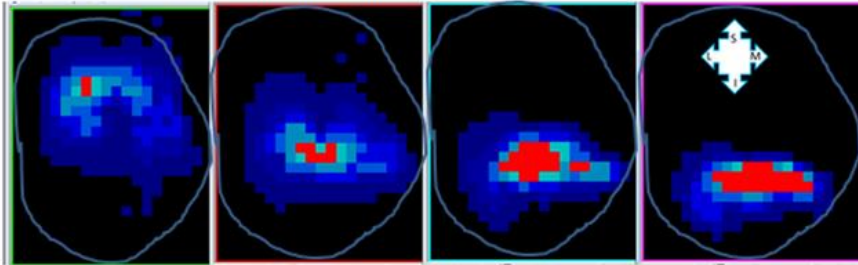
Figure 8-11: Mean peak pressure over a gait cycle .Data is presented as the mean (n=6) ± 95% confidence limits

The trends in peak contact pressure and mean contact pressure throughout the different stages in the gait cycle were similar. However, the error bars in the peak contact pressure were higher compared to the mean contact pressure. The highest contact pressure was observed in stage #4. The mean contact pressure reached 1.81 ± 0.19 MPa and the peak pressure reached 4.62 ± 1.15 MPa at this stage. The lowest pressure was at the end of the swing phase (stage #5) where the mean contact pressure was 1.29 ± 0.25 MPa and the peak pressure reached 3.42 ± 0.77 MPa.

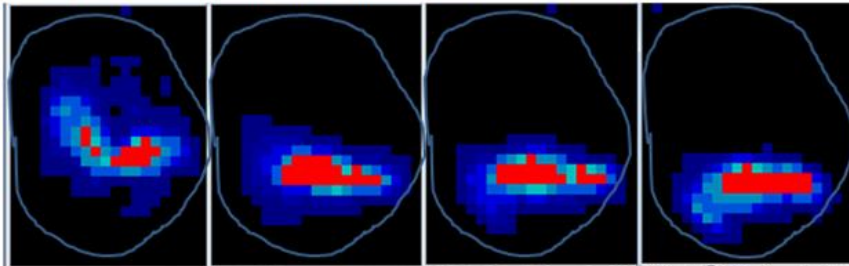
8.3.2 Fundamental study

The typical pressure maps for pattern 1 and 2 observed in the fundamental study are shown in Figure 8.12. In pattern 1, the area decreased from superior to inferior displacement whereas the contact area increased from superior to inferior displacement in pattern 2. In pattern 1, the contact area decreased with increasing flexion. The contact also moved from superior-lateral position to Inferior-medial position for each flexion angle. However, these trends were not evident in pattern 2.

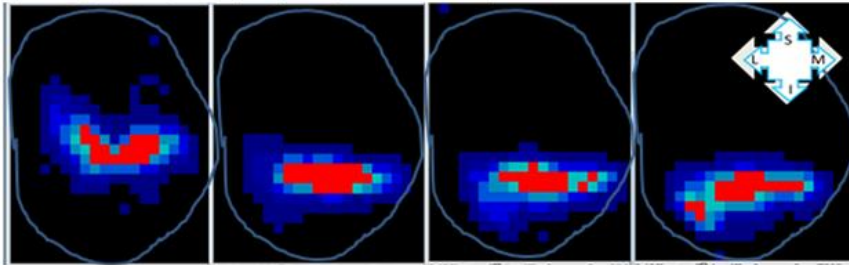
(A) FE=0°, AF=300N, SI=5mm, 0mm, -5mm, -10mm respectively



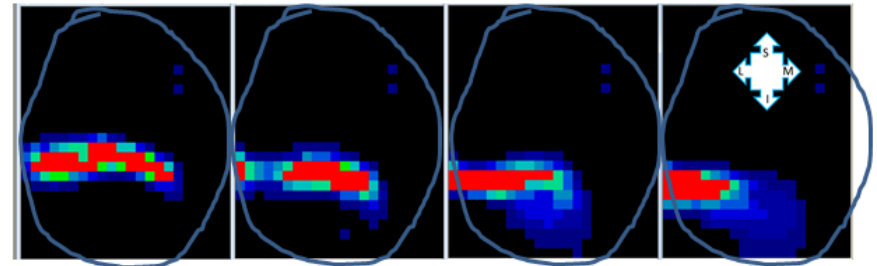
(B) FE=5°, AF=300N, SI=5mm, 0mm, -5mm, -10mm respectively



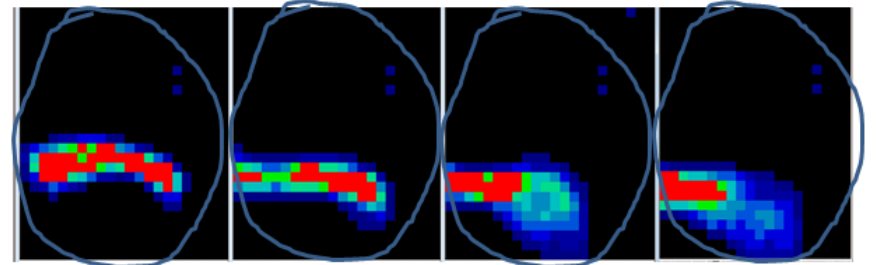
(C) FE=10°, AF=300N, SI=5mm, 0mm, -5mm, -10mm respectively



(A) FE=0°, AF=300N, SI=5mm, 0mm, -5mm, -10mm respectively



(B) FE=5°, AF=300N, SI=5mm, 0mm, -5mm, -10mm respectively



(C) FE=10°, AF=300N, SI=5mm, 0mm, -5mm, -10mm respectively

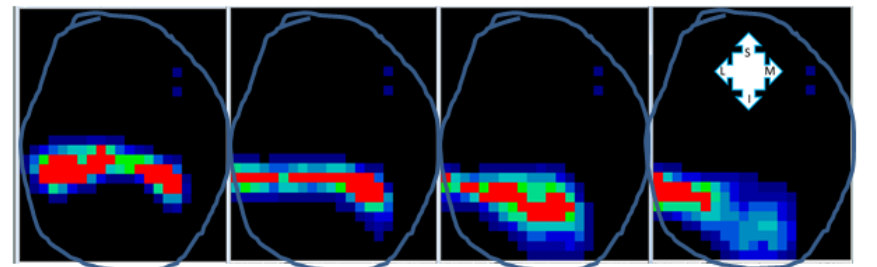


Figure 8-12: Pattern type 1 (left) and pattern type 2 (right) showing the change in contact mechanics with respect to SI (left to right) and FE (top to bottom)

The effect of flexion on contact area and pressure at different load and displacement is shown in Figure 8.13 and 8.14 respectively.

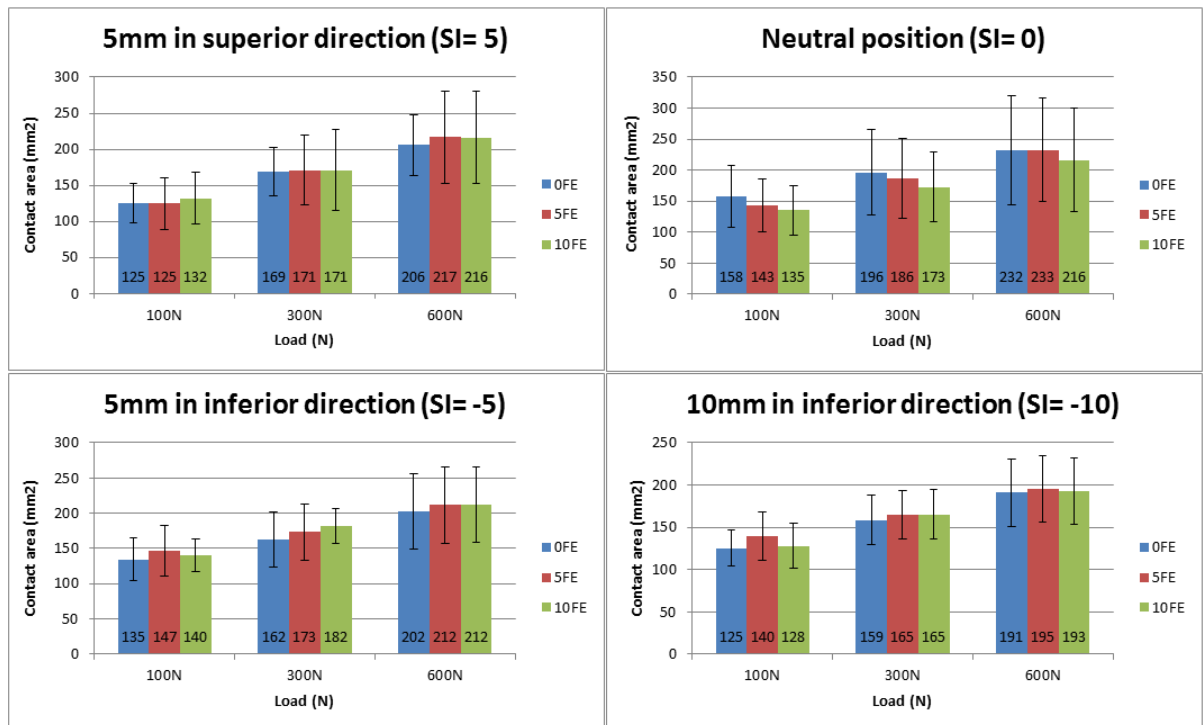


Figure 8-13: Effect of flexion on the contact area at different loads and displacements (Mean (n=6) ± 95% confidence limits)

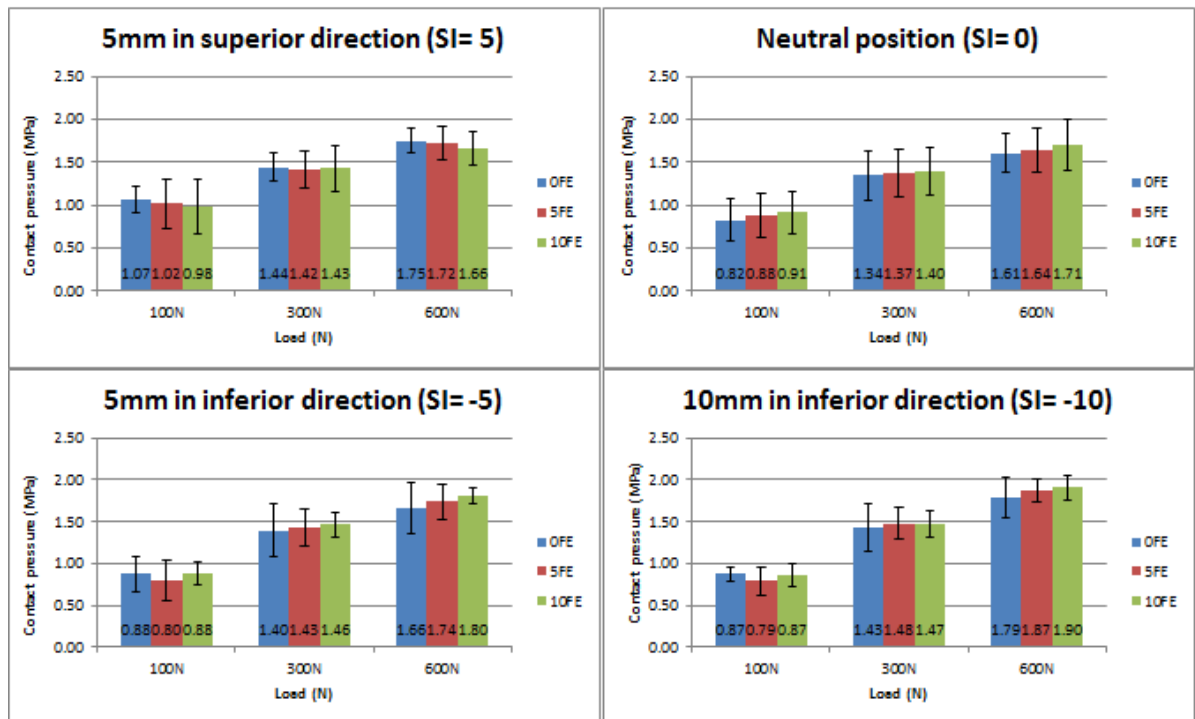


Figure 8-14: Effect of flexion in the contact pressure at different loads and displacements (Mean (n=6) ± 95% CL)

There were no significant differences ($p > 0.05$) between the flexions at any given load or displacement. However, the contact pressure significantly ($p= 0.013$) increased with increasing load. The 95% confidence limits also showed a larger variation in the contact area at higher loads.

There was almost no change in the contact area across various flexion angles at a displacement of 5 mm in the superior direction and at the neutral position the contact pressure also stayed the same across all three flexion angles. On the other hand, the contact pressure decreased with increasing flexion at a displacement of 5 mm in the superior direction and at the neutral position the contact area decreased with flexion.

The effect of displacement and flexion on the contact area and contact pressure at 300 N is shown in Figure 8.15 and 8.16 respectively.

Across various loads, flexion had no effect on the mean contact area or pressure at the 5 mm superior position ($SI=5$) and the 10 mm inferior position ($SI= -10$). However, at neutral position ($SI= 0$) the contact area decreased with increase in flexion and at 5 mm inferior ($SI= -5$) the area increased with the flexion.

As shown in Figure 8.15, from neutral to the inferior position the contact pressure increased with an increase in flexion. Similar trends were also observed at axial loads of 100 N and 600 N. At the different flexion angles the overall contact area was maximum at the neutral position ($SI=0$) and minimum at 10 mm inferior ($SI= -10$).

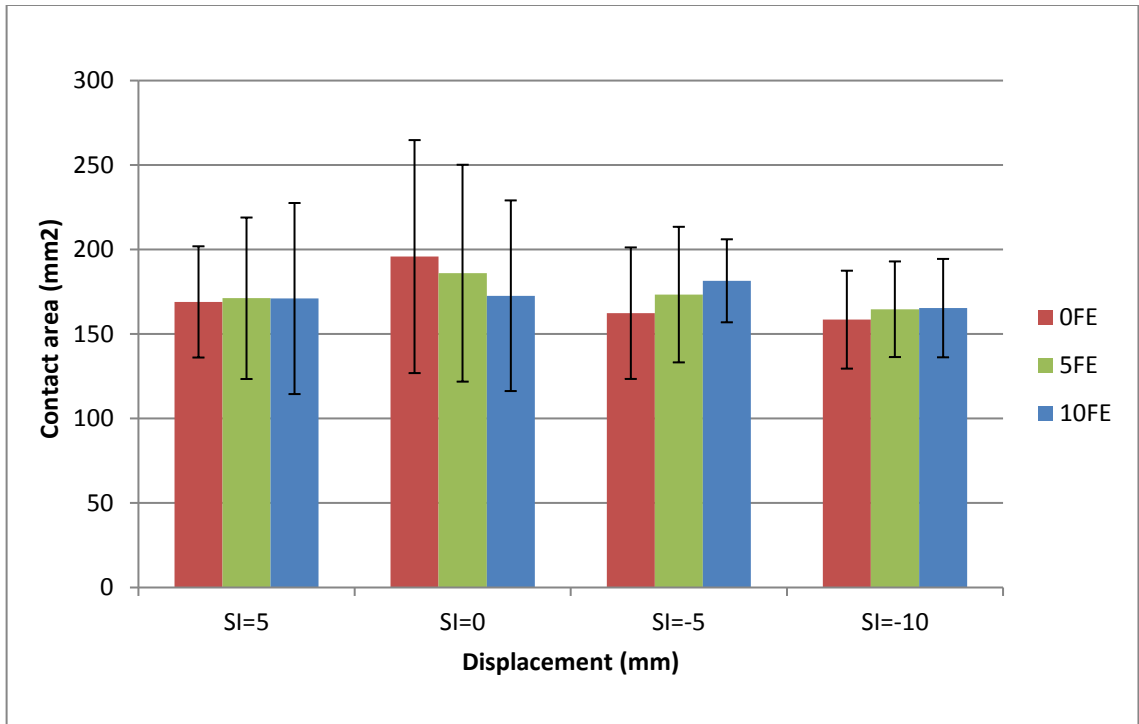


Figure 8-15: Contact area at 300N (Mean (n=6) ± 95% confidence limits)

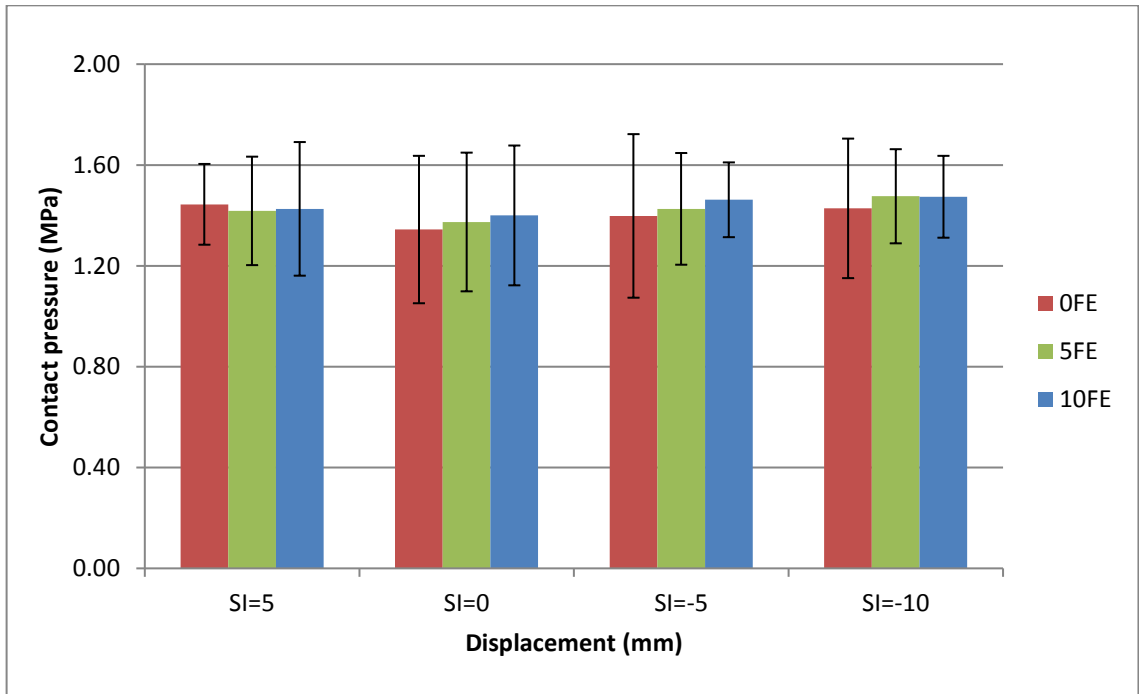


Figure 8-16: Contact pressure at 300N (Mean (n=6) ± 95% confidence limits)

8.4 Discussion

Contact area and contact pressure have been an area of interest for many (Clark, Herzog and Leonard, 2002; Hsieh *et al.*, 2002; Lee, Morris and Csintalan, 2003; Bachus *et al.*, 2006; Merkher *et al.*, 2006; Li *et al.*, 2011). Contact mechanics studies have contributed to the understanding of load distribution and pathology in diarthroidal joints, using a range of methodologies. Different researchers have used different methods and tools; in vitro studies using pressure sensitive films such as Tekscan and Fuji films, in vivo studies using MRI scans and the use of computational methods are common. However, there has been little research carried out to investigate the contact mechanics in the PFJ, especially using Tekscan sensors (Leichtle *et al.*, 2014; Wang *et al.*, 2015; Kim *et al.*, 2016; Lorbach *et al.*, 2016).

This chapter discusses the development and application of a methodology using Tekscan pressure sensors to investigate the contact area and contact pressure in the porcine PFJ. A fundamental study was carried out to systematically investigate the effect of flexion/extension, axial force and superior/inferior displacement on the contact mechanics of the joint. This showed the change in contact mechanics when all the test conditions were kept the same and just one variable was changed. A gait cycle study was also carried out to replicate the conditions in five different stages in the gait cycle and the contact mechanics was investigated.

In the gait cycle study, the contact area changed across the 5 points in the gait cycle. The contact area in the stance phase was larger compared to the contact area in the swing phase. This is because, during swing phase the feet do not touch the ground and there is no body weight applied. The highest contact pressure was observed in stage #4, just after the toe off region at the end of stance. This change in contact pressure was an indication of how the load is distributed during a normal walking cycle. At stance phase almost the entire body weight is applied but at swing phase, the leg lifts off the ground and the full body weight is not applied. Therefore, these points showed lower values.

In the fundamental study, an increase in contact area was observed with increasing load. This was consistent with the contact area results presented by Clark *et al.* using Fuji films in feline PFJs. They observed an exponential increase in contact area with force (Clark, Herzog and Leonard, 2002). The forces in the PFJ decreased across the gait cycle. The contact area

decreased with this decreasing load but there was no trend in the mean and contact pressures. This is because as the contact load increases, the contact area will increase to maintain a constant contact pressure in the joint.

In the fundamental study, the pressure increased with increasing flexion. A similar influence of flexion was noted by Geeslin et al. (2015) who investigated the influence of ligaments in the contact mechanics of cadaveric TFJ using Tekscan. They also observed a greater change in contact mechanics at larger flexion angles. TFJs with a meniscal tear showed 37- 52% decrease in contact area and 55-87% increase in contact pressure when flexion increased from 0-90°. The current study also observed larger contact pressures in conditions with lower contact area.

The contact pressure showed an increase with respect to the position of the patella. There was a larger contact pressure in the inferior displacement compared to the superior. This trend was more noticeable at lower loads. The contact area and contact pressure increased with increasing load despite the change in displacement or flexion.

The contact area obtained in this study agrees with the results from the literature. Brechter et al. (2003) measured contact area in human cadaveric PFJ using Fuji Film and MRI. A custom-made apparatus was used to apply a compressive load at 30° flexion. In the current study, similar to Brechter et al, there was a large variation between the samples, ranging from a contact area of 1.4 - 4.5 cm². However, the mean contact area in Brechter et al method was larger than the mean contact area in this study. They were in the range of 3 cm² and the current study was below 2.4 cm². Their study was on human cadaveric joints that would have a larger surface area compared to the porcine joints in this study.

There was also a large variation between the samples in the contact pressure, ranging from 1.06-2 MPa across the gait cycle. As seen from the fundamental study, the position did not have much effect on the contact pressure at higher loads. The position moved from superior to inferior across the gait cycle while the load was increasing.

Pattern 1 and pattern 2 were seen on both the fundamental and the gait cycle study, ie, the same pattern on the same samples was observed. This implies that the pattern was related to the shape of the samples rather than the test conditions. The change in pattern observed under

the same test conditions clearly shows that the variation was due to the geometry of the individual patello-femoral joint as the curvature of the surface can influence the contact points on the pressure sensors.

Other studies have also observed this change in contact mechanics across the samples. Brechter et al. observed a large variation between the 6 samples tested, ranging from 1.4 – 4 cm² in Fuji film and 1.5 – 4.5 cm² in MRI (Brechter *et al.*, 2003). Wang et al. (2015) investigated the contact pressure on the tibial plateau at various meniscal conditions using Tekscan pressure sensors. They observed a site dependent variation in all conditions and specimens. This also suggests the influence of the geometry of the joint in its contact mechanics.

The geometry of the joints was shown to have an effect on the contact mechanics. The tests were conducted with exactly the same conditions on each sample but the results varied across the samples. The geometry of each sample was different in terms of the area of the patella and the curvature of the groove. All the samples used in this study were from pigs of the same age range obtained from the same abattoir. No visible correlation was observed between the weight of the animal and the geometry of their joints. Some of the heavier animals had the smallest patella and the flattest groove.

Biological variation exists incoherently and the change in geometry between the samples is one of the reasons for the variation in contact mechanics across the samples. Larger patellae would have larger contact area as they simply had a larger surface area for the contact (Besier *et al.*, 2005; Gorniak, 2009). Nevertheless, this is not always true because other factors such as the curvature of the joint will also contribute to the contact area.

The contact mechanics of the joint can change with the anatomy of the patella and femoral groove. This was observed in several studies conducted on human samples in the past (Wiberg, 1941; Kwak *et al.*, 1997). Kwak et al. (1997) characterised the surface topography of the joint and found the types of patella found among the population. Through clinical images and surface analysis of these joints they observed a link between the anatomy and pathology caused by unequal distribution of loads such as patellar misalignment.

Although not measured during the dissection process, it was observed that some patellae had a more distinct ridge between the odd and medial facet compared to others. This was supported by Gunnar Wiberg's statement that there was a higher contact pressure between a convex patellar facet articulate against a convex femoral condyle. In these types of joints, the ridge between the medial and odd facet of the patella were distinctive (Wiberg, 1941).

During the dissection process in this study, a difference in the geometry of the joint in terms of the curvature of the femoral condyles and patella facets was observed. In some patellae the ridge between medial and lateral facet was not distinct although the femoral groove was deep and defined. This scenario could explain the two different patterns observed in this study. When the geometry allows the articulating surfaces to mate appropriately, the contact area will be larger as seen in pattern 1. Otherwise, there will be a larger concentration of stress in areas where the mating of the surfaces is difficult. This is why pattern 1 had a larger contact area compared to pattern 2 and pattern 1 showed lower peak pressures compared to pattern 2.

Studies conducted using pressure sensitive films often use minimal dissection techniques to allow the film to be inserted between the joint with minimal disruption to the surrounding tissue to keep the joint as intact as possible (Leichtle *et al.*, 2014; Padalecki *et al.*, 2014; Lorbach *et al.*, 2016). This is often carried out using arthroplasty technique and the sensors are sutured in place (Jansson *et al.*, 2013; Wang *et al.*, 2015; Lorbach *et al.*, 2016). However, the current study was carried out on a knee model that had all the soft tissues removed. This simplifies the process and allows the sensors to be placed without surgical interventions. Although this was a static study, the Tekscan method had advantages over other techniques used by several studies in the past. The sensors were capable of calculating static and dynamic contact mechanics and were also more accurate than other techniques such as Fuji film. Bachus *et al.* (2006) compared Fuji and Tekscan on a known surface using Instron and found that Tekscan can produce an accuracy of over 95% on plain surfaces. However, the results from this study showed a larger discrepancy between Tekscan and actual applied load.

Studies using intact knee joints usually fix the sensors within the joint using sutures (Lorbach *et al.*, 2016). In the current study it was fixed to the patella using plastic tape to ensure that the

film did not move during testing. Fixing the sensors allowed adequate and constant fixation of the sensors in each sample. This ensured that the position was comparable in every sample.

Many researchers have investigated the contact mechanics using Tekscan pressure sensors in an intact whole joint (Padalecki *et al.*, 2014; Geeslin *et al.*, 2015; Wang *et al.*, 2015; Kim *et al.*, 2016; Lorbach *et al.*, 2016). Having a simple model like the one developed in this study has several advantages.

As the kinematics was displacement driven rather than force driven, it did not require the presence of muscles and other soft tissues around the bones. Unlike the whole intact joint that require a specially trained individual to carry out the arthroplasty to insert the sensors at the correct position, the placement of the sensors in this model could be done very easily without prior training. The simplicity in dissection, setting up and conducting the experiment makes it a consistent method that could be followed by researchers from various skill sets and background. The presence of soft tissue was a risk to the sensors in an intact joint. Exposure to an aqueous environment has been shown to degrade the sensors and affect the results (Jansson *et al.*, 2013).

There is limited data in the literature that investigates the limitations of Tekscan and the variations in the results. Jansson *et al.* showed a reduction of 4.6% load output per hour when Tekscan was exposed to aqueous environment. This suggested diminished Tekscan output on tests carried out in moist environment (Jansson *et al.*, 2013). The verification tests carried out on the sensors in the current study showed an up to 7% increase in Tekscan load at the end of the contact mechanics study. This may have affected the contact pressure results in this study. However, as the same conditions were followed for both the fundamental and gait cycle study, the comparison between the studies were still reasonable.

The accuracy of Tekscan on uneven complex geometries such as the knee is not as accurate as the results on an even plane. This could be due to a number of reasons. There were possible risks of the crinkling of the sensor and excess load saturation over the calibration limit (LaPrade *et al.*, 2014; Padalecki *et al.*, 2014; Geeslin *et al.*, 2015). During the experiment, although it did not occur in this case, crinkling of the sensors could damage individual sensels that could lower the outputs. In the future the chances of these errors could be minimised by adjusting the data

set with respect to the neighbouring cells by taking the mean of the surrounding rows and columns of sensels.

The small sample size of this study was another limitation. Patterns and trends would be easier to identify if the sample size was larger. Increased sample size could also reduce the effect of factors such as geometry that causes the large variation between the samples. However, at this stage for developing the methodology this sample size was adequate to demonstrate the feasibility of this method.

8.5 Conclusions

This study showed the capability of Tekscan pressure sensor in determining the contact area and contact pressure between the patella and its groove at various points in a gait cycle using a joint simulator. There was a significant increase in contact area and pressure with increasing load. Through the fundamental study it was concluded that the significance of displacement and flexion on the contact mechanics can be influenced by other factors. The results showed that the geometry of the joints had an effect on the contact mechanics.

Chapter 9. Overall Discussion and Conclusions

Preclinical testing is a vital stage before administering a new drug or implanting a new device or tissue. It helps to assess the safety and reliability of the product and can identify potential adverse effects on the patient. It is a requirement before a drug, device or tissue is considered safe for clinical trials in humans. These preclinical tests are often carried out *in vivo* in animals and the choice of animal model based on that which most closely represents the anatomy and/or physiology and/or mechanism of the condition being treated in humans (Suzuki et al. 2008; Ding 2016; Yang 2016; Bar-Cohen 2015). Such *in vivo* animal trials can be costly and are not always successful. This highlights the need for *in vitro* preclinical testing, which is less costly and able to screen out interventions that are not likely to be successful, reducing costly failures.

According to the U.S Food and Drug Administration (FDA.gov, 2016), animal testing is required for most medical devices. Many in-vitro studies are not yet validated scientifically as an alternative for animal testing. However, FDA and many other institutions have ongoing research and development work aiming to replace the need for animal testing (FDA.gov, 2016). This is where the work in this thesis contributes. It fills the gap before *in vivo* animal testing, screening out devices and interventions that are likely to fail.

This final chapter discusses how the thesis has met the overall aims and objectives of the project. The main aim was to develop a methodology using a tribological knee simulator to investigate the biomechanics and wear in natural patello-femoral joints (PFJs). The first objective was to choose an appropriate animal model for the study. Secondly, a single station knee simulator (SSKS) was modified to test the natural PFJs. Finally, various methodologies were developed and tested to investigate the contact mechanics and wear in the joints.

In this chapter, the methods established and the conclusions made from the investigations will be evaluated. The limitations of the studies and improvements that can be implemented will also be discussed. There are future works that can continue from the studies discussed in this thesis. These were either not in the scope of this current project or not achievable due to the timescale of the project. However, these will benefit the long term goals of this project which is the pre-clinical assessment of the biotribological performance of osteochondral substitutions.

Developing the methodology to investigate the wear in porcine PFJs was one of the most novel aspects of this project. Simple geometrical pin-on-plates systems are a well-established model for the study of cartilage tribology (Lipshitz and Glimcher, 1974, 1979, Lipshitz, Etheredge and Glimcher, 1975, 1980; Krishnan, Mariner and Ateshian, 2005; Northwood and Fisher, 2007; Kock *et al.*, 2008) . A more complex model has been developed in this thesis to investigate a whole natural PFJ. A porcine tibio-femoral (TFJ) model has been previously developed in the same lab to investigate the tribology of the natural joint using a knee simulator (Liu *et al.*, 2015). This thesis reports a practical and consistent method that was established to investigate the biomechanics and biotribology of the PFJ using the same simulator.

This thesis describes the development of an in-vitro model that can be used for the pre-clinical testing of tissue substitutions in the PFJ. A methodology that simulated the wear in natural joints using a simulator with 6 degrees of freedom has been developed. The wear was assessed using ICRS grading, wear area measurements and surface roughness measurements. The contact area and pressure at different conditions were measured using Tekscan sensors. The simulator model and the experiments conducted in this study provide a platform for replicating the in-vivo behaviour of the natural PFJ under different physiological conditions.

Choosing an animal model

The first stage of this project investigated an appropriate animal model for the PFJ. The animal joint was required to be similar in size to the human joint in order to carry out comparative studies. Bovine and porcine PFJ were available as the possible alternatives for the animal model. The geometry and size of the porcine joint was more comparable to the human joint than the bovine joint. It was also more accurate to prepare the porcine samples for the tests than using a bovine joint as it was easier to handle. A porcine model was previously developed under similar conditions for investigating the tribology and biomechanics of a TFJ (Liu *et al.* 2015). Therefore, using the same model for the PFJ was also advantageous in terms of repeatability of tests and comparing the results between the two joints. Therefore, the porcine joint was chosen as the animal model.

Tissue substitutions methods such as osteochondral transplantation are minimally invasive treatments required to repair damaged articular cartilage in diarthrodial joints. This project

developed a PFJ model that can be potentially used for applications such as the testing of tissue substitutions that repair PFJ cartilage lesions. Therefore, the cartilage in the animal model must also have similar material properties to the human cartilage that would potentially require osteochondral transplantation. The porcine and human patello-femoral cartilage was characterised by measuring the thickness, equilibrium elastic modulus and the permeability of the cartilage. The results did not show any significant differences between porcine and human patello-femoral cartilage and hence porcine cartilage was concluded to be suitable for this study. However, the difference in the age and species may affect the biological composition of the tissue. Since the porcine tissue was sourced from young (6 months) animals the skeletal maturity of the porcine tissue was a limitation of this model with noticeable differences in the bone density, presence of growth plate and difference in material properties of its cartilage.

Developing the simulator study

The contact point study investigated the position of the patella with respect to the femur. This was required to define the starting (neutral) position of the patella during the gait cycle. It was concluded that at the beginning of flexion the patella sits on the superior end of the femur and travels inferiorly as flexion progresses. This kinematics was similar to that observed in human PFJs (Herrmann *et al.*, 2012). The results from the experimental method and the theoretical model created in SolidWorks based on findings from literature (Akbar *et al.*, 2012; Herrmann *et al.*, 2012; Kittl, Schmeling and Amis, 2015) were used to define the neutral position of the PFJ. The assumptions described in Chapter 6 to create the simplified SolidWorks model were a limitation to the computational part of this study. This simple model was however appropriate for the purpose of this study as described in Chapter 6. In the future, a complex model (for example, a dynamic model) that can provide more intricate geometrical analysis of the joint could be explored to provide a stronger validation for this contact point study.

Custom made fixtures were designed and manufactured in order to mount the sample into the simulator in a consistent and repeatable manner. One of the challenges of using natural tissue is the variability between samples. There was a large variation in the geometry of the centre of rotation of the patello-femoral groove so a method was developed to determine the radius of curvature of the patello femoral groove. This was used to determine the centre of rotation for

each sample before it was cemented into the fixtures. Therefore, this ensured consistency throughout the study.

Once the samples were cemented in the fixtures, they were mounted on the SSKS for testing. In terms of kinematics, a porcine gait cycle was developed for the dynamic testing profile, which was adapted from the artificial PFJ gait cycle and porcine TFJ gait cycle (Ellison *et al.*, 2008; Maiti *et al.*, 2014; Liu *et al.*, 2015) used previously in the same laboratory.

Wear study

A single station knee simulator (SSKS) was modified to carry out the contact mechanics and wear study on the porcine PFJ. New fixtures were designed and manufactured to hold the specimens in the simulator. The wear study introduced the use of an Alicona IF G5 optical profilometer to assess the change in cartilage topography in natural joints. It was used to analyse the surface roughness at each test condition which showed that the roughness values in the positive control of cartilage on metal was larger than the negative control of cartilage on cartilage.

Alicona IF G5 is not yet recorded in the literature as a tool for assessing cartilage wear. It has several advantages over other profilometers. Unlike surface measurement tools such as AFM and Talysurf, this does not require a contacting stylus for surface measurements. The current study established the use of Alicona for surface roughness measurement carried out on rubber replicas obtained from the surface of the samples tested. The results obtained using this method underestimated the surface roughness of cartilage by ~40%.

Alicona IF G5 is capable of scanning large surfaces in 3D which can help to better understand the surface topography compared to a 2D trace. In future studies this feature could be used to explore the potential for volumetric measurements to quantitatively measure the cartilage loss from wear studies. The volume measurement module located in the analysis software (IF Measure Suite) of the Alicona can be used to calculate the volume of cartilage defects (mm^3) as the total volume below the surface. A reference plane/mesh can be placed on the sample surface and the volume between the plane and the material underneath can be measured. In order to quantify the change in volume extending below cartilage surface level (volume of wear/

deformation) a baseline measurement of the volume that extends below the cartilage surface of negative control samples can be compared to the volume of wear in the experimental groups. This method can quantify the wear/ deformation by measuring the change in geometrical volume of the cartilage samples. It is a promising technique to compare the effect of different types of substitutions and their implant techniques on the wear of cartilage.

The current wear study was carried out for 5hrs at room temperature. The positive control of cartilage against metal showed cartilage deformation and increased surface roughness. However, there was no visible cartilage damage or loss. Longer test duration, higher loads and motions may all produce higher wear but this will require the joint to be sustained in the simulator for a longer period of time. Since natural tissue degrades, further extended duration testing over 24 hrs is not currently feasible using the current set up and conditions.

However, this may be possible in the future if PFJs can be mounted aseptically and tissue kept alive for longer with the addition of special design features to the simulator. Compared to previous simulators in the lab, the test volume in the current machine can be significantly increased to permit the setup of a sealed test chamber under aseptic conditions, with direct temperature control. There are certain chemicals that can be added to the lubricator to keep the tissue alive for longer. These methods can be used in the future to prolong the duration of wear tests to obtain quantitative wear data. This will broaden the scope for the tissue substitutions that can be tested using this system.

The current wear study did not produce significant wear in the positive control and therefore was not successful as a test protocol. The gait cycle representing the walking motion is not sufficiently severe to produce wear and therefore future studies must apply a larger flexion angle representative of daily activities such as stair climbing. This will increase the motion and severity of the test which can produce greater wear comparable to worse case scenarios.

Contact mechanics

Contact area and pressure can be used to predict the wear and failure of osteochondral substitutions. This thesis discussed the development and application of a methodology to investigate the contact mechanics of the PFJ using a Tekscan. The contact mechanics of the joint

was investigated by measuring the contact area and contact pressure at various points in a porcine patello-femoral gait cycle. Several researchers have reported the study of contact mechanics in natural joints using different techniques. Although the current study was able to provide quantitative area and pressure measurements, the variations in parameters such as load, flexion and type of joint used by other researchers has made it difficult for a direct comparison.

Two types of test were carried out; the fundamental contact mechanics study and the contact mechanics at five different stages in the gait cycle. The same 6 samples were used for the two studies to ensure that the results from the fundamental study could be compared to the gait cycle study without any variation among samples within the two tests. The fundamental study was carried out to systematically investigate the effect of flexion, load and displacement. There were two patterns of contact mechanics observed in the 6 samples in each test type, which indicated the difference in the geometry of the samples.

In the gait cycle study, the contact area decreased across the gait cycle. The contact area in the stance phase was larger compared to the contact area in the swing phase. This was because, during swing phase the feet do not touch the ground and there is no body weight applied. The highest contact pressure was observed just after the toe off region at the end of stance. This change in contact pressure was an indication of how the load is distributed during a normal walking cycle.

The fundamental study showed that the contact area increased with increasing load and the pressure increased with increasing flexion. It also displayed larger contact pressures in conditions with lower contact area. The contact pressure showed an increase with respect to the position of the patella, with a larger contact pressure in the inferior position compared to the superior. This trend was more noticeable at lower loads. The contact area and contact pressure increased with increasing load despite the change in displacement or flexion.

The complexity of the surface geometry of the knee can affect the accuracy of Tekscan. It works well on plane surfaces as there is risk of uneven load saturation in sensors around curved surfaces (LaPrade *et al.*, 2014; Padalecki *et al.*, 2014; Geeslin *et al.*, 2015). This is usually caused

by the creasing in the sensors around the curved surfaces, in which case it could be resolved by adjusting the challenging data set with respect to the neighbouring cells by taking the mean of the surrounding rows and columns of sensels.

Future work

This thesis has established the suitability of a porcine model as a valid biomechanical surrogate for human joints for the purposes of developing a preclinical test method for the PFJ. The model/method developed in this research project will in the future be used for testing the performance of tissue engineered solutions for the treatment of osteochondral lesions in the PFJ and will aid the understanding of the biomechanics of the joint under various conditions.

The sample size of $n=6$ could be considered a limitation of this study. Patterns, trends and significance would be easier to identify if the sample size was larger. It could also reduce the effect of inherent biological factors such as geometry that causes the large variation between the samples. In future studies, to reduce variation, the samples could be measured and divided into batches depending on the size and geometry of the samples. Measuring the radius of curvature of the groove, femoral sulcus angle, length and width of the femoral groove and patella, the curvature on the femoral condyles and the patellar facets could all contribute towards categorising the samples. However, at this stage for developing the methodology this sample size was adequate to demonstrate the feasibility and applications of the methods.

The purpose of this model was to simulate the dynamic motions of the PFJ using displacement control in an SSKS. The displacement control system does not require the muscles and soft tissue around the joint to apply the kinematics. This simplified the experiment, eliminated any discrepancies that could have been caused by the disruptions in the muscle forces and gave consistent input kinematics for each sample. A more complex model comprising the entire soft tissues could be developed in the future for more applications. It could investigate the effect of various muscle forces or surgical techniques on the contact mechanics and wear of the joint.

The methodology established in this study could be developed further to establish longer duration of test method. Future studies to determine porcine kinematic data and patella position parameters could be carried out to improve the test profiles for porcine kinematics.

Certain in-vivo studies currently carried out on live animals (Martinez-Carranza et al. 2016) could be simulated at least on some level using the in-vitro test methodologies and cadaveric human tissue. The animal model developed could be used to generate pre-clinical data to transition many lab based tissue engineered products to the treatments in patients. This could also reduce the number of live animal needed for the pre-clinical studies.

The integrity of the graft and subsequent loosening from the recipient site is a common challenge in OAT procedure (Trattnig *et al.*, 2007; Turtel *et al.*, 2015). The biomechanics of the graft in an in-vitro animal joint has never been investigated before. The model could be used to investigate the interactions of osteochondral grafts and substitutions within a natural joint. The capability of this system to apply physiological loading and kinematics will make this a perfect simulation for these types of studies.

The contact mechanics study could be used to investigate the integrity of grafts in the joint. It could provide the pressure difference on the graft interface and assess how well the plugs fit into the recipient site. Although in the current study, Tekscan was used for static loading on natural joints, these sensors are capable of real time data acquisition. Future work could investigate the use of Tekscan sensors on dynamic loading of the joints which could provide a visual representation of how the plugs interact within the joint during the gait cycle.

Conclusion

The methodologies developed and tested in this study have the potential to investigate the contact mechanics and wear in human PFJ under different conditions and to develop the pre-clinical testing of the osteochondral substitutions. This thesis has established the suitability of a porcine model as a valid biomechanical surrogate for human joints for this purpose.

Bibliography

Abdelgaied Latif, M. J., Jin, Z. and Wilcox, R. K. (2012) 'Biomechanical characterisation of ovine spinal facet joint cartilage', *Journal of Biomechanics*. Elsevier, 45(8), pp. 1346–1352.

Abdelgaied, A., Stanley, M., Galfe, M., Berry, H., Ingham, E. and Fisher, J. (2015) 'Comparison of the biomechanical tensile and compressive properties of decellularised and natural porcine meniscus', *Journal of Biomechanics*. Elsevier, 48(8), pp. 1389–1396.

Abu-Amer, Y., Darwech, I. and Clohisy, J. C. (2007) 'Aseptic loosening of total joint replacements: mechanisms underlying osteolysis and potential therapies.', *Arthritis research & therapy*. BioMed Central, 9 Suppl 1(Suppl 1), p. S6.

Accardi, M. A., Dini, D. and Cann, P. M. (2011) 'Experimental and numerical investigation of the behaviour of articular cartilage under shear loading—Interstitial fluid pressurisation and lubrication mechanisms', *Tribology International*. Elsevier, 44(5), pp. 565–578.

AccuTrans (2015) *What is AccuTrans - AccuTrans*. Available at: http://www.accutrans.info/overview/what_is_accutrans/ (Accessed: 1 July 2015).

Ahmad, C. S., Cohen, Z. a, Levine, W. N., Ateshian, G. a and Mow, V. C. (2001) 'Biomechanical and topographic considerations for autologous osteochondral grafting in the knee.', *The American journal of sports medicine*, 29(2), pp. 201–6.

Ahmed, a M., Burke, D. L. and Yu, a (1983) 'In-vitro measurement of static pressure distribution in synovial joints--Part II: Retropatellar surface.', *Journal of biomechanical engineering*, 105(3), pp. 226–36.

Akbar, M., Farahmand, F., Jafari, A. and Foumani, M. S. (2012) 'A detailed and validated three dimensional dynamic model of the patellofemoral joint.', *Journal of biomechanical engineering*. American Society of Mechanical Engineers, 134(4), p. 41005.

Al-Turaiki, M. H. S. (1990) *The Human Knee Functional Anatomy Biomechanics and Instabilities & Assessment Techniques*. The Joint Center for Research in Prosthetics. ASIN: B002M0L9OC

Amir, G., Pirie, C. J., Rashad, S. and Revell, P. a (1992) 'Remodelling of subchondral bone in osteoarthritis: a histomorphometric study.', *Journal of clinical pathology*, 45(11), pp. 990–2.

Andrus, B. W. and O'Rourke, D. J. (2007) 'Aortic stenosis: An update on current and emerging therapeutic options', pp. 99–106.

Arendt, E. A., Fithian, D. C. and Cohen, E. (2002) 'Current concepts of lateral patella dislocation.', *Clinics in sports medicine*, 21(3), pp. 499–519.

Ateshian, G. a., Chahine, N. O., Basalo, I. M. and Hung, C. T. (2004) 'The correspondence

between equilibrium biphasic and triphasic material properties in mixture models of articular cartilage', *Journal of Biomechanics*, 37(3), pp. 391–400.

Ateshian, G. A. and Hung, C. T. (2005) 'Patellofemoral Joint Biomechanics and Tissue Engineering', *Clinical Orthopaedics and Related Research*, (81), pp. 81–90.

Ateshian, G. A. and Hung, C. T. (2006) 'The natural synovial joint : properties of cartilage', *Structure*, 220, pp. 657–670.

Ateshian, G. A. and Wang, H. (1995) 'A theoretical solution for the frictionless rolling contact of cylindrical biphasic articular cartilage layers', *Journal of Biomechanics*, 28(11), pp. 1341–1355.

Ateshian, G. A., Warden, W. H., Kim, J. J., Grelsamer, R. P. and Mow, V. C. (1997) 'Finite deformation biphasic material properties of bovine articular cartilage from confined compression experiments', *Journal of Biomechanics*. Elsevier Science Ltd, 30(11–12), pp. 1157–1164.

Athanasίου, K. A., Rosenwasser, M. P., Buckwalter, J. A., Malinin, T. I. and Mow, V. C. (1991) 'Interspecies comparisons of in situ intrinsic mechanical properties of distal femoral cartilage.', *Journal of orthopaedic research : official publication of the Orthopaedic Research Society*, 9(3), pp. 330–40.

Bachus, K. N., DeMarco, A. L., Judd, K. T., Horwitz, D. S. and Brodke, D. S. (2006) 'Measuring contact area, force, and pressure for bioengineering applications: using Fuji Film and TekScan systems.', *Medical engineering & physics*, 28(5), pp. 483–8.

Balasubramanian, P., Prabhakaran, M. P., Sireesha, M. and Ramakrishna, S. (2013) 'Collagen in Human Tissues: Structure, Function, and Biomedical Implications from a Tissue Engineering Perspective', *Advances in Polymer Science*. Edited by A. Abe, H.-H. Kausch, M. Möller, and H. Pasch. Berlin, Heidelberg: Springer Berlin Heidelberg (Advances in Polymer Science), 251, pp. 173–206.

Baldwin, J. L. and House, C. K. (2005) 'Anatomic Dimensions of the Patella Measured During Total Knee Arthroplasty', *The Journal of Arthroplasty*, 20(2), pp. 250–257.

Balazs, E. (1982) "The physical properties of synovial fluid and the special role of hyaluronic acid" *Disorders of the knee*, Lippincott, p. 504.

Bannasch, H., Unterberg, T., Föhn, M., Weyand, B., Horch, R. E. and Stark, G. B. (2008) 'Cultured keratinocytes in fibrin with decellularised dermis close porcine full-thickness wounds in a single step', 34(7), pp. 1015–1021.

Baykal, D. (2013) *Tribological Assessment of Hydrogels for Replacing Damaged Articular*

Cartilage. PhD thesis, Drexel University.

B-cube (2016) *Micro-Computed Tomography*, b-cube AG, Switzerland. Available at: http://www.b-cube.ch/index.php?option=com_content&view=article&id=21&Itemid=19 (Accessed: 31 July 2016).

Benders, K. E. M., van Weeren, P. R., Badylak, S. F., Saris, D. B. F., Dhert, W. J. a and Malda, J. (2013) 'Extracellular matrix scaffolds for cartilage and bone regeneration.', *Trends in biotechnology*, 31(3), pp. 169–76.

Berta, Á., Duska, Z., Tóth, F. and Hangody, L. (2015) 'Clinical experiences with cartilage repair techniques: outcomes, indications, contraindications and rehabilitation.', *Joint diseases & related surgery*, 26(2), pp. 84–96.

Besier, T. F., Draper, C. E., Gold, G. E., Beaupré, G. S. and Delp, S. L. (2005) 'Patellofemoral joint contact area increases with knee flexion and weight-bearing.', *Journal of orthopaedic research : official publication of the Orthopaedic Research Society*, 23(2), pp. 345–50.

Bobinac, D., Spanjol, J., Zoricic, S. and Maric, I. (2003) 'Changes in articular cartilage and subchondral bone histomorphometry in osteoarthritic knee joints in humans', *Bone*, 32(3), pp. 284–290.

Bolland, F., Korossis, S., Wilshaw, S. P., Ingham, E., Fisher, J., Kearney, J. N. and Southgate, J. (2007) 'Development and characterisation of a full-thickness acellular porcine bladder matrix for tissue engineering', 28(6), pp. 1061–1070.

Boschetti, F., Pennati, G., Gervaso, F., Peretti, G. M. and Dubini, G. (2004) 'Biomechanical properties of human articular cartilage under compressive loads.', *Biorheology*, 41(FEBRUARY 2004), pp. 159–166.

Bosman, R. (2010) 'Mild microscopic wear in the boundary lubrication regime', *Materialwissenschaft und Werkstofftechnik*, 41(1), pp. 29–32.

Bosman, R. (2011) *Mild Microscopic Wear Modeling in the Boundary Lubrication Regime*. PhD thesis, University of Twente.

Bowland, P., Ingham, E., Jennings, L., Fisher, J. (2015) '*Journal of engineering in medicine*', 229(12), pp. 879–888.

Brechtler, H. J., Powers, C. M., Terk, M. R., Ward, S. R. and Lee, T. Q. (2003) 'Quantification of patellofemoral joint contact area using magnetic resonance imaging', *Magnetic Resonance Imaging*, 21(9), pp. 955–959.

Brien, M. O. (2001) 'Clinical Anatomy of the Patellofemoral Joint', *Most*, 2(1), pp. 1–8.

Brill, N., Riedel, J., Rath, B., Tingart, M., Jahr, H., Betsch, M., Quack, V., Pufe, T., Schmitt, R. and Nebelung, S. (2015) 'Optical coherence tomography-based parameterization and quantification of articular cartilage surface integrity.', *Biomedical optics express*, 6(7), pp. 2398–411.

Bruker (2013) *MicroCT methods*. Available at: <http://www.skyscan.be/company/methods.htm> (Accessed: 31 July 2013).

Burroughs, B. R., Rubash, H. E., Estok, D., Jasty, M., Krevolin, J. and Muratoglu, O. K. (2006) 'Comparison of conventional and highly crosslinked UHMWPE patellae evaluated by a new in vitro patellofemoral joint simulator.', *Journal of biomedical materials research. Part B, Applied biomaterials*, 79(2), pp. 268–74.

Callaghan, J. J. (2003) 'Biomechanics of the articular cartilage and menisci of the adult knee', in *The adult knee, Volume 1*. Lippincott Williams & Wilkins, pp. 81–99.

De Caro, F., Bisicchia, S., Amendola, A. and Ding, L. (2015) 'Large Fresh Osteochondral Allografts of the Knee: A Systematic Clinical and Basic Science Review of the Literature', *Arthroscopy: The Journal of Arthroscopic & Related Surgery*, 31(4), pp. 757–765.

Castañeda, S., Roman-Blas, J. a, Largo, R. and Herrero-Beaumont, G. (2012) 'Subchondral bone as a key target for osteoarthritis treatment.', *Biochemical pharmacology*, 83(3), pp. 315–23.

Chan, S. M. T., Neu, C. P., Komvopoulos, K. and Reddi, a H. (2011) 'Dependence of nanoscale friction and adhesion properties of articular cartilage on contact load.', *Journal of biomechanics*. Elsevier, 44(7), pp. 1340–5.

Charles Swann, A. (1988) *The effect of mechanical stress on the stiffness of articular cartilage and its role in the aetiology of osteoarthrosis*. PhD thesis, University of Leeds.

Chen, A. C., Bae, W. C., Schinagl, R. M. and Sah, R. L. (2001) 'Depth- and strain-dependent mechanical and electromechanical properties of full-thickness bovine articular cartilage in confined compression.', *Journal of biomechanics*, 34(1), pp. 1–12.

Chen, S. S., Falcovitz, Y. H., Schneiderman, R., Maroudas, A. and Sah, R. L. (2001) 'Depth-dependent compressive properties of normal aged human femoral head articular cartilage: relationship to fixed charge density.', *Osteoarthritis and cartilage / OARS, Osteoarthritis Research Society*, 9(6), pp. 561–9.

Chian, K. S., Leong, M. F. and Kono, K. (2015) 'Regenerative medicine for oesophageal reconstruction after cancer treatment'. Lancet Publishing Group, pp. e84–e92.

Chinkulprasert, C., Vachalathiti, R. and Powers, C. M. (2011) 'Patellofemoral joint forces and stress during forward step-up, lateral step-up, and forward step-down exercises.', *The Journal*

of orthopaedic and sports physical therapy, 41(4), pp. 241–8.

Clark, a L., Herzog, W. and Leonard, T. R. (2002) 'Contact area and pressure distribution in the feline patellofemoral joint under physiologically meaningful loading conditions.', *Journal of biomechanics*, 35(1), pp. 53–60.

Coakley, D. N., Shaikh, F. M., O'Sullivan, K., Kavanagh, E. G., Grace, P. A. and McGloughlin, T. M. (2015) 'In vitro evaluation of acellular porcine urinary bladder extracellular matrix - A potential scaffold in tissue engineered skin'. Elsevier GmbH, 10–11, pp. 9–16.

Coats, a. M., Zioupos, P. and Aspden, R. M. (2003) 'Material Properties of Subchondral Bone from Patients with Osteoporosis or Osteoarthritis by Microindentation testing and Electron Probe Microanalysis', *Calcified Tissue International*, 73(1), pp. 66–71.

Cooke, A. F., Dowson, D. and Wright, V. (1978) 'The pressure-viscosity characteristics of synovial fluid.', *Biorheology*, 15(2), pp. 129–35.

Crapo, P. M., Gilbert, T. W. and Badylak, S. F. (2011) 'An overview of tissue and whole organ decellularization processes.', *Biomaterials*, 32(12), pp. 3233–43.

Czichos, H. (1978) *Tribology: a systems approach to the science and technology of friction, lubrication, and wear*. 1st edn. Elsevier. ISBN: 9780080875651

Day, J. S., Van Der Linden, J. C., Bank, R. a, Ding, M., Hvid, I., Sumner, D. R. and Weinans, H. (2004) 'Adaptation of subchondral bone in osteoarthritis.', *Biorheology*, 41(3–4), pp. 359–68.

Dhafer, Y. Y. and Kahn, L. E. (2002) 'The effect of vastus medialis forces on patello-femoral contact: a model-based study.', *Journal of biomechanical engineering*, 124(6), pp. 758–67.

Dowson, D. (1981) 'Basic tribology', in *Introduction to the biomechanics of joints and joint replacement*. London: Mechanical engineering publications, pp. 486–510.

Draper, C. E., Besier, T. F., Fredericson, M., Santos, J. M., Beaupre, G. S., Delp, S. L. and Gold, G. E. (2011) 'Differences in patellofemoral kinematics between weight-bearing and non-weight-bearing conditions in patients with patellofemoral pain.', *Journal of orthopaedic research : official publication of the Orthopaedic Research Society*, 29(3), pp. 312–7.

Draper, C. E., Besier, T. F., Gold, G. E., Fredericson, M., Fiene, A., Beaupre, G. S. and Delp, S. L. (2006) 'Is cartilage thickness different in young subjects with and without patellofemoral pain?', *Osteoarthritis and cartilage / OARS, Osteoarthritis Research Society*, 14(9), pp. 931–7.

Duif, C., Koutah, M. A., Ackermann, O., Spyrou, G., Von Engelhardt, L. V., Kaya, D., Willburger, R. E. and Lahner, M. (2015) 'Combination of autologous chondrocyte implantation (ACI) and osteochondral autograft transfer system (OATS) for surgical repair of larger cartilage defects

of the knee joint. A review illustrated by a case report'. IOS Press, pp. 531–537.

Eckstein, F., Lemberger, B., Gratzke, C., Hudelmaier, M., Glaser, C., Englmeier, K.-H. and Reiser, M. (2005) 'In vivo cartilage deformation after different types of activity and its dependence on physical training status.', *Annals of the rheumatic diseases*, 64(2), pp. 291–5.

von Eisenhart-Rothe, R., Siebert, M., Bringmann, C., Vogl, T., Englmeier, K.-H. and Graichen, H. (2004) 'A new in vivo technique for determination of 3D kinematics and contact areas of the patello-femoral and tibio-femoral joint.', *Journal of biomechanics*, 37(6), pp. 927–34.

Elder, B. D., Eleswarapu, S. V and Athanasiou, K. a (2009) 'Extraction techniques for the decellularization of tissue engineered articular cartilage constructs.', *Biomaterials*. Elsevier Ltd, 30(22), pp. 3749–56.

Ellison, P. (2007) *Investigation of Wear within the Patellofemoral Joint of Total Knee Replacements*. PhD thesis, University of Leeds.

Ellison, P., Barton, D. C., Esler, C., Shaw, D. L., Stone, M. H. and Fisher, J. (2008) 'In vitro simulation and quantification of wear within the patellofemoral joint replacement.', *Journal of biomechanics*, 41(7), pp. 1407–16.

Eyre, D. (2002) 'Collagen of articular cartilage.', *Arthritis research*, 4(1), pp. 30–5.

FDA.gov (2016) *FDA Basics- Why are animals used for testing medical products?*, U S Food And Drug Administration. Office of the Commissioner. Available at: <http://www.fda.gov/AboutFDA/Transparency/Basics/ucm194932.htm> (Accessed: 25 August 2016).

Fermor, H. L. (2013) *Engineering of Natural Cartilage Substitution Biomaterials*. PhD thesis, University of Leeds.

Fermor, H. L., Russell, S. L., Williams, S., Fisher, J. and Ingham, E. (2015) 'Development and characterisation of a decellularised bovine osteochondral biomaterial for cartilage repair'. Kluwer Academic Publishers, 26(5).

Ficat, C. and Maroudas, A. (1975) 'Cartilage of the patella. Topographical variation of glycosaminoglycan content in normal and fibrillated tissue.', *Annals of the rheumatic diseases*, 34(6), pp. 515–9.

Fin-Ceramica Faenza Spa (2013) *MaioRegen® - Osteochondral regeneration, Product handbook*.

Fitzpatrick, C. K., Baldwin, M. a, Laz, P. J., Fitzpatrick, D. P., L Lerner, A. and Rullkoetter, P. J. (2011) 'Development of a statistical shape model of the patellofemoral joint for investigating

relationships between shape and function.’, *Journal of biomechanics*. Elsevier, 44(13), pp. 2446–52.

Forster, H. and Fisher, J. (1999) ‘The influence of continuous sliding and subsequent surface wear on the friction of articular cartilage.’, *Proceedings of the Institution of Mechanical Engineers. Part H, Journal of engineering in medicine*, 213(4), pp. 329–45.

Forster, H., Fisher, J., Dowson, D. and Wright, V. (1995) ‘The effect of stationary loading on the friction and boundary lubrication of articular cartilage in the mixed lubrication regime’, *Tribology Series*. Elsevier, 30, pp. 71–83.

Freeman, M. E., Furey, M. J., Love, B. J. and Hampton, J. M. (2000) ‘Friction, wear, and lubrication of hydrogels as synthetic articular cartilage’, *Wear*, 241(2), pp. 129–135.

Froimson, M. I., Ratcliffe, A., Gardner, T. R. and Mow, V. C. (1997) ‘Differences in patellofemoral joint cartilage material properties and their significance to the etiology of cartilage surface fibrillation.’, *Osteoarthritis and cartilage / OARS, Osteoarthritis Research Society*, 5(6), pp. 377–86.

Fulkerson, J. and Hungerford, D. (1990) ‘Patellar tilt/compression and the excessive lateral pressure syndrome’, in *Disorders of the patellofemoral joint*, pp. 102–23.

Furey, M. J. and Burkhardt, B. M. (1997) ‘Biotribology: Friction, wear, and lubrication of natural synovial joints’, *Lubrication Science*, 9(3), pp. 255–271.

Gan, X., Cai, Z., Qiao, M., Gao, S., Zhu, M. and Yu, H. (2013) ‘Fretting wear behaviors of mandibular condylar cartilage of nature temporomandibular joint in vitro’, *Tribology International*, 63, pp. 204–212.

Gannon, A. R., Nagel, T., Bell, A. P., Avery, N. C. and Kelly, D. J. (2015) ‘The changing role of the superficial region in determining the dynamic compressive properties of articular cartilage during postnatal development.’, *Osteoarthritis and cartilage / OARS, Osteoarthritis Research Society*, 23(6), pp. 975–84.

Garretson, R. B. (2004) ‘Contact Pressure at Osteochondral Donor Sites in the Patellofemoral Joint’, *American Journal of Sports Medicine*, 32(4), pp. 967–974.

Geeslin, A. G., Civitarese, D., Turnbull, T. L., Dornan, G. J., Fuso, F. A. and LaPrade, R. F. (2015) ‘Influence of lateral meniscal posterior root avulsions and the menisiofemoral ligaments on tibiofemoral contact mechanics.’, *Knee surgery, sports traumatology, arthroscopy : official journal of the ESSKA*. Springer Berlin Heidelberg, pp. 1–9.

Ghosh, S., Bowen, J., Jiang, K., Espino, D. M. and Shepherd, D. E. T. (2013) ‘Investigation of techniques for the measurement of articular cartilage surface roughness.’, *Micron (Oxford*,

England : 1993), 44(1), pp. 179–84.

Goldberg-bockhorn, E., Seitz, A. M., Sc, M., Du, L., Ph, D., Ignatius, A., Walther, P., Breiter, R. and Rotter, N. (2012) 'Decellularized Cartilage Matrix as a Novel Biomatrix for Cartilage Tissue-Engineering Applications', 18.

Gorniak, G. C. (2009) 'Patterns of patellofemoral articular cartilage wear in cadavers.', *The Journal of orthopaedic and sports physical therapy*, 39(9), pp. 675–83.

Graindorge, S., Ferrandez, W., Jin, Z., Ingham, E., Grant, C., Twigg, P. and Fisher, J. (2005) 'Biphasic surface amorphous layer lubrication of articular cartilage.', *Medical engineering & physics*, 27(10), pp. 836–44.

Gray, H. (1918) 'Chapter 2: Osteology', in *Gray's Anatomy of the Human Body*. 20th edn. Philadelphia; Lea & Febiger. ISBN-139781782124269

Greaves, N. S., Morris, J., Benatar, B., Alonso-Rasgado, T., Baguneid, M. and Bayat, A. (2015) 'Acute cutaneous wounds treated with human decellularised dermis show enhanced angiogenesis during healing'. *Public Library of Science*, 10(1).

Greco, K. V., Francis, L., Somasundaram, M., Greco, G., English, N. R., Roether, J. A., Boccaccini, A. R., Sibbons, P. and Ansari, T. (2015) 'Characterisation of porcine dermis scaffolds decellularised using a novel non-enzymatic method for biomedical applications'. *SAGE Publications Ltd*, 30(2), pp. 239–253.

Grelsamer, R. P. and Weinstein, C. H. (2001) 'Applied biomechanics of the patella.', *Clinical orthopaedics and related research*, (389), pp. 9–14.

Grynpas, M. D., Alpert, B., Katz, I., Lieberman, I. and Pritzker, K. P. (1991) 'Subchondral bone in osteoarthritis.', *Calcified tissue international*, 49(1), pp. 20–6.

Gudas, R., Gudaitė, A., Pocius, A., Gudienė, A., Čekanauskas, E., Monastyreckienė, E. and Basevičius, A. (2012) 'Ten-Year Follow-up of a Prospective, Randomized Clinical Study of Mosaic Osteochondral Autologous Transplantation Versus Microfracture for the Treatment of Osteochondral Defects in the Knee Joint of Athletes', *Am J Sports Med*, 40, pp. 2499–2508.

Gudas, R., Kalesinskas, R. J., Kimtys, V., Stankevičius, E., Toliušis, V., Bernotavičius, G. and Smailys, A. (2005) 'A prospective randomized clinical study of mosaic osteochondral autologous transplantation versus microfracture for the treatment of osteochondral defects in the knee joint in young athletes', *Arthroscopy - Journal of Arthroscopic and Related Surgery*, 21(9), pp. 1066–1075.

Haberth, D. (2002) *Use of Lasers in Medicine : Tissue Soldering and Precise Cutting*. Philosophisch-Naturwissenschaftliche Fakultät, Universität Bern.

Hamrock, B. (1984) 'Lubrication of Machine Elements', *NASA Reference Publication 1126*. NASA.

Hangody, L., Kish, G., Karpati, Z., Szerb, I. and Eberhardt, R. (1997) 'Treatment of Osteochondritis Dissecans of the Talus: Use of the Mosaicplasty Technique--A Preliminary Report', *Foot & Ankle International*. SAGE Publications, 18(10), pp. 628–634.

Hangody, L., Vasarhelyi G, Sukosd Z. (2008) Autologous osteochondral grafting - technique and long-term results. *'Injury'*, 39(1), pp.32-39

Hauser, R. (2009) 'The Deterioration of Articular Cartilage in Osteoarthritis by Corticosteroid Injections', *Journal of Prolotherapy*, 2, pp. 107–123.

Van Haver, A., Mahieu, P., Claessens, T., Li, H., Pattyn, C., Verdonk, P. and Audenaert, E. A. (2014) 'A statistical shape model of trochlear dysplasia of the knee.', *The Knee*. Elsevier, 21(2), pp. 518–23.

Van Haver, A., De Roo, K., Claessens, T., De Beule, M., Verdonk, P. and De Baets, P. (2013) 'Pilot validation study on a quasi-static weight-bearing knee rig.', *Proceedings of the Institution of Mechanical Engineers. Part H, Journal of engineering in medicine*, 227(3), pp. 229–33.

Heino, J. G., Powers, C. M., Terk, M. and Lee, T. (1999) 'Measurement of patellofemoral joint contact area using magnetic resonance imaging', in *Orthopaedic Resaerch Society 45th Annual Meeting*.

Herrmann, S., Lenz, R., Geier, A., Lehner, S., Souffrant, R., Woernle, C., Tischer, T. and Bader, R. (2012) '[Musculoskeletal modeling of the patellofemoral joint. Dynamic analysis of patellar tracking].', *Der Orthopäde*, 41(4), pp. 252–9.

Herrmann, S., Lenz, R., Woernle, C., Kreuz, P., Bader, R. and Tischer, T. (2013) 'Displacement of the medial patellofemoral ligament in relation to varying attachment positions at the femoral condyle', in *ORS Conference Abstract*.

Hinman, R. S., Lentzos, J., Vicenzino, B. and Crossley, K. M. (2014) 'Is Patellofemoral Osteoarthritis Common in Middle-Aged People With Chronic Patellofemoral Pain?', *Arthritis Care & Research*, 66(8), pp. 1252–1257.

Hoch, D. H., Grodzinsky, A. J., Koob, T. J., Albert, M. L. and Eyre, D. R. (1983) 'Early changes in material properties of rabbit articular cartilage after meniscectomy.', *Journal of Orthopaedic Research*, 1(1), pp. 4–12.

Horas, U., Pelinkovic, D., Herr, G., Aigner, T. and Schnettler, R. (2003) 'Autologous chondrocyte implantation and osteochondral cylinder transplantation in cartilage repair of the knee joint. A prospective, comparative trial.', *The Journal of bone and joint surgery. American volume*. The

American Orthopedic Association, 85–A(2), pp. 185–92.

Hori, R. Y. and Mockros, L. F. (1976) 'Indentation tests of human articular cartilage.', *Journal of biomechanics*, 9(4), pp. 259–68.

Hsieh, Y.-F., Draganich, L. F., Ho, S. H. and Reider, B. (2002) 'The effects of removal and reconstruction of the anterior cruciate ligament on the contact characteristics of the patellofemoral joint.', *The American journal of sports medicine*, 30(1), pp. 121–7.

Hsu, H. P. and Walker, P. S. (1989) 'Wear and deformation of patellar components in total knee arthroplasty.', *Clinical orthopaedics and related research*, (246), pp. 260–5.

Hungerford, D. S. and Barry, M. (1979) 'Biomechanics of the patellofemoral joint.', *Clinical orthopaedics and related research*, (144), pp. 9–15.

Hussainova, I. (2007) *Biotribology Problems of Human Joints*. PhD thesis, Tallinn University of Technology.

ICRS (2016) *ICRS Chondral Injury Classification*. Available at: <http://cartilage.org/> (Accessed: 20 August 2015).

James, C. B. and Uhl, T. L. (2001) 'A review of articular cartilage pathology and the use of glucosamine sulfate.', *Journal of athletic training*, 36(4), pp. 413–9.

Jansson, K. S., Michalski, M. P., Smith, S. D., LaPrade, R. F. and Wijdicks, C. A. (2013) 'Tekscan pressure sensor output changes in the presence of liquid exposure.', *Journal of biomechanics*, 46(3), pp. 612–4.

Jay, G. D. (1992) 'Characterization of a bovine synovial fluid lubricating factor. I. Chemical, surface activity and lubricating properties.', *Connective tissue research*, 28(1–2), pp. 71–88.

Joda, A., Korossis, S., Summers, J., Fisher, J. and Jin, Z. (2011) 'Numerical simulations of decellularised aortic valve scaffolds', in, p. 37.

Julkunen, P., Harjula, T., Iivarinen, J., Marjanen, J., Seppänen, K., Närhi, T., Arokoski, J., Lammi, M. J., Brama, P. A., Jurvelin, J. S. and Helminen, H. J. (2009) 'Biomechanical, biochemical and structural correlations in immature and mature rabbit articular cartilage.', *Osteoarthritis and cartilage / OARS, Osteoarthritis Research Society*, 17(12), pp. 1628–38.

Jurvelin, J. S., Buschmann, M. D. and Hunziker, E. B. (1997) 'Optical and mechanical determination of Poisson's ratio of adult bovine humeral articular cartilage.', *Journal of biomechanics*, 30(3), pp. 235–41.

Katta, J. (2007) *Self-assembling Peptide Networks for Treatment of Cartilage Degenerative Diseases*. PhD thesis, University of Leeds.

- Katta, J., Jin, Z., Ingham, E. and Fisher, J. (2008) 'Biotribology of articular cartilage — A review of the recent advances', *Medical Engineering & Physics*, 30, pp. 1349–1363.
- Katta, J., Jin, Z., Ingham, E. and Fisher, J. (2009) 'Effect of nominal stress on the long term friction, deformation and wear of native and glycosaminoglycan deficient articular cartilage.', *Osteoarthritis and cartilage / OARS, Osteoarthritis Research Society*. Elsevier Ltd, 17(5), pp. 662–8.
- Katta, J., Pawaskar, S. S., Jin, Z. M., Ingham, E. and Fisher, J. (2007) 'Effect of load variation on the friction properties of articular cartilage', *Proceedings of the Institution of Mechanical Engineers, Part J: Journal of Engineering Tribology*, 221(3), pp. 175–181.
- Katta, J., Stapleton, T., Ingham, E., Jin, Z. M. and Fisher, J. (2008) 'The effect of glycosaminoglycan depletion on the friction and deformation of articular cartilage.', *Proceedings of the Institution of Mechanical Engineers. Part H, Journal of engineering in medicine*, 222(1), pp. 1–11.
- Kawcak, C. E., McIlwraith, C. W., Norrdin, R. W., Park, R. D., James, S. P., Ilwraith, C. W. M. C., Norrdin, R. W., Park, R. D. and James, S. P. (2001) 'The role of subchondral bone in joint disease: a review', *Equine veterinary journal*, 33(2), pp. 120–6.
- Kelc Robi, N. J. (2013) *Current Issues in Sports and Exercise Medicine*. Edited by M. Hamlin. InTech. ISBN 978-953-51-1031-6
- Kempson, G. E., Spivey, C. J., Swanson, S. A. V. and Freeman, M. A. R. (1971) 'Patterns of cartilage stiffness on normal and degenerate human femoral heads', *Journal of Biomechanics*, 4(6), pp. 597–609.
- Kheir, E., Stapleton, T., Shaw, D., Jin, Z., Fisher, J. and Ingham, E. (2011) 'Development and characterization of an acellular porcine cartilage bone matrix for use in tissue engineering.', *Journal of biomedical materials research. Part A*, 99(2), pp. 283–94.
- Khorramirouz, R., Sabetkish, S., Akbarzadeh, A., Muhammadnejad, A., Heidari, R. and Kajbafzadeh, A. M. (2014) 'Effect of three decellularisation protocols on the mechanical behaviour and structural properties of sheep aortic valve conduits'. *Medical University of Bialystok*, 59(2), pp. 299–307.
- Kim, D., Chung, H., Yi, C.-H., Yoon, Y.-S., Son, J., Kim, Y., On, M.-G. and Yang, J. (2016) 'Effect of glenohumeral position on contact pressure between the capsulolabral complex and the glenoid in free ALPSA and Bankart lesions.', *Knee surgery, sports traumatology, arthroscopy : official journal of the ESSKA*. Springer Berlin Heidelberg, 24(2), pp. 350–6.
- Kittl, C., Schmeling, A. and Amis, A. A. (2015) 'The patellofemoral joint: Anatomy, biomechanics, and surgical interventions', *Arthroscopie*. Springer Verlag, 28(3), pp. 172–180.

- Kock, N. B., Smolders, J. M. H., van Susante, J. L. C., Buma, P., van Kampen, A. and Verdonschot, N. (2008) 'A cadaveric analysis of contact stress restoration after osteochondral transplantation of a cylindrical cartilage defect.', *Knee surgery, sports traumatology, arthroscopy : official journal of the ESSKA*, 16(5), pp. 461–8.
- Koh J., Kowalski A. and Lautenschlager E. (2004) The effect of angled osteochondral grafting on contact pressure - a biomechanical study. *Am J Sport Med* 2006; 34(1), pp. 116-119
- Kon, E., Vannini, F., Buda, R., Filardo, G., Cavallo, M., Ruffilli, A., Nanni, M., Di Martino, A., Marcacci, M. and Giannini, S. (2012) 'How to treat osteochondritis dissecans of the knee: surgical techniques and new trends: AAOS exhibit selection.', *The Journal of bone and joint surgery. American volume. The Journal of Bone and Joint Surgery*, 94(1), p. e1(1-8).
- Korduba, L., Longaray, J., Essner, A. and Meneghini, R. (2008) 'Development of an aggressive wear test for patella implants', in *54th Orthopaedic Research society*. San Fransisco, California.
- Korhonen, R. ., Laasanen, M. ., Töyräs, J., Rieppo, J., Hirvonen, J., Helminen, H. . and Jurvelin, J. . (2002) 'Comparison of the equilibrium response of articular cartilage in unconfined compression, confined compression and indentation', *Journal of Biomechanics*, 35(7), pp. 903–909.
- Koskinen, S. (1993) *Measurement of patellofemoral relationships at 0-30 degrees of knee flexion*. PhD thesis, University of Turku.
- Krishnan, R., Mariner, E. N. and Ateshian, G. a (2005) 'Effect of dynamic loading on the frictional response of bovine articular cartilage.', *Journal of biomechanics*, 38(8), pp. 1665–73.
- Kuster, M. S., Podsiadlo, P. and Stachowiak, G. W. (1998) 'Shape of wear particles found in human knee joints and their relationship to osteoarthritis.', *British journal of rheumatology*, 37(9), pp. 978–84.
- Kwak, S. D., Colman, W. W., Ateshian, G. A., Grelsamer, R. P., Henry, J. H. and Mow, V. C. (1997) 'Anatomy of the human patellofemoral joint articular cartilage: surface curvature analysis.', *Journal of orthopaedic research : official publication of the Orthopaedic Research Society*. Raven Press Ltd, 15(3), pp. 468–72.
- Lai, W. M., Hou, J. S. and Mow, V. C. (1991) 'A triphasic theory for the swelling and deformation behaviors of articular cartilage.', *Journal of biomechanical engineering*, 113(3), pp. 245–58.
- Lai, W. M. and Mow, V. C. (1980) 'Drag-induced compression of articular cartilage during a permeation experiment.', *Biorheology*, 17(1–2), pp. 111–23.
- Landínez-Parra, N. S., Garzón-Alvarado, D. A. and Vanegas-Acosta, J. C. (2012) 'Mechanical

- Behavior of Articular Cartilage', in Goswami, T. (ed.) *Injury and Skeletal Biomechanics*. InTech.
- LaPrade, C. M., Jansson, K. S., Dornan, G., Smith, S. D., Wijdicks, C. A. and LaPrade, R. F. (2014) 'Altered tibiofemoral contact mechanics due to lateral meniscus posterior horn root avulsions and radial tears can be restored with in situ pull-out suture repairs.', *The Journal of bone and joint surgery. American volume*, 96(6), pp. 471–9.
- Leal, A., Pereira, R., Pereira, H., Flores, P. and Silva, F. S. (2015) *New Trends in Mechanism and Machine Science*. Edited by P. Flores and F. Viadero. Cham: Springer International Publishing ISBN 978-94-007-4902-3
- Lee, T. Q., Morris, G. and Csintalan, R. P. (2003) 'The influence of tibial and femoral rotation on patellofemoral contact area and pressure.', *The Journal of orthopaedic and sports physical therapy*, 33(11), pp. 686–93.
- Lee, T. Q., Yang, B. Y., Sandusky, M. D. and McMahon, P. J. (2001) 'The effects of tibial rotation on the patellofemoral joint: assessment of the changes in in situ strain in the peripatellar retinaculum and the patellofemoral contact pressures and areas.', *Journal of rehabilitation research and development*, 38(5), pp. 463–9.
- Leichtle, U. G., Wünschel, M., Leichtle, C. I., Müller, O., Kohler, P., Wülker, N. and Lorenz, A. (2014) 'Increased patellofemoral pressure after TKA: an in vitro study.', *Knee surgery, sports traumatology, arthroscopy : official journal of the ESSKA*, 22(3), pp. 500–8.
- Levangie, P. K. and Norkin, C. C. (2011) *Joint Structure and Function: A Comprehensive Analysis*. F. A. Davis Company.
- Li, B. and Aspden, R. M. (1997) 'Mechanical and material properties of the subchondral bone plate from the femoral head of patients with osteoarthritis or osteoporosis.', *Annals of the rheumatic diseases*, 56(4), pp. 247–54.
- Li, B., Marshall, D., Roe, M. and Aspden, R. M. (1999) 'The electron microscope appearance of the subchondral bone plate in the human femoral head in osteoarthritis and osteoporosis.', *Journal of anatomy*, 195 (Pt 1, pp. 101–10.
- Li, G., DeFrate, L. E., Zayontz, S., Park, S. E. and Gill, T. J. (2004) 'The effect of tibiofemoral joint kinematics on patellofemoral contact pressures under simulated muscle loads.', *Journal of orthopaedic research : official publication of the Orthopaedic Research Society*, 22(4), pp. 801–6.
- Li, L., Patil, S., Steklov, N., Bae, W., Temple-Wong, M., D'Lima, D. D., Sah, R. L. and Fregly, B. J. (2011) 'Computational wear simulation of patellofemoral articular cartilage during in vitro testing.', *Journal of biomechanics*, 44(8), pp. 1507–13.

Liang, J. (2008) *Investigation of synthetic and natural lubricants*. PhD Thesis, NC State University.

Liggins, A. B., Hardie, W. R. and Finlay, J. B. (1995) 'The Spatial and Pressure Resolution of Fuji Pressure-sensitive Film', *Experimental Mechanics*, pp. 166–173.

Lipshitz, H., Etheredge, R. and Glimcher, M. J. (1975) 'In vitro wear of articular cartilage.', *The Journal of bone and joint surgery. American volume*, 57(4), pp. 527–34.

Lipshitz, H., Etheredge, R. and Glimcher, M. J. (1980) 'In vitro studies of the wear of articular cartilage—III. The wear characteristics of chemically modified articular cartilage when worn against a highly polished characterized stainless steel surface', *Journal of Biomechanics*, 13(5), pp. 423–436.

Lipshitz, H. and Glimcher, M. J. (1974) 'A technique for the preparation of plugs of articular cartilage and subchondral bone', *Journal of Biomechanics*, 7(3), p. 293–IN18.

Lipshitz, H. and Glimcher, M. J. (1979) 'In vitro studies of the wear of articular cartilage II. Characteristics of the wear of articular cartilage when worn against stainless steel plates having characterized surfaces', *Wear*, 52(2), pp. 297–339.

Little, C. J., Bawolin, N. K. and Chen, X. (2011) 'Mechanical properties of natural cartilage and tissue-engineered constructs.', *Tissue engineering. Part B, Reviews*, 17(4), pp. 213–227.

Liu, A., Jennings, L. M., Ingham, E. and Fisher, J. (2015) 'Tribology studies of the natural knee using an animal model in a new whole joint natural knee simulator', *Journal of Biomechanics*, 48(12), pp. 3004–3011.

Lizhang, J. (2010) *Tribology of hemiarthroplasty*. PhD thesis, University of Leeds.

Lorbach, O., Hauptert, A., Efe, T., Pizanis, A., Weyers, I., Kohn, D. and Kieb, M. (2016) 'Biomechanical evaluation of MPFL reconstructions: differences in dynamic contact pressure between gracilis and fascia lata graft.', *Knee surgery, sports traumatology, arthroscopy : official journal of the ESSKA*. Springer Berlin Heidelberg, pp. 1–9.

Lu, X. L. and Mow, V. C. (2008) 'Biomechanics of articular cartilage and determination of material properties', *Medicine and Science in Sports and Exercise*, 40(2), pp. 193–199.

Luo, J., Fisher, J., Jin, Z., Ingham, E. and Korossis, S. (2011) 'Biomechanical testing of low-concentration SDS decellularised porcine pulmonary valves', in, p. 63.

Lynch, T. S., Patel, R. M., Benedick, A., Amin, N. H., Jones, M. H. and Miniaci, A. (2015) 'Systematic Review of Autogenous Osteochondral Transplant Outcomes', *Arthroscopy: The Journal of Arthroscopic & Related Surgery*, 31(4), pp. 746–754.

- Ma, R., Xiong, D., Miao, F., Zhang, J. and Peng, Y. (2010) 'Friction properties of novel PVP/PVA blend hydrogels as artificial cartilage.', *Journal of biomedical materials research. Part A*, 93(3), pp. 1016–9.
- Maiti, R. (2012) *Bio tribology of the Patella Femoral Joint in Total Knee Replacement*. PhD thesis, PhD thesis, University of Leeds.
- Maiti, R., Fisher, J., Rowley, L. and Jennings, L. M. (2014) 'The influence of kinematic conditions and design on the wear of patella-femoral replacements.', *Proceedings of the Institution of Mechanical Engineers. Part H, Journal of engineering in medicine*, 228(2), pp. 175–81.
- Malcom, L. L. (1976) *An experimental investigation of the frictional and deformational responses of articular cartilage interfaces to static and dynamic loading*. PhD thesis, University of California, San Diego.
- Maquet, P. (1990) 'Biomechanics of the patello-femoral joint', *Acta orthopaedica Belgica*, 44(1), pp. 41–54.
- Maroudas, A. (1968) 'Physicochemical properties of cartilage in the light of ion exchange theory.', *Biophysical journal*, 8(5), pp. 575–95.
- Maroudas, A. and Bullough, P. (1968) 'Permeability of Articular Cartilage', *Nature*, 219(5160), pp. 1260–1261.
- Mason, J. J., Leszko, F., Johnson, T. and Komistek, R. D. (2008) 'Patellofemoral joint forces.', *Journal of biomechanics*, 41(11), pp. 2337–48.
- Matthews, L. S., Sonstegard, D. a and Henke, J. a (1977) 'Load bearing characteristics of the patello-femoral joint.', *Acta orthopaedica Scandinavica*, 48(5), pp. 511–6.
- McCann, L. (2009) *A Computational and Experimental Investigation of the Tribological Properties of Articular Cartilage Defect Repair*. PhD thesis, University of Leeds.
- Mccutchen, C. (1962) 'The frictional properties of animal joints', *Wear*, 5(1), pp. 1–17.
- McGann, M. E., Vahdati, A. and Wagner, D. R. (2012) 'Methods to assess in vitro wear of articular cartilage.', *Proceedings of the Institution of Mechanical Engineers. Part H, Journal of engineering in medicine*, 226(8), pp. 612–22.
- McLure, S. W. D. (2012) *Improving models for translational reasearch in osteoarthritis*. Univeristy fo Leeds.
- McNary, S., Athanasiou, K. and Reddi, A. H. (2011) 'Engineering Lubrication in Articular Cartilage.', *Tissue engineering. Part B, Reviews*.

- Mehl, J., Feucht, M. J., Bode, G., Dovi-Akue, D., Südkamp, N. P. and Niemeyer, P. (2014) 'Association between patellar cartilage defects and patellofemoral geometry: a matched-pair MRI comparison of patients with and without isolated patellar cartilage defects.', *Knee surgery, sports traumatology, arthroscopy : official journal of the ESSKA*. Springer Verlag, 24(3), pp. 838–846.
- Merchant, A. C. (1988) 'Classification of patellofemoral disorders.', *Arthroscopy : the journal of arthroscopic & related surgery : official publication of the Arthroscopy Association of North America and the International Arthroscopy Association*, 4(4), pp. 235–40.
- Merkher, Y., Sivan, S., Etsion, I., Maroudas, A., Halperin, G. and Yosef, A. (2006) 'A rational friction test using a human cartilage-on-cartilage arrangement', in *International Conference on Tribology*.
- Moa-Anderson, B. J., Costa, K. D., Hung, C. T. and Ateshian, G. A. (2003) 'Bovine articular cartilage surface topography and roughness in fresh versus frozen tissue samples using atomic force microscopy', in *Summer Bioengineering Conference*. Florida.
- Mow, V. C. (1969) 'The Role of Lubrication in Biomechanics Joints', *American Society of Mechanical Engineers*, pp. 320–326.
- Mow, V. C., Hou, J. S., Owens, J. M. and Ratcliffe, A. (1990) 'Biphasic and Quasilinear Viscoelastic Theories for hydrated soft tissues', in *Biomechanics of Diarthrodial Joints: Volume I*. Springer, pp. 215–260.
- Mow, V. C., Kuei, S. C., Lai, W. M. and Armstrong, C. G. (1980) 'Biphasic Creep and Stress Relaxation of Articular Cartilage in Compression: Theory and Experiments', *Journal of Biomechanical Engineering*. American Society of Mechanical Engineers, 102(1), p. 73.
- Mow, V. C. and Huiskes, R. (2005); 'Chapter 5: Structure and Function of articular cartilage and Meniscus'. *Basic Orthopaedic Biomechanics and Mechano-Biology*. 3rd edition, Philadelphia: Lippincott Williams & Wilkins. ISBN 9780781739337
- Mrosek, E. H., Lahm, a, Erggelet, C., Uhl, M., Kurz, H., Eissner, B. and Schagemann, J. C. (2006) 'Subchondral bone trauma causes cartilage matrix degeneration: an immunohistochemical analysis in a canine model.', *Osteoarthritis and cartilage / OARS, Osteoarthritis Research Society*, 14(2), pp. 171–8.
- Muraoka, T., Hagino, H., Okano, T., Enokida, M. and Teshima, R. (2007) 'Role of subchondral bone in osteoarthritis development: a comparative study of two strains of guinea pigs with and without spontaneously occurring osteoarthritis.', *Arthritis and rheumatism*, 56(10), pp. 3366–74.
- Nebelung, S., Brill, N., Müller, F., Tingart, M., Pufe, T., Merhof, D., Schmitt, R., Jahr, H. and

- Truhn, D. (2016) 'Towards Optical Coherence Tomography-based elastographic evaluation of human cartilage.', *Journal of the mechanical behavior of biomedical materials*, 56, pp. 106–19.
- Newman, A. P. (1998) 'Articular cartilage repair.', *The American journal of sports medicine*, 26(2), pp. 309–24.
- Nho, S. J., Foo, L. F., Green, D. M., Shindle, M. K., Warren, R. F., Wickiewicz, T. L., Potter, H. G. and Williams, R. J. (2008) 'Magnetic resonance imaging and clinical evaluation of patellar resurfacing with press-fit osteochondral autograft plugs.', *The American journal of sports medicine*, 36(6), pp. 1101–9.
- Nishida, K., Iwasaki, N., Fujisaki, K., Funakoshi, T., Kamishima, T., Tadano, S. and Minami, A. (2012) 'Distribution of bone mineral density at osteochondral donor sites in the patellofemoral joint among baseball players and controls.', *The American journal of sports medicine*, 40(4), pp. 909–14.
- Nordin, M. and Frankel, M. N. V. H. (2001) *Basic Biomechanics of the Musculoskeletal System*. Lippincott Williams & Wilkins. ISBN 9781609133351
- Northwood, E. and Fisher, J. (2007) 'A multi-directional in vitro investigation into friction, damage and wear of innovative chondroplasty materials against articular cartilage.', *Clinical biomechanics (Bristol, Avon)*, 22(7), pp. 834–42.
- Northwood, J. E. (2007) *Cartilage Wear simulation models for Surface and Spacer Hemiarthroplasty and Tissue Engineering*. PhD thesis, University of Leeds.
- Nukavarapu, S. P. and Dorcemus, D. L. (2013) 'Osteochondral tissue engineering: Current strategies and challenges.', *Biotechnology advances*. Elsevier Inc., 31(5), pp. 706–21.
- Ohba, S., Yano, F. and Chung, U. (2009) 'Tissue engineering of bone and cartilage', *IBMS BoneKEy*, 6(11), pp. 405–419.
- Osterhoff, G., Löffler, S., Steinke, H., Feja, C., Josten, C. and Hepp, P. (2011) 'Comparative anatomical measurements of osseous structures in the ovine and human knee.', *The Knee*, 18(2), pp. 98–103.
- Oungoulian, S. R., Bortz, O., Hehir, K. E., Zhu, K., Hung, C. T. and Ateshian, G. A. (2012) 'Articular Cartilage Wear Characterization With a Particle Sizing and Counting Analyzer', in *ASME 2012 Summer Bioengineering Conference, Parts A and B*. ASME, p. 503.
- Padalecki, J. R., Jansson, K. S., Smith, S. D., Dornan, G. J., Pierce, C. M., Wijdicks, C. A. and Laprade, R. F. (2014) 'Biomechanical consequences of a complete radial tear adjacent to the medial meniscus posterior root attachment site: in situ pull-out repair restores derangement of joint mechanics.', *The American journal of sports medicine*, 42(3), pp. 699–707.

- Park, S., Costa, K. D. and Ateshian, G. a (2004) 'Microscale frictional response of bovine articular cartilage from atomic force microscopy.', *Journal of biomechanics*, 37(11), pp. 1679–87.
- Pawaskar, S. S. (2006) *Contact Mechanics Modelling of Articular Cartilage and Applications*. PhD thesis, University of Leeds.
- Pawaskar, S. S., Fisher, J. and Jin, Z. (2010) 'Robust and general method for determining surface fluid flow boundary conditions in articular cartilage contact mechanics modeling.', *Journal of biomechanical engineering*, 132(3), p. 31001.
- Peng, Z. and Wang, M. (2013) 'Three dimensional surface characterization of human cartilages at a micron and nanometre scale', *Wear*, 301(1–2), pp. 210–217.
- Radin, E. L. and Paul, I. L. (1971) 'Response of Joints to Impact Loading. I. In Vitro Wear', *Arthritis & Rheumatism*, 14(3), pp. 356–362.
- Radin, E. L. and Rose, R. M. (1986) 'Role of subchondral bone in the initiation and progression of cartilage damage.', *Clinical orthopaedics and related research*, (213), pp. 34–40.
- Radins, E. L. and Paulq, I. L. (1972) 'Response of Joints to Impact Loading. II. In Vitro Wear', pp. 267–272.
- Reddi, A. H. (2008) 'The Interface of Functional Biotribology and Regenerative Medicine in Synovial Joints', 14(3).
- Redman, S. N., Oldfield, S. F. and Archer, C. W. (2005) 'Current strategies for articular cartilage repair.', *European cells & materials*, 9(0), pp. 23-32-32.
- Reilly, D. T. and Martens, M. (1972) 'Experimental analysis of the quadriceps muscle force and patello-femoral joint reaction force for various activities.', *Acta orthopaedica Scandinavica*, 43(2), pp. 126–37.
- Revell, P. A. (2008) 'The combined role of wear particles, macrophages and lymphocytes in the loosening of total joint prostheses.', *Journal of the Royal Society, Interface / the Royal Society*. The Royal Society, 5(28), pp. 1263–78.
- Roba, M., Bruhin, C., Ebnetter, U., Ehrbar, R., Crockett, R. and Spencer, N. D. (2010) 'Latex on Glass: an Appropriate Model for Cartilage-Lubrication Studies?', *Tribology Letters*, 38(3), pp. 267–273.
- Robinson, D. L., Kersh, M. E., Walsh, N. C., Ackland, D. C., de Steiger, R. N. and Pandey, M. G. (2016) 'Mechanical properties of normal and osteoarthritic Human articular cartilage', *Journal of the Mechanical Behavior of Biomedical Materials*, 61, pp. 96–109.

- Rössner, E., Smith, M. D., Petschke, B., Schmidt, K., Vitacolonna, M., Syring, C., Von Versen, R. and Hohenberger, P. (2011) 'Epiflex® A new decellularised human skin tissue transplant: Manufacture and properties', *12*(3), pp. 209–217.
- Russell, S. (2011) *SOP . 02 . 2 Long term Friction / Wear Pin-on-Plate Simulator, Tissue Engineering*.
- Russell, S. L. (2010) *Friction , Wear , Wear Debris and Functional Biocompatibility of Cartilage Substitution Biomaterials*. PhD thesis, University of Leeds.
- Saarakkala, S., Töyräs, J., Hirvonen, J., Laasanen, M. S., Lappalainen, R. and Jurvelin, J. S. (2004) 'Ultrasonic quantitation of superficial degradation of articular cartilage.', *Ultrasound in medicine & biology*, *30*(6), pp. 783–92.
- Saarakkala, S., Wang, S.-Z., Huang, Y.-P. and Zheng, Y.-P. (2009) 'Quantification of the optical surface reflection and surface roughness of articular cartilage using optical coherence tomography.', *Physics in medicine and biology*. IOP Publishing, *54*(22), pp. 6837–52.
- Saikko, V. (2003) 'Effect of Lubricant Protein Concentration on the Wear of Ultra-High Molecular Weight Polyethylene Sliding Against a CoCr Counterface', *Journal of Tribology*, *125*(3), p. 638.
- Saleh, K. J., Arendt, E. A., Eldridge, J., Fulkerson, J. P., Minas, T. and Mulhall, K. J. (2005) 'Symposium. Operative treatment of patellofemoral arthritis.', *The Journal of bone and joint surgery. American volume*, *87*(3), pp. 659–71.
- Scanlon, C. (2012) *Cartilage Tissue Engineering Using a Modified Decellularized Porcine Cartilage Scaffold and a Novel Centrifugation Cell Seeding Technique*. PhD thesis, University of Miami.
- Schmidt, T. A. and Sah, R. L. (2007) 'Effect of synovial fluid on boundary lubrication of articular cartilage.', *Osteoarthritis and cartilage / OARS, Osteoarthritis Research Society*, *15*(1), pp. 35–47.
- Schwartz, C. J. and Bahadur, S. (2007) 'Investigation of articular cartilage and counterface compliance in multi-directional sliding as in orthopedic implants', *Wear*, *262*(11–12), pp. 1315–1320.
- Schwarz, S., Koerber, L., Elsaesser, A. F., Goldberg-Bockhorn, E., Seitz, A. M., Dürselen, L., Ignatius, A., Walther, P., Breiter, R. and Rotter, N. (2012) 'Decellularized Cartilage Matrix as a Novel Biomatrix for Cartilage Tissue-Engineering Applications', *Tissue Engineering Part A*, *18*, pp. 12-17.
- Scott, N. (2011) *Insall & Scott Surgery of the Knee*. 5th edn. Churchill Livingstone. ISBN

9780323400466

Serway, R. A. and Jewett, J. W. (2012) *Physics for Scientists and Engineers, Chapters 1-39*. Cengage Learning.

Setton, L. a, Zhu, W. and Mow, V. C. (1993) 'The biphasic poroviscoelastic behavior of articular cartilage: role of the surface zone in governing the compressive behavior.', *Journal of biomechanics*, 26(4-5), pp. 581-92.

Shekhawat, V. K., Laurent, M. P., Muehleman, C. and Wimmer, M. A. (2009) 'Surface topography of viable articular cartilage measured with scanning white light interferometry.', *Osteoarthritis and cartilage / OARS, Osteoarthritis Research Society*, 17(9), pp. 1197-203.

Shepherd, D. E. and Seedhom, B. B. (1999) 'Thickness of human articular cartilage in joints of the lower limb.', *Annals of the rheumatic diseases*, 58(1), pp. 27-34.

Shi, L., Sikavitsas, V. I. and Striolo, A. (2011) 'Experimental friction coefficients for bovine cartilage measured with a pin-on-disk tribometer: testing configuration and lubricant effects.', *Annals of biomedical engineering*, 39(1), pp. 132-46.

Shirazi, R., Shirazi-Adl, a and Hurtig, M. (2008) 'Role of cartilage collagen fibrils networks in knee joint biomechanics under compression.', *Journal of biomechanics*, 41(16), pp. 3340-8.

Smith and Nephew (2013) *TRUFIT™ CB Plug, Product handbook*.

Smyth, P. a, Rifkin, R. E., Jackson, R. L. and Hanson, R. R. (2012) 'A surface roughness comparison of cartilage in different types of synovial joints.', *Journal of biomechanical engineering*, 134(2), p. 21006.

A. J. Sophia Fox, A. Bedi, and S. a Rodeo, (2009) "The basic science of articular cartilage: structure, composition, and function.," *Sports health*, vol. 1, no. 6, pp. 461-8

Stachowiak, G. W. and Podsiadlo, P. (1997) 'Analysis of wear particle boundaries found in sheep knee joints during in vitro wear tests without muscle compensation', *Journal of Biomechanics*, 30(4), pp. 415-419.

Stewart, T. (2007) 'The natural synovial joint', in *MECH 3835 Biomedical engineering lecture notes*. University of Leeds, pp. 11-27.

Stewart, T. D. (2010) 'Tribology of artificial joints', *Orthopaedics and Trauma*. Elsevier Ltd, 24(6), pp. 435-440.

Stockwell, R. A. (1971) 'The interrelationship of cell density and cartilage thickness in mammalian articular cartilage.', *Journal of anatomy*, 109(Pt 3), pp. 411-21.

- Sullivan, N. P. T., Robinson, P. W., Ansari, A., Hassaballa, M., Robinson, J. R., Porteous, A. J., Eldridge, J. D. and Murray, J. R. D. (2014) 'Bristol index of patellar width to thickness (BIPWiT): a reproducible measure of patellar thickness from adult MRI.', *The Knee*, 21(6), pp. 1058–62.
- Suzuki, T., Hosseini, A., Li, J.-S., Gill, T. J. and Li, G. (2012) 'In vivo patellar tracking and patellofemoral cartilage contacts during dynamic stair ascending.', *Journal of biomechanics*. Elsevier, 45(14), pp. 2432–7.
- Taylor, C. (2013) *Development and characterisation of mechanical and enzymatic models of cartilage degeneration*. PhD thesis, University of Leeds.
- Taylor, S. (2012) *An In-vitro Medium Term Simulation of Hip Hemiarthroplasty*. PhD thesis, University of Leeds.
- Trattng, S., Millington, S. A., Szomolanyi, P. and Marlovits, S. (2007) 'MR imaging of osteochondral grafts and autologous chondrocyte implantation.', *European radiology*. Springer, 17(1), pp. 103–18.
- Treppo, S., Koepp, H., Quan, E. C., Cole, A. A., Kuettner, K. E. and Grodzinsky, A. J. (2000) 'Comparison of biomechanical and biochemical properties of cartilage from human knee and ankle pairs.', *Journal of orthopaedic research : official publication of the Orthopaedic Research Society*, 18(5), pp. 739–48.
- Turtel, A., DeBerardino, T., Talavera, F. and Pearsell, A. (2015) *Osteochondral Grafting of Articular Cartilage Injuries: Background, Indications, Contraindications*.
- Ulstein, S., Engebretsen, L. and Heir, S. (2014) 'Microfracture technique versus osteochondral autologous transplantation mosaicplasty in patients with articular chondral lesions of the knee: A prospective randomized trial with long-term follow-up', *Knee Surgery, Sports Traumatology, Arthroscopy*, 22(6), pp. 1207–1215.
- Walker, P. S., Dowson, D., Longfield, M. D. and Wright, V. (1968) "'Boosted lubrication" in synovial joints by fluid entrapment and enrichment.', *Annals of the rheumatic diseases*, 27(6), pp. 512–20.
- Wallace, D. a, Salem, G. J., Salinas, R. and Powers, C. M. (2002) 'Patellofemoral joint kinetics while squatting with and without an external load.', *The Journal of orthopaedic and sports physical therapy*, 32(4), pp. 141–8.
- Wang, C. C.-B., Deng, J.-M., Ateshian, G. A. and Hung, C. T. (2002) 'An automated approach for direct measurement of two-dimensional strain distributions within articular cartilage under unconfined compression.', *Journal of biomechanical engineering*, 124(5), pp. 557–67.
- Wang, C. C.-B., Hung, C. T. and Mow, V. C. (2001) 'An analysis of the effects of depth-

dependent aggregate modulus on articular cartilage stress-relaxation behavior in compression', *Journal of Biomechanics*. Elsevier Science Ltd, 34(1), pp. 75–84.

Wang, H., Chen, T., Gee, A. O., Hutchinson, I. D., Stoner, K., Warren, R. F., Rodeo, S. A. and Maher, S. A. (2015) 'Altered regional loading patterns on articular cartilage following meniscectomy are not fully restored by autograft meniscal transplantation.', *Osteoarthritis and cartilage / OARS, Osteoarthritis Research Society*, 23(3), pp. 462–8.

Wang, M. and Peng, Z. (2015) 'Investigation of the nano-mechanical properties and surface topographies of wear particles and human knee cartilages', *Wear*, 324–325, pp. 74–79.

Wang, M., Sharkey, P. and Tuan, R. (2004) 'Particle bioreactivity and wear-mediated osteolysis', *The Journal of Arthroplasty*, 19(8), pp. 1028–1038.

Wiberg, G. (1941) 'Roentgenographic and Anatomic Studies on the Femoropatellar Joint', *Acta Orthopaedica Scandinavica*, 12(November), pp. 319–410.

Williams, R. J. and Gamradt, S. C. (2008) 'Articular cartilage repair using a resorbable matrix scaffold.', *Instructional course lectures*, 57, pp. 563–71.

Wright, V. and Dawson, D. (1976) 'Lubrication and cartilage', *Journal of anatomy*, (121), pp. 107–118.

Wu J., Herzog W and Hasler E. (2002) Inadequate placement of osteochondral plug mau induce abnormal stress-strain distributions in articular cartilage - finite element simulations. *Med Eng Phys*; 24(2), pp.85-97

Wyndow, N., Collins, N., Vicenzino, B., Tucker, K. and Crossley, K. (2016) 'Is There a Biomechanical Link Between Patellofemoral Pain and Osteoarthritis? A Narrative Review', *Sports Medicine and Arthroscopy Review*, pp. 1–12.

Zaffagnini, S., Dejour, D., Grassi, A., Bonanzinga, T. and Marcheggiani Muccioli, G. M. (2016) 'Patellofemoral anatomy and biomechanics: current concepts.', *Joints*, 1(2), pp. 15–20.

Zhang, L., Hu, J. and Athanasiou, K. A. (2009) 'The role of tissue engineering in articular cartilage repair and regeneration.', *Critical reviews in biomedical engineering*, 37(1–2), pp. 1–57.